Author:
Tijssen, Teuntje

Title:
Spin manifestations in light and matter waves

Spin manifestations in structured light and matter waves

Teuntje Tijssen

H. H. Wills Physics Laboratory
University of Bristol

A thesis submitted to the University of Bristol in
accordance with the requirements of the degree of
Ph.D. in the Faculty of Science

School of Physics, December 2018

41168 words

“The greater the circle of light, the greater is the boundary of the darkness by which it is confined"

Joseph Priestly

Abstract

Fields in free space are able to carry orbital angular momentum, which may arise when a system is invariant under rotations. Such systems favour a description in cylindrical polar coordinates. Solutions of the wave equation in these coordinates are Bessel beams, invariant under propagation in the longitudinal direction.

Some fields also possess spin angular momentum, such as the optical vector field and the electron spinor field. These fields are described by multi-component wavefunctions, in contrast to a scalar (spinless) field. The resulting spin degree of freedom can be quantized by either the longitudinal direction (spin) or the momentum vector (helicity). Differences between helicity and spin states are in general small and disappear in suitable limits.

Spin and orbital angular momentum couple to each other, yielding fields that are eigenstates of the total angular momentum. The effects of this coupling can be studied by considering the mechanical properties of the fields. There is an orbital contribution, arising from the multi-component nature of the wavefunctions, and a spin contribution.

Combining fields with circular polarization gives rise to states with linear polarization, analogous to constructing standing waves from travelling waves, or creating a real Majorana field from two complex spinor fields. Fermionic Majorana modes, rather than particles, can be constructed with equal contributions of positive and negative frequencies. These modes carry no charge and are invariant under charge conjugation, conditions optical modes satisfy trivially. However, symmetry considerations lead to the conclusion that optical Majorana modes are linearly polarized. There exist bound optical modes analogous to fermionic Majorana modes, but there are also photonic Majorana modes possible that do not have fermionic counterparts.

The coupling between orbital and spin angular momentum changes considerably in systems described in parabolic coordinates, as the basis states are eigenstates of the parabolic momentum instead. There is only an effective spin-to-orbital angular momentum coupling and a spin-to-parabolic-momentum coupling close to one Cartesian coordinate axis.

Acknowledgements

During my PhD I have been supported to great lengths by my supervisor Mark Dennis. With his extensive knowledge of many fields in physics there was never a moment in which he did not have a new idea or a new direction in which I could take my research. It must have been very difficult to juggle all responsibilities he had at the same time. I want to thank him for everything that he has done for me over the last four years to bring me in the position I am now in, with my thesis being completed. In this context I definitely also need to mention Martin Gradhand, who was appointed as my second supervisor. He has given me some very helpful advice, especially during my last year concerning the writing of my thesis. I would also like to thank the two postdocs in our group, Sandy Taylor and Dave Foster. Although my work was not related to theirs, they could always help in shining a new light on problems concerning my research.

I have received plenty of support from my fellow PhD students, which I consider now my friends. These are Danica Sugic, Elena Boniolo, Keith Alexander, Ben Bode and Lauren Scanlon. I would also like to mention Xi Peng and Tom Saunderson. You all brightened up my office in your own way.

Other members of the School of Physics I would like to mention are Sven Friedemann, with whom I frequently had conversations about rowing, and Nic Tomkins, who I usually saw in the morning in the common room. Some afternoons I would run into Ben Lang, with whom I had interesting discussions about our work. Lastly, I would like to thank Matt Coles who I met during my week at BIRS for some good advice every now and then.

I moved to Bristol for my PhD, leaving my family behind. I phoned my sister Marij regularly for over an hour, discussing everything in our lives. When I came back home, I received a lot of support from Rob, Reina and Gon. But I was also very lucky with my housemates Sue Kilroe, Floor Kellerman and Rachel Pougnet. They understood what I was going through and it helped me a lot to exchange our experiences. I would also like to thank Arthur La Rooij for his advice, understanding what doing a PhD is like.

I would also like to mention some people I have met over the last years and with whom I am now good friends; Jason Mueller, Lea Glaubig and Isabella Burdess. I could not have done this without our conversations over lunch and your support.

My big passion throughout my PhD has been rowing, and this has definitely helped me to unwind from work. I would like to thank my coaches, Cam Kennedy and Edward Bloomfield, for supporting me in busy times when my performance was effected by work-related issues. Thanks also to the Women's captains over the last four years, accommodating for my absences on Wednesday afternoons and research related travels.

Author's Declaration

I declare that the work in this dissertation was carried out in accordance with the requirements of the University's *Regulations and Code of Practice for Research Degree Programmes* and that it has not been submitted for any other academic award. Except where indicated by specific reference in the text, the work is the candidate's own work. Work done in collaboration with, or with the assistance of, others, is indicated as such. Any views expressed in the dissertation are those of the author.

SIGNED: ..... DATE:.....

Teuntje Tijssen

Contents

List of Figures

List of Tables

Acronyms and frequently used symbols

OAM	orbital angular momentum
SAM	spin angular momentum
TAM	total angular momentum
EVB	electron vortex beam
TE	transverse electric
TM	transverse magnetic
$\mathbf{L}$	orbital angular momentum
$\mathbf{S}$	spin angular momentum
$\mathbf{K}$	Runge-Lenz vector
K	parabolic momentum operator
$\boldsymbol{\mathcal{S}}$	Poynting vector
$\hat{\mathbf{p}}$	$\frac{\mathbf{p}}{p}$
$T^{\mu\nu}$	canonical energy-momentum tensor
$\Theta^{\mu\nu}$	symmetrized energy-momentum tensor
H	Hamiltonian
$\mathcal{H}$	helicity operator
σ	optical helicity
ϕ	polar angle in x, y-plane
θ	azimuthal angle
p, q	general transverse coordinates
u, v	parabolic coordinates
$k_\perp$	transverse wavenumber
k_r	radial wavenumber
$k_z \ll k_\perp$	paraxial limit
ℓ	azimuthal winding number, measure of OAM
φ	scalar wavefunction
ψ	spinor wavefunction
S_j	spin-1 matrices
σ_j	Pauli spin matrices
w_s	spin-polarization spinor
w_h	helicity spinor
$\mathcal{M}^{\mu\nu}$	spin-1 generators of the Lorentz group transformations
$\Sigma^{\mu\nu}$	spin-$\frac{1}{2}$ generators of the Lorentz group transformations
$\epsilon = \sqrt{\frac{\mathcal{E}-m}{\mathcal{E}+m}}$	measure of relativistic effects; $\mathcal{E}$ is the total energy and m is the mass of the particle

1 Introduction

A rotating object is said to possess a mechanical quantity called angular momentum. Picture, for example, a solid object such as a ball. This ball is said to have orbital angular momentum if it is moving in a circular trajectory; it orbits around an external point of reference. It could also rotate around its own axis, in which case it has spin angular momentum. The combined motion for any point on the ball, therefore, is described by a circular spiral-like trajectory. The rotational energy of the ball will depend on the sum of both angular momenta. These are usually independent of each other.

However, in some physical systems the magnitude of the spin and orbital angular momenta are related to each other, and this is the main focus of this thesis. The interplay between the two angular momenta will be studied for two different particles; photons (light) and electrons. These particles both carry an intrinsic spin angular momentum, while the wavefunctions describing them can be designed to carry orbital angular momentum. These wavefunctions are conveniently described in cylindrical polar coordinates that have a rotational axis of symmetry. However, physical systems can be described in many different coordinate systems, for example cylindrical parabolic or cylindrical elliptic coordinates. In these coordinates the angular momentum will manifest itself differently.

Electrons and photons can both be described as wave phenomena, due to the particle-wave duality principle in quantum mechanics. Further, the spin angular momentum of both can only take two distinct values. This allows for a similar description between the two particles. Differences arise because electrons and photons have different particle properties; photons are massless particles with spin 1 while electrons are massive particles with spin $\frac{1}{2}$. Manifestations of these differences can be studied by considering mechanical properties of the fields such as the probability, energy and momentum densities.

Angular momentum is a vector quantity, defined by both a magnitude and a direction. The direction of the spin angular momentum of the particle can be chosen relative to an external axis or its momentum. This distinction gives rise to states that differ in minute details. Further, the relative alignment of OAM and SAM can be chosen freely. They can be perpendicular or parallel to each other, enhancing or decreasing the total angular momentum. These different alignments have measurable effects on the mechanical properties.

It turns out that specific photon states, standing or travelling waves with linear polarization, are similar to the Majorana states of electrons. Majorana particles are a curious result of describing electrons by the Dirac formalism; they are their own antiparticle and described by a real wavefunction instead of a complex one. This is analogous to the distinction between travelling and standing waves. Although photons share the characteristic properties of Majorana particles naturally, these specific photon states obey extra conditions, similar to those that the Majorana states of electrons need to satisfy.

1.1 Outline of this thesis

This thesis will focus on the interaction between the orbital angular momentum (OAM) and spin angular momentum (SAM) of both electrons and photons. To study the effects of this interaction, a number of mechanical properties will be considered. The properties of the electron and photon fields will be compared to those of the scalar field (that has no SAM), to identify contributions from the spin and the spin-orbit coupling effects.

Only those properties that are conserved quantities under transformations respecting the symmetry of the system will be considered. The derivation of their expressions, using Noether's theorem, will be discussed in chapter 2. This chapter will also discuss some fundamental issues considering the Dirac equation and the Majorana particles, and examine the angular momenta of light.

An important degree of freedom of fields carrying SAM is its direction; the polarization. The direction can be defined by an external axis (spin) or by the momentum direction (helicity). In systems that comprise collections of plane waves, such as beams, the momentum of the individual plane waves is not necessarily aligned with the direction of propagation of the beam as a whole. This has as result that the spin states (a state with an overall polarization) and helicity states (a states that contains only plane waves with the same helicity) are different

from each other. These differences are discussed in chapter 3.

However, the spin can also be directed into a transverse direction, perpendicular to the propagation direction. This can be interpreted as a superposition of two spin states that are oppositely polarized in the longitudinal direction. Similarly, there exist superpositions of two states with opposite helicity. The differences between these two superpositions will be discussed in chapter 4.

Superimposing two states with opposite spin is closely related to the construction of standing waves. Moreover, the distinction between travelling and standing waves is analogous to the distinction between real and complex fields. The Dirac equation, describing complex electron states, also allows for real solutions. These are the Majorana states and closely related to linearly polarized electron beams. This raises the question what the optical analogues of Majorana states are, and what restrictions are imposed on the polarization of these optical fields. This will be addressed in chapter 5.

Systems with an axis-rotational symmetry are preferably described in the cylindrical polar system. Solutions of the wave equation in this coordinate system are OAM carrying Bessel beams. Angular momentum manifests itself differently in other cylindrical coordinate systems, such as the cylindrical parabolic coordinate system. This will be studied in chapter 6.

1.2 The cylindrical polar coordinate system

OAM is in classical mechanics described by the cross product of the position vector and the momentum:

$$\mathbf{L} = \mathbf{r} \times \mathbf{p}. \tag{1.1}$$

The dimensions of angular momentum are $(\text{kg m}^2\ \text{s}^{-1})$ in SI-units. Since OAM is a measure of the motion of the particle about an external point, it is extrinsic and depends on the choice of origin of the coordinate system. In cylindrical polar coordinates (r, ϕ, z), defined by

$$x = r\cos(\phi), \quad y = r\sin(\phi), \quad z = z, \tag{1.2}$$

the $\hat{\mathbf{z}}$-component of the OAM is given by a simple form in both classical and quantum mechanics:

$$L_{z,\text{classical}} = xp_y - yp_x = mr^2\partial_t\phi, \ \rightarrow \ L_{z,\text{quantum}} = -i\hbar\partial_\phi. \tag{1.3}$$

The components of the quantummechanical angular momentum operator satisfy the commutation relations $[L_i, L_i] = 0$ and $[L_i, L_j] = \epsilon_{ijk}L^k$, with ϵ_{ijk} the anti-symmetric Levi-Civita tensor. This definition of the OAM operator implies that the essential condition for having OAM is an azimuthal variation of the wavefunction. Solving the wave equation in cylindrical polar coordinates shows that this arises naturally in these coordinates.

1.2.1 Separability in cylindrical coordinates; Bessel beams

Wave phenomena in free space are described by the wave equation

$$\nabla^2\varphi(t,\mathbf{r}) - \frac{1}{v^2}\partial_t^2\varphi(t,\mathbf{r}) = 0, \tag{1.4}$$

where ∇^2 is the three-dimensional Laplacian and v is the wave velocity. Separation of $\varphi(t,\mathbf{r})$ into $A(p,q)Z(z)T(t)$ allows for separating out the dependence on time and the $\hat{\mathbf{z}}$-coordinate [1]:

$$\nabla^2 A(p,q)Z(z) = -k^2 A(p,q)Z(z) \begin{cases} \nabla_\perp^2 A(p,q) = -k_\perp^2 A(p,q), & \\ \partial_z^2 Z(z) = -k_z^2 Z(z), & \end{cases} \tag{1.5a}$$

$$\partial_t^2 T(t) = -v^2k^2T(t). \tag{1.5b}$$

The left-hand side of the equation for the spatial part (1.5a) is called the Helmholtz equation. This separation shows that the scalar field is correctly described by $A(p,q)e^{ik_z z}e^{-i\omega t}$, with $\omega = vk$ and the total wavenumber $k^2 = k_\perp^2 + k_z^2$. If the transverse wavenumber $k_\perp$ is constant, the wave will retain its shape upon propagation.

The Helmholtz equation is separable in different transverse-cylindrical coordinate systems (p,q,z) with the transverse coordinates defined in different ways, including Cartesian, cylindrical polar, cylindrical elliptic and cylindrical parabolic coordinates. The cylindrical parabolic coordinate system will be discussed in chapter 6. The rest of this thesis will focus on cylindrical polar coordinate systems. Separation of variables $\varphi(r,\phi,z) \mapsto R(r)\Phi(\phi)Z(z)$ transforms the Helmholtz equation (1.5a) into the following set of equations:

$$k_r^2r^2R'' + k_rrR' + k_r^2r^2R = \ell^2R, \tag{1.6a}$$

$$\Phi'' = -\ell^2\Phi, \tag{1.6b}$$

$$Z'' = -k_z^2Z. \tag{1.6c}$$

Here $k_\perp = k_r$ as the transverse momentum is pointing in the radial direction only. Solutions of the radial equation (1.6a) are Bessel functions $R(r) = J_\ell(k_r r)$, while solutions of the azimuthal equation (1.6b) are $\Phi(\phi) \sim e^{\pm i\ell\phi}$ and of the longitudinal equation (1.6c) are $Z(z) \sim e^{\pm ik_z z}$. As a result, the scalar field solution of the wave equation (1.4) in cylindrical polar coordinates is a scalar Bessel beam:

$$\varphi(t, \mathbf{r}) = J_\ell(k_r r) e^{i\ell\phi} e^{ik_z z} e^{-i\omega t}. \tag{1.7}$$

The intensity distribution of this field is given by $|\varphi(\mathbf{r}, t)|^2 = J_\ell^2(k_r r)$, which is a pattern of concentric rings. The azimuthal phase dependence is not directly observable. Since the phase winds around the $\hat{\mathbf{z}}$ axis, the field carries OAM in the $\hat{\mathbf{z}}$ direction of magnitude $\hbar\ell$ and it is said that the angular spectrum is given by $A(\phi) = e^{i\ell\phi}$. Continuity of the phase (modulo 2π) requires that this number ℓ is an integer, $\ell \in \mathbb{Z}$. Whether it is positive or negative depends on the direction of the increase in phase with ϕ [2]. The value is not restricted, which means that fields can carry any amount of OAM.

From (1.7) it can be concluded that a scalar Bessel beam is invariant under translations in the ϕ- and $\hat{\mathbf{z}}$-directions and in time; it carries OAM, is *propagation invariant* and a stationary solution. These scalar Bessel beams, sometimes called cylindrical harmonics, are basis states for any field that is described in cylindrical coordinates, similar to plane waves in Cartesian coordinates.

Plane waves, described by cosines and sines, are the natural choice for basis functions in these coordinates as they are orthogonal to each other and invariant under translations, respecting the translational symmetries of the coordinate system. This is exploited by the Fourier transform, decomposing any function described in Cartesian coordinates in cosines and sines, or complex exponentials. Transforming the Fourier transform to cylindrical polar coordinates gives the zeroth order Hankel transform [3]:

$$F_0(k) = \int_0^\infty r f(r) J_0(kr) dr.$$

In general, any function of the radial coordinate $f(r)$ can be expressed in Bessel functions by the Hankel transform of arbitrary order n, as Bessel functions form an orthogonal basis of functions in cylindrical polar coordinates [1]:

$$\int_0^\infty r J_n(k_r r) J_n(k_r' r)\, dr = \frac{1}{k_r}\delta(k_r - k_r').$$

Hence the scalar Bessel beams (1.7) of arbitrary order ℓ define a set of basis states of functions in cylindrical polar coordinates.

However, the intensity pattern of a Bessel beam arises as the interference pattern of a collection of plane waves. Since the longitudinal and transverse wavenumbers are related to each other by $k_r^2 = k^2 - k_z^2$, the momentum vectors of the plane waves lie on a cone making an angle θ with the propagation axis such that $k_z = k\cos(\theta)$ and $k_r = k\sin(\theta)$. A field can only be propagation invariant if, when propagating over a distance Δz, all waves obtain the same phase shift $k_z \Delta z$ [4]. This can only be realized if all the plane waves have the same longitudinal wavevector, i.e. the field is monochromatic. Further, to form a Bessel beam the waves need to be evenly distributed over the azimuthal angle ϕ, as the intensity only varies with the radial distance. These conditions give rise to an important property of Bessel beams: they are *self-healing* [5]. When part of the beam is obstructed, the rest of the beam can pass, ultimately reforming to the initial beam profile. The spectrum of a Bessel beam of order ℓ is thus described by:

$$\tilde{\varphi}(\mathbf{k}) = \frac{1}{2\pi i^\ell k_{r,0}} A(\phi_k)\delta(k_r - k_{r,0}) = \frac{1}{2\pi i^\ell k_{r,0}} e^{i\ell\phi_k}\delta(k_r - k_{r,0}). \tag{1.8}$$

This spectrum is shown in figure 1.1.

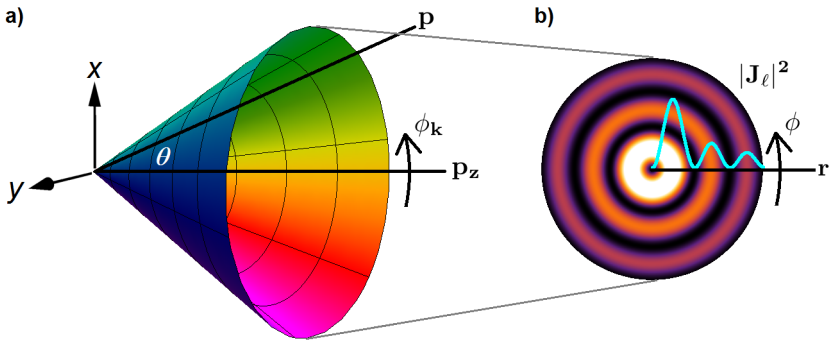

Figure 1.1: The spectrum of a Bessel beam. a): The plane waves forming a Bessel beam lie on a cone making an opening angle θ with the $\hat{\mathbf{z}}$-axis, distributed over the azimuthal angle ϕ_k in Fourier space. b): Intensity distribution of the first order Bessel function $J_1(k_r r)$ in real space, in the range $|k_r r| \leq 10$.

The spatial dependence of a propagation-invariant field can be found by solving the Whittaker integral in the transverse plane [6]:

$$\varphi(\mathbf{r}) = e^{ik_z z} \int d^2\mathbf{k}\, e^{i\mathbf{k}_\perp \cdot \mathbf{r}_\perp} \widetilde{\varphi}(\mathbf{k}) \tag{1.9a}$$

$$= e^{ik_z z} \int_0^{2\pi} \int_0^{\infty} k_r A(\phi_k) \exp\left[ik_r(x\cos(\phi_k) + y\sin(\phi_k)\right] dk_r d\phi_k. \tag{1.9b}$$

Here $\widetilde{\varphi}(\mathbf{k})$ is the spectrum of the field, with $A(\phi_k)$ the angular spectrum. The transverse coordinates $x(p,q)$ and $y(p,q)$ can be expressed in the transverse coordinates (p,q) of the preferred transverse cylindrical coordinate system. Solutions in elliptical coordinates are called Mathieu functions and in parabolic coordinates Weber functions. These will be discussed further in chapter 6.

For a Bessel beam with the spectrum given by (1.8) the integral over k_r in (1.9b) is trivial. Combining this with the transformations $x = r\cos(\phi_r)$ and $y = r\sin(\phi_r)$, and using an integral identity[1] gives the following Fourier transform:

$$\varphi(r,\phi,z) = e^{ik_z z}\frac{e^{i\ell\phi_r}}{2\pi i^\ell}\int_0^{2\pi} d\phi_k\; e^{i\ell(\phi_k-\phi_r)}e^{ik_r r\cos(\phi_k-\phi_r)} = J_\ell(k_r r)e^{i\ell\phi_r}e^{ik_z z}.$$

This method can be used to find the spatial dependence of a field when only the angular spectrum $A(\phi)$ is known, for example in creating optical beams with a desired intensity pattern.

1.2.2 Scalar optical beams carrying OAM

From the Bessel beam expression (1.7) it can be concluded that to create a propagation invariant field that carries OAM it is necessary to have a phase winding around the propagation axis; all phases occur along a path that is traced around this direction. Shrinking the path implies that there must be a point inside the loop where the full 2π range of phases coincides; a phase singularity where the phase is undefined. This change in phase generates a current, (see equation (2.19)) and hence (optical) fields where these phase singularities occur are also called (optical) vortices. An ambiguity in phase is physically not allowed, hence the amplitude of the field drops to zero [2]. Singularities in light fields can hence be detected as points of darkness, that form lines of darkness as the light propagates.

These lines were described by Dirac in general three-dimensional wavefunctions as early as 1931 [7], with the first study of these lines in electromagnetic fields by Nye and Berry in 1974 [8]. However, the first observation of vortices in optical fields was in 1950 by Wolter [9], who found a vortex in the interference of incident, reflected and refracted waves near a glass-air transition.

[1] Bessel functions can be represented by the integral

$$\oint d\tau\; e^{in\tau}e^{ix\cos(\tau)} = 2\pi i^n J_n(x). \tag{1.10}$$

In the same paper [8], Nye and Berry considered optical vortices as dislocations in the phase of the optical field, similar to dislocations as seen in crystals. This inspired the authors of [10] to study the use of diffractive elements with a dislocation to create an optical vortex in 1990. A collection of diffracted beams that were spatially separated was created, with the different orders of diffraction corresponding to different values of OAM. This made it possible to block out unwanted orders of diffraction.

However, it took until 1992 when Allen at al. [11] realized that this OAM could be manipulated, and all beams with helical phase fronts carry OAM in units of $\hbar$. The same group also introduced another method to create optical vortex beams in 1994 [12]; a spiral phase plate with varying thickness can be placed in a laser beam to introduce the azimuthal phase winding.

These works started a whole new area of research into light beams carrying OAM, created by holograms [13], using laser cavities [14] or by three-wave interference [15], inspired by the work performed in 1951 [16]. This demostrated that vortices can be created by the superposition of three or more plane waves. In 1996 an experimental group [17] started to use light of frequencies $\sim 10^{11}$ Hz (instead of visible light of frequency $\sim 10^{15}$ Hz). The increased wavelength simplified the production of a suitable phase plate, that was now of the order of 10 mm instead of 10^{-6} m. More unconventional methods to create a vortex beam have also been studied, such as the generation of optical fields with vortices by using a molecular array of specific geometry [18]. These molecules can absorb or emit light at a specific frequency, creating an excited state with a desired symmetry.

The OAM state of the light can be measured by detecting interference patterns with plane waves, or by shining the light on an annular grating [19]; the diffraction pattern that appears shows a number of dark fringes corresponding to the OAM value. Another method is based on compressing the OAM mode in one transverse direction, creating linearly-shaped light [20]. The interference patterns show a number of fringes that is related to the amount of OAM the beam carries.

The darkness in the center of OAM carrying beams makes them very suitable for applications such as trapping, guiding and transferring OAM to dielectric particles. A review of applications is given in the paper [21].

Any physically realizable field, for example a laser beam, needs to be square-integrable. This means that the integral of the field squared over all space is finite, as this is proportional to the total energy stored in the field [22]. The indefinite integral of a function is finite if the function decreases faster than $1/x$; $f(x) \sim x^{-\alpha}$

with $\alpha > 1$. In cylindrical coordinates, since the Jacobian gives a factor of r, this leads to the condition that $f(r) \sim r^{-\beta}$ with $\beta > 2$. Since the *square* of the field needs to be integrable the field should decrease faster than $1/r$ in the radial direction.

However, Bessel functions approximate to $1/\sqrt{r}$ for large r and are thus not square integrable. Thus any scalar field that is described by (1.7) needs to be regularized. This can be done with a Gaussian envelope $\sim e^{-r^2/w_0^2}$ in the transverse plane. The parameter w_0 is the minimum waist of the beam. At the focus plane $z = 0$, the Bessel-Gauss beam is given by [23]

$$\varphi_\ell^{BG}(t, r, \phi, z = 0) \propto J_\ell(k_r r) e^{-r^2/w_0^2} e^{i\ell\phi} e^{-i\omega t}. \tag{1.11}$$

This creates a physical beam; the field is localized around the $\hat{\mathbf{z}}$-axis and decreases in size further away from the axis. However, this modification has as consequence that the Bessel-Gauss beam will spread (diffract) upon propagation. The full expression for Bessel-Gauss beams, dependent on the longitudinal coordinate z, is given in Appendix A.

If the longitudinal wavenumber is much greater than the transverse wavenumber, $k_z \gg k_\perp$, this defocussing is a slow process over long distances and the beam is said to propagate paraxially [24]. From the Bessel beam spectrum as shown in figure 1.1 it can be concluded that the paraxial regime, $k_z \gg k_r$ corresponds to a value $\theta \simeq 0$.

In the paraxial approximation, the longitudinal wave number can be expressed in terms of the total and transverse wave numbers:

$$k_z = \sqrt{k^2 - k_\perp^2} \approx k - \frac{k_\perp^2}{2k}.$$

Since in this regime the inequality, $|\partial_z^2 Z(z)| \ll |k\partial_z Z(z)|$ holds, the Helmholtz equation (1.5a) gets modified to the paraxial Helmholtz equation[2]:

$$\nabla_\perp^2 A(p, q) Z(z) + 2ik\partial_z A(p, q) Z(z) = 0, \tag{1.12}$$

where the Laplacian is only taken in the transverse plane. This equation resembles the time dependent Schrödinger equation from quantum mechanics, with the

[2]This equation can be derived from the Helmholtz equation, assuming that the field is described by $\varphi(\mathbf{r}) = u(\mathbf{r})e^{ikz}$. The Helmholtz equation for this field then transforms to

$$e^{ikz}\left(\nabla_\perp^2 + \partial_z^2 + 2ik\partial_z\right) u(\mathbf{r}),$$

which reduces to the paraxial Helmholtz equation using the aforementioned inequality.

time derivative replaced by the derivative with respect to z. This shows that for a paraxial wave propagation in z is comparable to propagation in time.

The fact that Bessel beams are not square-integrable makes them impossible to generate in an experiment. The beams that are created will always be an approximation to the ideal theoretical beam, as described first by Durnin in 1987 [5]. The first experimental generation of a zeroth order Bessel beam, based on creating a beam with the desired angular spectrum by shining a laser beam on an annular slit, followed in the same year [25]. Proceeding from this experiment were others, using holographic techniques [26], and conical or aberrating spherical lenses [27] to create zeroth order Bessel beams. In 2001 a finite approximation of a Bessel beam was realised [28] by using an axicon, a conical glass element. This creates a phase difference between the plane waves as the length of the path travelled is changed. The incident Gaussian beam was refracted, creating the wave spectrum of a zeroth order Bessel beam.

Higher order Bessel beams were realized by different experimental groups between 1989 and 2000, such as [29, 30] that used computer generated holograms to convert Gaussian modes into Bessel-like beams. Bessel beams can also be created from Laguerre-Gaussian modes [28], with differences between these beams and ideal Bessel beams increasing with the order of the Bessel beam [31].

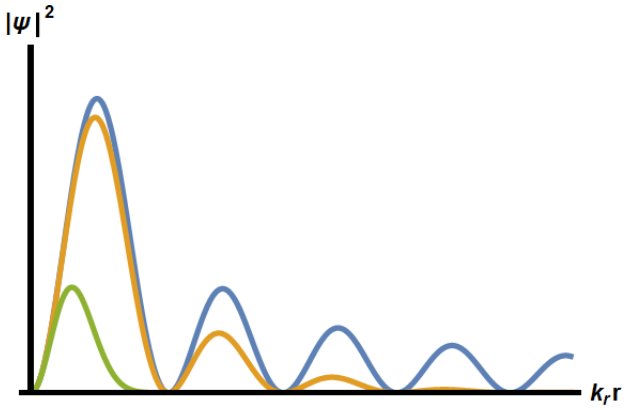

Figure 1.2: Comparison between Bessel and Bessel Gauss profiles. All Bessel functions are of order $\ell = 1$, with $w_0 = \{0, 0.1,\ 0.5\}$ for the blue, yellow and green graphs respectively, see (1.11).

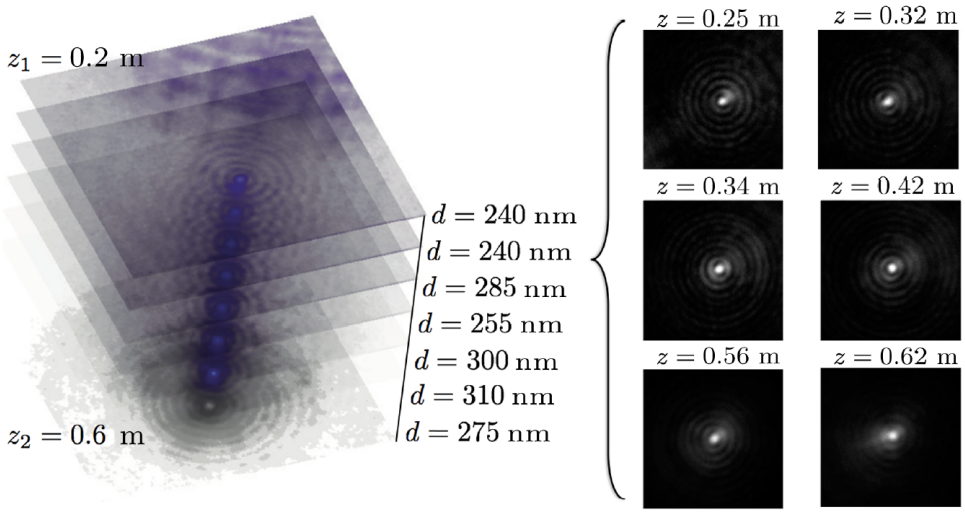

Figure 1.3: The non-diffractive nature of an electron Bessel beam. Observation of the probability density of a zeroth order electron Bessel beam as a function of propagation distance. The beam holds its shape very well between 0.2 and 0.6m, while a theoretical prediction of the non-diffractive distance is 0.75m [35].

In contrast to Bessel beams, Bessel-Gauss beams are physically realizable solutions, first described by Gori [22] with non-paraxial corrections of BG beams discussed by [23, 32]. Other beams that carry OAM, such as the Laguerre-Gauss beams, are similar to Bessel-Gauss beams [23, 33] under specific conditions[3].

1.2.3 Scalar electron beams carrying OAM

There are many examples of electron states that carry OAM, for example when bound to atoms, in quantum Hall states, ferromagnets and Bose-Einstein condensates. However, vortex electron states in free space had not been studied until in 2007 wave packet solutions of the Schrödinger equation with phase vortices were discussed [34]. This proposal was based on the particle-wave duality in quantum mechanics; since any particle can be described by waves, free electron vortex states could also exist, similar to optical vortex beams.

This paper was followed by theoretical work [36] and the first experimental generations of electron vortex beams (EVBs) in 2010, using a holographic construction technique [37], or a spiral phase plate [38], similar to the creation of optical vortex beams. Both experiments created beams with one quantum $\hbar$ of OAM. EVBs with an OAM of up to $100\hbar$ were generated in 2011 [39]. These

[3]This is discussed further in Appendix A

electron vortex beams were all created with electrons that were accelerated in an electron microscope.

These electrons have a typical kinetic energy of 200 keV, which is a non-relativistic energy since the rest mass of an electron is about 500 keV. At these energies a spiral phase plate needs to have a step height of 42 nm [40], complicating the fabrication of a plate that has a continually varying thickness. A spiral-like phase plate can be used instead, for example from layers of graphite, that changes its height in steps. These initiating papers were followed in later years by more advanced techniques such as a mode converter to create HG beams [41] or exploiting lens aberrations to create Bessel-like beams [42], with about 65% of the electron density in the mode with one quantum of OAM. The first electron Bessel beam was generated in 2014 by Grillo et al. [35] by using a non-absorbing kinoform, followed by [43] using an annular slit to generate the Bessel beam spectrum. A completely different method that can be used to create an electron vortex beam is based on the interaction of an electron beam with an (approximate) magnetic monopole, simulated by a thin magnetic needle with a width of 200 nm [44].

Mechanical properties of the EVBs have been studied in the non-relativistic paraxial regime [45]. EVBs carry only longitudinal and azimuthal momentum, of which the latter disappears when integrating over all space. The induced electromagnetic fields are a radial electric field and azimuthal and longitudinal magnetic fields [46]. These fields can be used to measure the OAM of the beam non-destructively [47]. Another method to measure the OAM is by measuring the transition radiation of an electron, associated with its magnetic moment, when it is passing from one medium to another [48]. Possible applications for electron vortex beams include the creation of electronic tweezers or a new type of electron energy loss spectroscopy [38], using the OAM instead of the SAM of the electrons. These Bessel beams, similar to optical Bessel beams, are not ideal beams and spread a little upon propagation.

1.3 A Lorentz covariant description of spinor and vector fields

All theoretical and experimental work mentioned up to now considered the optical fields and electron fields as scalar fields. The intensity (or probability density of the field) showed the vortex signature of a phase singularity in the centre of

the beam. The fact that both electrons and photons have spin and can hence be polarized differently, or that this SAM could interact with the OAM, was not considered. Describing these fields, while taking their spin into account in a Lorentz covariant manner, requires (classical) field theory. The basic aspects of this theory will be discussed in this section[4].

1.3.1 4-vectors and spacetime

Throughout this thesis, a relativistically covariant notation will be adopted. Space and time coordinates are combined in one vector $x^\mu = (t, \mathbf{r})$, with the derivative $\partial^\mu = (\partial_t, -\nabla)$. Greek indices take values including 0; $\mu = 0, 1, 2, 3$, where 0 is the temporal coordinate, while Roman indices only take non-zero values $j = 1, 2, 3$. The Minkowski metric is expressed by $\eta^{\mu\nu} = \text{diag}(1, -1, -1, -1)$ and can be used to raise or lower the index of 4-vectors; $x_\mu = \eta_{\mu\nu} x^\nu = (t, -\mathbf{r})$. When indices are repeated, summation is implicit; $dx^\mu dx_\mu = dt^2 - d\mathbf{r}^2$.

The metric $\eta^{\mu\nu}$ contains factors of r in cylindrical polar coordinates. To avoid problems in calculations that involve 4-vector manipulation, all calculations will be performed in Cartesian coordinates. The results can then be transformed to their cylindrical polar equivalents by the usual relationships (1.2). One exception is the calculation of the energy-momentum tensor components, these were performed in both Cartesian coordinates and cylindrical polar coordinates as an extra confirmation that the right quantities were found.

1.3.2 Fields with spin angular momentum

The two types of angular momentum, spin and orbital, have the same origin in classical mechanics; a rotation about either an external or internal axis. However, SAM is not associated with a spinning motion in quantum mechanics, in spite of having the same dimensions as orbital angular momentum and the total angular momentum being the vector sum of the spin and orbital angular momentum.

Rather, the SAM determines how a particle couples to a magnetic field [52], and the existence of SAM can be deduced by experiments such as the Stern-Gerlach experiment [53]. Here particles, that can be either electrons or atoms, are being led through an inhomogeneous magnetic field. It is found that they are deflected into distinct spots. Treating the particles as spinning magnetic dipoles, they will precess in an external magnetic field and get deflected if this field is

[4]Textbooks used include [49, 50, 51].

inhomogeneous. However, if the particles were "spinning" in random ways, the beam would spread out in every direction equally. The detection of distinct spots signifies that the particle can only "spin" in specific ways.

It turns out that if a particle has spin s, there are $2s+1$ different substates. These are labelled by the magnetic spin quantum number m_s, which can take values $\{-s, -s+1, \ldots, +s-1, +s\}$. The different spin states are degenerate in the absence of a magnetic field. If there is a magnetic field, the spin couples to it and causes the energy to shift by the Zeeman effect[5]. If $m_s = s$ the spin is completely aligned with the magnetic field, and anti-aligned if $m_s = -s$. The states in between are partially aligned.

A field with spin 0 is called a scalar field, as its wavefunction has a single component only. Higher spin fields, for example photons, have spin 1 and are described by a vector field with 3 components. Electrons have spin $\frac{1}{2}$ and are described by a spinor field with 2 components. Depending on whether the spin of a particle is integer or half-integer they behave very differently. Particles with spin $\frac{1}{2}, \frac{3}{2}, \ldots$ are fermions, which obey the Pauli exclusion principle, while particles with integer spins are bosons.

Throughout this thesis field theory will be used, describing OAM and SAM in terms of fields rather than single particles. However, these fields will not be quantized at a single-particle level but rather considered as a continuous entity. This is to avoid complicated problems such as the mutual interaction between electrons in a collective system. As a result, all field quantities discussed are *densities* instead of single-particle properties. An important difference between the OAM and SAM is that the OAM can take any integer value, while the SAM is restricted by the particle properties.

1.3.3 Polarization coordinates

When describing fields with SAM it is convenient to use the circular polarization basis $(\hat{\mathbf{e}}_+, \hat{\mathbf{e}}_-, \hat{\mathbf{e}}_z)$ with

$$\hat{\mathbf{e}}_\pm = \frac{1}{\sqrt{2}}(\hat{\mathbf{p}} \pm i\hat{\mathbf{q}}). \tag{1.14}$$

[5]The Zeeman effect raises or lowers the energy of the particle, depending on the alignment of the spin relative to the magnetic field. For electrons this is:

$$H_Z = -\boldsymbol{\mu} \cdot \mathbf{B} = -\frac{g_s \mu_B}{\hbar} \mathbf{S} \cdot \mathbf{B}, \tag{1.13}$$

where $\boldsymbol{\mu}$ is the magnetic moment, g_s the g-factor of the electron, approximately 2 [54], and μ_B the Bohr magneton.

In these coordinates, the transverse derivatives and field components are transformed to

$$\partial_\pm = \frac{1}{\sqrt{2}}(\partial_p \pm i\partial_q) = U^\pm, \qquad F_\pm = \frac{1}{\sqrt{2}}(F_p \mp iF_q),$$

and the identity of the divergence is transformed to

$$\nabla \cdot \mathbf{F} = U^+F_+ + U^-F_- + \partial_z F_z. \tag{1.15}$$

A consequence of using (1.14) is that the transverse derivatives $U^\pm$ in cylindrical coordinates are given by

$$U^\pm = \frac{e^{\pm i\phi}}{\sqrt{2}}(\partial_r \pm \frac{i}{r}\partial_\phi) \tag{1.16}$$

and these operators have the special property that they act on a scalar Bessel beam as ladder operators, raising or lowering the OAM value [55][6]

$$U^\pm J_\ell(k_r r)e^{i\ell\phi}e^{ik_z z} = \mp\frac{k_r}{\sqrt{2}}J_{\ell\pm1}(k_r r)e^{i(\ell\pm1)\phi}e^{ik_z z}. \tag{1.17}$$

This can also be deduced from the commutator of L_z and $U^\pm$ in cylindrical polar coordinates:

$$[U^\pm, L_z] = -\frac{i}{\sqrt{2}}\left\{e^{\pm i\phi}\left[\partial_r \pm \frac{i}{r}\partial_\phi\right]\partial_\phi - \partial_\phi e^{\pm i\phi}\left[\partial_r \pm \frac{i}{r}\partial_\phi\right]\right\} = \mp U^\pm.$$

Thus, if φ is an eigenstate of L_z with eigenvalue ℓ, the state $U^\pm\varphi$ will have eigenvalue $\ell \pm 1$. Using these derivatives, the Laplacian takes on the form $\nabla^2 = 2U^\pm U^\mp + \partial_z^2$, which shows that subsequent acting with a raising and lowering operator on a Bessel function gives

$$U^\pm U^\mp J_\ell(k_r r) = -\frac{k_r^2}{2}J_\ell(k_r r). \tag{1.18}$$

1.3.4 Rotation matrices

A vector quantity such as SAM can be rotated from one spatial direction to another. These rotations are described by matrices that form the group $SO(3)$ for three-component vectors. Take for example the rotation about the $\hat{\mathbf{z}}$-axis, given by the matrix $\widetilde{R}_z(\theta)$:

$$\widetilde{R}_z(\theta) = \begin{pmatrix} \cos(\theta) & \sin(\theta) & 0 \\ -\sin(\theta) & \cos(\theta) & 0 \\ 0 & 0 & 1 \end{pmatrix}.$$

[6] Applying the quantummechanical operator formalism is a very powerful analytical method in many areas of physics, especially optics [56].

This matrix can also be expressed as the exponential[7] of another matrix, called the *generator* S_z; $\widetilde{R}_z = \exp(-\theta S_z)$. The matrices S_j for rotations about all three spatial directions are the spin-1 matrices:

$$S_x = \begin{pmatrix} 0 & 0 & 0 \\ 0 & 0 & -1 \\ 0 & 1 & 0 \end{pmatrix}, \quad S_y = \begin{pmatrix} 0 & 0 & 1 \\ 0 & 0 & 0 \\ -1 & 0 & 0 \end{pmatrix}, \quad S_z = \begin{pmatrix} 0 & -1 & 0 \\ 1 & 0 & 0 \\ 0 & 0 & 0 \end{pmatrix}. \tag{1.19}$$

These matrices obey the commutation relations for angular momentum operators; $[S_i, S_j] = \epsilon_{ijk} S^k$ and $[S_i, S_i] = 0$. However, it is commonly used to express these spin matrices in the polarization basis (1.14), $\hat{\mathbf{e}}_\pm = \frac{1}{\sqrt{2}}(\hat{\mathbf{x}} \pm i\hat{\mathbf{y}})$, such that the S_z matrix is diagonal, with its expectation values the values of the SAM of the vector components. These matrices are related to (1.19) by a unitary matrix transformation that transforms the vector components from Cartesian to polarization coordinates:

$$S_j^* = V^\dagger S_j V\,; \qquad V = \frac{1}{\sqrt{2}} \begin{pmatrix} 1 & 1 & 0 \\ i & -i & 0 \\ 0 & 0 & \sqrt{2} \end{pmatrix}, \qquad S_z^* = \begin{pmatrix} 1 & 0 & 0 \\ 0 & -1 & 0 \\ 0 & 0 & 0 \end{pmatrix}.$$

As a result, the vector components described in this basis are distinguished from each other by the SAM they carry; the top component has $s = +1$, while the middle component has $s = -1$ and the bottom component $s = 0$.

Different from vectors, the rotation of spinors is described by the group $SU(2)$, which is homomorphic with the group $SO(3)$. Elements of this group are the 2×2 Pauli spin matrices:

$$\sigma_x = \begin{pmatrix} 0 & 1 \\ 1 & 0 \end{pmatrix}, \; \sigma_y = \begin{pmatrix} 0 & -i \\ i & 0 \end{pmatrix}, \; \sigma_z = \begin{pmatrix} 1 & 0 \\ 0 & -1 \end{pmatrix}. \tag{1.20}$$

The spin is conventionally chosen to be pointing in the $\pm\hat{\mathbf{z}}$ direction, being described by the spinor w_s that is an eigenstate of σ_z:

$$w_{s=+\frac{1}{2}} = \begin{pmatrix} 1 \\ 0 \end{pmatrix} \quad \text{spin “up”}, \qquad w_{s=-\frac{1}{2}} = \begin{pmatrix} 0 \\ 1 \end{pmatrix} \quad \text{spin “down”}. \tag{1.21}$$

Hence the top component of a general 2-spinor has spin $s = +\frac{1}{2}$ and the bottom component has $s = -\frac{1}{2}$.

[7] The exponential of a matrix A can be found in a similar way as the exponential of a scalar, using the Taylor expansion: $e^A = \mathbb{1} + A + \frac{1}{2}A^2 + \frac{1}{6}A^3 + \ldots$.

1.3.5 Transformations of the Lorentz group and their generators

Describing fields Lorentz covariantly means that they transform correctly under all transformations in the Lorentz group. This group contains all rotations and boosts of 4-dimensional Minkowski spacetime that preserve the spacetime interval $ds^2 = dt^2 - dx^2 - dy^2 - dz^2$. It is denoted by $O(1,3)$, of which only a subgroup of transformations will be considered in this thesis, $SO^+(1,3)$. This group consists of 3 rotations and 3 boosts.

There are also two discrete spacetime transformations that preserve ds^2; parity and time reversal. These change the sign of the spatial and time coordinates respectively. These transformations are discussed in chapter 2 and will become important in chapter 5.

The Lorentz group is usually described in terms of its generators. Similar to the vector rotations, the 4-vector transformations can each be expressed as the exponential of a generator. For example the 4-vector rotation about $\hat{\mathbf{z}}$ over θ:

$$R_z(\theta) = \begin{pmatrix} 1 & 0 & 0 & 0 \\ 0 & \cos(\theta) & \sin(\theta) & 0 \\ 0 & -\sin(\theta) & \cos(\theta) & 0 \\ 0 & 0 & 0 & 1 \end{pmatrix} = \exp(-\theta J_z);\ J_z = \begin{pmatrix} 0 & 0 & 0 & 0 \\ 0 & 0 & -1 & 0 \\ 0 & 1 & 0 & 0 \\ 0 & 0 & 0 & 0 \end{pmatrix}. \quad (1.22)$$

Similarly, boosts are represented by the matrices $B_j(\zeta)$ where ζ is the rapidity; $v = \tanh(\zeta)$ and $\beta = v/c = \cosh(\zeta)$. All 6 generators are given by:

$$J_x = \begin{pmatrix} 0 & 0 & 0 & 0 \\ 0 & 0 & 0 & 0 \\ 0 & 0 & 0 & -1 \\ 0 & 0 & 1 & 0 \end{pmatrix}, \quad K_x = \begin{pmatrix} 0 & -1 & 0 & 0 \\ -1 & 0 & 0 & 0 \\ 0 & 0 & 0 & 0 \\ 0 & 0 & 0 & 0 \end{pmatrix},$$

$$J_y = \begin{pmatrix} 0 & 0 & 0 & 0 \\ 0 & 0 & 0 & 1 \\ 0 & 0 & 0 & 0 \\ 0 & -1 & 0 & 0 \end{pmatrix}, \quad K_y = \begin{pmatrix} 0 & 0 & -1 & 0 \\ 0 & 0 & 0 & 0 \\ -1 & 0 & 0 & 0 \\ 0 & 0 & 0 & 0 \end{pmatrix}, \quad (1.23)$$

$$J_z = \begin{pmatrix} 0 & 0 & 0 & 0 \\ 0 & 0 & -1 & 0 \\ 0 & 1 & 0 & 0 \\ 0 & 0 & 0 & 0 \end{pmatrix}, \quad K_z = \begin{pmatrix} 0 & 0 & 0 & -1 \\ 0 & 0 & 0 & 0 \\ 0 & 0 & 0 & 0 \\ -1 & 0 & 0 & 0 \end{pmatrix}.$$

Comparing these with (1.19) shows that the spin-1 matrices are the spatial, 3×3 dimensional versions of the J_i.

The generators (1.23) can be expressed in one basis of antisymmetric matrices $\mathcal{M}^{\rho\sigma}$, with $J_i = \epsilon_{ijk}M^{jk}$ and $K_i = M_{0i}$. These obey the *Lorentz algebra* [57]:

$$[\mathcal{M}^{\rho\sigma}, \mathcal{M}^{\mu\nu}] = \eta^{\sigma\mu}\mathcal{M}^{\rho\nu} - \eta^{\rho\mu}\mathcal{M}^{\sigma\nu} + \eta^{\rho\nu}\mathcal{M}^{\sigma\mu} - \eta^{\sigma\nu}\mathcal{M}^{\rho\mu}. \tag{1.24}$$

This algebra plays an important role in the relativistic spinor description of electrons.

1.3.6 The Dirac equation

The fundamental equation of quantum mechanics is the Schrödinger equation, describing the time dependence of the wavefunction:

$$i\partial_t\psi(t,\mathbf{r}) = \hat{H}\psi(t,\mathbf{r}) = \left(-\frac{\hbar^2}{2m}\nabla^2 + V(\mathbf{r})\right)\psi(t,\mathbf{r}).$$

This is a scalar equation and applicable in the non-relativistic regime, as the Hamiltonian $\hat{H}$ is the energy operator given by the classical relationship of the sum of kinetic and potential energy. If the wave function is an energy eigenstate, $\hat{H}\psi(t,\mathbf{r}) = \mathcal{E}\psi(t,\mathbf{r})$, the time dependence is given by $e^{-i\mathcal{E}t}$.

However, electrons have spin. If the spin states of the electron need to be taken into account, for example when describing a particle in an electromagnetic field, the Pauli equation[8] needs to be used. Similarly for particles with relativistic energies, the Klein-Gordon equation[9] is required, as this considers the relativistic energy-momentum relationship $\mathcal{E}^2 = |\mathbf{p}|^2 + m^2$.

To describe the OAM and SAM of electrons in a relativistically covariant way, both these aspects need to be taken into account. They are combined in the Dirac equation, given by [58, 59]:

$$(i\gamma^\mu\partial_\mu - m)\psi = 0. \tag{1.27}$$

[8]The Pauli equation describes the coupling of the electron spin with the electromagnetic field, given in terms of the vector potential $\mathbf{A}$ and scalar potential V by

$$\left[\frac{1}{2m}\left(\boldsymbol{\sigma}\cdot(\mathbf{p} - q\mathbf{A})\right)^2 + qV\right]\psi = i\hbar\partial_t\psi. \tag{1.25}$$

[9]The Klein-Gordon equation is given by

$$(\partial_t^2 - \nabla^2 - m^2)\psi(t,\mathbf{r}) = 0. \tag{1.26}$$

The γ^μ are 4×4 matrices that are related to the generators of Lorentz transformations for spin$-\frac{1}{2}$ particles. Consequently the Dirac equation, and its related quantities, are Lorentz covariant[10]. The γ-matrices can be expressed in terms of the Pauli spin matrices (1.20) by

$$\gamma^0 = \begin{pmatrix} \mathbb{1} & 0 \\ 0 & -\mathbb{1} \end{pmatrix} \quad , \quad \boldsymbol{\gamma} = \begin{pmatrix} 0 & \boldsymbol{\sigma} \\ -\boldsymbol{\sigma} & 0 \end{pmatrix}. \tag{1.29}$$

Another commonly used notation of the γ-matrices is $\boldsymbol{\alpha} = \gamma^0\boldsymbol{\gamma}$ and $\beta = \gamma^0$. The definitions (1.29) make up the standard (Dirac) representation. There are many choices (representations) for the γ-matrices possible, but these are all physically equivalent. The only condition is that they need to satisfy the *Clifford algebra* [58]:

$$\{\gamma^\mu, \gamma^\nu\} = 2\eta^{\mu\nu}\mathbb{1}_4. \tag{1.30}$$

These matrices define a 4-dimensional representation $\Sigma^{\mu\nu}$ of the Lorentz algebra that satisfy the commutation relations (1.24):

$$\Sigma^{\mu\nu} = \frac{i}{4}[\gamma^\mu, \gamma^\nu]. \tag{1.31}$$

The transformations generated by $\Sigma^{\mu\nu}$ act on the Dirac spinor field ψ^μ, similarly to how the matrices generated by (1.23) acts on a 4-vector. The generators of spinor and vector fields cannot be the same, as vector fields describe bosons and spinor fields describe fermions that obey the Pauli exclusion principle; the total wavefunction is antisymmetric with respect to the exchange of two identical particles[11].

A consequence of this 4×4 description is that electrons are not described by a 2-component spinor but by a bi-spinor with 4 components. Hence all operators need to be 4-dimensional, for example the spin operator:

$$\mathbf{S} = \frac{1}{2}\text{diag}(\boldsymbol{\sigma}, \boldsymbol{\sigma}). \tag{1.32}$$

[10]Multiplying the Dirac equation by $(-i\gamma^\mu\partial_\mu - m)$ from the left shows that every component of ψ should satisfy the Klein-Gordon equation;

$$(-i\gamma^\mu\partial_\mu - m)(i\gamma^\nu\partial_\nu - m)\psi = (\gamma^\mu\partial_\mu\gamma^\nu\partial_\nu + m^2)\psi = (\partial^\nu\partial_\nu + m^2)\psi = 0. \tag{1.28}$$

Here the anticommutation relations of γ-matrices (1.30) were used.

[11]This can be observed from studying the rotations over 2π. The rotation generated by $\mathcal{M}^{12}$ simplifies to $+\mathbb{1}_4$, while the rotation generated by Σ^{12} reduces to $-\mathbb{1}_4$[60]. Thus spinors do not return to themselves under a rotation over 2π, but gain a minus sign.

Finding solutions of the Dirac equation starts with writing the equation (1.27) in a 2×2 matrix form, using the standard representation (1.29):

$$\begin{pmatrix} i\partial_t - m & i\nabla \cdot \boldsymbol{\sigma} \\ -i\nabla \cdot \boldsymbol{\sigma} & -i\partial_t - m \end{pmatrix} \psi(t, \mathbf{r}) = 0,$$

where the bi-spinor can be written as two spinors $\psi = (\psi_A, \psi_B)^T$. The components of ψ_A correspond to particles with positive energy, and ψ_B to particles with negative energy. However, a moving particle is in general described by a spinor with four non-zero components, for which the total plane wave solution then becomes [61]

$$\psi_1(t, \mathbf{r}) = \frac{e^{-i(\mathcal{E}t - \mathbf{p}\cdot\mathbf{r})}}{\sqrt{2\mathcal{E}(\mathcal{E}+m)}} \begin{pmatrix} (\mathcal{E}+m)w \\ (\mathbf{p}\cdot\boldsymbol{\sigma})w \end{pmatrix}, \quad \psi_2(t, \mathbf{r}) = \frac{e^{+i(\mathcal{E}t - \mathbf{p}\cdot\mathbf{r})}}{\sqrt{2\mathcal{E}(\mathcal{E}+m)}} \begin{pmatrix} (\mathbf{p}\cdot\boldsymbol{\sigma})w \\ (\mathcal{E}+m)w \end{pmatrix}. \tag{1.33}$$

The solutions are normalized as $\psi^\dagger\psi = 1$ and the spin state is determined by w, a 2-spinor. From the sign of the exponential it can be deduced that ψ_1 has a positive and ψ_2 a negative energy. In the rest of this thesis only the positive energy solutions ψ_1 will be considered, as the negative energy solutions correspond to antiparticle (positron) states. Dropping the subscript, plane wave solutions of positive energy are thus given by

$$\widehat{\psi}(t, \mathbf{r}) = e^{-i\mathcal{E}t + i\mathbf{p}\cdot\mathbf{r}} \sqrt{\frac{\mathcal{E}+m}{2\mathcal{E}}} \begin{pmatrix} w \\ \varepsilon(\hat{\mathbf{p}}\cdot\boldsymbol{\sigma})w \end{pmatrix}. \tag{1.34}$$

Here $\varepsilon = \sqrt{\frac{\mathcal{E}-m}{\mathcal{E}+m}}$ and $\hat{\mathbf{p}} = \mathbf{p}/p$. The dimensionless parameter $\varepsilon < 1$ approaches 1 smoothly in the massless limit.

1.3.7 Maxwell's equations

Describing light as a scalar field is sufficient when only the intensity of the light is relevant, for example the OAM carrying beams as described in section 1.2.2. However, many optical phenomena require a vector description. Light is the manifestation of not one oscillating vector field, but both an electric and a magnetic field. These are related to each other by the Maxwell's equations, in vacuum given by [62]:

$$\nabla \cdot \mathbf{E} = 0, \qquad \nabla \cdot \mathbf{B} = 0, \tag{1.35a}$$

$$\nabla \times \mathbf{E} = -\partial_t \mathbf{B}, \qquad \nabla \times \mathbf{B} = \partial_t \mathbf{E}. \tag{1.35b}$$

where $\epsilon_0 = \mu_0 = c = 1$. From these equations a number of important characteristics of light can be derived. First of all, the electric and magnetic fields obey the vector wave equation:

$$\nabla \times \nabla \times \mathbf{E} = \nabla(\nabla \cdot \mathbf{E}) - \nabla^2 \mathbf{E} = -\partial_t \nabla \times \mathbf{B} = -\partial_t^2 \mathbf{E},$$

with a similar equation for the magnetic field. This implies that each component of the vector field needs to be a solution of the *scalar* wave equation (1.4) individually, as the operators act on each component separately. Solutions are given by $\mathbf{E}(t, \mathbf{r}) = \widetilde{\mathbf{E}}\, e^{-i\omega t + i\mathbf{k}\cdot\mathbf{r}}$, where $\widetilde{\mathbf{E}}$ is a vector that gives the magnitude of the electric field, and k the wavenumber.

The second consequence is that the fields are perpendicular to the momentum direction, i.e. light is a *transverse* wave

$$\mathbf{k} \cdot \mathbf{E} = \mathbf{k} \cdot \mathbf{B} = 0. \tag{1.36}$$

This implies that there are only two degrees of freedom, instead of the expected three spin states for a spin-1 field. Why this is will be explained in section 1.5. Moreover, the electric and magnetic fields are also perpendicular to each other, since the curl of the fields (1.35b) in Fourier space is given by

$$\mathbf{k} \times \begin{pmatrix} \mathbf{E} \\ \mathbf{B} \end{pmatrix} = i\omega \begin{pmatrix} \mathbf{B} \\ -\mathbf{E} \end{pmatrix}.$$

Assuming that both fields are oscillating sinusoidally, they need to oscillate in phase.

1.3.8 Invariance under coordinate transformations

Systems can be characterized by mechanical properties that are conserved quantities under symmetry transformations. A symmetry transformation of a system is a transformation under which the Lagrangian is unchanged. For example: the conservation of energy if the system is invariant under translations in time or the conservation of momentum for translations in space. This principle is expressed by Noether's theorem [57, 50].

Considering the translations in time and space (i.e. the spacetime 4-vector), the conserved quantities form the 4-current of energy and momentum. This 4-current has a vanishing 4-divergence; a change in energy must be compensated by a flow in momentum. Energy, momentum and stresses are combined into the energy-momentum tensor, a matrix of which the components correspond to these

quantities. Which element corresponds to which quantity will be explained in section 2.3.

This tensor can be derived from considering the effect of translations on the Lagrangian, but this calculation only works well for scalar fields that carry no spin. As soon as a multi-component field is considered, contributions to the energy-momentum tensor are overlooked due to the spin of the field. This can be illustrated by considering a rotation of a vector field. The different field components are not just rotated, but also mixed up amongst each other. To find the right energy-momentum tensor that takes the spin into account, it is necessary to consider rotations or Lorentz transformations instead of translations. The derivation of the modified energy-momentum tensor using these transformations will be explained in chapter 2.

1.4 Spin-orbit interactions

The optical vortices and EVBs consist of particles that carry SAM, and these two angular momenta couple to each other. This spin-orbit coupling is extensively studied in the field of atomic physics. A relatively simple system where these effects can be observed is the hydrogen atom. This system will be discussed first, before moving on to the derivation of the wavefunctions for both spinor and vector fields carrying OAM. These solutions demonstrate spin-orbit coupling effects.

1.4.1 A spin-orbit coupling example from atomic physics

A simple example for studying spin-orbit effects is the hydrogen atom, in which a single electron experiences a spherically symmetric attractive force from the nucleus. As the electron is moving through this electric field, it effectively sees a magnetic field [63]:

$$\mathbf{B} = \frac{1}{m_e e c^2} \frac{1}{r} \frac{\partial V(r)}{\partial r} \mathbf{L},$$

with m_e the mass of the electron, e the elementary charge, c the speed of light, $V(r)$ the electrostatic radial potential and $\mathbf{L}$ the angular momentum operator. The electron spin interacts with this magnetic field through the Zeeman effect (1.13). Since the magnetic field arises from the orbital angular momentum, there is effectively a coupling between the OAM and SAM of the electron, in which the alignment of the momenta determines how the energy is shifted:

$$H_Z = \frac{g_s \mu_B}{\hbar m_e e c^2} \frac{1}{r} \frac{\partial V(r)}{\partial r} \mathbf{S} \cdot \mathbf{L}.$$

This is the Zeeman Hamiltonian, that is added to the Hamiltonian describing the energy of the electron as sum of the kinetic and potential energies. The spin-orbit coupling effects occurring in optical and electron vortex beams will be discussed in chapter 3.

In general, there needs to be an extrinsic spatial movement to have a spin-orbit interaction, which can also occur in classical systems. For example, the rotation of the moon around its axis is correlated to its movement around the earth; the tidal forces that are generated by the orbital movement have slowed down the spinning motion of the moon, until the two movements are now (almost) in resonance.

To study this spin-orbit coupling it is necessary to derive a wavefunction with both OAM and SAM. Spinor and vector fields that carry OAM can be derived from the scalar field solution of the Helmholtz equation (1.7). The derivation of propagation invariant vector fields [6, 55, 64] and a similar derivation for spinor fields [65, 66] will be discussed.

1.4.2 Vector Bessel beams

If φ is a solution of the Helmholtz equation (1.5a), a general propagation invariant vector field can be given in terms of two fields [55, 6]:

$$\mathbf{T} = \hat{\mathbf{k}} \times \nabla\varphi = \left(\hat{\mathbf{p}}\frac{1}{h_p}\partial_q - \hat{\mathbf{q}}\frac{1}{h_q}\partial_p\right)(\hat{\mathbf{k}}\varphi), \tag{1.37a}$$

$$\mathbf{S} = \nabla \times (\hat{\mathbf{k}} \times \varphi) = \frac{1}{k}\left(ik_z\nabla_\perp + k_\perp^2\hat{\mathbf{k}}\right)\varphi. \tag{1.37b}$$

Here h_p, h_q are the scale factors corresponding to the transverse coordinates (p, q). The propagation direction $\hat{\mathbf{k}}$ is in the $\hat{\mathbf{z}}$ direction.

The fields (1.37) form a group under the curl operator; $\frac{1}{k}\nabla \times \mathbf{S} = \mathbf{T}$ [6]. Combined with the transversality of $\mathbf{T}$, these fields are suitable to describe transverse electric and magnetic fields; from (1.35b) it follows that if the transverse electric (TE) mode is described by $\mathbf{T}$, the corresponding magnetic field is proportional to by $\mathbf{S}$, and vice versa for the transverse magnetic (TM) modes. Further, the TE and TM modes form a complete basis set to describe the electromagnetic field in, and all other polarization states can be derived from these modes [55].

The general vector fields (1.37) can be transformed to polarization coordinates, which gives the expression of a general electric field [55]:

$$\mathbf{E}(p,q,z,t) = \left[c_1 \begin{pmatrix} U^- \\ -U^+ \\ 0 \end{pmatrix} \varphi_1(p,q) + c_2 \begin{pmatrix} U^- \\ U^+ \\ -i\sqrt{2}\frac{k_\perp^2}{k_z} \end{pmatrix} \varphi_2(p,q) \right] \times e^{-i\omega t + ik_z z}, \quad (1.38)$$

with $\varphi_{1,2}$ scalar solutions of the Helmholtz equation. This is indeed a correct description of an electric or magnetic field, as it can be seen from (1.15) that (1.38) has a vanishing divergence. Taking the scalar Bessel beam solution (1.7) in cylindrical polar coordinates with arbitrary value of ℓ, and the action of $U^\pm$ as in (1.17), it is shown that the orders of Bessel functions are restricted, as a field with zero divergence will always be of the form

$$\mathbf{E}(r,\phi,z,t) = \left[c_1 \begin{pmatrix} J_{\ell-1}(k_r r)e^{-i\phi} \\ -J_{\ell+1}(k_r r)e^{i\phi} \\ 0 \end{pmatrix} + c_2 \begin{pmatrix} J_{\ell-1}(k_r r)e^{-i\phi} \\ J_{\ell+1}(k_r r)e^{i\phi} \\ -i\frac{k_\perp^2}{k_z} J_\ell \end{pmatrix} \right] \times e^{-i\omega t + ik_z z + i\ell\phi}. \quad (1.39)$$

This is an example of spin-orbit coupling: the component of right-handed polarization has a lower OAM value, such that the sum of OAM and SAM is conserved. These fields are sometimes called "spin-weighted harmonics" [67, 68]; the field components are weighted by their spin value. An important consequence of the form of these solutions is that an electromagnetic field cannot be correctly described by a solution that is completely polarized in one direction. Every component is of the form (1.7), which depends on all three coordinates (r, ϕ, z). A field that has one component only does not have a zero divergence.

Further, in the non-paraxial regime the z-component is not negligible compared to the transverse field components. Due to the different orders of Bessel functions that these components are described by, the intensity distribution will shift in radial position [69].

The direction in which the electric field oscillates is called the polarization direction. This direction can be fixed upon propagation, which is called linear polarization. It can also rotate around the propagation axis, tracing out a corkscrew motion; circular polarization. States with a specific polarization can be constructed from (1.38) by choosing the constants c_1, c_2 suitably. In this thesis the convention will be used that if the polarization direction rotates *anticlockwise*

upon propagation this corresponds to *right-handed* polarization. The direction is determined from the viewpoint of the object, not the observer.

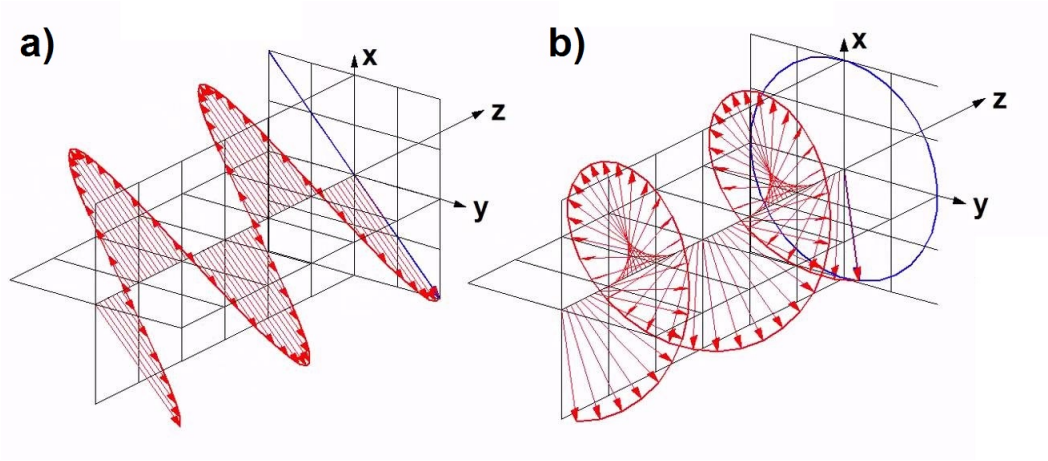

Figure 1.4: Polarization states of light in vacuum. a): Linear polarization. b): Circular (right-handed) polarization.

A beam consist of plane waves that all propagate under slightly different angles and as a result the OAM and SAM operators do not commute in the non-paraxial regime [70]. The spin and orbital angular momentum cannot be completely distinguished from each other. Further, part of the SAM is transferred to the OAM [71], this is called *spin-to-orbital AM conversion*. This will be explained further in chapter 2.

1.4.3 Spinor Bessel beams

The expressions of spinor beams can be derived in a way similar to the vector beams; if φ is a scalar solution of the Helmholtz equation, the spinor ψ can be found by acting with the operator $(i\gamma^\mu\partial_\mu + m)$ on φ [66]. This is a useful consequence of the condition (1.28), see footnote on page 19. A general spinor can hence be expressed as

$$\psi(p,q,z,t) = i\left[c_1\begin{pmatrix}\partial_t + m\\ 0\\ -\partial_z\\ -\sqrt{2}U^+\end{pmatrix}\varphi_1(p,q) + c_2\begin{pmatrix}0\\ \partial_t + m\\ -\sqrt{2}U^-\\ \partial_z\end{pmatrix}\varphi_2(p,q)\right]\times e^{-i\omega t + ik_z z}. \quad (1.40)$$

These spinors correspond to spin-polarized states; taking the spin-up spinor w_s (1.21) in (1.34) gives the same states but then in the momentum representation, $\widehat{\psi}(\mathbf{k})$, where the derivatives are replaced by their corresponding energy and momentum components; $\partial_t \to -i\omega$ and $\nabla \to i\mathbf{k}$. Performing the Hankel transform on this spinor

$$\psi(\mathbf{r}) = \frac{(-i)^\ell}{2\pi k_r} \int_0^\infty k_r \, dk_r \int_0^{2\pi} d\phi_k \, e^{i\ell\phi_k} \widehat{\psi}(\mathbf{k}) e^{ik_r r\cos(\phi_r - \phi_k)} \tag{1.41}$$

gives the solutions in cylindrical coordinates. The transverse derivatives $U^\pm$ contain a factor $e^{\pm i\phi}$, as $\partial_x \pm i\partial_y = \partial_r e^{\pm i\phi_r}$, which gets transformed to $k_r e^{\pm i\phi_k}$. These factors will raise or lower the order ℓ of the resulting Bessel function. However, the factor $(-i)^\ell$ in front of the integral (1.41) remains unchanged, hence the Bessel functions are multiplied by $\pm i$ beside shifting in value. To conclude, a generally polarized spinor field is given by

$$\psi(r,\phi,z,t) = \left[c_1 \begin{pmatrix} (\omega+m)J_\ell(k_r r) \\ 0 \\ k_z J_\ell(k_r r) \\ ik_r J_{\ell+1}(k_r r)e^{i\phi} \end{pmatrix} + c_2 \begin{pmatrix} 0 \\ (\omega+m)J_\ell(k_r r) \\ -ik_r J_{\ell-1}(k_r r)e^{-i\phi} \\ -k_z J_\ell(k_r r) \end{pmatrix} \right] \times e^{i\ell\phi} e^{-i\omega t + ik_z z}. \tag{1.42}$$

This could also be derived directly by acting with the derivatives $U^\pm$ in (1.40) on the scalar solution (1.7). Similar to the vector fields, these operators $U^\pm$ are responsible for the appearance of the $J_{\ell\pm1}$ terms in the Bessel beam solutions. Due to this shift, spin and orbital angular momentum are coupled. Solutions of the Dirac equation that are energy eigenstates can only be eigenstates of the *total* angular momentum. This can be deduced from the commutation relations between the Hamiltonian and AM operators.

The Dirac Hamiltonian can be derived from the Dirac equation (1.27) by multiplication by γ^0 from the left:

$$(i\partial_t + i\gamma^0\boldsymbol{\gamma}\cdot\nabla - \gamma^0 m)\psi = \gamma^0(\boldsymbol{\gamma}\cdot\mathbf{p} + m)\psi = i\partial_t\psi = H_D\psi. \tag{1.43}$$

With the SAM operator for a spinor field given by (1.32), the commutator with (1.43) is given by

$$[\hat{H}, \mathbf{S}] = i \begin{pmatrix} 0 & 1 \\ 1 & 0 \end{pmatrix} (\boldsymbol{\sigma} \times \mathbf{p}) = -[\hat{H}, \mathbf{L}]$$

as the OAM operator is given by (1.3). This shows that only the total angular momentum operator $\mathbf{L} + \mathbf{S}$ commutes with the Hamiltonian.

In 2011, Bliokh et al. [72] described electron vortex beams relativistically by the Dirac equation. It was observed that part of the SAM is transferred to the OAM; a spin-to-orbital conversion similar to the effects observed in optical vortex beams. Further, it was observed that the probability densities are dependent on both the OAM and SAM values. The Bessel functions of order $J_{\ell\pm1}$ appear in the spinor components that are small in the paraxial limit, but these components have a similar effect on the probability density as the longitudinal vector components of the optical vortices [69]. The effects will further be studied in chapter 3. Electron vortex states have also been described in spinor form [73] to study the modifications that an external electromagnetic field has on the electron vortex states. Research into the Cherenkov radiation emitted by vortex electrons suggests that the angular distribution of the radiation depends on the orbital angular momentum and polarization state of the electrons [74].

To conclude, vector and spinor field expressions can be derived from the scalar solution in a similar way. When describing the fields in cylindrical polar coordinates the operators $U^{\pm}$ appear, that shift the OAM value of the component to compensate for the SAM value. As a result, both the spinor and vector fields are eigenstates of the total AM operator.

1.5 Spin and helicity states

The sense of rotation about the propagation axis of the electric and magnetic fields of a plane wave is expressed in the quantity helicity; $\mathcal{H} = \hbar\sigma$, where $\sigma = \pm1$ for right(left)-handed polarization, and $\sigma = 0$ for linear polarization [75]; the direction of rotation is projected onto the direction of the momentum, as experienced by the fields and not the observer. In optics usually the frame of the observer is chosen. However, since the photon states will be compared with electron states, the conventions as used in particle physics are adopted here. Helicity has the same dimensions as SAM and is also an intrinsic quantity. It can therefore be *considered* as the SAM of a single photon. In 1909 Poynting [76] realized that this SAM is related to the polarization of light, and in 1936 it was shown that this is indeed an angular momentum, which can exert a torque on an optically sensitive material [77].

An important difference between helicity and SAM is that SAM is determined

by the projection of the spin onto an external axis. The spin can be completely (anti-) aligned, but if there are more than two spin substates it can also be partially aligned. In contrast, there are only two helicity states possible, completely aligned (right-handed) or anti-aligned (left-handed).

The correspondence between the SAM and helicity of a plane wave is possible as a photon has only two degrees of freedom instead of three. This is because photons are massless particles, and hence they are described by irreducible representations of the Lorentz group[12]. Generators of the Lorentz group only correspond to rotations with $\pm s$ [78], hence massless particles can only occupy the spin states $\pm s$. Light can only have a transverse polarization, not longitudinal. If the fields were pointing in the longitudinal direction, they would be infinitely Lorentz contracted [14] as the photon travels at the speed of light.

The correspondence between circular polarization and helicity is only true for plane waves. As soon as beams are considered, there is a distinction possible between helicity and polarization (spin) states. A beam with a well-defined helicity consists of plane waves that all have the same helicity, but these do not necessarily propagate parallel to each other. A well-defined spin state cannot be created as a superposition of plane waves that are all polarized in the same way; it is a property of the total field as it is defined by an external axis. These spin-polarized fields are created by using polarization filters to cancel one of the polarization directions present in a helical beam. Consequently, vector and spinor fields that are spin eigenstates are different from helicity eigenstates.

Electrons are usually not described in terms of helicity. This is because helicity is not a conserved quantity for massive particles. As a massive particle always travels at speeds slower than the speed of light, there are Lorentz boosts possible that reverse the direction of motion. This Lorentz boost will reverse the helicity of the particle; it is not a relativistically invariant property. However, these transformations will not be considered in this thesis, allowing the study of helicity-polarized electron states.

The difference between spin and helicity beams is the main point of focus in chapter 3. Now a short description of how to derive these different fields will be given.

[12]This will be discussed in the context of Dirac fermions in section 2.1.1.

1.5.1 Vector fields

With a general vector field described by (1.38), electromagnetic fields with a specific polarization can be constructed by choosing the constants c_1, c_2 suitably.

Spin-polarized Bessel beams The expression of a spin-polarized Bessel beam can be derived by describing the component with the desired polarization by the scalar solution (1.7). In this thesis the convention will be adopted that a right-handed circularly polarized beam has a zero left-handed component, and vice versa. Bessel beams that are spin-polarized in the right- or left-handed sense correspond to choosing $c_1 = \pm c_2$ in (1.38), but it is also possible to construct an $\hat{\mathbf{x}}$ or $\hat{\mathbf{y}}$-polarized Bessel beam.

Helicity-polarized Bessel beams Helicity Bessel beams consist of plane waves that all have the same helicity. The theoretical derivation of these beams is described in [79]. To create the conical wave vector distribution, the wave vectors are each rotated away from the propagation axis, rotating the electric field of every plane wave with it. Starting with a wave travelling in the $\hat{\mathbf{z}}$ direction, $k = k_z$, the wave vectors after the rotation will be given by $\mathbf{k} = (k_x, k_y, k_z) = (k\sin(\theta)\cos(\phi), k\sin(\theta)\sin(\phi), k\cos(\theta))$, as shown in figure 1.5. This is the vector equivalent of the original work by Durnin to create Bessel beams [25] and obtained by a purely geometrical transformation [79]:

$$U(\theta, \phi) = R_z(-\phi)R_y(\theta)R_z(\phi), \tag{1.44}$$

where the rotations in three dimensions are generated by (1.19). These rotations are described by a unitary matrix in the circular polarization basis [79]:

$$\mathbf{E}' = U(\theta,\phi)\mathbf{E} = \begin{pmatrix} a & -be^{-2i\phi} & \sqrt{2ab}e^{-i\phi} \\ -be^{2i\phi} & a & \sqrt{2ab}e^{i\phi} \\ -\sqrt{2ab}e^{i\phi} & -\sqrt{2ab}e^{-i\phi} & a-b \end{pmatrix}\mathbf{E}, \tag{1.45}$$

with $a = \cos^2(\theta/2)$ and $b = \sin^2(\theta/2)$. For example, if all plane waves are right-handed circularly polarized, $\mathbf{E} = (1, 0, 0)^T$, the resulting field will be given by [79]

$$\mathbf{E}' = (\cos^2(\theta/2), -\sin^2(\theta/2)e^{2i\phi}, -\sin(\theta)e^{i\phi}/\sqrt{2}).$$

For a tightly-focused beam, $\theta \sim 0$, the right-handed component is the largest component in the resulting field. However, the rotation has created small left-handed circularly and longitudinally polarized fields.

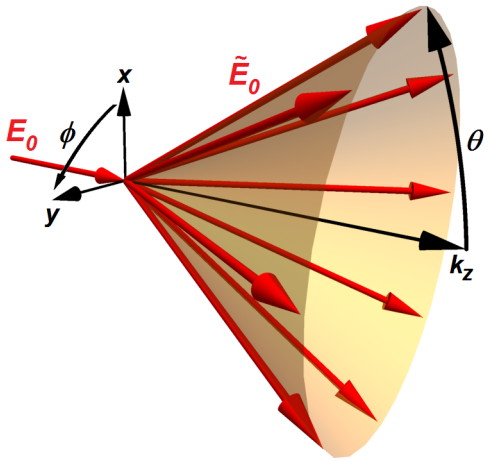

Figure 1.5: Rotation of electric field vectors over the opening angle θ, away from the $\hat{\mathbf{z}}$ axis, to create the Bessel beam spectrum. The field vectors are evenly spread out over the azimuthal angle ϕ.

Fields with a well-defined helicity return to themselves under the curl operation, and are therefore called *curl eigenstates*[13]. This can be shown by considering the definition of the curl operator in Fourier space, i.e. taking the cross product of the wave vector with the field; $\nabla \times \mathbf{F} \rightarrow i\mathbf{k} \times \mathbf{F}$. If the field is a helicity state, it can be written as $\mathbf{F} \sim \mathbf{p} \pm i\mathbf{q}$ with $\mathbf{p}, \mathbf{q}$ general transverse coordinates. Since $\mathbf{p} \times \mathbf{q} = \mathbf{k}$, this field is an eigenstate of the curl operator:

$$i\mathbf{k} \times \mathbf{F} = i\mathbf{k} \times \mathbf{p} \mp \mathbf{k} \times \mathbf{q} = \pm(\mathbf{p} \pm i\mathbf{q}).$$

Thus, for a helical field the curl operator gives the helicity value:

$$\nabla \times \mathbf{F} = \pm\mathbf{F}.$$

The difference between spin-polarized and helicity beams is illustrated in figure 1.6 and will be discussed in chapter 3.

1.5.2 Spinor fields

Describing the electrons in spin states with respect to the $\hat{\mathbf{z}}$-axis, the spinor w_s (1.21) can be inserted into the plane wave solution (1.34). Followed by the Hankel

[13]Fields that are curl eigenstates are also known as Chandrasekhar-Kendall functions [80] and are a special case of cylindrical vector harmonics. Curl eigenstates are intensively studied in astrophysics, as magnetic fields that satisfy the equation $\nabla \times \mathbf{B} = \alpha\mathbf{B}$ cannot exert a (magnetic) Lorentz force on conductive particles. With the electric field parallel to the magnetic field, as $\nabla \times \mathbf{B} = \partial_t \mathbf{E}$, the electric field will give these particles a speed parallel to the magnetic field; $\mathbf{v} \| \mathbf{B}$. Thus the magnetic field cannot exert a Lorentz force, since $\mathbf{v} \times \mathbf{B} = 0$ [81].

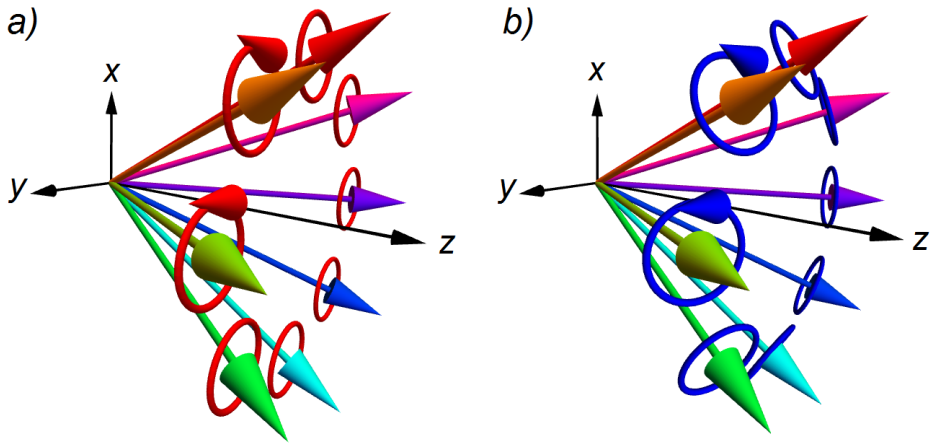

Figure 1.6: The different polarization states of a Bessel beam; a) a Bessel beam with overall (right-handed) polarization. The circles denote the *overall* polarization. This polarization state can only be achieved by using polarization filters to cancel one polarization direction, or by taking suitable combinations for helical beams. b) a Bessel beam consisting of right-handed polarized plane waves.

transform (1.41) the spin-polarized spinor Bessel beams (1.42) are found.

To describe fermions in helicity states, the same procedure can be followed. Instead of w_s the spinor w_h is now used, an eigenstate of the helicity operator. This operator is in spinor and bi-spinor form:

$$\hat{\mathbf{p}}\cdot\boldsymbol{\sigma} = \frac{1}{p}\begin{pmatrix} p_z & p_x - ip_y \\ p_x + ip_y & -p_z \end{pmatrix} = \begin{pmatrix} \cos(\theta) & \sin(\theta)e^{-i\phi} \\ \sin(\theta)e^{i\phi} & -\cos(\theta) \end{pmatrix}, \tag{1.46}$$

$$\mathcal{H} = \hat{\mathbf{p}}\cdot\mathbf{S} = \frac{1}{2}\begin{pmatrix} \hat{\mathbf{p}}\cdot\boldsymbol{\sigma} & 0 \\ 0 & \hat{\mathbf{p}}\cdot\boldsymbol{\sigma} \end{pmatrix}. \tag{1.47}$$

with the corresponding eigenvectors given by

$$w_{h=+\frac{1}{2}} = \begin{pmatrix} \cos(\theta/2) \\ \sin(\theta/2)e^{i\phi} \end{pmatrix}, \qquad w_{h=-\frac{1}{2}} = \begin{pmatrix} -\sin(\theta/2)e^{-i\phi} \\ \cos(\theta/2) \end{pmatrix}. \tag{1.48}$$

These states can also be found from applying the spinor variant of the geometric rotation (1.44) on the spinors w_s, with the rotations generated by (1.20) [82]:

$$\widetilde{U}(\theta,\phi) = \begin{pmatrix} \cos(\theta) & \sin(\theta)e^{i\phi} \\ -\sin(\theta)e^{-i\phi} & \cos(\theta) \end{pmatrix}. \tag{1.49}$$

Commutators of (1.47) with the AM operators show that helicity commutes with the total angular momentum only:

$$[\mathcal{H}, \mathbf{L}] = -i\mathbb{1}_2(\boldsymbol{\sigma} \times \mathbf{p}) = -[\mathcal{H}, \mathbf{S}].$$

Combined with the fact that $[H, \mathcal{H}] = 0$, it can be concluded that states can simultaneously be eigenstates of the Hamiltonian, helicity and total angular momentum, but not the spin or orbital angular momenta separately. The differences between electron spin and helicity states will be studied in chapter 3.

1.6 Real and complex states

The circular polarization basis is constructed from combining the coordinates x and y as $x \pm iy$. This shows that a circularly polarized state is a superposition of two linearly polarized states, and vice versa. This fact will be used to derive expressions for linearly polarized Bessel beams, discussed further in chapter 4.

Similarly, a complex field can be described by two real fields; one for the real part and one for the imaginary part as in $re^{i\phi} = x + iy$. There is physically no difference between these two, as they both have two degrees of freedom. However, the complex notation is usually easier to work with. An example is the optical field. It is a real field as the photon does not carry charge, but can be represented by a complex field $\widetilde{\mathbf{E}}$, of which the actual field is given by $\mathbf{E} = \mathrm{Re}(\widetilde{\mathbf{E}})$. All conserved quantities, given in terms of the real fields, can be expressed in the complex fields, where one has to remember that the real part of these quantities is the physical part that needs to be considered.

This similarity is mathematically equivalent to the distinction between standing and travelling waves. Travelling waves are typically described by $e^{i\alpha}$, while standing waves are described by $\cos(\alpha)$ and $\sin(\alpha)$. However, this shows that a travelling wave can be created by superimposing two standing waves and vice versa. Further, whether a wave is observed as standing or travelling depends on the frame of the observer. Moving along with a travelling wave, a standing wave is observed. The same is true for an observer that is moving along a standing wave, observing a travelling wave.

The distinction between a real or complex description, or between standing and travelling waves has a fermionic analogue; the description of real spinors as solutions of the Dirac equation.

1.6.1 Majorana representation

As explained in section 1.3.6, there are different representations of the gamma matrices possible. One particular representation, the Majorana representation, has completely imaginary gamma matrices. It was developed around 80 years ago by Ettore Majorana [83, 84]. The γ-matrices in this representation are given by [85]:

$$\begin{aligned} \gamma^0 &= \begin{pmatrix} 0 & \sigma^y \\ \sigma^y & 0 \end{pmatrix}, \qquad \gamma^1 = \begin{pmatrix} i\sigma^z & 0 \\ 0 & i\sigma^z \end{pmatrix}, \\ \gamma^2 &= \begin{pmatrix} 0 & \sigma^y \\ -\sigma^y & 0 \end{pmatrix}, \qquad \gamma^3 = \begin{pmatrix} -i\sigma^x & 0 \\ 0 & -i\sigma^x \end{pmatrix}. \end{aligned} \tag{1.50}$$

The Majorana representation is related to the Dirac representation by the unitary matrix transformation

$$\gamma_M = V\gamma_D V^\dagger; \qquad \psi_M = V\psi_D; \qquad V = \frac{1}{\sqrt{2}} \begin{pmatrix} \mathbb{1} & \sigma_y \\ \sigma_y & -\mathbb{1} \end{pmatrix}. \tag{1.51}$$

A consequence of completely imaginary gamma matrices is that the corresponding spinors are real, $\psi = \psi^*$, and invariant under complex conjugation. Complex conjugation is closely related to the concept of charge conjugation in field theory.

Charge conjugation describes the transformation between particles and antiparticles; antiparticles have the same properties as particles but carry opposite charge. However, they can also be considered as particles (i.e. with the same charge) that move backwards in time. For example an electrical current of electrons; this is indistinguishable from a current of positrons moving in the opposite direction. As a result, a scalar complex particle described by a plane wave $\varphi = e^{-i\mathcal{E}t+i\mathbf{p}\cdot\mathbf{r}}$ is related to its antiparticle by complex conjugation; charge conjugation and complex conjugation are the same operation. However, this is not true for a Dirac spinor, as an antiparticle needs to have opposite spin. Charge conjugation can now be accomplished by the following operator:

$$\mathcal{C} : \psi(t, \mathbf{r}) \mapsto -i\gamma^2\psi^*(t, \mathbf{r}), \tag{1.52}$$

as it needs to incorporate both a spin-flip and complex conjugation. A spinor that is invariant under charge conjugation does not carry electric charge[14] and satisfies the condition $\psi_D = -i\gamma^2\psi_D^* = \psi_D^c$. The Majorana representation diagonalises

[14] See section 2.3.1

this relationship [86], with as result that Majorana spinors are eigenstates of the charge conjugation operator with eigenvalue $-i$:

$$\psi_M^c = V\psi_D^c = V(i\gamma^2(V^{-1}\psi_M)^*) = iV\gamma^2(V^*)^{-1}\psi_M^* = -i\psi_M^* = -i\psi_M. \quad (1.53)$$

This eigenvalue (the charge conjugation phase) will become important when considering the Majorana mass states, further explained in chapter 2 and relevant in chapter 5.

1.6.2 Construction of spinor charge conjugation eigenstates

Being an eigenstate of charge conjugation brings consequences with it, that can be derived from the form of the solutions. Under $\mathcal{C}$ as given by (1.52) a spinor with spin up is tranformed into a spinor with spin down, negative energy and opposite momentum. Thus, a Majorana spinor must incorporate both [86]; it is a superposition of two spinors with opposite spin.

This superposition restricts the number of degrees of freedom for a Majorana fermion; instead of the four solutions of the Dirac equation (2 spin states and either positive or negative energy) there are only two different states possible. These states, when transformed to the Majorana representation, are described by cosines and sines instead of complex exponentials.

Due to similarities between optical and electron vortex states, one could wonder what a Majorana state of the optical field is. What effects does the superposition of opposite spin states have, for example on the polarization? The superposition of two waves with opposite spin can be interpreted in two different ways. Consider a right-handed and a left-handed wave, both travelling in the same direction. This gives a travelling, linearly polarized wave. However, since helicity is coupled to the momentum direction, the left-handed wave can also be interpreted as a right-handed wave travelling in the opposite direction. This gives a standing wave.

This demonstrates the analogy between complex fields and travelling waves, in contrast with real fields and standing waves. Majorana fields are real and hence describe standing waves, even when they are constructed from photons that are inherently real. This is reflected in the observation that states in the Majorana representation are described by sines and cosines instead of complex exponentials.

The similarities between the different distinctions, real vs. complex, linear vs. circular and standing vs. travelling waves, will be discussed in chapter 5, where the optical equivalent of Majorana states will be discussed.

2 Fundamental theoretical principles

This chapter will cover the framework of several different theories that will be used in the rest of this thesis. First the Weyl and Majorana spinors are considered, including a discussion about chirality, the matrix γ^5 and its connection with the mass of the particle. The appearance of fermionic Majorana excitations in solid state systems will also be discussed, followed by an explanation of discrete spacetime symmetries. Next is a description of symmetries of the fields and Lagrangian, the Euler-Lagrange equations and Noether's theorem. These are helpful tools to derive the energy-momentum tensor, which will be studied in chapters 3 and 4 for optical vortices and EVBs. This chapter will conclude with a discussion about the different angular momenta of light and the distinction between optical spin angular momentum and helicity.

2.1 Weyl and Majorana fermions

The solutions of the Dirac equation as derived in (1.33) are completely unconstrained. They describe a field with two spin degrees of freedom and either positive or negative energy. However, as mentioned in section 1.6, there are only two basis spinors in the Majorana representation, as there is a constraint that halves the number of solutions of the Dirac equation. This is the sign of the charge conjugation phase. There are other constraints possible, for example chirality, demonstrated by the Weyl representation.

Chirality is a fundamental property of a particle, determined by under which of the two irreducible representations of the Lorentz group this particle transforms. Weyl spinors transform under either of these, while Dirac spinors transform under a reducible representation that is a direct sum of the two. The Weyl spinors can therefore be considered as fundamental building blocks of the spinor field [85].

Majorana fermions can be constructed from either Weyl or Dirac spinors, but in this section the construction from Weyl spinors only will be considered, simplifying the derivations. A number of important properties of Majorana spinors will be discussed. These will become relevant when considering the optical Majorana states in chapter 5. Textbook references for this section include [58, 59, 60].

2.1.1 The Weyl representation and chirality

There are different choices for the gamma matrices in the Dirac equation possible. These are related to each other by unitary transformations as $\gamma^{(2)} = U\gamma^{(1)}U^\dagger$, with $U^\dagger U = \mathbb{1}$. The spinors are hence related to each other by $\psi^{(2)} = U\psi^{(1)}$. All representations are physically equivalent, since the γ-matrices in the Dirac equation (1.27) are multiplied by the spinor, cancelling the unitary transformation. The difference in representations is expressed in the form of the eigenstates of specific operators. Every representation diagonalises a specific operator, favouring the corresponding eigenstates.

Apart from the Dirac and Majorana representation, a commonly used representation of the Dirac equation is the Weyl representation. This representation is given by:

$$\gamma^0 = \begin{pmatrix} 0 & -\mathbb{1} \\ -\mathbb{1} & 0 \end{pmatrix} \quad , \quad \boldsymbol{\gamma} = \begin{pmatrix} 0 & \boldsymbol{\sigma} \\ -\boldsymbol{\sigma} & 0 \end{pmatrix}. \tag{2.1}$$

Another convention for the Weyl representation is $\gamma^0 = \begin{pmatrix} 0 & \mathbb{1} \\ \mathbb{1} & 0 \end{pmatrix}$ with $\boldsymbol{\gamma}$ unchanged. The effect of switching between these two representations is that the spinors with right-handed and left-handed helicities are interchanged. In this thesis the representation (2.1) will be used.

The unitary transformation relating these matrices to the standard representation (1.29) is

$$\gamma^W = U^\dagger \gamma^D U, \qquad U = \frac{1}{\sqrt{2}} \begin{pmatrix} 1 & -1 \\ 1 & 1 \end{pmatrix}. \tag{2.2}$$

The Weyl representation is conventionally used to describe massless particles, as in the limit of zero mass the Dirac equation is block diagonal in this representation; massless particle solutions are given by only the upper two or lower two components of the spinor:

$$\psi_+^W(t,\mathbf{r}) = \frac{e^{-i\mathcal{E}t+i\mathbf{p}\cdot\mathbf{r}}}{2\mathcal{E}} \begin{pmatrix} (\mathcal{E}+\mathbf{p}\cdot\boldsymbol{\sigma})w \\ 0 \end{pmatrix},$$
$$\psi_-^W(t,\mathbf{r}) = \frac{e^{-i\mathcal{E}t+i\mathbf{p}\cdot\mathbf{r}}}{2\mathcal{E}} \begin{pmatrix} 0 \\ (\mathcal{E}-\mathbf{p}\cdot\boldsymbol{\sigma})w \end{pmatrix}.$$

The states with subscript $+(-)$ describe particles with right-(left-)handed helicity, as inserting the definition of w_h (1.48) gives only two helicity eigenstates, the spinor ψ_+^W combined with $w_{h=+\frac{1}{2}}$ and ψ_-^W with $w_{h=-\frac{1}{2}}$, while the other combinations are zero:

$$\psi_+^W(t,\mathbf{r}) = e^{-i\mathcal{E}t+i\mathbf{p}\cdot\mathbf{r}} \begin{pmatrix} \cos(\theta/2) \\ \sin(\theta/2)e^{i\phi} \\ 0 \\ 0 \end{pmatrix},\ \psi_-^W(t,\mathbf{r}) = e^{-i\mathcal{E}t+i\mathbf{p}\cdot\mathbf{r}} \begin{pmatrix} 0 \\ 0 \\ \sin(\theta/2)e^{-i\phi} \\ -\cos(\theta/2) \end{pmatrix}. \tag{2.3}$$

The Weyl spinors must be constrained by a specific property, that halves the number of allowed states from four to two. This property is chirality. There is also an optical quantity that is called chirality that will be discussed in section 2.5.4.

The chirality of a spinor denotes the irreducible representation of the Lorentz group that it transforms under. The generators (1.31) of both rotations and boosts are diagonal in the Weyl representation [60], which means that it is reducible; it can be split into two irreducible representations that either act only on the upper two or lower two components of the 4-spinor:

$$\Sigma^{ij} = \begin{pmatrix} e^{+i\theta\cdot\sigma^k/2} & 0 \\ 0 & e^{+i\theta\cdot\sigma^k/2} \end{pmatrix}, \qquad \Sigma^{0k} = \begin{pmatrix} e^{+\zeta\sigma^k/2} & 0 \\ 0 & e^{-\zeta\sigma^k/2} \end{pmatrix}.$$

The 4-component bi-spinor can be split in two spinors with opposite chirality as a result, that transform the same under rotations, but with opposite signs under boosts:

$$\psi = \begin{pmatrix} u_+ \\ u_- \end{pmatrix}. \tag{2.4}$$

The upper spinor u_+ is in the so-called $\left(\frac{1}{2},0\right)$ representation of the Lorentz group, while u_- is in the $\left(0,\frac{1}{2}\right)$ representation [87]. It is possible to define projection operators that project a state onto $u_\pm$, as in $P_\pm\psi = u_\pm$:

$$\left.\begin{aligned} P_+ &= \begin{pmatrix} 1 & 0 \\ 0 & 0 \end{pmatrix} \\ P_- &= \begin{pmatrix} 0 & 0 \\ 0 & 1 \end{pmatrix} \end{aligned}\right\} P_\pm = \frac{1}{2}(1\pm\gamma^5) \to \gamma^5 = \begin{pmatrix} 1 & 0 \\ 0 & -1 \end{pmatrix}. \qquad \text{(Weyl rep)}$$

This matrix $\gamma^5 = i\gamma^0\gamma^1\gamma^2\gamma^3$ is called the *chirality* operator and the Weyl spinors $u_\pm$ have chirality ± 1. From the Weyl spinors (2.3) it can be concluded that the spinor u_+ corresponds to right-handed helicity and chirality $+1$, and the spinor u_- to left-handed helicity and chirality -1. Hence there is a one-to-one correspondence between chirality and helicity.

This is only true for massless particles[1] as helicity and chirality are distinct quantities for massive particles: re-introducing the mass in the Weyl representation shows that a massive spinor is described by a combination of spinors with positive and negative chirality, transforming under the representation $(\frac{1}{2}, 0) \oplus (0, \frac{1}{2})$. Hence the Dirac spinor is completely unconstrained.

This can also be concluded from considering the commutator of the Hamiltonian[2] with γ^5:

$$[\hat{H}, \gamma^5] = -2m\gamma^5\gamma^0 = 2m \begin{pmatrix} 0 & 1 \\ -1 & 0 \end{pmatrix}.$$

This commutator does not depend on the representation chosen, as both the Hamiltonian and the matrix γ^5 do. As this commutator is proportional to the mass, an energy eigenstate can only be a chirality eigenstate if it is massless. However, a particle can always be designed to be a helicity eigenstate, since the helicity operator (1.47) is diagonal and commutes with the Hamiltonian.

It can be concluded that Weyl spinors transform under different representations of the Lorentz group, characterized by their chirality. They can hence be considered as "more fundamental" than spinors in other representations. Chirality corresponds to helicity only in the massless limit.

2.1.2 Constructing Majorana spinors

The defining property of Majorana particles is to be invariant under charge conjugation. This is equivalent to the condition of being its own antiparticle, since particles are transformed into antiparticles by charge conjugation and vice versa. However, no elementary Majorana particles have been found yet; all known particles in the Standard Model behave as Dirac fermions. The only exception

[1] The action of γ^5 can be expressed by the matrix: $\gamma^5 u_\pm = \begin{pmatrix} \frac{\mathbf{p}\cdot\boldsymbol{\sigma}}{\mathcal{E}+m} & 0 \\ 0 & \frac{\mathbf{p}\cdot\boldsymbol{\sigma}}{\mathcal{E}-m} \end{pmatrix} u_\pm \underset{m\to 0}{\to} (\boldsymbol{\Sigma}\cdot\hat{\mathbf{p}})u_\pm$ which reduces to the helicity operator in the massless limit [61].

[2] The Hamiltonian in the Weyl representation is given by

$$H_W = \begin{pmatrix} \boldsymbol{\sigma}\cdot\mathbf{p} & 0 \\ 0 & -\boldsymbol{\sigma}\cdot\mathbf{p} \end{pmatrix}. \tag{2.5}$$

is the neutrino, of which it is still unknown whether this is a Dirac or Majorana fermion [88]. The only way to construct a fermionic field that is invariant under charge conjugation, $\psi^c = \psi$, with the charge conjugation operator given by (1.52), is by making a superposition of a fermionic field and its charge conjugate. For this purpose the Weyl spinors will be used, as these are the most fundamental spinors and this will simplify the calculations as there are no mixing terms.

In terms of the Weyl spinors $u_\pm$ [86], a bi-spinor can be defined with the property $\psi = -i\gamma^2\psi^*$:

$$\psi = \left\{ \begin{pmatrix} u_+ \\ i\sigma^2 u_+^* \end{pmatrix}, \begin{pmatrix} -i\sigma^2 u_-^* \\ u_- \end{pmatrix} \right\}. \tag{2.6}$$

It turns out that there are only two distinct Majorana solutions instead of four [86]. The constraint responsible for this is the sign of the *charge conjugation phase*. This phase shows up when transforming the charge conjugation operator to the Majorana representation (1.53):

$$\mathcal{C}\psi = -i\psi^*.$$

This phase, being imaginary, has an important consequence. Its effect can be deduced from modifying the Dirac equation to the Majorana equation, using that $\psi^c = \psi$:

$$i\gamma^\mu\partial_\mu\psi - m\psi^c = i\gamma^\mu\partial_\mu\psi + im\psi^* = 0. \tag{2.7}$$

If a Dirac spinor is multiplied by a complex phase it remains a solution of the Dirac equation, but this is not the case for Majorana spinors. Multiplying the Majorana spinor by $+i$ changes the sign of charge conjugation:

$$(i\psi)^c = -\psi^*; \qquad \mathcal{C} : i\psi \to i(i\psi^*).$$

This changes the form of (2.7):

$$i\gamma^\mu\partial_\mu(i\psi) - m(i\psi)^c = i\gamma^\mu\partial_\mu(i\psi) + m\psi^* = i\gamma^\mu\partial_\mu(i\psi) - im(i\psi^*) = 0. \tag{2.8}$$

It can be concluded that the multiplication by a complex phase changes the sign of the mass [86]. In fact, the Majorana equation (2.7) describes four particle states that are degenerate and can only be told apart by their charge conjugation phase. This explains why there are only two solutions instead of four. In fact, a four-component Majorana spinor can represent two 2-spinors with different (or even opposite) masses [86]. As a result, Majorana fermions in solid state systems have been observed on the interface of two regions that differ in the sign of the (effective) mass.

2.1.3 Majorana excitations in solid state systems

In this subsection the Majorana excitations in solid state systems will be discussed. This gives an insight into the conditions that need to be fulfilled for Majorana excitations to appear. The optical equivalents of these conditions will be discussed in chapter 5, allowing for the appearance of optical Majorana states.

Up to now, theoretical work and experiments have focused on creating or finding fermionic Majorana states as a superposition of a fermion and an anti-fermion. This can be achieved by creating an exciton, a concept from solid state physics. It is a bound state of an electron and a hole (an empty space below the Fermi energy), hence electrically neutral [89] and described by:

$$\gamma = \frac{1}{\sqrt{2}} \left(u c_\sigma^\dagger + u^* c_\sigma \right). \tag{2.9}$$

with c_σ the creation operator for an electron with spin σ, and $c_\sigma^\dagger$ the annihilation operator, i.e. the creation operator for a hole. Hence this exciton is Hermitian and its own anti-exciton; $\gamma^\dagger = \gamma$ [90]. An exciton is a pseudo-particle that can *behave* as a Majorana particle, while the physical particle is still the electron.

An important consequence of (2.9) is that a Majorana excitation has zero energy, as the creation of an electron with energy $\mathcal{E}$ is equivalent to annihilating a hole with energy $-\mathcal{E}$ [89]. Thus there is a degeneracy in the ground state of a system between a state with a Majorana excitation and a state without one. Further, as a Majorana fermion can be considered as "half a fermion", Majorana fermions always appear in pairs. A fermion operator is equivalent to two Majorana operators that are localized in the same position [90], and Majorana excitations need to be spatially separated to be able to speak of a Majorana particle.

The energy of a fermionic excitation is a function of the momentum p; $\mathcal{E}(p) = \pm\sqrt{p^2 + m^2}$. This energy is described by two bands separated by the non-zero mass. The mass does not have to be the physical (rest) mass; in a solid-state system it can also be a parameter depending on the electrostatic or chemical potential. Consequently, this mass parameter can change value with position or even change sign. The place where it changes sign and goes through zero is called a domain wall, marking the transition between two phases of matter. Due to their zero energy, Majorana excitations can only appear at these boundaries. Edges of a system are also domain walls, and these are the domain walls that will be considered in this section.

Superconducting systems are promising candidates for finding Majorana fermions as they respect the electron-hole symmetry. Electrons in supercon-

ductors couple to each other to form Cooper pairs, that can form a condensate due to their bosonic nature. A change in the total number of Cooper pairs does not substantially change the physical properties of the superconductor [91]. As a result, a hole in the vicinity of a Cooper pair can be regarded as a single electron; the rigid distinction between electrons and holes has disappeared.

The modes in the superconducting state are called Bogoliubov excitations, described by [90]:

$$b = uc_\sigma^\dagger + vc_\sigma.$$

These modes clearly have an electron and a hole component, but they do not have to appear in equal proportions; $v \neq u^*$. However, in some systems the conditions are exactly right and the Bogoliubov excitations are of the Majorana type (2.9), with $v = u^*$.

It is important that these superconductors are p-wave superconductors as a necessary condition for *unpaired* Majorana fermions to appear is that the spin degeneracy of the electrons is lifted [89]. The reason for this is that introducing spin to a system doubles the eigenstates of the Hamiltonian; instead of having a single Majorana state there will be two states in the same position, which is equivalent to a fermionic state [92]. In a spinless system all electrons are in the same spin state, hence when they combine into Cooper pairs they cannot combine into a total state with zero spin (s-wave coupling) but couple into a state with spin $s = 1$; this is p-wave coupling. However, it was shown theoretically in 2008 that Majorana excitations could also appear in s-wave superconductors when brought in contact with a topological insulator [93].

Well-known theoretical works on Majorana excitations in one-dimensional [94] and two-dimensional [95] p-wave superconductors will be discussed next. These works demonstrate the fundamental properties of Majorana excitations; they have zero energy and hence appear as boundary states on opposite sides of the system, being spatially separated. These excitations in solid state systems can be compared to optical systems where similar effects occur, discussed in chapter 5.

The Majorana-like modes in a 1-dimensional superconductor were first described by Kitaev [94] in 2001. This system can be considered as a chain consisting of a large number of sites. Each site only accommodates one electron each, being effectively spinless. This can be realized by applying a small magnetic field. Electrons can both hop from their site to a neighbouring one, parametrized by t, and couple to each other forming a Cooper pair. This coupling is parametrized by Δ, the energy that it costs to form a Cooper pair (the superconducting gap function).

The interaction Hamiltonian of this system is given by

$$H \sim \sum_{i}^{N-1} \left(t c_i^\dagger c_{i+1} + \Delta c_i c_{i+1} + h.c. \right). \tag{2.10}$$

The Cooper pairs are formed from electrons on different sites due to the Pauli exclusion principle.

Splitting the fermion operators on each site i gives the Majorana operators:

$$\gamma_{i,1} = c_i^\dagger + c_i, \qquad \gamma_{i,2} = i(c_i^\dagger - c_i).$$

With these new operators, under the condition $t = \Delta$, the Hamiltonian (2.10) becomes [90]:

$$H = -it \sum_{i=1}^{N-1} \gamma_{i,2}\gamma_{i+1,1} = 2t \sum_{i=1}^{N-1} \tilde{c}_i^\dagger \tilde{c}_i. \tag{2.11}$$

This shows two important effects: the sum runs over i up to $N-1$ instead of N, and the operators on neighbouring sites are combined; $\tilde{c}_i = (\gamma_{i+1,1} + i\gamma_{i,2})/2$. From the new Hamiltonian (2.11) the two operators $\gamma_{1,1}$ and $\gamma_{N,2}$ are missing, while these were present in the old Hamiltonian (2.10). These two operators can be combined in one operator

$$\tilde{c}_M = \frac{1}{2}(\gamma_{N,2} + i\gamma_{1,1}).$$

The state created by this operator is a Majorana state. Firstly, it is a localized state concentrated on the two endpoints of the chain. Secondly, it does not contribute to the energy since it does not appear in the expression of the Hamiltonian. Thus there is a two-fold degeneracy of the ground state between a state with the sites at the ends unpaired and a state where all sites are paired, see figure 2.1.

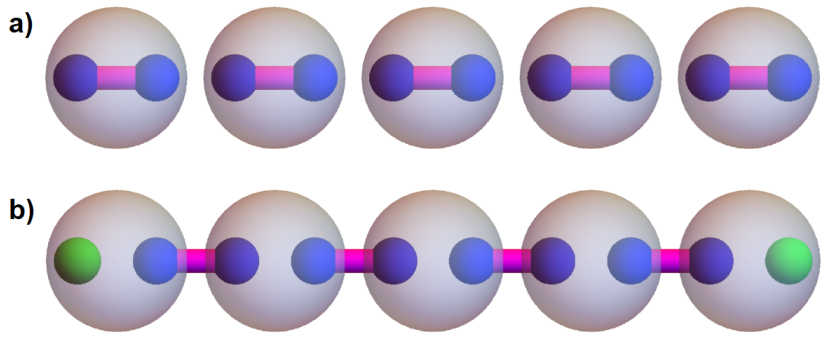

Figure 2.1: Two different ways to pair electrons in Kitaev's chain. Each fermion site is described by two Majorana operators, shown by the small blue spheres. a): all sites are paired to a neighbour; there is no Majorana state. b): the sites at the ends are unpaired, corresponding to a chain with a Majorana state.

It can be concluded that the fermionic operators on each site can be split into two parts, that can be recombined in two different ways; as in the original configuration or by pairing neighbouring sites, giving rise to edge states with zero energy.

However, Majorana excitations can also occur in two-dimensional systems, demonstrating another important characteristic of Majorana modes: the halving of the degrees of freedom. This is a result of the coupling between the energy and the momentum vector on the boundary of the system. Two-dimensional p-wave superconductors with Majorana excitations are described by [95]. It was found that the creation and annihilation operators can be combined in excitation modes u, v. These are described by a set of first-order equations compatible with $u = v^*$; the excitations can be considered to be their own antiparticle. This has as important consequence that there is only *one excitation mode* for each wavevector $\mathbf{k}$ [95].

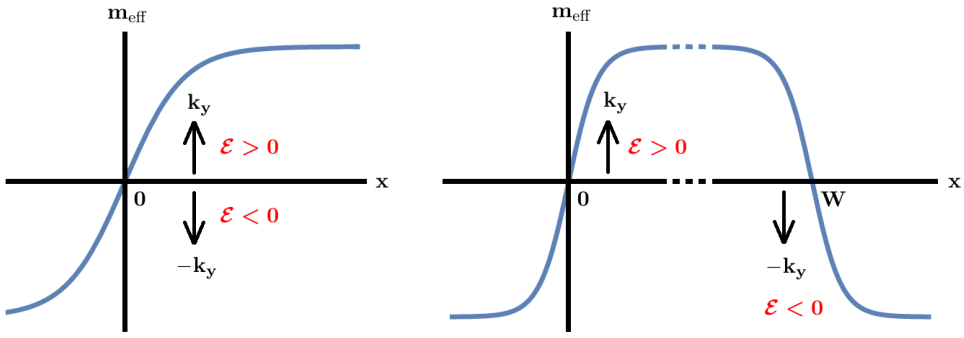

Figure 2.2: The effective mass changes sign at the edges of the system or a domain wall. Left: a single edge. The direction of motion depends on the sign of the energy. Right: two edges separated by a distance W. Positive energy solutions become concentrated on one side, negative energy solutions on the other. The direction of the momentum and the sign of the energy are coupled.

If the domain wall is parallel to the $\hat{\mathbf{y}}$-direction, the energy of these excitations is given by $\mathcal{E} = \Delta k_y$; the solutions are bound to the domain wall, and travel in one direction only depending on their energy. If the system has a finite width, the pair of first-order equations describing u and v separately is replaced by one second-order equation for the mode $u \pm iv$. This equation has a positive and a negative energy solution. The eigenstates with $\mathcal{E} > 0$ become concentrated on one edge, and the eigenstates with $\mathcal{E} < 0$ on the other. This set of eigenstates can

be seen as a single Majorana mode, divided over the two edges; the left-moving states on one edge and right-moving states on the other [95].

These results show that the Majorana excitations appear as edge states, reflecting the condition that they are massless. The energy and momentum vector become coupled to each other, which limits the degrees of freedom. This coupling determines on which edge the states appear, separating the two states from each other.

These theoretical works were followed by the first "creation" of Majorana particles in nanowires by Kouwenhoven [96] in 2012. This work inspired other experiments focussing on Majorana signatures in nanowires connecting a superconductor and semiconductor [97, 98]. Further, in 2014 a topological superconductor was created by placing a chain of ferromagnetic atoms on the surface of a superconductor. It was observed that zero-energy edge states appear, the characteristic of Majorana modes [99].

To conclude, important characteristics of Majorana states are having a zero energy, which can be accomplished by being a superposition of positive and negative energy, and the sign of the energy is coupled to the momentum direction; positive energy states move in one direction and negative energy states move in the opposite direction. This is a constraint that halves the number of states, and there is only one excitation for every wavevector $\mathbf{k}$.

Similarities between these fermionic Majorana excitations and optical Majorana states will be discussed in chapter 5, where is it shown that for optical states the spin direction, instead of the sign of the energy, is coupled to the momentum direction.

2.2 Discrete spacetime transformations for spinor fields

Charge conjugation is one of three discrete spacetime transformations. The other two are parity ($\mathcal{P}$) and time ($\mathcal{T}$) reversal. Parity is the reversal of all spatial components; $(t, \mathbf{r}) \rightarrow (t, -\mathbf{r})$, while time reversal only changes the sign of the time coordinate: $(t, \mathbf{r}) \rightarrow (-t, \mathbf{r})$.

As mentioned in section 1.3.5, only a subgroup of the Lorentz group $O(1,3)$ will be considered in this thesis. This subgroup, $SO^{+}(1,3)$, is called the proper ortochronous group. Elements of this group conserve the direction of time and orientation. There are other subgroups of the Lorentz group that are connected to $SO^{+}(1,3)$ by $\mathcal{P}$ and $\mathcal{T}$ reversal.

By careful consideration of the Dirac spinors under these transformations, conclusions can be drawn about how these are represented in terms of the $\gamma-$matrices [50, 57, 100]. This leads to important conclusions of the effect of charge conjugation $\mathcal{C}$, that appears to be related to the sign of mass for Majorana spinors.

Parity The parity operator inverts the direction of the spatial components of spacetime. This means that it reverses the direction of the momentum of a particle and its helicity, but not its spin, as parity commutes with rotations. Considering helicity eigenstates in the Weyl representation (2.3), a parity transformation can be obtained by multiplication by the γ^0 matrix and inversion of the spatial coordinates $\mathbf{r}$ [50]:

$$\mathcal{P} : \psi(t, \mathbf{r}) \mapsto \gamma^0 \psi(t, -\mathbf{r}). \tag{2.12}$$

Time The time reversal operator inverts only the time coordinate, which implies that momentum and spin are reversed, but helicity is not. This can be realized by the operation [50]

$$\widetilde{\mathcal{T}} : \psi(t, \mathbf{r}) \mapsto \gamma^0 \gamma^2 \psi^*(-t, \mathbf{r}). \tag{2.13}$$

However, Wigner [101] found that this time reversal operator does not comply with Kramer's theorem.

This theorem states that, if a Hamiltonian is time-reversal symmetric, energy eigenstates will always appear in pairs. If a wavefunction ψ is a solution of the Schrödinger equation,

$$i\partial_t \psi(t, \mathbf{r}) = H\psi(t, \mathbf{r}),$$

and the Hamiltonian commutes with $\mathcal{T}$, then $\mathcal{T}\psi$ is also a solution with the same energy. However, simply reversing time is not enough to satisfy this condition. It needs to be combined with complex conjugation, making $\mathcal{T}$ an anti-linear operator:

$$i\partial_t \psi^*(-t, \mathbf{r}) = H\psi^*(-t, \mathbf{r}).$$

It follows that $\psi^*(-t, \mathbf{r})$ is also an energy eigenstate [50]. This can be interpreted as follows: time reversal symmetry implies that there is no distinction possible between a process and the same process reversed in time. A time-reversed process looks like it is going forward in time, but with momenta and spins inverted[3].

[3]Time reversal alone is not enough to change a particle into an antiparticle. Take for example an electron with spin up travelling in the positive $\hat{\mathbf{x}}$-direction. The time-reversed system is an electron with spin down moving in the negative $\hat{\mathbf{x}}$-direction, which is equivalent to a positron moving in the positive $\hat{\mathbf{x}}$-direction, but with spin up. This can be explained from the conservation of charge and

Since the γ^2 matrix is imaginary, the right form of the time reversal operator is $\gamma^1\gamma^3$, as this product leaves the Dirac Lagrangian invariant [50]:

$$\mathcal{T} : \psi(t, \mathbf{r}) \mapsto \gamma^1\gamma^3\psi(-t, \mathbf{r}). \tag{2.14}$$

It was mentioned in section 2.1.3 that Majorana fermions can only appear in p-wave superconductors that are effectively spinless, as in this situation only a *single* mode for each $\mathbf{k}$ is allowed. The spin state is determined by the direction of $\mathbf{k}$, while the other spin state does not appear. These combinations break time-reversal symmetry, as opposite spin states are connected to each other by time-reversal. As a result the Majorana states are isolated on either side of the domain. Thus the condition for Majorana excitations to appear in p-wave superconductors can be recast as the breaking of time-reversal symmetry.

$\mathcal{CPT}$ and the connection with the sign of mass and γ^5 It turns out that there is a connection between the signs of mass and energy, as they can be related to the transformation of a spinor under $\mathcal{CPT}$ reversal. Multiplication of a Majorana spinor by γ^5 changes the sign of mass; since $\{\gamma^5, \gamma^\mu\} = 0$, the Dirac equation gets modified to

$$(i\gamma^\mu\partial_\mu - m)\gamma^5\psi = -\gamma^5(i\gamma^\mu\partial_\mu + m)\psi.$$

In its own turn, multiplication by γ^5 is also observed as part of the combined transformation of $\mathcal{C}$, $\mathcal{P}$ and $\mathcal{T}$;

$$\begin{aligned}\mathcal{CPT}\psi(t, \mathbf{r}) &= \mathcal{CP}\gamma^1\gamma^3\psi(-t, \mathbf{r}) = \mathcal{C}\gamma^0\gamma^1\gamma^3\psi(-t, -\mathbf{r}) \\ &= -i\gamma^2\gamma^0\gamma^1\gamma^3\psi^*(-t, -\mathbf{r}) = -\gamma^5\psi^*(-t, -\mathbf{r}).\end{aligned} \tag{2.15}$$

An important difference between these two transformations is that $\mathcal{CPT}$ also involves the inversion of both t and $\mathbf{r}$. These inversions compensate for the change in sign of the mass, ensuring that the transformed particle is still a solution of the Dirac equation

$$\begin{aligned}(i\gamma^\mu\partial_\mu - m)(-\gamma^5\psi(-t, -\mathbf{r})) &= -(-i\gamma^\mu\partial_\mu - m)\gamma^5\psi(t, \mathbf{r}), \\ &= -\gamma^5(i\gamma^\mu\partial_\mu - m)\psi(t, \mathbf{r}).\end{aligned}$$

It turns out that the conservation of $\mathcal{CPT}$ provides a relation between a process involving particles and the reverse process involving antiparticles [58].

spin. The charge-conjugated system would be a positron with spin down moving in the positive $\hat{\mathbf{x}}$-direction.

Since $\mathcal{CPT}$ leaves the Dirac equation invariant, particles and antiparticles have the same sign of energy and mass; they are either both positive or negative. The connection between the signs can be deduced from applying the transformation $\gamma^0 \mapsto -\gamma^0$ to the Dirac equation [102]. This transformation needs to be combined with the transformation $m \mapsto -m$ to keep the Dirac equation unchanged. However, since γ^0 is multiplied by the derivative with respect to time (the energy operator) the sign of the energy also needs to change. As a result, states that are superpositions of positive and negative energy states (Majorana excitations) need to be superpositions of positive and negative mass states.

The situation is different for optical states, as photons are massless, hence the condition $m = 0$ is trivially fulfilled. However, instead of states with positive and negative energies, states with opposite helicities need to be combined to create a Majorana state. This will be shown in chapter 5, and is also reflected in the observation that fermionic Majorana states couple the energy to the wavevector, while optical Majorana states will be shown to couple the spin to the wavevector instead.

2.3 Symmetries of the Lagrangian

This section will discuss the concept of symmetries of a field, and its associated conserved quantities. These are important characteristics of a field when described in relativistic field theory. A field is symmetric under a transformation if this transformation does not physically change the field. For example, if the field has a conserved angular momentum, it is invariant under rotations. There are different types of transformations depending on whether they change the spacetime coordinates or the field itself. The Euler-Lagrange equations can be derived from considering a change in only the fields themselves. These are the field equations; the Klein-Gordon equation for scalar fields, the Dirac equation for spinor fields and Maxwell's equations for (massless) vector fields. Considering a 4-coordinate transformation that changes both the coordinates and the fields leads to a conserved 4-current, as described by Noether's theorem [57, 58]. This current is the energy-momentum tensor when spacetime translations are considered, and the components of this tensor will be used in later chapters to compare the spinor and vector fields with the scalar fields.

The principle of least action states that the dynamics of a system described by a Lagrangian $\mathcal{L}$ is such that the action, a path integral of the Lagrangian in field

configuration space, is minimized. The fields can be perturbed along this path, as long as the end points are kept fixed.

A simple transformation perturbs the fields as $\phi'(x) = \phi(x) + \delta_0\phi(x)$ while keeping the coordinates unchanged. It is found that the action is minimized when the fields satisfy the Euler-Lagrange equations (the field equations) [103]:

$$\frac{\partial \mathcal{L}}{\partial \phi} - \partial_\mu \left(\frac{\partial \mathcal{L}}{\partial(\partial_\mu \phi)} \right) = 0. \tag{2.16}$$

There are also transformations that change the coordinates, transforming the fields with them:

$$\phi'(x) = \phi(x) + \delta_0\phi(x), \qquad \delta_0\phi(x) = \delta\phi(x) - \delta x^\mu \partial_\mu \phi(x).$$

The action is minimized if there is a conserved current. This is the Noether current, given by the expression

$$j^\mu = \frac{\partial \mathcal{L}}{\partial(\partial_\mu \phi)}\delta\phi - \left[\frac{\partial \mathcal{L}}{\partial(\partial_\mu \phi)}\partial^\nu \phi - \mathcal{L}\eta^{\mu\nu} \right] \delta x_\nu. \tag{2.17}$$

2.3.1 Gauge symmetries

The Euler-Lagrange equations leave the fields with some degrees of freedom. This means that the fields can be changed from one configuration to the other without changing the Lagrangian or the field equations derived from it. Transformations between these different configurations can be either global or local. For example, complex (charged) fields are invariant under a phase transformation

$$\psi(x) \to e^{i\alpha}\psi(x),$$

as the Lagrangian contains both φ and φ^*, see equation (2.18). This is a global invariance, as the phase α does not depend on the position x. If it did, this would be a local phase transformation

$$\psi(x) \to e^{i\alpha(x)}\psi(x).$$

Physical quantities should be gauge-*invariant* and are degenerate under a gauge transformation; they do not depend on the gauge that is chosen.

Gauge symmetry and current of scalar fields

The Lagrangian density of a complex scalar field described by the Klein-Gordon equation is given by:

$$\mathcal{L} = \frac{1}{2}\left(\partial^\mu \varphi^* \partial_\mu \varphi - m^2 \varphi^* \varphi\right). \tag{2.18}$$

This Lagrangian is invariant under a $U(1)$ transformation of the field; multiplying the field by $e^{-i\alpha}$ does not change the Lagrangian, as both φ and φ^* appear here, cancelling the complex phases. Associated with this symmetry is the charge 4-current consisting of the charge density and currents. The transformation in infinitesimal form is:

$$\varphi \to \varphi - i\alpha\varphi, \qquad \varphi^* \to \varphi^* + i\alpha\varphi^*.$$

and the conserved current, using the first term of (2.17), is given by

$$j^\mu = -\frac{i}{2}(\varphi^*\partial^\mu\varphi - (\partial^\mu\varphi^*)\varphi) = \text{Im}(\varphi^*\partial^\mu\varphi). \tag{2.19}$$

Gauge symmetry and current of the Dirac field

The symmetries of the Dirac field can be found from the Dirac Lagrangian. This is given by [60]:

$$\mathcal{L}_{\text{Dirac}} = \bar{\psi}(i\gamma^\mu\partial_\mu - m)\psi. \tag{2.20}$$

Remarkable here is that $\bar{\psi} = \gamma^0\psi^\dagger$ appears, the adjoint spinor, and not $\psi^\dagger$, the Hermitian conjugate. This is because the quantities $\bar{\psi}\psi$ and $\bar{\psi}\gamma^\mu\psi$ transform as a Lorentz scalar and Lorentz current respectively, but the same quantities with $\psi^\dagger$ instead do not [60]. It follows that this Lagrangian is invariant under a $U(1)$ gauge transformation $\psi \to e^{i\alpha}\psi$ and $\bar{\psi} \to e^{-i\alpha}\bar{\psi}$ [88].

Similarly, the conserved gauge current of the Dirac field is $\bar{\psi}\gamma^\mu\psi$, which can be found by subtracting the Dirac equation from its adjoint. This gives $\partial_\mu(\bar{\psi}\gamma^\mu\psi) = 0$. Hence the probability density and current are given by

$$j^\mu = \bar{\psi}\gamma^\mu\psi \to \begin{cases} \rho = \bar{\psi}\gamma^0\psi = \psi^\dagger\psi, \\ \\ \mathbf{J} = \bar{\psi}\boldsymbol{\gamma}\psi = \psi^\dagger\boldsymbol{\alpha}\psi. \end{cases} \tag{2.21}$$

These quantities arise as a result of the $U(1)$ gauge symmetry associated with the complex phase. The Majorana equation is not invariant under a complex phase transformation (2.8). However, there exists another transformation that is a symmetry of the Majorana field; the transformation $\psi \to e^{i\gamma^5\alpha}\psi$. The conserved quantity related to this transformation is the *axial* vector current. For Dirac spinors, the four-divergence of this current is equal to [60]

$$\partial_\mu j_A^\mu = 2im\bar{\psi}\gamma^5\psi,$$

and hence the current is only conserved for $m = 0$. The axial transformation is in infinitesimal form given by:

$$\psi \to \psi(1 + i\gamma^5).$$

Since both the multiplication of a Majorana spinor by $+i$ and by γ^5 have as effect that the sign of the mass in the Majorana equation (2.7) gets inverted, the combined multiplication gives a spinor that is again a solution of (2.7):

$$(i\gamma^5\psi)^c = -i(i\gamma^5\psi)^* = \gamma^5\psi^*,$$

$$i\gamma^\mu\partial_\mu(i\gamma^5\psi) - m(i\gamma^5\psi)^c = i\gamma^\mu\partial_\mu(i\gamma^5\psi) - m\gamma^5\psi^* = i\gamma^\mu\partial_\mu(i\gamma^5\psi) + im(i\gamma^5\psi^*).$$

It can be concluded that the axial transformation is a symmetry of the field, and the Majorana field has a non-zero axial current [104].

Gauge symmetry of the optical field

The Lagrangian of the optical field is given in terms of the electromagnetic field tensor $F_{\mu\nu} = \partial_\mu A_\nu - \partial_\nu A_\mu$, with A_μ the 4-potential $(V, -\mathbf{A})$:

$$\mathcal{L} = -\frac{1}{4}F_{\mu\nu}F^{\mu\nu}; \qquad F_{\mu\nu} = \begin{pmatrix} 0 & E_x/c & E_y/c & E_z/c \\ -E_x/c & 0 & -B_z & B_y \\ -E_{y/c} & B_z & 0 & -B_x \\ -E_z/c & -B_y & B_x & 0 \end{pmatrix}. \tag{2.22}$$

This Lagrangian is expressed in terms of the field tensor $F^{\mu\nu}$, as it transforms correctly under Lorentz transformations while the field A^μ does not [58]. However, A^μ is the correct parameter to describe the optical field by. The interaction matrix[4] can be constructed in terms of either A^μ or $F^{\mu\nu}$. Using $F^{\mu\nu}$ gives an interaction strength that falls off faster than the expected r^{-2} behaviour from Coulomb's law, while using A^μ gives the right behaviour [58]. This is why the Lagrangian is given in terms of the field tensor $F^{\mu\nu}$, but the actual field is the field vector A^μ.

Since the field tensor $F_{\mu\nu}$ is real there is no $U(1)$ symmetry for the optical field[5]. The absence of a gauge current is in general proved by Weinberg and

[4] An object frequently used in particle physics; the S-matrix denotes the complex probability amplitudes for transitions caused by interactions with an external field [58].

[5] However, the Lagrangian can be "complexified" by adding a dual-symmetric field tensor. This will be explained in chapter 5. This dual-symmetric Lagrangian *is* invariant under a $U(1)$ gauge transformation, and there exists a corresponding conserved current; the helicity density and spin currents.

Witten [105]: there is no Lorentz covariant current with a non-vanishing charge density for a massless field with spin $s > \frac{1}{2}$.

However, since the electric and magnetic fields can be expressed in terms of the scalar potential V and vector potential $\mathbf{A}$ as $\mathbf{E} = -\nabla V - \partial_t \mathbf{A}$ and $\mathbf{B} = \nabla \times \mathbf{A}$, there are other transformations possible that do not change the fields. Under the combined transformations of the potentials by any scalar function $\varphi(t, \mathbf{r})$,

$$V \to V - \partial_t \varphi, \quad \mathbf{A} \to \mathbf{A} + \nabla\varphi; \quad A^\mu \to A^\mu - \partial^\mu \varphi,$$

the fields are unchanged:

$$\mathbf{E} \to -\nabla V + \nabla\partial_t\varphi - \partial_t \mathbf{A} - \nabla\partial_t\varphi, \qquad \mathbf{B} \to \nabla \times \mathbf{A} + \nabla \times \nabla\varphi.$$

These transformations define the gauge transformations for the optical field. This is a local gauge transformation, in contrast to the $U(1)$ gauge transformation of complex fields. There are different ways to fix this gauge, of which the two most common choices are the Coulomb gauge and the Lorenz gauge [106].

Physical quantities need to be *gauge independent*; they do not change value depending on the method chosen to fix the gauge [107]. For example, the value of the scalar potential depends on the choice in gauge, so it is not a physical quantity.

Lorenz gauge In the Lorenz gauge the divergence of the vector potential is Lorentz covariant:

$$\partial_\mu A^\mu = 0 \to \nabla \cdot \mathbf{A} = \partial_t V.$$

This does not completely fix the 4-potential, as this condition is also satisfied when the derivative of a scalar function f is added to the potential, $A^\mu \to A^\mu + \partial^\mu f$, under the condition that $\Box^2 f = 0$. The Lorenz gauge is usually used for time-dependent electromagnetic fields.

Coulomb gauge In the Coulomb gauge, the divergence of the vector potential is zero:

$$\nabla \cdot \mathbf{A} = 0.$$

As a consequence, the scalar potential is determined by the charge density distribution at this very moment, $\rho = -\nabla^2 V$. When the electric charges move, the potential is changed instantaneously anywhere in space. This does not violate special relativity as the scalar potential is not something that can be measured absolutely. Hence there is no information transferred with a speed greater than

the speed of light. In the rest of this thesis the Coulomb gauge will be used. This is done for simplicity reasons; both the electric and magnetic fields are dependent on the same vector field only, without having to take the scalar potential into account, which can be chosen to be zero.

The gauge currents of the scalar and spinor fields will be discussed and compared with each other in chapter 3, while for the optical field other quantities need to be considered. These turn out to be the helicity and SAM densities. Why this is will be explained in section 2.5.2.

2.3.2 Translation symmetries; the energy-momentum tensor

The $U(1)$ gauge symmetry of a complex field is a global symmetry. There are also local symmetries to consider, of which symmetry under a translation (either in time or space) is the simplest example. These transformations give in classical mechanics rise to the conservation of energy and momentum. An infinitesimal spacetime translation changes the coordinates $(x^\mu)' = x^\mu - \epsilon^\mu$, translating the fields, although they are not changed themselves. With these transformations the Noether current (2.17) is the canonical energy-momentum tensor:

$$T^\mu_{\ \nu} = \frac{\partial \mathcal{L}}{\partial(\partial_\mu \phi)} \partial_\nu \phi - \mathcal{L}\eta^\mu_{\ \nu}. \tag{2.23}$$

This energy-momentum tensor $T^{\mu\nu}$ describes the flow of the μ-component of the relativistic 4-momentum through a surface of constant coordinate ν; T^{00} gives the energy density, while T^{0j} describes the flow of energy in the j-direction and T^{j0} describes the flow of j-momentum through time. The T^{ij} components describe stresses; when $i \neq j$ these are shear stresses and the components with $i = j$ are normal stresses (pressures). From the conservation of energy and momentum, and the principle of inertial movement (the momentum is the product of the energy density and velocity) it is expected that the energy-momentum tensor is symmetric [108]. This is indeed the case for scalar fields, but not for multicomponent fields that carry spin. The energy-momentum tensor (2.23) for the scalar Lagrangian (2.18) becomes:

$$T^{\mu\nu} = \frac{1}{2}[\partial^\mu \varphi^* \partial^\nu \varphi + \partial^\mu \varphi \partial^\nu \varphi^*] - \eta^{\mu\nu} \frac{1}{2} \left[\partial_\alpha \varphi^* \partial^\alpha \varphi - m^2 \varphi^* \varphi\right]. \tag{2.24}$$

The energy density, momentum densities and stress components, described by their corresponding components, are hence given by

$$\begin{aligned}
\mathcal{E} = T^{00} &= \frac{1}{2}\left(\partial_t\varphi^*\partial_t\varphi + \nabla\varphi^*\nabla\varphi + m^2\varphi^*\varphi\right), \\
p_j = T^{0j} &= \mathrm{Re}\left[(\partial_t\varphi^*)\nabla^j\varphi\right], \\
\sigma_{jj} = T^{jj} &= \mathrm{Re}\left[(\nabla^j\varphi^*)\nabla^j\varphi\right] - \eta^{jj}\frac{1}{2}\left[\partial_\alpha\varphi^*\partial^\alpha\varphi - m^2\varphi^*\varphi\right], \\
\sigma_{ij} = T^{ij} &= \mathrm{Re}\left[(\nabla^i\varphi^*)\nabla^j\varphi\right].
\end{aligned}$$

By the same method the energy-momentum tensor for the Dirac field can be derived; the Dirac Lagrangian is given by (2.20), and application of (2.23) gives:

$$T^{\mu\nu} = \frac{i}{2}\left(\bar{\psi}\gamma^\mu\partial^\nu\psi - (\partial^\nu\bar{\psi})\gamma^\mu\psi\right). \tag{2.25}$$

Similarly for the optical field, with the Lagrangian given by (2.22), the canonical energy-momentum tensor (2.23) is given by:

$$T^{\mu\nu} = -F^\mu_{\ \gamma}(\partial^\nu A^\gamma) + \frac{1}{4}\eta^{\mu\nu}F^{\alpha\beta}F_{\alpha\beta}. \tag{2.26}$$

Comparisons between (2.24), (2.25) and (2.26) show that the energy-momentum tensor of the scalar field is symmetric in the indices, while the tensors of the spinor and vector field are not.

This is problematic, as a non-symmetric tensor breaks the principles of inertial movement [108]; the flow of energy in a specific direction (given by component T^{0j}) needs to be equal to the flow of momentum in that direction through time (given by component T^{j0}). The energy-momentum tensor can be symmetrized by a method contributed to Rosenfeld [109] and Belinfante [110]. This method takes the spin current of the field into account.

To conclude, from global $U(1)$ symmetries of the Lagrangian the gauge density and currents can be derived. Implementation of translations of the fields gives the energy-momentum tensor from Noether's theorem, which is not symmetric if the fields carry spin.

2.4 Symmetric energy-momentum tensor and the spin contribution

The canonical energy-momentum tensor is not symmetric due to the presence of a spin current. Non-scalar fields are described by a multicomponent wavefunction, and under spacetime translations these transform all in slightly different ways.

Symmetric energy-momentum tensors are studied in general relativity, where the Einstein equations relate the curvature of space to the energy-momentum tensor. This implies that the energy-momentum tensor is symmetric. However, general relativity is a classical field theory in the sense that it does not consider spin interactions, which are quantum effects. The absence of an antisymmetric part of the energy-momentum tensor signifies this absence of a spin current [107].

Rosenfeld [109] realised that the symmetric tensor can be split into two parts, contributed by different sources of gravity. This is comparable to how bound and free currents are the source of a magnetic field. It turns out that one of these sources of gravity is analogous to the spin current of a field. Due to the curvature of spacetime in the presence of gravity, a translation in space mixes field components. Hence a field that carries spin is affected, but a scalar field is not. By adding an intrinsic spin-dependent part to the canonical energy-momentum tensor, it can be made a symmetric tensor $\Theta^{\mu\nu}$.

For the Dirac field, this extra contribution is given by the Gordon decomposition [111] of the conserved gauge current. The energy-momentum tensor components are directly related to this gauge current, and hence symmetrized this way. Since there is no gauge current for the optical field, there is only the energy-momentum tensor to consider. The separation of this tensor into a scalar part and a spin part is given by Belinfante's procedure [110].

2.4.1 Gordon decomposition

The conserved Dirac current j^μ (2.21) can be split in a scalar-like part and a spin part by the Gordon decomposition [111]. This is found by multiplying the Dirac equation by γ^ν from the left:

$$0 = i\gamma^\mu\partial_\mu\psi - m\psi = i\gamma^\nu\gamma^\mu\partial_\mu\psi - m\gamma^\nu\psi = \frac{i}{m}\bar{\psi}\gamma^\nu\gamma^\mu\partial_\mu\psi - \bar{\psi}\gamma^\nu\psi.$$

And similarly for the adjoint equation $\frac{-i}{m}(\partial_\mu\bar{\psi})\gamma^\mu\gamma^\nu\psi - \bar{\psi}\gamma^\nu\psi = 0$. Using this, the conserved gauge current (2.21) is given by

$$j^\nu = \frac{1}{2}\left[\bar{\psi}\gamma^\nu\psi + \bar{\psi}\gamma^\nu\psi\right] = \frac{i}{2m}\left[\bar{\psi}\gamma^\nu\gamma^\mu\partial_\mu\psi - (\partial_\mu\bar{\psi})\gamma^\mu\gamma^\nu\psi\right].$$

Using anticommutation (1.30) and commutation (1.31) relations of the γ-matrices, the products of γ-matrices become:

$$\gamma^\mu\gamma^\nu = \frac{1}{2}\left([\gamma^\mu,\gamma^\nu] + \{\gamma^\mu,\gamma^\nu\}\right) = -2i\Sigma^{\mu\nu} + \eta^{\mu\nu}.$$
$$\gamma^\nu\gamma^\mu = 2i\Sigma^{\mu\nu} + \eta^{\mu\nu}.$$

And with these the gauge current becomes

$$j^\nu = -\frac{1}{m}\partial_\mu \left[\bar{\psi}\Sigma^{\mu\nu}\psi\right] + \frac{i}{2m}\left(\bar{\psi}\partial^\nu\psi - (\partial^\nu\bar{\psi})\psi\right).$$

The blue term is the *spin* part, while the second part resembles the Klein-Gordon current (2.19) for a relativistic particle, but with $\bar{\psi}$ replacing ψ^*;

$$\frac{i}{2m}\left(\bar{\psi}\partial^\nu\psi - (\partial^\nu\bar{\psi})\psi\right) = -\frac{1}{m}\mathrm{Im}(\bar{\psi}\partial^\nu\psi).$$

Since the Dirac spinor ψ is multi-component, it can be written as one scalar component φ and multiple extra, smaller, components; $\psi = \varphi + \Phi$. Then the "spinor Klein-Gordon current" splits up as follows:

$$\frac{i}{2m}\left(\bar{\psi}\partial^\nu\psi - (\partial^\nu\bar{\psi})\psi\right) = \frac{i}{2m}\left(\bar{\varphi}\partial^\nu\varphi - (\partial^\nu\bar{\varphi})\varphi\right) + \frac{i}{2m}\left(\mathcal{O}(\bar{\varphi}\Phi, \bar{\Phi}\varphi, \bar{\Phi}\Phi)\right).$$

The first part is by definition equal to the Klein-Gordon current[6], and the terms in red are the *orbital* terms. Thus, the Dirac current can be split into three parts:

$$j^\mu = j^\mu_{\text{orbital, scalar}} + j^\mu_{\text{orbital, spin}} + j^\mu_{\text{spin}}. \tag{2.27}$$

The spin part $+j^\mu_{\text{spin}}$ can be expressed as the curl of the spin operator, using (1.31) in the standard representation:

$$\Sigma^{\mu\nu} = \frac{i}{4}[\gamma^\mu, \gamma^\nu] = \begin{cases} \Sigma^{00} = \Sigma^{pp} = 0, \\ \Sigma^{0p} = -\Sigma^{p0} = \frac{i}{2}\begin{pmatrix} 0 & \sigma^p \\ \sigma^p & 0 \end{pmatrix}, \\ \Sigma^{pq} = -\frac{1}{2}\epsilon^{pqr}\sigma_r \mathbb{1}_2 = -\epsilon^{pqr}S_r. \end{cases} \tag{2.28}$$

As a result of this, the spin part of the gauge density ρ can be expressed as:

$$\rho_{\text{spin}} = -\frac{1}{m}\partial_p\left[\bar{\psi}\Sigma^{p0}\psi\right] = \frac{i}{2m}\nabla\cdot\left[\bar{\psi}\begin{pmatrix} 0 & \boldsymbol{\sigma} \\ \boldsymbol{\sigma} & 0 \end{pmatrix}\psi\right].$$

This contribution will turn out to be zero for helicity states, but not for spin states. The spin part of the gauge current j^q can be rewritten as:

$$\begin{aligned} j^q_{\text{spin}} = -\frac{1}{m}\partial_\nu(\bar{\psi}\Sigma^{\nu q}\psi) &= -\frac{1}{m}\partial_t(\bar{\psi}\Sigma^{0q}\psi) + \frac{1}{m}\partial_p(\bar{\psi}\Sigma^{pq}\psi), \\ &= \frac{1}{m}[\nabla\times(\bar{\psi}\mathbf{S}\psi)]^q. \end{aligned}$$

[6] Since γ^0 is given by (1.29) in the standard Dirac representation, the first two components of $\bar{\psi}$ are equal to the first two components of $\psi^\dagger$. These two components are the larger, scalar-like components of the bi-spinor.

To conclude the total gauge density and currents become:

$$\rho = \frac{1}{m}\mathrm{Im}(\bar{\psi}\partial_t\psi) + \frac{i}{2m}\nabla\cdot\left[\bar{\psi}\begin{pmatrix} 0 & \boldsymbol{\sigma} \\ \boldsymbol{\sigma} & 0 \end{pmatrix}\psi\right], \tag{2.29}$$

$$\mathbf{J} = \frac{1}{m}\mathrm{Im}(\bar{\psi}\nabla\psi) + \frac{1}{m}[\nabla\times(\bar{\psi}\mathbf{S}\psi)]. \tag{2.30}$$

This shows that both quantities have a part that is similar to the corresponding Klein-Gordon current for the scalar field, although the spinor ψ is multicomponent function. There is also an extra contribution from the spin current.

2.4.2 Derivation of the Belinfante-Rosenfeld tensor

This section will explain the derivation of the Belinfante-Rosenfeld tensor, based on [58], relevant for the energy-momentum tensor of the optical field. A crucial step in this derivation is to consider a *Lorentz transformation* instead of a translation when deriving the Noether current, acting on both vector fields and coordinates:

$$\begin{aligned}(x^\mu)' &= x^\mu + \omega^\mu{}_\nu x^\nu,\\ (\phi^\mu)' &= \phi^\mu + \frac{1}{2}\Omega_{\rho\sigma}(\mathcal{M}^{\rho\sigma})^\mu{}_\nu\phi^\nu.\end{aligned}$$

Here $\omega^{\mu\nu}$ and $\Omega^{\mu\nu}$ are antisymmetric matrices, and $\mathcal{M}^{\rho\sigma}$ are the generators of the Lorentz transformations, as in (1.24). The conserved Noether current (2.17) becomes under this transformation

$$j^\mu = \frac{\partial\mathcal{L}}{\partial(\partial_\mu\phi^\lambda)}\frac{1}{2}\Omega_{\rho\sigma}(\mathcal{M}^{\rho\sigma})^\lambda{}_\nu\phi^\nu - T^{\mu\rho}\Omega_{\rho\sigma}x^\sigma. \tag{2.31}$$

Using the facts that $\Omega_{\rho\sigma}$ is an antisymmetric matrix and that indices that are summed over can be relabelled, the energy-momentum tensor term can be split in two parts:

$$\begin{aligned}j^\mu &= \frac{1}{2}\Omega_{\rho\sigma}\left[\frac{\partial\mathcal{L}}{\partial(\partial_\mu\phi^\lambda)}(\mathcal{M}^{\rho\sigma})^\lambda{}_\nu\phi^\nu - T^{\mu\rho}x^\sigma + T^{\mu\sigma}x^\rho\right],\\ &= \frac{1}{2}\Omega_{\rho\sigma}\left[S^{\mu\rho\sigma} - T^{\mu\rho}x^\sigma + T^{\mu\sigma}x^\rho\right].\end{aligned} \tag{2.32}$$

The tensor $S^{\mu\rho\sigma}$ is antisymmetric in the last two indices [112] and can be regarded as the spin density:

$$S^{\mu\rho\sigma} = \frac{\partial\mathcal{L}}{\partial(\partial_\mu\phi^\lambda)}(\mathcal{M}^{\rho\sigma})^\lambda{}_\nu\phi^\nu = \frac{\partial\mathcal{L}}{\partial(\partial_\mu\phi^\rho)}\phi^\sigma - \frac{\partial\mathcal{L}}{\partial(\partial_\mu\phi^\sigma)}\phi^\rho. \tag{2.33}$$

Conservation of the current (2.31) implies that the 4-divergence of $S^{\mu\rho\sigma}$ is the asymmetric part of the canonical energy-momentum tensor

$$\partial_\mu S^{\mu\rho\sigma} = T^{\sigma\rho} - T^{\rho\sigma}.$$

This confirms that the canonical energy-momentum tensor is not symmetric due to a non-zero spin current.

In general, a symmetric tensor $\Theta^{\mu\nu}$ can be constructed from the canonical tensor by subtracting the antisymmetric part; $\Theta^{\mu\nu} = T^{\mu\nu} + \partial_\alpha B^{\alpha\mu\nu}$. The condition that this tensor is symmetric can then be used to relate $B^{\alpha\mu\nu}$ to $S^{\alpha\mu\nu}$:

$$B^{\alpha\mu\nu} = \frac{1}{2}(S^{\alpha\mu\nu} + S^{\mu\nu\alpha} - S^{\nu\alpha\mu}).$$

The symmetric energy-momentum tensor now becomes [58]

$$\Theta^{\mu\nu} = T^{\mu\nu} + \frac{1}{2}\partial_\alpha \left(S^{\alpha\mu\nu} + S^{\mu\nu\alpha} - S^{\nu\alpha\mu}\right). \tag{2.34}$$

Inserting the definition of $S^{\alpha\mu\nu}$ (2.33) in this expression gives the final expression of the symmetric energy-momentum tensor:

$$\Theta^{\mu\nu} = T^{\mu\nu} + \frac{1}{2}\partial_\gamma \left[\frac{\partial\mathcal{L}}{\partial(\partial_\gamma\phi^\lambda)}(\mathcal{M}^{\mu\nu})^\lambda{}_\alpha\phi^\alpha + \frac{\partial\mathcal{L}}{\partial(\partial_\mu\phi^\lambda)}(\mathcal{M}^{\nu\gamma})^\lambda{}_\alpha\phi^\alpha - \frac{\partial\mathcal{L}}{\partial(\partial_\nu\phi^\lambda)}(\mathcal{M}^{\gamma\mu})^\lambda{}_\alpha\phi^\alpha\right]. \tag{2.35}$$

This expression will be used to derive the spin current contribution to the energy-momentum tensor for the different fields. To make the distinction more clear, different colours will be used for the canonical and spin parts:

$$\Theta^{\mu\nu} = T^{\mu\nu} + \partial_\gamma K^{\gamma\mu\nu}. \tag{2.36}$$

However, there are also spin terms that contribute to the canonical energy-momentum tensor due to the multi-component wavefunctions describing a non-scalar field. Hence there is an *orbital* contribution (this will be shown in red) to the canonical energy-momentum tensor, and the final distinction can be made as follows:

$$\Theta^{\mu\nu} = \text{scalar quantity } + T^{\mu\nu} - \text{scalar quantity } + \partial_\gamma K^{\gamma\mu\nu}. \tag{2.37}$$

The terms in red are related to the non-zero spin of the field, while the contribution $+\partial_\gamma K^{\gamma\mu\nu}$ is related to the spin current. This becomes apparent when considering the angular momentum tensor, that can be constructed from the energy-momentum tensor by taking the cross product with the position vector. When using the canonical energy-momentum tensor, the angular momentum tensor is not conserved;

$$\partial_\mu(T^{\mu\rho}x^\sigma - T^{\mu\sigma}x^\rho) = T^{\sigma\rho} - T^{\rho\sigma}.$$

However, a conserved angular momentum tensor can be constructed from the symmetric energy-momentum tensor, and is given by

$$M^{\mu\sigma\rho} = \Theta^{\mu\rho}x^\sigma - \Theta^{\mu\sigma}x^\rho = T^{\mu\rho}x^\sigma - T^{\mu\sigma}x^\rho + \partial_\alpha K^{\alpha\mu\rho}x^\sigma - \partial_\alpha K^{\alpha\mu\sigma}x^\rho. \tag{2.38}$$

This angular momentum tensor will also be used in section 2.5.2 to discuss the spin-to-orbital conversion in light, as it incorporates the spin angular momentum. This spin contribution can be rewritten in the form

$$\begin{aligned}\partial_\alpha K^{\alpha\mu\rho}x^\sigma - \partial_\alpha K^{\alpha\mu\sigma}x^\rho &= \partial_\alpha\left[K^{\alpha\mu\rho}x^\sigma - K^{\alpha\mu\sigma}x^\rho\right] - K^{\alpha\mu\rho}\delta^\sigma_\alpha + K^{\alpha\mu\sigma}\delta^\rho_\alpha,\\ &= \partial_\alpha F^{\alpha\mu\rho\sigma} - S^{\mu\rho\sigma}.\end{aligned}$$

The tensor $F^{\alpha\mu\rho\sigma}$ is asymmetric in (ρ,σ) and, from the definition of $B^{\alpha\mu\rho}$, also in (α,μ). However, the angular momentum tensor $M^{\mu\rho\sigma}$ is antisymmetric in (ρ,σ) only, so $F^{\alpha\mu\rho\sigma}$ does not have the right properties to be part of the angular momentum. Further, it does not change the conservation law $\partial_\mu M^{\mu\sigma\rho}=0$ and it can be left out from the definition of $M^{\mu\rho\sigma}$ [113]. This leads to the new expression for the angular momentum tensor, equivalent to the one found for the conserved current (2.32) under rotations and boosts [112]:

$$M^{\mu\sigma\rho} = T^{\mu\rho}x^\sigma - T^{\mu\sigma}x^\rho - S^{\mu\rho\sigma}. \tag{2.39}$$

This clearly shows that the tensor $S^{\mu\rho\sigma}$ gives the intrinsic (spin) part of the angular momentum tensor. The total angular momentum density is given by the integral of the angular momentum density over all space $\int M^{0ij}dV$, hence the spin angular momentum is given by $\int S^{0ij}dV$.

All quantities mentioned here are derived from the Lagrangian. If this Lagrangian is of first order in derivatives, constant field terms can be added without any effect on the energy-momentum tensor, as the symmetrized energy-momentum (2.36) and angular momentum (2.39) tensors only differ from the canonical tensors by a divergence term. This divergence term vanishes for fields that vanish at infinity, which seems to pose a problem as Bessel beams extend to infinity in the longitudinal direction. However, since they are also invariant in the longitudinal direction, none of the quantities considered depend on the longitudinal coordinate and are effectively line densities.

Spin is an important characteristic to distinguish particles. The spin quantum number s is related to the square of the Pauli-Lubanski pseudovector:

$$C_2 = W_\mu W^\mu = -m^2 s(s+1),$$

where m is the mass of the particle. This operator C_2 is one of two *Casimir operators* of the Poincaré group; operators that commute with all generators of transformations in that group. The Poincaré group combines translations with the

Lorentz group. These need to be included as translations are generated by the momentum operators, defining the first Casimir operator

$$C_1 = P_\mu P^\mu.$$

The two Casimir operators describe the two kinematic properties that are used to characterize a particle: spin and mass [49]. The second Casimir operator, although it is related to spin, cannot be the square of the spin operator $\mathbf{S}^2$ as this does not commute with all generators of the Lorentz group[7]. Instead it is determined by the Pauli-Lubanski pseudovector, incorporating the total angular momentum (derived from (2.39)), given by:

$$W^\mu = \frac{1}{2}\epsilon^{\mu\nu\rho\sigma} M_{\nu\rho} P_\sigma. \tag{2.40}$$

with P_σ the momentum vector and $M_{\nu\rho}$ the total angular momentum. This expression confirms that the total AM is given by the integral over all space of the angular momentum density (2.39):

$$M_{\nu\rho} = \int d^3\mathbf{r}\; M_{0\nu\rho} = \int d^3\mathbf{r}\; T_{0\rho} x_\nu - T_{0\nu} x_\rho - S_{0\rho\nu},$$

where $S_{0\rho\nu}$ is given by (2.33). Using these definitions, the Pauli-Lubanski tensor can be expressed in terms of the canonical momentum $\pi_\lambda = \frac{\partial \mathcal{L}}{\partial(\partial_t \phi^\lambda)}$ as [114]

$$W^\mu = -\frac{1}{2}\epsilon^{\mu\nu\rho\sigma} \int d^3\mathbf{r}\; \pi_\lambda (\mathcal{M}_{\rho\nu})^\lambda{}_\nu \phi^\nu,$$

which agrees with the expression (2.40).

2.4.3 Symmetric energy-momentum tensor for spinor and vector fields

The symmetrization procedure (2.35) can be implemented to derive the symmetrized energy-momentum tensor of both the spinor and vector field. For the spinor field the substitution $\mathcal{M}^{\mu\nu} \to \Sigma^{\mu\nu}$ is made as now the spinor generators of the Lorentz group (1.31) need to be used. With the Dirac Lagrangian given by (2.20), the derivative terms are given by $\frac{\partial \mathcal{L}}{\partial(\partial_\mu \psi)} = i\bar{\psi}\gamma^\mu$. Inserting these in (2.35) gives

$$\begin{aligned}\Theta^{\mu\nu} - T^{\mu\nu} &= -\frac{1}{2}\partial_\kappa \left[\bar{\psi}_\ell \gamma^\kappa (\Sigma^{\mu\nu})^\ell{}_m \psi^m - \bar{\psi}_\ell \gamma^\mu (\Sigma^{\kappa\nu})^\ell{}_m \psi^m - \bar{\psi}_\ell \gamma^\nu (\Sigma^{\kappa\mu})^\ell{}_m \psi^m\right], \\ &= -\frac{i}{4}\left(\bar{\psi}\gamma^\mu \partial^\nu \psi + \bar{\psi}\gamma^\nu \partial^\mu \psi + (\partial^\mu \bar{\psi})\gamma^\nu \psi + (\partial^\nu \bar{\psi})\gamma^\mu \psi\right).\end{aligned} \tag{2.41}$$

[7] Further, spin also corresponds to a rotation group symmetry $SU(2)$, but only when $m^2 > 0$ [78]. This explains why the polarization states of massless particles are $S_z = \pm S$ only.

This expression could also be found by inspection; it can be deduced that adding two terms to the canonical Dirac energy-momentum tensor (2.25) with the indices interchanged will give a symmetric tensor:

$$\Theta^{\mu\nu} = \frac{i}{4}\left(\bar{\psi}\gamma^{\mu}\partial^{\nu}\psi + \bar{\psi}\gamma^{\nu}\partial^{\mu}\psi - (\partial^{\mu}\bar{\psi})\gamma^{\nu}\psi - (\partial^{\nu}\bar{\psi})\gamma^{\mu}\psi\right). \tag{2.42}$$

Working out the different components in matrix form separately gives a relationship similar to the Gordon decomposition, (2.29) and (2.30) but now for energy and momentum densities, and in terms of $\psi^{\dagger}$ instead of $\bar{\psi}$:

$$\Theta^{00} - T^{00} = \frac{i}{2}\nabla\cdot\left[\psi^{\dagger}\begin{pmatrix} 0 & \boldsymbol{\sigma} \\ \boldsymbol{\sigma} & 0 \end{pmatrix}\psi\right],$$
$$\Theta^{0j} - T^{0j} = \frac{1}{2}\left[\nabla\times(\psi^{\dagger}\mathbf{S}\psi)\right]^{j} = -\Theta^{j0} + T^{j0}.$$

For the shear stresses, since the canonical normal stresses are diagonal, the spin contribution becomes:

$$\Theta^{pq} - T^{pq} = \frac{1}{2}\epsilon^{pqr}\partial_t\left[\psi^{\dagger}S_r\psi\right] + \frac{1}{4}\epsilon^{pqr}\partial_r\left[\bar{\psi}\begin{pmatrix} 0 & \mathbb{1} \\ -\mathbb{1} & 0 \end{pmatrix}\psi\right].$$

It can be expected that the first term is zero, since the product $\psi^{\dagger}\psi$ is not time-dependent. Neither does this product depend on z, predicting that the $r\phi-$ and $\phi r-$ stresses have no spin correction.

With the electromagnetic Lagrangian given by (2.22), the derivative terms in (2.35) are given by $\frac{\partial\mathcal{L}}{\partial(\partial_\gamma\Psi^{\ell})} = -F^{\gamma}_{\ell}$. Inserting these into the Belinfante-Rosenfeld tensor the extra contributions to the energy-momentum tensor are given by:

$$\begin{aligned}\Theta^{\mu\nu} - T^{\mu\nu} &= \frac{1}{2}\partial_\gamma\left[F^{\gamma}_{\lambda}(\mathcal{M}^{\mu\nu})^{\lambda}_{\rho}A^{\rho} - F^{\mu}_{\lambda}(\mathcal{M}^{\gamma\nu})^{\lambda}_{\rho}A^{\rho} - F^{\nu}_{\lambda}(\mathcal{M}^{\gamma\mu})^{\lambda}_{\rho}A^{\rho}\right], \\ &= F^{\mu\gamma}\partial_\gamma A^{\nu}.\end{aligned} \tag{2.43}$$

The canonical tensor components and the spin contributions are given in the following table, for different values of μ and ν:

$\mu\nu$	Canonical	Spin contribution
00	$(-\partial_t\mathbf{A})\cdot\mathbf{E} + \frac{1}{2}(-E^2+B^2)$	$-\mathbf{E}\cdot\nabla V$
$j0$	$-E_j\partial_t V - (\partial_t\mathbf{A}\times\mathbf{B})_j$	$E_j\partial_t V + (\mathbf{E}\times\mathbf{B})_j + (\partial_t\mathbf{A}\times\mathbf{B})_j$
$0j$	$\mathbf{E}\cdot\partial^j\mathbf{A}$	$-(\mathbf{E}\cdot\nabla)\mathbf{A}_j$
ij	$(\partial_j V)E_i - (\mathbf{B}\times\nabla_j\mathbf{A})_i$	$E_i\partial_t A_j + (\mathbf{B}\times\nabla A_j)_i$
jj	$(\partial_j V)E_j - (\mathbf{B}\times\nabla_j\mathbf{A})_j + \frac{1}{2}(E^2-B^2)$	$E_j\partial_t A_j + (\mathbf{B}\times\nabla A_j)_j$

Table 2.1: The separation of the energy-momentum tensor of the electromagnetic field in a canonical and spin part.

Combining the canonical energy-momentum tensor (2.26) with (2.43) gives the total symmetrized energy-momentum tensor:

$$\Theta^{\mu\nu} = F^{\mu}_{\ \gamma} F^{\gamma\nu} + \frac{1}{4}\eta^{\mu\nu} F^{\alpha\beta} F_{\alpha\beta}. \tag{2.44}$$

This energy-momentum tensor, also known as the electromagnetic stress-energy tensor, has the following familiar expressions:

$$\begin{aligned}
&\text{Energy density} && \Theta^{00} &&= \tfrac{1}{2}(E^2 + B^2),\\
&\text{Poynting vector } (\boldsymbol{\mathcal{S}}) && \Theta^{0j} = \Theta^{j0} &&= (\mathbf{E}\times\mathbf{B})_j,\\
&\text{Normal stress} && \Theta^{ij} = \Theta^{ji} &&= -E_iE_j - B_iB_j,\\
&\text{Shear stress} && \Theta^{jj} &&= -E_jE_j - B_jB_j + \tfrac{1}{2}(E^2+B^2).
\end{aligned} \tag{2.45}$$

Similar to the Gordon decomposition of the Dirac gauge current into an orbital and spin part (2.30), the spin contribution to the Poynting vector can be expressed as the curl of the spin current, $\mathbf{S} = \mathbf{E}\times\mathbf{A}$ [115]:

$$\boldsymbol{\mathcal{S}} - \mathbf{T} = -(\mathbf{E}^*\cdot\nabla)\mathbf{A} = \frac{i}{2\omega}\nabla\times(\mathbf{E}^*\times\mathbf{E}) = \frac{1}{2}\nabla\times\mathbf{S}.$$

In the following chapters, the Poynting vector and its canonical part will be calculated. The spin part can be found by calculating the difference between the two. The canonical part of the Poynting vector, T^{0j} is given by

$$\mathbf{T} = \mathbf{E}\cdot\nabla\mathbf{A}. \tag{2.46}$$

When calculating these vector products in cylindrical coordinates, care has to be taken as the derivatives are replaced by the covariant derivatives:

$$\nabla_j\mathbf{u} \to D_j\mathbf{u} = \left(\frac{\partial u_i}{\partial x^j} + \Gamma^{i}_{\ kj}u^k\right)\hat{\mathbf{e}}_i.$$

Here $\Gamma^{i}_{\ kj}$ are the Christoffel symbols describing the metric connection

$$\Gamma^{\mu}_{\ \nu\rho} = \frac{1}{2}g^{\mu\alpha}\left(\partial_\rho g_{\alpha\nu} + \partial_\nu g_{\alpha\rho} - \partial_\alpha g_{\nu\rho}\right),$$

with the metric given by $g_{\mu\nu} = \text{diag}(1,-1,-r^2,-1)$. The only non-zero Christoffel symbols are $\Gamma^{\phi}_{\ r\phi} = \Gamma^{\phi}_{\ \phi r} = r^{-1}$ and $\Gamma^{r}_{\ \phi\phi} = -r$. This gives for the derivatives on $\mathbf{A}$ the following changes:

$$\partial_\phi A_r \to \tfrac{1}{r}\partial_\phi A_r - \tfrac{1}{r}A_\phi, \quad \partial_\phi A_\phi \to \tfrac{1}{r}\partial_\phi A_\phi + \tfrac{1}{r}A_r, \quad \partial_\phi A_z \to \tfrac{1}{r}\partial_\phi A_z.$$

These modifications need to be taken into account when calculating the components of the canonical energy-momentum tensor $\mathbf{T}$, as can be verified by

calculating them in Cartesian coordinates first and then transforming them to cylindrical polar coordinates.

In this section, the contribution from the spin current of non-scalar fields to the energy-momentum tensor was considered, and to the gauge current for the Dirac field, described by the Gordon decomposition. All these quantities can be split into a spin part, an orbital part and a scalar part. These quantities will be calculated for both optical vortex beams and EVBs in chapter 3, to compare these fields and draw conclusions about the effects of describing massless fields compared to massive fields, and spinor fields compared to vector fields.

2.5 The optical angular momenta

In this section, the concepts of optical helicity, chirality and spin angular momentum will be explained. Optical chirality is closely related to optical helicity, but different from the chirality for Dirac fields. The differences between helicity and spin angular momentum will be discussed, and considerations of the optical angular momenta operators will lead to an explanation for the spin-to-orbital AM conversion mentioned in section 1.4.2. In this section the conventions as for circular polarization as explained in section 1.5 will be used.

2.5.1 Helicity

The spin angular momentum of a plane wave is measured in units of helicity; a right-handed circularly polarized wave has one positive unit of angular momentum, corresponding to helicity $+1$. A left-handed circularly polarized wave has helicity -1 and a linearly polarized wave has helicity 0. By convention, right-handed polarization means an anti-clockwise rotation relative to the propagation direction; the sense of rotation is in the direction of the momentum. As helicity depends on the momentum direction, the helicity of a collection of waves is a measure of circular polarization in the momentum representation [116]. Expanding a field in circularly polarized waves gives the helicity operator form

$$\hat{\mathcal{H}} = \sum_{\mathbf{k}} \hbar(\hat{n}_{\mathbf{k},R} - \hat{n}_{\mathbf{k},L}),$$

where $\hat{n}_{\mathbf{k},R/L}$ is the number operator for plane waves with right/left-handed helicity. Using the conventions mentioned in section 1.5, this expression is equivalent to the one in [117, 118] up to a factor (-1).

The electric and magnetic fields associated with a circularly polarized wave rotate about the propagation axis upon propagation; there is no preferred direction of the fields. This makes the fields invariant under a rotation over $\pm\alpha$ in the transverse plane [119]:

$$\begin{aligned}\mathbf{E}' &= \cos(\alpha)\mathbf{E} + \sin(\alpha)\mathbf{B},\\ \mathbf{B}' &= -\sin(\alpha)\mathbf{E} + \cos(\alpha)\mathbf{B},\end{aligned} \tag{2.47}$$

as this transformation does not change the phase difference between $\mathbf{E}$ and $\mathbf{B}$. It can be concluded that helicity is the generator of rotations of the fields around the momentum direction, see figure 2.3. This symmetry is called the Heaviside-Larmor symmetry or duality symmetry and is conserved by Maxwell's equations. Boundaries between different media can break or conserve the duality symmetry, depending on the values of ϵ and μ of the different media [120]. This will be discussed in more detail in chapter 5.

The Heaviside-Larmor symmetry (2.47) suggest that there is a similar symmetry connecting the *vector* potentials of $\mathbf{E}$ and $\mathbf{B}$. For this purpose a vector potential $\mathbf{C}$ for the electric field needs to be introduced: $\mathbf{E} = -\nabla \times \mathbf{C}$. Working in the Coulomb gauge, the two potentials are related to each other in a way similar to the relation between the electric and magnetic fields; $\nabla \times \mathbf{C} = \partial_t \mathbf{A}$ and $\nabla \times \mathbf{A} = -\partial_t \mathbf{C}$.[8] The potentials are also related to each other by a duality rotation:

$$\begin{aligned}\mathbf{A}' &= \cos(\alpha)\mathbf{A} + \sin(\alpha)\mathbf{C},\\ \mathbf{C}' &= -\sin(\alpha)\mathbf{A} + \cos(\alpha)\mathbf{C}.\end{aligned} \tag{2.48}$$

With these definitions, a quantity that has the desired properties of helicity, a time-even pseudoscalar with units of angular momentum, can be defined as;

$$\mathcal{H} = \int d^3\mathbf{r}\; h = \int d^3\mathbf{r}\; \frac{1}{2}\left(\mathbf{A}\cdot\mathbf{B} - \mathbf{C}\cdot\mathbf{E}\right). \tag{2.49}$$

This helicity density is the conserved quantity associated with duality transformations. These transformations are symmetry transformations of the field equations and not of the Lagrangian, and hence the helicity cannot be found by Noether's theorem. However, there are ways to modify the Lagrangian such that the duality

[8] It is also possible to develop a dual-symmetric theory of electromagnetism with non-zero scalar potentials [121]. The vector potentials are split in a perpendicular and parallel part and are hence related as follows:

$$\begin{aligned}\partial_t \mathbf{A}^{\perp} &= -\nabla \times \mathbf{C}^{\perp} \quad & -\partial_t \mathbf{A}^{\parallel} &= \nabla V,\\ \partial_t \mathbf{C}^{\perp} &= \nabla \times \mathbf{A}^{\perp} \quad & -\partial_t \mathbf{C}^{\parallel} &= \nabla \Theta.\end{aligned}$$

with Θ the scalar potential of the magnetic field; $\mathbf{B} = -\nabla\Theta - \partial_t \mathbf{C}$. However, throughout this thesis the Coulomb gauge will be adopted, choosing $V = 0$.

transformations become symmetry transformations of the Lagrangian with an associated conserved current [122].

Maxwell's equations (1.35) in terms of the field tensor $F^{\mu\nu} = \partial^\mu A^\nu - \partial^\nu A^\mu = (\mathbf{E}, \mathbf{B})$ can be written in four-vector notation as:

$$\partial_\nu F^{\mu\nu} = 0 \quad , \quad \tfrac{1}{2}\epsilon^{\mu\nu\sigma\tau}\partial_\nu F_{\sigma\tau} = 0.$$

A dual-symmetric field tensor $G^{\mu\nu}$ can be defined in terms of the vector potential C^μ;

$$G^{\mu\nu} = \partial^\mu C^\nu - \partial^\nu C^\mu = (\mathbf{B}, -\mathbf{E}).$$

Since $G^{\mu\nu} = \frac{1}{2}\epsilon^{\mu\nu\sigma\tau}F_{\sigma\tau}$, the second Maxwell equation becomes $\partial_\nu G^{\mu\nu} = 0$. With these two field tensors the dual-symmetric Lagrangian becomes:

$$\mathcal{L} = -\frac{1}{8}(F^{\mu\nu}F_{\mu\nu} + G^{\mu\nu}G_{\mu\nu}).$$

If the duality transformation (2.48) is a symmetry transformation of this Lagrangian, the current h^γ is conserved;

$$h^\gamma = \frac{1}{2}(A_\alpha G^{\alpha\gamma} - C_\alpha F^{\alpha\gamma}).$$

The 0-component of this current is of the same form as (2.49). The spatial components turn out to be the SAM components, as discussed in the next section.

2.5.2 Orbital and Spin AM

As mentioned in section 1.4.2, the spin and orbital angular momentum of light cannot be completely distinguished from each other. This can be explained by considering the total angular momentum (2.38), given by the cross product of the position and momentum density that is described by the Poynting vector:

$$\mathbf{J} = \int d^3\mathbf{r}\ \mathbf{r} \times \mathbf{p} = \int d^3\mathbf{r}\ \mathbf{r} \times (\mathbf{E} \times \mathbf{B}).$$

This integral can be split into an intrinsic and extrinsic part, using the identities of both vector potentials:

$$\mathbf{J} = \int d^3\mathbf{r}\ \frac{1}{2}\left(E_i(\mathbf{r}\times\nabla)A_i + B_i(\mathbf{r}\times\nabla)C_i\right) + \int d^3\mathbf{r}\ \frac{1}{2}\left(\mathbf{E}\times\mathbf{A} + \mathbf{B}\times\mathbf{C}\right). \quad (2.50)$$

The first integral is extrinsic, as it depends on the choice of the origin of the coordinate system. This is the quantity that is identified with the OAM. The second

integral is intrinsic, and henceforth identified with the SAM. In the momentum representation it is given by [116]:

$$\mathbf{S} = \int d^3\mathbf{r}\, \frac{1}{2}\left(\mathbf{E}\times\mathbf{A} + \mathbf{B}\times\mathbf{C}\right) = \sum_{\mathbf{k}} \hbar(\hat{n}_{\mathbf{k},R} - \hat{n}_{\mathbf{k},L})\frac{\mathbf{k}}{|\mathbf{k}|}. \tag{2.51}$$

However, in 1994 van Enk and Nienhuis [70] realized that the optical spin and orbital angular momentum operators do not follow the commutation rules for AM operators[9]:

$$[S_i, S_j] = 0, \quad [L_i, L_j] = i\epsilon_{ijk}(L_k - S_k), \quad [L_i, S_j] = i\epsilon_{ijk}S_k.$$

This implies that the AM operators are not independent of each other. This observation can be explained by considering the rotations that the OAM and SAM generate; both rotate the electric and magnetic fields in ways that do not preserve the transversality. The SAM is associated with the vector nature of the field, and should rotate the directions of $\mathbf{E}$ and $\mathbf{B}$, while the OAM is associated with the spatial dependence and should rotate the fields in space while leaving their directions unchanged. These rotations are ideally described by [124]:

$$\begin{aligned} &\text{OAM} \quad \mathbf{E}' = \mathbf{E} + \boldsymbol{\alpha}\cdot(\mathbf{r}\times\nabla)\mathbf{E}, && \nabla\cdot\mathbf{E}' = \boldsymbol{\alpha}\cdot\partial_t\mathbf{B}, \\ &\text{SAM} \quad \mathbf{E}' = \mathbf{E} - \boldsymbol{\alpha}\times\mathbf{E}, && \nabla\cdot\mathbf{E}' = -\boldsymbol{\alpha}\cdot\partial_t\mathbf{B}. \end{aligned} \tag{2.52}$$

However, the action of the optical SAM actually corresponds to a rotation through $\boldsymbol{\alpha}\cdot\hat{\mathbf{k}}$, see figure 2.3. The OAM and SAM operators have the following effect on the fields [124]:

$$\begin{aligned} &\text{“OAM”} \quad \mathbf{E}' = \mathbf{E} + \left[(\boldsymbol{\alpha}\cdot(\mathbf{r}\times\nabla)\mathbf{E}\right]^{\perp}, \\ &\text{“SAM”} \quad \mathbf{E}' = \mathbf{E} - (\boldsymbol{\alpha}\times\mathbf{E})^{\perp}. \end{aligned} \tag{2.53}$$

However, this is an approximation of the true rotations, since only the transverse part is taken into account, and reflects that the optical spin is not a true angular momentum [116].

[9] There is another separation of the Poynting vector possible: the separation into helicity components $\mathbf{E}_{\pm}$ [123]. The orbital current splits into three parts; two that are purely right- or left-handed and one mixed part. The spin current does not have this mixed part. However, when applying the duality symmetry, the mixed term splits up as well:

$$\begin{aligned} \mathcal{S}_{\text{orb}} &= \frac{1}{2}(\mathcal{S}_{\text{orb},E_+} + \mathcal{S}_{\text{orb},E_-} + \mathcal{S}_{\text{orb},H_+} + \mathcal{S}_{\text{orb},H_-}), \\ \mathcal{S}_{\text{spin}} &= \frac{1}{2}(\mathcal{S}_{\text{spin},E_+} + \mathcal{S}_{\text{spin},E_-} + \mathcal{S}_{\text{spin},H_+} + \mathcal{S}_{\text{spin},H_-}). \end{aligned}$$

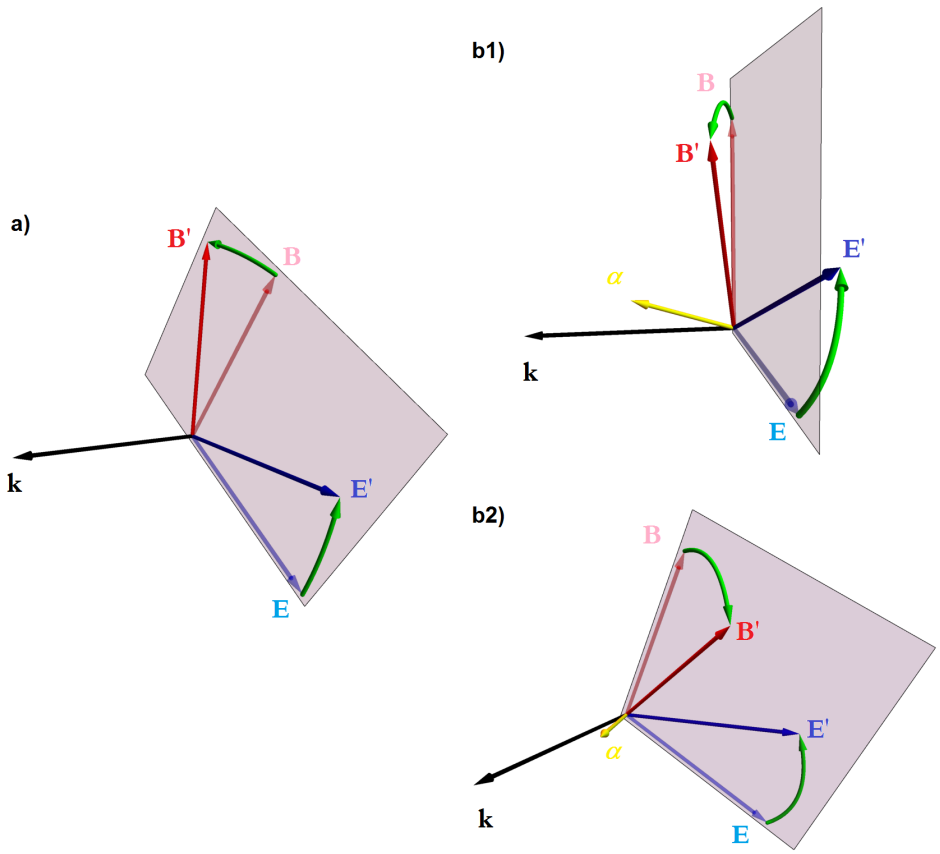

Figure 2.3: Rotations of the electromagnetic field generated by helicity and spin. a): Rotations generated by helicity, conserving the transversality of the electric and magnetic field. b1) and b2): Rotations generated by spin, as described by (2.53). These figures show clearly that the electric field is rotated *away* from the wavevector, and with a positive sense in the xy-plane, while the magnetic field is rotated *towards* the momentum vector with a negative rotation in the xy-plane. It can be concluded that the rotations generated by the SAM do not conserve transversality.

These rotations do not individually conserve transversality, only the combined action of both does. This is also reflected in the expectation values of the AM operators; it was found [71] that these are coupled to each other:

$$\mathbf{S} = \sigma \cos(\theta)\hat{\mathbf{P}}; \qquad \mathbf{L} = (\ell + \sigma\,[1 - \cos(\theta)])\,\hat{\mathbf{P}}. \tag{2.54}$$

where $\hat{\mathbf{P}} = \frac{\mathbf{P}}{P}$ and θ is the azimuthal opening angle of the waves, as illustrated in figure 1.1. Although the total angular momentum $\mathbf{J}$ is conserved, $J_z = S_z + L_z = \sigma + \ell$, equation (2.54) shows that part of the SAM is transferred to OAM; this is called *spin-to-orbital AM conversion*. A direct consequence of this is that the OAM

becomes helicity-dependent. In the limit of the opening angle $\theta \to \pi/2$, all SAM will be converted to OAM.

However, in the paraxial limit $\theta \to 0$ the values for a plane wave are recovered: $\mathbf{S} = \sigma\hat{\mathbf{P}},\ \mathbf{L} = \ell\hat{\mathbf{P}}$. This is in agreement with the observation that, since the longitudinal components of the fields are very small [124], the expressions for the rotated fields (2.53) are close to the ideal ones (2.52).

Expressions of the angular momenta could also be derived from the Belinfante AM tensor. The components of this tensor obey the commutation relations of the angular momentum operators, but are not gauge invariant as only the transverse parts of the tensor are gauge invariant. Laser experiments show that the gauge-invariant quantities are the physically relevant ones [107]. These are the OAM and SAM operators as derived by van Enk and Nienhuis (2.50), that have the problem that they do not commute. However, the helicity can be derived from either operator, and is meaningful for both.

It can be concluded that SAM and OAM are not separable from each other as the rotations that generate them do not conserve Maxwell's equations. They are only approximately independent in the paraxial limit. This will be confirmed in chapter 3 when calculating the expectation values of the SAM and OAM operators for optical Bessel beams.

2.5.3 Conservation of helicity and spin

The expressions for the optical helicity (2.49) and spin (2.51) resemble the expressions for the energy and momentum densities of the optical field:

$$\begin{aligned} \mathcal{H} &= \tfrac{1}{2}\left(\mathbf{A}\cdot\mathbf{B} - \mathbf{C}\cdot\mathbf{E}\right), & \mathcal{E} &= \tfrac{1}{2}\left(\mathbf{B}\cdot\mathbf{B} + \mathbf{E}\cdot\mathbf{E}\right), \\ & & \leftrightarrow & \\ \mathbf{S} &= \tfrac{1}{2}\left(\mathbf{E}\times\mathbf{A} + \mathbf{B}\times\mathbf{C}\right), & \mathcal{S} &= \tfrac{1}{2}\left(\mathbf{E}\times\mathbf{B} - \mathbf{B}\times\mathbf{E}\right). \end{aligned}$$

The transition from the expressions on the left to the right is made by the substitutions $\mathbf{A} \to \mathbf{B},\ \mathbf{C} \to -\mathbf{E}$. This shows that spin describes the flow of helicity; the helicity density h and spin density $\mathbf{s}$ form a conserved four-current:

$$\partial_t \mathcal{H} + \nabla\cdot\mathbf{S} = 0. \tag{2.55}$$

However, momentum is also a conserved quantity

$$\partial_t P_i + \partial_j \Theta_{ij} = 0,$$

where Θ_{ij} is symmetric energy-momentum tensor (2.45). Following this analogy, an expression for the tensor that describes the flow of optical spin can be found. The components of this tensor are the ij-infra-zilches [116]:

$$n_{ij} = \frac{1}{2}\left((\mathbf{A}\cdot\mathbf{B} - \mathbf{C}\cdot\mathbf{E})\delta_{ij} - A_iB_j - A_jB_i + C_iE_j + C_jE_i\right).$$

The optical helicity density and spin currents of Bessel beams will be considered in chapter 3.

2.5.4 Chirality

The substitutions $\mathbf{A} \to \mathbf{B},\ \mathbf{C} \to -\mathbf{E}$, to transform the helicity density to the energy density of the electromagnetic field, are equivalent to $\mathbf{A} \to \nabla\times\mathbf{A},\ \mathbf{C} \to \nabla\times\mathbf{C}$. However, Maxwell's equations retain their form under the transformation $\mathbf{F} \to \nabla\times\mathbf{F}$ for any field, and replacing *all* fields in the expression of the optical helicity density (2.49) gives the expression of the optical chirality:

$$\mathcal{H} = \frac{1}{2}\left(\mathbf{A}\cdot\mathbf{B} - \mathbf{E}\cdot\mathbf{C}\right) \quad \to \quad \chi = \frac{1}{2}\left(\mathbf{B}\cdot(\nabla\times\mathbf{B}) + \mathbf{E}\cdot(\nabla\times\mathbf{E})\right).$$

Chirality for spinor fields was discussed in section 2.1.1, indistinguishable from helicity for massless fermions. However, optical chirality is distinguishable from the optical helicity, as the field expansion in the momentum representation shows that chirality can be considered as the energy-weighted helicity [118]:

$$\chi = \hbar\sum_{\mathbf{k}} k^2(\hat{n}_{\mathbf{k},R} - \hat{n}_{\mathbf{k},L}).$$

For monochromatic fields, chirality is proportional to helicity: $\chi = k^2\mathcal{H}$. It is associated[10] with the following symmetry transformation of the fields [125]:

$$\begin{array}{l}\mathbf{A}' = \mathbf{A} + \eta\nabla\times\partial_t\mathbf{A} \\ V' = V\end{array} \quad\to\quad \begin{array}{l}\mathbf{E}' = \mathbf{E} - \eta\nabla^2\mathbf{B} \\ \mathbf{B}' = \mathbf{B} + \eta\nabla^2\mathbf{E}\end{array}.$$

To conclude, helicity and SAM are indistinguishable for plane waves. For a collection of plane waves the SAM describes the flow of optical helicity. The SAM and OAM are not conserved separately as they do not conserve Maxwell's equations individually, only approximately in the paraxial limit.

[10] The conserved quantity related to this transformation is equal to the chirality density, up to a divergence term:

$$\partial_i\left(-\frac{1}{2}V\partial_tB^i + A_j(\partial^iB^j - \partial^jB^i)\right).$$

The conserved quantities discussed in this chapter, the gauge currents for the spinor field, the optical helicity and spin currents and the energy-momentum tensor components for both spinor and vector fields, will be calculated in the next two chapters. Chapter 3 will focus on the difference between spin-polarized and helical beams, while chapter 4 will consider linearly polarized beams. Further, chapter 5 will consider the optical Majorana states, and draw parallels with the fermionic Majorana states and the description of $\mathcal{C}, \mathcal{P}$ and $\mathcal{T}$ reversal for spinor fields.

3

Vector and spinor Bessel beams quantized by spin or helicity

The optical vortex beams created in the experiments mentioned in chapter 1 were all scalar beams; only the intensity and not the polarization of the light was considered. Similarly for electron vortex beams, all electron vortex beams that have been generated are scalar beams. The only studies into spinor Bessel beams have been theoretical, although vector Bessel beams have been studied both theoretically and experimentally[1].

When the spin of the fields is considered, a distinction can be made between different polarization states; circularly or linearly polarized, or helical. This chapter will focus on the differences between the circularly polarized beams and the helical beams. It can be predicted from the Bessel beam spectrum that these beams are very similar and even coincide in the paraxial limit.

The small differences become noticeable when investigating the conserved quantities of the vortex beams, such as the energy and probability density. By comparing these quantities with the corresponding quantities for a scalar Bessel beam, conclusions can be drawn about the manifestation of spin- and spin-orbit coupling effects.

These differences appear because the Bessel beam spectrum consists of a collection of plane waves spread out over a cone centred on the propagation axis (1.8). A longitudinally polarized beam has a distinct polarization direction, while a helical beam is constructed from waves that all have the same helicity. Every plane wave is rotated away from the propagation direction given by the spherical angles (θ, ϕ). This rotation is described by equations (1.45) for vector and (1.49) for spinor fields. The helical vector (spinor) fields, indicated by the superscript h, are as a result related to the spin-polarized vector (spinor) fields, indicated by the superscript s, by

[1] For relevant bibliography see chapter 1

$$\begin{pmatrix} \mathbf{F}^h_+ \\ \mathbf{F}^h_- \\ \vdots \end{pmatrix} = U(\theta,\phi) \begin{pmatrix} \mathbf{F}^s_+ \\ \mathbf{F}^s_- \\ \mathbf{F}^s_0 \end{pmatrix}, \qquad \begin{pmatrix} \psi^h_+ \\ \psi^h_- \end{pmatrix} = \widetilde{U}(\theta,\phi) \begin{pmatrix} \psi^s_+ \\ \psi^s_- \end{pmatrix}.$$

Since photons do not have a longitudinal polarization state $\mathbf{F}^s_0$, i.e. electromagnetic waves are transverse, the relationship between the optical helicity and spin states becomes:

$$\mathbf{F}^h_\pm = \cos^2(\theta/2)\mathbf{F}^s_\pm - \sin^2(\theta/2)e^{\pm 2i\phi}\mathbf{F}^s_\mp. \tag{3.1}$$

And spinor helicity states can be expressed in spinor spin states as follows:

$$\psi^h_\pm = \cos(\theta/2)\psi^s_\pm \pm \sin(\theta/2)e^{\pm i\phi}\psi^s_\mp. \tag{3.2}$$

This shows that in the paraxial limit $\theta \to 0$, the helicity and spin states indeed coincide, but if $\theta \neq 0$ a helicity state comprises a small contribution from the state with opposite spin. An important difference between spinor and vector fields is that the proportionality constants for the vector fields are those of the spinor fields squared, a result from (1.45) being the 2^{nd}-induced matrix of (1.49) [126, 127].

3.1 Vector Bessel beams

In this section the vector Bessel beams will be derived, both polarized by helicity or spin. These can be compared with each other to draw conclusions about the differences between helicity and spin polarization for optical beams. Vector Bessel beams can be described in different polarization states, for example linearly [128] or azimuthally [129]. In reference [130] various different polarization states, and the possibility of generating these beams with axicons, conically shaped optical elements, were discussed. Vector Bessel-Gauss beams were also described in 1996 [131] and 1998 [132].

The first experiment that considered the mechanical effects of both the SAM and OAM of the light beams simultaneously was in 2003 [133], where the transfer of AM to a particle positioned in the beam was studied. The beam was created with an axicon, and circularly polarized by inserting a quarter-wave plate.

The experimental generation of a vector Bessel beam can be described in a couple of steps. First a Bessel beam is created in the way pioneered by Durnin [25], using a diffraction grating. This is followed by passing the beam through a polarization filter to create a linearly polarized Bessel beam [134]. Confusingly,

this is sometimes called a scalar beam in the literature [135]. This linearly polarized beam can then be converted into a radially or azimuthally polarized beam by a q-plate[2] [134]. Helical Bessel beams can, technically speaking, be generated by Durnin's initial method, while approximations to helicity-polarized Bessel beams are created by converting a linearly polarized beam into a circularly polarized beam with the aid of a quarter-wave plate [137]. The authors make no distinction between helical or circularly polarized Bessel beams.

Other methods to generate vector Bessel beams include using a spatial light modulator to create a scalar Bessel beam and converting this to a vector beam using an azimuthally varying birefringent plate [135]. In addition, metasurfaces can be used to manipulate the polarization of the beams [138] and Bessel beams that have a spatially varying polarization can be generated by superimposing oppositely polarized Bessel beams [139].

There have been a number of studies into the polarization effects on the properties of Bessel and Bessel-Gauss beams [140, 134, 141], comparing radially and azimuthally polarized beams. These will be discussed in chapter 4.

3.1.1 Helical optical Bessel beams

The first beams to consider are the helicity vector beams. These are optical fields consisting of plane waves that all have the same helicity.

The theoretical derivation of helical Bessel beams is described in [71, 79]. The rotation of the plane waves away from the propagation axis (1.45) gives rise to the following helicity fields in the polarization basis (1.14):

$$\mathbf{E}_{+}^{h,\ell}(t,\mathbf{r}) = \begin{pmatrix} J_\ell \\ \tan^2(\theta/2) J_{\ell+2} e^{2i\phi} \\ -i\sqrt{2}\tan(\theta/2) J_{\ell+1} e^{i\phi} \end{pmatrix} e^{-i\omega t + ik_z z + i\ell\phi}, \tag{3.3a}$$

$$\mathbf{E}_{-}^{h,\ell}(t,\mathbf{r}) = \begin{pmatrix} \tan^2(\theta/2) J_{\ell-2} e^{-2i\phi} \\ J_\ell \\ i\sqrt{2}\tan(\theta/2) J_{\ell-1} e^{-i\phi} \end{pmatrix} e^{-i\omega t + ik_z z + i\ell\phi}. \tag{3.3b}$$

All Bessel beams have argument $k_r r$, and the total field is rescaled by $\cos^2(\theta/2)$. The subscript $\pm$ denotes the polarization state of the *local* field, i.e. the individual plane waves and the superscript ℓ the OAM value of the largest component. These beams correspond to part b) of figure 1.6. There is a small longitudinal

[2] A q-plate is a slab of material with liquid crystal molecules that are aligned according to the azimuthal angle divided by a half-integer q; ϕ/q [136].

spin component proportional to $\tan(\theta/2)$. Further, the component with opposite polarization is also non-zero and proportional to $\tan^2(\theta/2)$. Hence these two components will vanish in the paraxial limit, as expected.

The corresponding magnetic fields, found by using $\partial_t \mathbf{B} = -i\omega\mathbf{B} = -\nabla \times \mathbf{E}$, are:

$$\mathbf{B}_+^{h,\ell}(t,\mathbf{r}) = -i \begin{pmatrix} J_\ell \\ \tan^2(\theta/2) J_{\ell+2} e^{2i\phi} \\ -i\sqrt{2}\tan(\theta/2) J_{\ell+1} e^{i\phi} \end{pmatrix} e^{-i\omega t + ik_z z + i\ell\phi}, \tag{3.4a}$$

$$\mathbf{B}_-^{h,\ell}(t,\mathbf{r}) = i \begin{pmatrix} \tan^2(\theta/2) J_{\ell-2} e^{-2i\phi} \\ J_\ell \\ i\sqrt{2}\tan(\theta/2) J_{\ell-1} e^{-i\phi} \end{pmatrix} e^{-i\omega t + ik_z z + i\ell\phi}. \tag{3.4b}$$

These magnetic fields are proportional to the electric field; $\mathbf{B}_\pm^{h,\ell} = \mp i \mathbf{E}_\pm^{h,\ell}$, which shows that these fields are indeed helicity fields, as explained in section 1.5.1; they are curl eigenstates. The largest components of the electric and magnetic fields correspond to the same polarization states as the fields are described in the polarization basis (1.14).

These helicity beams are eigenstates of the TAM operator in the $\hat{\mathbf{z}}$ direction, but with the helicity quantum number fulfilling the role of SAM:

$$\langle \mathbf{E}_\pm^{h,\ell} | L_z | \mathbf{E}_\pm^{h,\ell} \rangle = \ell \langle \mathbf{E}_\pm^{h,\ell} | \mathbf{E}_\pm^{h,\ell} \rangle \pm 2\tan^2(\theta/2) J_{\ell\pm1}^2 \pm 2\tan^4(\theta/2) J_{\ell\pm2}^2,$$

$$\langle \mathbf{E}_\pm^{h,\ell} | S_z | \mathbf{E}_\pm^{h,\ell} \rangle = h \langle \mathbf{E}_\pm^{h,\ell} | \mathbf{E}_\pm^{h,\ell} \rangle \mp 2\tan^2(\theta/2) J_{\ell\pm1}^2 \mp 2\tan^4(\theta/2) J_{\ell\pm2}^2.$$

Since the helicity h can only take values ± 1, the eigenvalues of the TAM operator are $\ell \pm 1$. The shift of angular momentum from the SAM to the OAM can be explained from a consideration of the geometric phases.

When the polarization vector is transported parallel along the cone a geometrical phase is induced[3], which effectively rotates the direction of polarization [142, 145]. For a Bessel beam this geometric phase is given by [71]:

$$\Phi_G = 2\pi(1 - \cos(\theta)).$$

This phase determines the change in SAM and OAM from their expected values $L_z = \ell$ and $S_z = \bar{\sigma}$, with $\bar{\sigma}$ the averaged helicity of the beam [71]:

$$L_z = \ell + \bar{\sigma}\tfrac{\Phi_G}{2\pi}, \quad S_z = \bar{\sigma}\left(1 - \tfrac{\Phi_G}{2\pi}\right); \quad J_z = \ell + \bar{\sigma}. \tag{3.5}$$

[3]This phase is induced by the coupling between the SAM and the coordinate axes. A circularly polarized wave travelling in the $\hat{\mathbf{z}}$ direction will obtain a phase shift when the $\hat{\mathbf{x}}$ and $\hat{\mathbf{y}}$ axes are rotated about the $\hat{\mathbf{z}}$ axis. The sign of the phase shift depends on the SAM of the plane wave [142]. An optical experiment that would measure this was proposed by [143] and confirmed by [144] in 1986.

Although the total angular momentum is unchanged, part of the SAM is transferred to the OAM, as expressed in (2.54). A direct consequence is that the OAM becomes helicity-dependent. In the limit of the opening angle $\theta \to \pi/2$, all SAM will be converted to OAM, while in the limit $\theta \to 0$ the values for a plane wave are recovered [71].

Since the shift (3.5) only depends on the *averaged* helicity, it occurs for any Bessel beam, independent of its overall polarization. This is possible as any beam can be decomposed in a set of plane waves with a well-defined helicity. The only exception is when the averaged helicity is zero, this will be discussed in chapter 4.

3.1.2 Spin-polarized optical Bessel beams

The helicity beams (3.3) have 3 non-zero field components, which is in contrast with spin-polarized Bessel beams, that can be defined by implementing the condition that the field component corresponding to the *opposite* polarization is identically zero. With only one non-zero transverse component, the longitudinal component can be derived by requiring that the divergence of the field vanishes. The following expressions for the electric fields are obtained:

$$\mathbf{E}_{+}^{s,\ell}(t,\mathbf{r}) = \begin{pmatrix} J_\ell \\ 0 \\ -\frac{i}{\sqrt{2}}\tan(\theta)J_{\ell+1}e^{i\phi} \end{pmatrix} e^{-i\omega t+ik_z z+i\ell\phi}, \tag{3.6a}$$

$$\mathbf{E}_{-}^{s,\ell}(t,\mathbf{r}) = \begin{pmatrix} 0 \\ J_\ell \\ \frac{i}{\sqrt{2}}\tan(\theta)J_{\ell-1}e^{-i\phi} \end{pmatrix} e^{-i\omega t+ik_z z+i\ell\phi}. \tag{3.6b}$$

These vector fields were derived earlier in [130]. The fields are rescaled by $\cos(\theta)$ with the subscript $\pm$ denoting the right- or left-handed polarization respectively. The superscript s stands for spin polarization. The longitudinal component is smaller than the non-zero transverse component and will vanish in the paraxial limit, similar to the longitudinal components of the helicity fields. However, the magnitude of this component is proportional to $\tan(\theta)$ instead of $\tan(\theta/2)$. These spin-polarized Bessel beams correspond to part a) of figure 1.6.

The magnetic fields can be calculated to be

$$\mathbf{B}_{+}^{s,\ell}(t,\mathbf{r}) = -\frac{i}{2\cos(\theta)} \begin{pmatrix} (1+\cos^2(\theta))J_\ell \\ \sin^2(\theta)J_{\ell+2}e^{2i\phi} \\ -i\sqrt{2}\sin(\theta)\cos(\theta)J_{\ell+1}e^{i\phi} \end{pmatrix} e^{-i\omega t+ik_z z+i\ell\phi}, \tag{3.7a}$$

$$\mathbf{B}_{-}^{s,\ell}(t,\mathbf{r}) = \frac{i}{2\cos(\theta)} \begin{pmatrix} \sin^2(\theta) J_{\ell-2} e^{-2i\phi} \\ (1+\cos^2(\theta)) J_\ell \\ i\sqrt{2}\sin(\theta)\cos(\theta) J_{\ell-1} e^{-i\phi} \end{pmatrix} e^{-i\omega t + ik_z z + i\ell\phi}. \tag{3.7b}$$

In contrast to the electric fields, the magnetic fields have three non-zero components. However, the component corresponding to the polarization direction of the beam is again the largest term, just as for the helical fields. The component with opposite polarization is proportional to $\sin^2(\theta)/\cos(\theta)$, instead of $\sin^2(\theta/2)$. The magnetic fields are related to the electric fields as follows:

$$\mathbf{B}_{\pm}^{s,\ell} = \mp \frac{i}{2\cos(\theta)} \left[(1+\cos^2(\theta)) \mathbf{E}_{\pm}^{s,\ell} + \sin^2(\theta) \mathbf{E}_{\mp}^{s,\ell\pm2} \right].$$

This shows that in the paraxial limit the plane-wave relationship $\mathbf{B}_{\pm}^{s,\ell} = \mp i \mathbf{E}_{\pm}^{s,\ell}$ is recovered, as the contribution from $\mathbf{E}_{\pm}^{s,\ell\pm2}$ vanishes.

Similarly to the helical beams, the spin-polarized beams are not eigenstates of the OAM and SAM operators separately, but of the total angular momentum, as the eigenvalues of the angular momenta separately show the spin-to-orbital AM conversion:

$$\left.\begin{aligned} \langle \mathbf{E}_{\pm}^{s,\ell} | L_z | \mathbf{E}_{\pm}^{s,\ell} \rangle &= \ell |\mathbf{E}_{\pm}^{s,\ell}|^2 \rangle \pm \tfrac{1}{2}\tan^2(\theta) J_{\ell\pm1}^2 \\ \langle \mathbf{E}_{\pm}^{s,\ell} | S_z | \mathbf{E}_{\pm}^{h,\ell} \rangle &= s |\mathbf{E}_{\pm}^{s,\ell}|^2 \mp \tfrac{1}{2}\tan^2(\theta) J_{\ell\pm1}^2 \end{aligned}\right\} (L_z + S_z)\mathbf{E}_{\pm}^{s,\ell} = (\ell \pm 1)\mathbf{E}_{\pm}^{s,\ell}.$$

This confirms the observation that the spin-to-orbital conversion (3.5) is valid for any polarization.

3.1.3 Comparing optical spin and helical fields

The helical fields (3.3) and spin polarized fields (3.6) can be expressed into each other:

$$\mathbf{E}_{\pm}^{h,\ell} = \mathbf{E}_{\pm}^{s,\ell} + \tan^2(\theta/2)\mathbf{E}_{\mp}^{s,\ell\pm2}. \tag{3.8}$$

This equation is not exactly equal to the relationship found earlier (3.1). There are two reasons for this. First of all, the helical fields are rescaled by $\cos(\theta/2)$. Secondly, the minus sign is replaced by a plus sign, a consequence of the integral identity for Bessel functions (1.10); a Bessel function of order ℓ contributes a factor i^ℓ, so a Bessel function of order $\ell \pm 2$ will contribute $-(i^\ell)$.

The helical fields and spin fields are equal to each other in the paraxial limit, while a non-zero θ mixes in the spin polarized field with opposite polarization. To compensate for this different spin value, the OAM needs to be raised or lowered

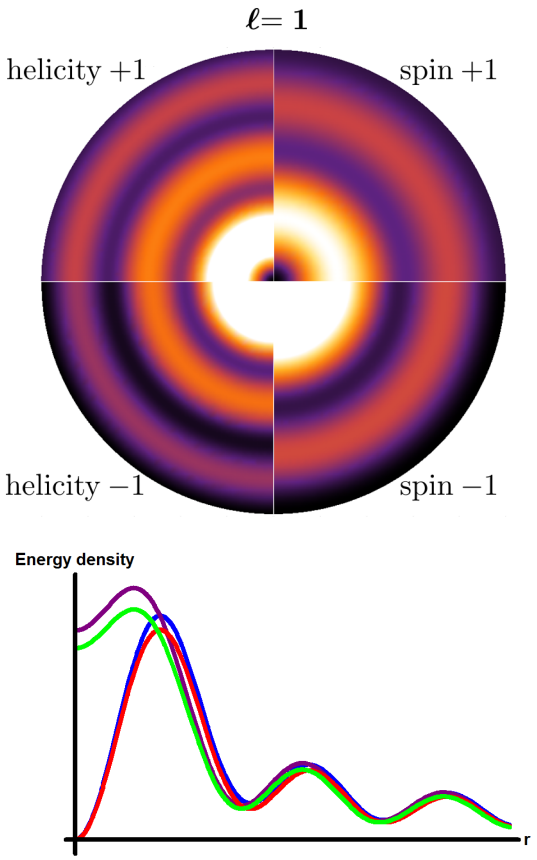

Figure 3.1: Energy density distribution for both the spin and helicity optical beams, for both right-handed $(+1)$ and left-handed (-1) polarization. Remarkable is the zero intensity on the beam axis for the right-handed beams, while there is light on the axis for the left-handed beams. This arises as the zeroth order Bessel function is non-zero on the beam axis. Red: helicity $+1$, blue: spin $+1$, green: helicity -1, purple: spin -1. This figure clearly shows that the spin down state has the largest intensity on the beam axis.

to conserve the sum $\ell + s$ or $\ell + h$. The energy distribution for the four different beams is shown in figure 3.1, all for $\ell = 1$.

Despite these differences, the helicity and spin fields both demonstrate a spin-to-orbital conversion that vanishes in the paraxial limit. Since this shift is determined by the average helicity, it can be expected that it will be larger for the helical beams compared to the spin-polarized beams. This is indeed the case, as for the helical fields the shift is proportional to $2\tan^2(\theta/2)$ and $2\tan^4(\theta/2)$, while it is proportional to $\frac{1}{2}\tan^2(\theta)$ for the spin fields. This difference will show up more

often in the other comparisons that will be made between the spin and helicity beams.

The effects of the appearance of these extra field components in LG beams on the spatial structure of the light were discussed recently by Krenn and Zeilinger [69]. They found that the contribution of the longitudinal component was out of phase with that of the transverse components, and proportional to ℓ^2/r^2 instead of ℓ/r. This translates to optical Bessel beams as the comparison between the radial behaviour of the Bessel functions J_ℓ and $J_{\ell\pm1}$. For large radii, a Bessel function can be approximated by $J_\ell(z) \approx \sqrt{\frac{1}{z}}\cos\left(z - \frac{\ell\pi}{2} - \frac{\pi}{4}\right)$, which indeed shows that the longitudinal component is out of phase with the transverse components. However, the order of the Bessel function does not have a significant effect on the spatial behaviour for large arguments. Further, for small arguments Bessel functions can be approximated by $J_\ell(z) \approx \frac{1}{\ell!}\left(\frac{z}{2}\right)^\ell$, which suggests that the radial behaviour is directly related to the order of the Bessel function. This implies that the longitudinal component can either depend on a larger or smaller power of r, depending on which spin state is considered.

3.2 Spinor Bessel beams

Electron beams can also be polarized by either their spin or helicity, similarly to optical vortex beams, as explained in section 1.5.2. EVBs are described relativistically by spinor Bessel beams. These were first discussed by Bliokh et al. in 2011 [72]. Electron vortex beams in spinor form were also derived by [73] to study the interaction between an external electromagnetic field and the electron OAM. These field solutions allow for a study into the effects of introducing spin on these vortex beams compared to scalar electron vortex beams.

3.2.1 Spin-polarized electron Bessel beams

The expressions for a generally polarized spinor field, described in cylindrical polar coordinates and decomposed as a sum of two fields that were spin-polarized in the $\hat{\mathbf{z}}$-direction, were derived earlier and are given by (1.42). Expressing the momentum components in spherical coordinates,

$$x = r\sin(\theta)\cos(\phi),\ y = r\sin(\theta)\sin(\phi),\ z = r\cos(\theta),$$

gives the vortex beams solutions of the electron spin states, as derived in [72]:

$$\psi_{\pm}^{\ell,s}(t,\mathbf{r}) = e^{-i(\omega t - k_z z - \ell\phi)}\sqrt{\frac{\mathcal{E}+m}{2\mathcal{E}}}\left\{ J_\ell \begin{pmatrix} \alpha \\ \beta \\ 0 \\ 0 \end{pmatrix} + \cos(\theta)\varepsilon\, J_\ell \begin{pmatrix} 0 \\ 0 \\ \alpha \\ -\beta \end{pmatrix} + i\sin(\theta)\varepsilon \begin{pmatrix} 0 \\ 0 \\ -\beta J_{\ell-1} e^{-i\phi} \\ \alpha J_{\ell+1} e^{i\phi} \end{pmatrix} \right\}. \quad (3.9)$$

Here α and β denote the spin state; $|\alpha|^2 + |\beta|^2 = 1$, with $\alpha = 1$ corresponding to spin up and $\beta = 1$ to spin down relative to the $\hat{\mathbf{z}}$ axis. The parameter $\epsilon = \sqrt{\frac{\mathcal{E}-m}{\mathcal{E}+m}}$ is a measure of the relativistic regime; the non-relativistic limit corresponds to $\epsilon = 0$.

It will become convenient to describe spin-polarized electron states in this way when comparing them with helicity-polarized electron states, as now the spin direction is solely a function of the two angles (ϕ, θ). In the non-relativistic limit, $\varepsilon \to 0$, the solution (3.9) reduces to a two-component solution of the Pauli equation (1.25):

$$\psi_{\pm}^{\ell,s}(t,\mathbf{r}) = e^{-i(\omega t - k_z z - \ell\phi)}\sqrt{\frac{\mathcal{E}+m}{2\mathcal{E}}} \begin{pmatrix} \alpha \\ \beta \end{pmatrix} J_\ell.$$

These two components are the top two components of (3.9). They are larger than the bottom two, even in the relativistic regime. For a fully polarized electron beam the Pauli solution will reduce to the scalar field expression. The bottom two components can therefore be considered as the spin contribution, resulting from the spinor description.

Similarly to the optical vortex beams, the EVB solutions (3.9) are no eigenstates of the OAM and SAM individually but of the TAM in the $\hat{\mathbf{z}}$ direction only, with eigenvalue $\ell \pm \frac{1}{2}$ [72]:

$$\langle L_z \rangle_{\pm}^{s} = \ell \langle \psi_{\pm}^{\ell,s} | \psi_{\pm}^{\ell,s} \rangle + \frac{1}{2}\Delta^s \left(\alpha^2 J_{\ell+1} - \beta^2 J_{\ell-1} \right),$$
$$\langle S_z \rangle_{\pm}^{s} = s \langle \psi_{\pm}^{\ell,s} | \psi_{\pm}^{\ell,s} \rangle - \frac{1}{2}\Delta^s \left(\alpha^2 J_{\ell+1} - \beta^2 J_{\ell-1} \right).$$

This shows that a part of the SAM is converted to the OAM, similar to spin-to-orbital AM conversion observed in optical vortex fields [71, 79]. The parameter Δ^s disappears in both the paraxial $\theta \to 0$ and non-relativistic $\mathcal{E} \to m$ limit:

$$\Delta^s = \left(1 - \frac{m}{\mathcal{E}}\right) \sin^2(\theta).$$

It was further observed that the probability densities depend on both the OAM and SAM values [72], as shown in figure 3.2. These effects will be studied in more detail later in this chapter, similar to [69] studying the effect of the different radial behaviours of the spinor components for exponential electron wavepackets.

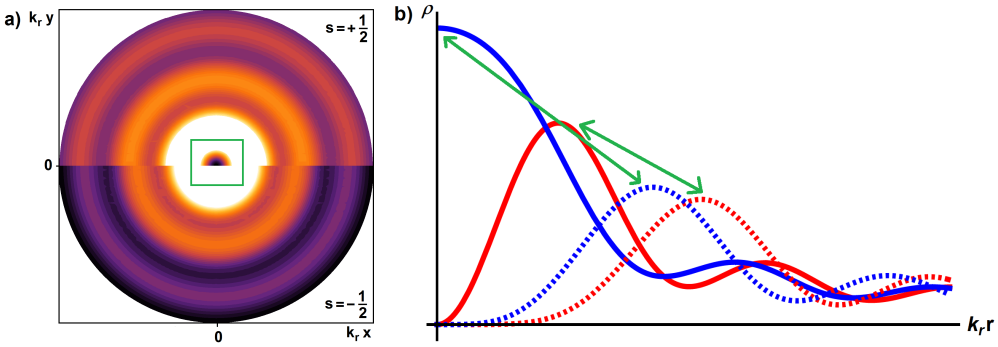

Figure 3.2: Spin-orbit effects for the density distribution of spin-polarized relativistic electron Bessel beams. a): The density distribution of the spin-up and -down states for $\ell = 1$, showing the non-vanishing density of spin down electrons at the centre of the beam. b): Effect of the azimuthal winding number ℓ on the radial density distribution for both spin states. Solid red graph: $\ell = 1, s = +1/2$, dashed red graph: $\ell = 3, s = +1/2$, solid blue graph: $\ell = 1, s = -1/2$, dashed blue graph: $\ell = 3, s = -1/2$. The different positions of the first bright ring as function of ℓ are indicated by the green arrows.

3.2.2 Helical electron Bessel beams

Using the helicity spinors (1.48) instead of the spinors (1.21) gives the helicity vortex solutions:

$$\psi_{\pm}^{\ell,h}(t,\mathbf{r}) = e^{-i(\mathcal{E}t - p_z z - \ell\phi)}\sqrt{\frac{\mathcal{E}+m}{2\mathcal{E}}}\left\{\cos(\theta/2)\begin{pmatrix}\alpha J_\ell\\ \beta J_\ell\\ 0\\ 0\end{pmatrix} + i\sin(\theta/2)\begin{pmatrix}\beta J_{\ell-1}e^{-i\phi}\\ \alpha J_{\ell+1}e^{i\phi}\\ 0\\ 0\end{pmatrix}\right.$$
$$\left. + \cos(\theta/2)\varepsilon\begin{pmatrix}0\\ 0\\ \alpha J_\ell\\ -\beta J_\ell\end{pmatrix} + i\sin(\theta/2)\varepsilon\begin{pmatrix}0\\ 0\\ -\beta J_{\ell-1}e^{-i\phi}\\ \alpha J_{\ell+1}e^{i\phi}\end{pmatrix}\right\}. \quad (3.10)$$

Now α and β denote the helicity state, where $\alpha = 1$ corresponds to right-handed helicity. These states were derived before in slightly different form [73]. Similar to the spin solutions, these states are also only eigenstates of the J_z operator with

eigenvalue $\ell \pm \frac{1}{2}$. The expectation values of the L_z and S_z operators are now:

$$\langle L_z \rangle_{\pm}^{h} = \ell \langle \psi_{\pm}^{\ell,h} | \psi_{\pm}^{\ell,h} \rangle + \frac{1}{2}\Delta^h \left(\alpha^2 J_{\ell+1} - \beta^2 J_{\ell-1} \right),$$
$$\langle S_z \rangle_{\pm}^{h} = h \langle \psi_{\pm}^{\ell,h} | \psi_{\pm}^{\ell,h} \rangle - \frac{1}{2}\Delta^h \left(\alpha^2 J_{\ell+1} - \beta^2 J_{\ell-1} \right).$$

where the parameter Δ^h is defined differently from Δ^s:

$$\Delta^h = 2\sin^2(\theta/2).$$

Similar to Δ^s, Δ^h vanishes in the paraxial limit. This shows that also for helicity states the OAM and SAM are only separable in the paraxial limit. However, the Δ^h parameter does not depend between the ratio of energy and mass, and this will be encountered more often for the helical electron beams. Since helicity is only well-defined for massless particles, adopting a helically polarized description effectively imposes the restriction to the massless regime. Therefore, when comparing the spin and helical electron beams, the massless (relativistic) limit of the spin polarized electron beams needs to be taken.

A question that arises now is whether these helicity electron beams are eigenstates of the helicity operator (1.47). This turns out not to be the case, as expectation values of this operator are given by

$$\langle \mathcal{H} \rangle = \langle \psi_{\pm}^{\ell,h} | \mathcal{H} | \psi_{\pm}^{h,\ell} \rangle = \pm \cos(\theta) \left[\cos^2(\theta/2) J_{\ell}^2 - \sin^2(\theta/2) J_{\ell\pm1}^2 \right].$$

However, plane waves would be eigenstates of the helicity operator, as the term in brackets would be equal to $[\cos^2(\theta/2) + \sin^2(\theta/2)] = 1$; the factor -1 comes from the Bessel function of order $\ell \pm 1$. Nonetheless, the overall sign of $\langle \mathcal{H} \rangle$ depends on the chosen helicity direction, while the factor $\cos(\theta)$ signifies that the propagation direction of the plane waves is not parallel to the $\hat{\mathbf{z}}$-axis.

3.2.3 Comparing spin and helicity electron fields

The spinor helicity states can be related to the spinor spin states, similar to the prediction (3.2):

$$\psi_{\pm}^{\ell,h} = \cos(\theta/2)\psi_{\pm}^{\ell,s} + i\sin(\theta/2)\psi_{\mp}^{\ell\pm1,s}.$$

Every factor of $e^{\pm i\phi}$ in the plane wave expression gives rise to a factor $\pm i$ in the vortex solution, as explained on page 26. This explains the discrepancy with equation (3.2). Similarly to the optical fields, the spin state with opposite polarization has its OAM shifted in such a way that both terms have the same

TAM; now $\ell \pm 1$ is enough to satisfy this condition. Rescaling the helicity states by $\cos(\theta/2)$, in analogy to (3.1), shows that the proportionality factor is $\tan(\theta/2)$ compared to $\tan^2(\theta/2)$ for photons;

$$\psi_{\pm}^{\ell,h} \sim \psi_{\pm}^{\ell,s} + i\tan(\theta/2)\psi_{\mp}^{\ell\pm1,s}. \tag{3.11}$$

Similarly to the optical field, the electron field also shows the spin-to-orbital AM conversion, for which the proportionality constants $\Delta^{s,h}$ were introduced. In contrast to the shift for optical Bessel beams, the shift is larger for electron spin states than for helicity states. Only in the *non-paraxial* limit and non-relativistic limit, when $\frac{m}{\mathcal{E}} > 0.5$, the shift Δ^s is smaller than Δ^h. Further, the same difference in proportionality between θ and $\theta/2$ as seen for the optical fields can be observed.

3.2.4 Is the spinor description of electron vortex beams necessary?

The need of a relativistic description of electron vortex beams is not widely accepted. It was argued in [146] that electrons behave as scalar fields in experiments, since electron vortex beams are created in electron microscopes with energies below 500 keV[4]. The SAM effects have a relatively small magnitude and require large electromagnetic fields to be measurable. Hence there have not been any experiments yet that considered the spin states of the vortex electrons.

Further, beams created in electron microscopes are always paraxial [148] and solutions of the Dirac equation are shown to be eigenstates of both $\mathbf{L}$ and $\mathbf{S}$ in this limit [146]. For example, an important relativistic effect is a non-zero intensity at the beam axis, as shown in part a) of figure 3.2. However, this intensity is approximately 10^{-5} of the maximum intensity, and the radius inside which this effect would be observable is of the order of 10^{-12} m. These two factors make these effects non-measurable [146]. It was concluded that the Pauli equation suffices as description of the electrons, with L_z a suitable quantum number.

In contrast, [66] argued that relativistic corrections may amount to 60% of the intensity for electron energies of 300 keV. In a relativistic description, the structure of vortex lines is completely different from the scalar description; the vorticity $\boldsymbol{\omega} = \nabla \times \mathbf{v}$ is not concentrated on the vortex line, but spread out over all space [66]. In response, [149] argued that Dirac electrons, described by a spinor wavefunction, are characterized by polarization singularities, not by vorticity, which is suitable to describe a scalar field. This is because the velocity in the Dirac

[4]These electrons have a wavelength that is about 10 times smaller than the distance between the electrons, hence there are no interaction effects that need to be considered [147].

description is not given by the gradient of the phase, and not proportional to the momentum. This leads to effects such as Zitterbewegung; a "trembling motion" of the electron as the expectation value of the velocity is $\pm c$ at all times.

Another paper that discussed the velocity and position operators [150] observed that there is, however, an azimuthal current associated with the region around the vortex. It was argued in [149] that the choice of the OAM and SAM operators in determined by the choice of the position operator, in an aim to resolve the apparent contradiction between [66] and [150].

The effect of choosing either the spin or helicity polarization can be studied by considering the conserved quantities of the spinor and vector fields. Comparisons with the corresponding scalar ones allows for the identification of orbital and spin contributions. The first conserved quantity to consider is the gauge current for the Dirac field.

3.3 Conserved gauge quantities

The complex scalar field and Dirac field are both described by a complex wavefunction and have a $U(1)$ gauge symmetry as a result. The conserved quantities associated with this symmetry are the gauge currents (2.19) and (2.21). As the optical field is a real field and has no complex $U(1)$ symmetry, there is no conserved current for massless spin-1 fields [105]. As an "alternative" the helicity density (2.49) and spin currents (2.51) will be considered.

The gauge density and currents of the scalar Bessel beam (1.7) can be found from (2.19):

$$\rho = 2\omega J_\ell^2, \tag{3.12}$$

$$\mathbf{J} = 2\left(\frac{\ell}{r}\widehat{\boldsymbol{\phi}} + k_z\hat{\mathbf{z}}\right) J_\ell^2. \tag{3.13}$$

These quantities reflect the harmonic dependence on time, the azimuthal and longitudinal coordinates. There is no radial gauge current.

3.3.1 Gauge quantities of the Dirac field

With the expressions for the spin (3.9) and helical (3.10) electron beams the probability density and currents (2.21) related to the $U(1)$ gauge symmetry can be calculated. The quantities of the spin and helical electron beams can be compared with each other to draw conclusions about the effects of the choice in polarization.

Probability density

The probability densities (2.21) for the spin and helical EVBs are given by:

$$(\rho_e)^s_\pm = \frac{\mathcal{E}+m}{2\mathcal{E}}\left[J_\ell^2(1+\varepsilon^2\cos^2(\theta)) + \varepsilon^2 J_{\ell\pm1}^2\sin^2(\theta)\right], \tag{3.14}$$

$$(\rho_e)^h_\pm = J_\ell^2\cos^2(\theta/2) + J_{\ell\pm1}^2\sin^2(\theta/2). \tag{3.15}$$

This shows that the density of the helicity beams does not depend on the ratio between the energy and mass, while the fields themselves do. This is similar to the observation that the parameter Δ^h does not depend on this ratio either.

The electron probability density and currents can be split into a scalar, orbital and a spin part by the Gordon decomposition (2.27). This works out for spin-polarized electrons as follows:

$$(\rho_e)^s_\pm = J_\ell^2 + \frac{\mathcal{E}-m}{2\mathcal{E}}\sin^2(\theta)\left[J_\ell^2 + J_{\ell\pm1}^2\right] - \frac{\mathcal{E}^2-m^2}{2m\mathcal{E}}\sin^2(\theta)\left[J_\ell^2 - J_{\ell\pm1}^2\right]. \tag{3.16}$$

In either the rest frame limit, $\mathcal{E}\to m$, or the paraxial limit, the gauge density approaches the scalar quantity, although the Bessel functions will be infinitely condensed on the beam axis since in this limit $k_r\to 0$. The proportionality factor of the spin part is about twice as large as the factor of the orbital part for small energies, $\mathcal{E}\sim m$:

$$\frac{\mathcal{E}^2-m^2}{2m\mathcal{E}} = \left(\frac{\mathcal{E}+m}{m}\right)\frac{\mathcal{E}-m}{2\mathcal{E}}.$$

Combined with the fact that $J_{\ell+1} < J_\ell$ for small radii, the spin part is larger in absolute value than the orbital part, whereas the sign depends on the spin state; for spin up the spin part counteracts the orbital part, where for spin down the spin part increases the shift. The spin correction is of the order of 10^{-4} and the orbital correction is of the order of 10^{-5} in magnitude compared to the scalar expression, in agreement with the observations made in [146].

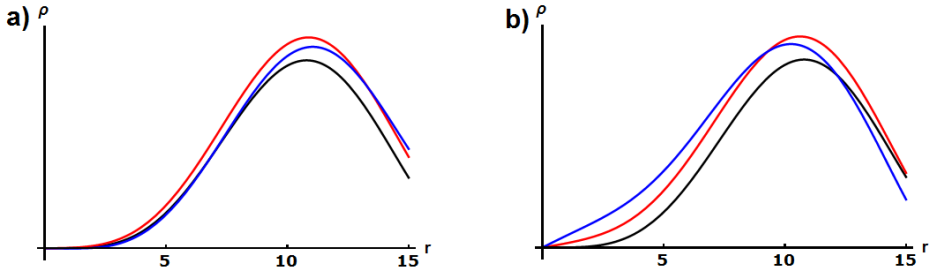

Figure 3.3: Decomposition of the electron density distribution for spin up (a) and spin down (b). Both for $\ell = 2, \theta = \pi/4$ and the ratio between energy and mass $\mathcal{E}/m = 1.1$, corresponding to an energy of 500keV. Shown are the scalar distribution (black), scalar and orbital part (red) and the combined scalar, orbital and spin part(blue). It can be seen that for spin up, the spin part counteracts the orbital shift (for small radii) while for spin down the spin part increases the shift from the orbital part.

There is no spin contribution to the density distribution of the helical electrons;

$$(\rho_e)^h_\pm = J^2_\ell + \sin^2(\theta/2)\left[-J^2_\ell + J^2_{\ell\pm1}\right]. \tag{3.17}$$

In the paraxial limit this density reduces to the scalar density; $(\rho_e)^h_\pm \underset{\theta\to0}{\to} J^2_\ell$. For both spin and helicity beams the orbital part of the probability density depends on the OAM and spin value, as Bessel functions of the order $\ell \pm 1$ appear. This is the result of the multi-component description by the Dirac equation. Describing electrons by the Schrödinger equation would give a density distribution that would only depend on the OAM of the field, being proportional to J^2_ℓ.

Quantum core radius

It is now worthwhile to ask at what distances from the beam axis the contributions from the $J_{\ell\pm1}$ terms are measurable. The density distribution of the electron beam with spin down is shifted closer to the beam axis by the orbital and spin contributions. This effect will be the largest for electron vortex beams with $\ell = 1$, as one component of the spinor will be proportional to a zeroth order Bessel function. This Bessel function is non-zero on the beam axis, while all higher order Bessel beams are zero, giving rise to a non-vanishing probability density. To quantify this effect a *quantum core radius* can be defined; the radius at which the terms proportional to J_0 will be larger than the terms proportional to J_1. It is not a problem that both spin and orbital parts contain the terms J_ℓ and $J_{\ell\pm1}$, as the definition of a quantum core radius has as purpose to distinguish between a spinor and scalar beam. Since the density distribution of a scalar beam

is simply proportional to J_ℓ^2, the part of the spinor beam proportional to J_ℓ^2 could be confused with the scalar density distribution when measured.

For this purpose, the gauge density distribution is split in two parts:

$$(\rho_e)_1^s = \tfrac{\mathcal{E}+m}{2\mathcal{E}}\left[J_1^2(1+\varepsilon^2\cos^2(\theta))\right], \quad (\rho_e)_0^s = \tfrac{\mathcal{E}+m}{2\mathcal{E}}\varepsilon^2 J_0^2\sin^2(\theta),$$

$$(\rho_e)_1^h = J_1^2\cos^2(\theta/2), \qquad (\rho_e)_0^h = J_0^2\sin^2(\theta/2).$$

The contribution of both parts are shown in figure 3.4. Equating these two contributions, and using the approximation $J_\ell(k_r r) \approx \frac{1}{\ell!}\left(\frac{k_r r}{2}\right)^\ell$ which leads to $J_0^2/J_1^2 \sim k_r^2 r^2/4$, gives a radius below which the $(\rho_e)_0^{s,h}$ part starts to dominate:

$$R_e^s = \frac{2}{k}\varepsilon\frac{1}{\sqrt{1+\varepsilon\cos^2(\theta)}} \underset{m\to 0}{\to} \frac{2}{k}\frac{1}{\sqrt{1+\cos^2(\theta)}} \underset{\theta\to 0}{\approx} \frac{\sqrt{2}}{k}\left(1+\frac{\theta^2}{4}+\dots\right),$$
$$R_e^h = \frac{1}{k}\frac{1}{\cos^2(\theta/2)} \underset{\theta\to 0}{\approx} \frac{1}{k}\left(1+\frac{\theta^2}{4}+\dots\right).$$

This shows that in the massless paraxial limit $R_e^s = \sqrt{2}R_e^h$. The radius is larger for the spin states as the large part of the probability density includes a factor J_1^2 that is independent of θ. In the non-relativistic limit the quantum core radius of the beams shrinks to zero as expected, as the spinor wavefunction reduces to the scalar wavefunction in this limit; the quantum core radius is a relativistic effect.

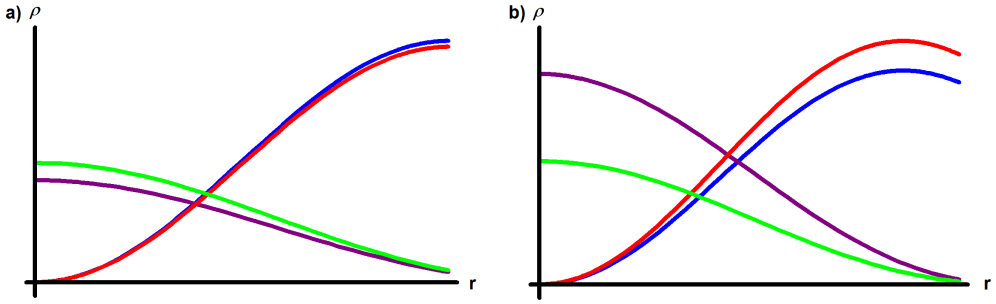

Figure 3.4: Different components of the probability density of the electron vortex beams, for (a) $m = \mathcal{E}/2$ and (b) $m = 0$. Large components are red (helicity) and blue (spin). Small components are green (helicity) and purple (spin). $\theta = \pi/4$.

For electrons in an electron microscope, with a typical kinetic energy $\mathcal{E} = 200$ keV and opening angle $\theta = \pi/90$, the quantum core radius is approximately $R_e^s \approx 7\times 10^{-14}$ m for spin polarized electrons and $R_e^h \approx 9\times 10^{-13}$ m for helicity electrons. This agrees with the observations made [146].

Longitudinal probability current

The probability currents for both the spin and helicity electron vortex beams are found by inserting (3.9) and (3.10) into (2.21). The probability current of the spin polarized electrons in the longitudinal direction can be separated as follows:

$$\begin{aligned}(\mathbf{J}_e^z)_\pm^s &= \frac{k}{\mathcal{E}}\cos(\theta)J_\ell^2, \\ &= \frac{k}{\mathcal{E}}\cos(\theta)J_\ell^2 + \frac{k}{\mathcal{E}}\cos(\theta)\sin^2(\theta)\left(\frac{\mathcal{E}-m}{2m}\right)[-J_\ell^2 + J_{\ell\pm1}^2] \\ &\qquad -\frac{k}{\mathcal{E}}\cos(\theta)\sin^2(\theta)\left(\frac{\mathcal{E}-m}{2m}\right)[-J_\ell^2 + J_{\ell\pm1}^2].\end{aligned} \tag{3.18}$$

The longitudinal momentum density is proportional to the scalar quantity (3.13) with proportionality factor $1/\mathcal{E}$. This factor comes from the Dirac normalization and can hence be ignored. The spin and orbital parts cancel exactly. Similar to the density distribution, the scalar quantity is retrieved in the paraxial limit.

The longitudinal gauge current of the helical electrons is quite different;

$$\begin{aligned}(\mathbf{J}^z)_\pm^h &= \frac{k}{\mathcal{E}}\left[\cos^2(\theta/2)J_\ell^2 - \sin^2(\theta/2)J_{\ell\pm1}^2\right], \\ &= \frac{k}{\mathcal{E}}\cos(\theta)J_\ell^2 + \frac{k\cos(\theta)}{\mathcal{E}}\sin^2(\theta/2)(-J_\ell^2 + J_{\ell\pm1}^2) \\ &\qquad +\frac{2k}{\mathcal{E}}\left(\cos^4(\theta/2)J_\ell^2 - \sin^4(\theta/2)J_{\ell\pm1}^2\right).\end{aligned} \tag{3.19}$$

In contrast to the spin polarized electrons, the longitudinal current of the helical states contains a term proportional to $J_{\ell\pm1}^2$, making the total current not proportional to the scalar current. However, this term disappears in the paraxial limit, while the spin part does not vanish in this limit.

The difference between the longitudinal Dirac and scalar gauge currents can be expressed as

$$\begin{aligned}(\mathbf{J}^z)_\pm^s - J_{z,\text{scalar}} &= \left(\frac{1}{\mathcal{E}} - 1\right)k\cos(\theta)J_\ell^2, \\ (\mathbf{J}^z)_\pm^h - J_{z,\text{scalar}} &= \left(\frac{1}{\mathcal{E}} - 1\right)k\cos(\theta)J_\ell^2 + \frac{k}{\mathcal{E}}\sin^2(\theta/2)(J_\ell^2 - J_{\ell\pm1}^2).\end{aligned}$$

This shows, as expected, that in the paraxial regime the scalar expression is retrieved. The differences between the scalar and spinor currents are very small, as this factor $\left(\frac{1}{\mathcal{E}} - 1\right)k\cos(\theta) \approx 1.23\times10^{-9}$, and the factor $\frac{k}{\mathcal{E}}\sin^2(\theta/2) \approx 4\times10^{-13}$, both for $\mathcal{E} \sim 500$ keV and $\theta \sim \pi/90$ radians. The difference between the helical spinor and scalar current has a term proportional to $J_\ell^2 - J_{\ell\pm1}^2$, similar to the difference between the probability density of the helical electrons and the scalar field, (3.17).

Azimuthal probability current

Remarkably, the azimuthal currents of the spin and helicity electrons are the same:

$$(\mathbf{J}_e^{\phi})^s_{\pm} = (\mathbf{J}_e^{\phi})^h_{\pm} = \frac{k}{\mathcal{E}}\sin(\theta) J_\ell J_{\ell\pm1}. \tag{3.20}$$

These currents vanish in the paraxial limit, as required. Calculating the orbital and spin part separately gives for the spin electrons:

$$\begin{aligned}(\mathbf{J}^{\phi})^s_{\pm} = &-\frac{1}{\mathcal{E}}\frac{\ell}{r}J_\ell^2 - \frac{\mathcal{E}-m}{2m\mathcal{E}}\sin^2(\theta)\left[\frac{\ell}{r}J_\ell^2 + \frac{\ell\pm1}{r}J_{\ell\pm1}^2\right] \\ &+\frac{1}{\mathcal{E}}\frac{\ell}{r}J_\ell^2 + \frac{k\sin(\theta)}{\mathcal{E}}J_\ell J_{\ell\pm1} + \frac{\mathcal{E}-m}{2m\mathcal{E}}\sin^2(\theta)\left[\frac{\ell}{r}J_\ell^2 + \frac{\ell\pm1}{r}J_{\ell\pm1}^2\right].\end{aligned} \tag{3.21}$$

In the restframe limit, the orbital part goes to zero but the spin part does not; only the last term vanishes. The first term of the spin part is automatically cancelled by the scalar term, while the remaining term only vanishes in the paraxial limit. The same can be seen for the helicity electrons:

$$\begin{aligned}(\mathbf{J}^{\phi})^h_{\pm} = &-\frac{1}{\mathcal{E}}\frac{\ell}{r}J_\ell^2 + \frac{\sin^2(\theta/2)}{\mathcal{E}}\left[\frac{\ell}{r}J_\ell^2 - \frac{\ell\pm1}{r}J_{\ell\pm1}^2\right] \\ &+\frac{1}{\mathcal{E}}\frac{\ell}{r}J_\ell^2 + \frac{k\sin(\theta)}{\mathcal{E}}J_\ell J_{\ell\pm1} - \frac{\sin^2(\theta/2)}{\mathcal{E}}\left[\frac{\ell}{r}J_\ell^2 - \frac{\ell\pm1}{r}J_{\ell\pm1}^2\right].\end{aligned} \tag{3.22}$$

The orbital part is cancelled by the spin part, which again contains a single term that is not cancelled by any other contribution.

Another correspondence between the scalar and spinor azimuthal currents can be found by writing the scalar azimuthal current (3.13) as $J_{\phi,\text{scalar}} = k\sin(\theta)J_\ell(J_{\ell+1}+J_{\ell-1})$. Using this definition, the difference between the scalar and electron azimuthal current becomes

$$(\mathbf{J}^{\phi})_{\pm} - J_{\phi,\text{scalar}} = k\sin(\theta)J_\ell\left[J_{\ell\pm1}\left(\frac{1}{\mathcal{E}}-1\right) - J_{\ell\mp1}\right].$$

Up to a proportionality factor of $\mathcal{E}$, the difference is exactly the azimuthal current of the electron state with opposite polarization, which implies that the scalar current is proportional to the average of the two Dirac currents;

$$\frac{\mathcal{E}}{2}\left[(\mathbf{J}_e^{\phi})_+ + (\mathbf{J}_e^{\phi})_-\right] = k\sin(\theta)J_\ell(J_{\ell+1}+J_{\ell-1}) = \frac{\ell}{r}J_\ell^2.$$

The azimuthal current of an unpolarized electron Bessel beam will thus be undistinguishable from the azimuthal current of a scalar beam.

Discussion

The differences between the spin and helicity quantities can be summarized in the following table. Every Bessel function is multiplied by the proportionality factor in the same row:

		orbital	spin	proportionality constant
Spin	ρ	$J_\ell^2 + J_{\ell\pm1}^2$	$J_\ell^2 - J_{\ell\pm1}^2$	$\sin^2(\theta)$
	J_z	$-J_\ell^2 + J_{\ell\pm1}^2$	$J_\ell^2 - J_{\ell\pm1}^2$	$\sin^2(\theta)$
	J_ϕ	$J_\ell^2 + J_{\ell\pm1}^2$	$J_\ell^2 + J_{\ell\pm1}^2$+ other terms	$\sin^2(\theta)$
Helicity	ρ	$J_\ell^2 - J_{\ell\pm1}^2$	n/a	$\sin^2(\theta/2)$
	J_z	$-J_\ell^2 + J_{\ell\pm1}^2$	$J_\ell^2 - J_{\ell\pm1}^2$ $^{(*)}$	$\sin^2(\theta/2)$, $\sin^4(\theta/2)$
	J_ϕ	$J_\ell^2 - J_{\ell\pm1}^2$	$-J_\ell^2 + J_{\ell\pm1}^2$+ other terms	$\sin^2(\theta/2)$

Table 3.1: The gauge current components of spin and helicity electron beams split into an orbital and spin part with corresponding proportionality factors. $^{(*)}$This term is $\cos^4(\theta/2)J_\ell^2 - \sin^4(\theta/2)J_{\ell\pm1}^2 = J_\ell^2 - \sin^4(\theta/2)(J_\ell^2 + J_{\ell\pm1}^2)$

Clearly, all contributions to the quantities of the spin electrons are proportional to $\sin(\theta)$, while for the helicity electrons this is $\sin^2(\theta/2)$. Remarkable is the fact that all contributions to the quantities of the helicity states are proportional to the *difference* $J_\ell^2 - J_{\ell\pm1}^2$, which will vanish for small radii (the case $\ell = 0$ excluded) while for larger radii this becomes equal to a periodically oscillating function of amplitude $\frac{1}{k_r r}$; for large radii the Bessel functions can be approximated by $J_\ell(k_r r) \approx \sqrt{\frac{2}{\pi k_r r}} \cos\left(k_r r - \ell\frac{\pi}{2} - \frac{\pi}{2}\right)$ and hence the difference will result into

$$J_\ell^2 - J_{\ell\pm1}^2 \approx \frac{2}{\pi k_r r}\left[\cos^2(k_r r) - \sin^2(k_r r)\right].$$

For the spin beams, the orbital and spin contributions are either proportional to this same factor, or to the *sum* $J_\ell^2 + J_{\ell\pm1}^2$. The latter approximates to a constant value $\frac{1}{k_r r}$.

Density distribution For the spin-polarized electron beams, the spin contribution dominates over the orbital contribution at small radii. At larger distances from the centre the orbital contribution becomes constant while the spin contribution oscillates, and hence the orbital contribution dominates. There is no spin contribution to the density distribution of the helicity beams. The quantum core radius is of the order 10^{-13} m, making it unlikely to be observed in experiments.

Longitudinal current The orbital and spin parts of the longitudinal gauge current exactly cancel for the spin beams. Whether the spin contribution is smaller

than the orbital contribution for the helicity beams depends on θ only; for paraxial beams the contribution from the spin term $\sim \cos^4(\theta/2)J_\ell^2$ dominates. Corrections with respect to the scalar current are of the order of 10^{-9} in magnitude.

Azimuthal current The total azimuthal currents of the spin and helicity electrons are equal to each other, although the orbital and spin parts are different. The orbital part is cancelled by the spin part for both types of electron beams, and the only contribution comes from the spin part; it even cancels the scalar part. The average of the azimuthal currents of oppositely polarized electron beams is proportional to the scalar current.

3.3.2 Helicity density and spin current of the optical field

The optical field has no $U(1)$ symmetry, which means that there is no conserved gauge current. Another conserved 4-current associated with the duality transformation (2.47) is formed by the helicity density and spin AM components (2.55). When describing optical fields by complex expressions, the real part of the conserved quantities corresponds to the physical quantity. Hence the spin current and helicity density are given by the complex versions of (2.49) and (2.51):

$$\mathcal{H} = \frac{1}{2}\mathrm{Re}(\mathbf{A}^* \cdot \mathbf{B} - \mathbf{C}^* \cdot \mathbf{E}), \tag{3.23a}$$

$$\mathbf{S} = \frac{1}{2}\mathrm{Re}(\mathbf{E} \times \mathbf{A}^* + \mathbf{B} \times \mathbf{C}^*). \tag{3.23b}$$

The helicity density of both the optical spin and helicity Bessel beams is given by:

$$\begin{aligned}\mathcal{H}^s_\pm &= \pm\frac{1}{2k\cos(\theta)}\left[J_\ell^2\left(1+\cos^2(\theta)\right) + J_{\ell\pm1}^2\sin^2(\theta)\right] \\ &\approx \pm\frac{1}{k}\left[J_\ell^2\left(1+\frac{\theta^4}{8}\right) + J_{\ell\pm1}^2\left(\frac{\theta^2}{2}+\frac{\theta^4}{12}\right)\right],\end{aligned} \tag{3.24a}$$

$$\begin{aligned}\mathcal{H}^h_\pm &= \pm\frac{1}{k}\left[J_\ell^2 + J_{\ell\pm1}^2\left(2\tan^2(\theta/2)\right) + J_{\ell\pm2}^2\tan^4(\theta/2)\right] \\ &\approx \pm\frac{1}{k}\left[J_\ell^2 + J_{\ell\pm1}^2\left(\frac{\theta^2}{2}+\frac{\theta^4}{12}\right) + \frac{1}{16}J_{\ell\pm2}^2\theta^4\right].\end{aligned} \tag{3.24b}$$

These densities are the same for small powers of θ, as differences arise for θ^4;

$$\mathcal{H}^h_\pm - \mathcal{H}^s_\pm \approx \frac{\theta^4}{16k}\left[J_{\ell\pm2}^2 - 2J_\ell^2\right]. \tag{3.25}$$

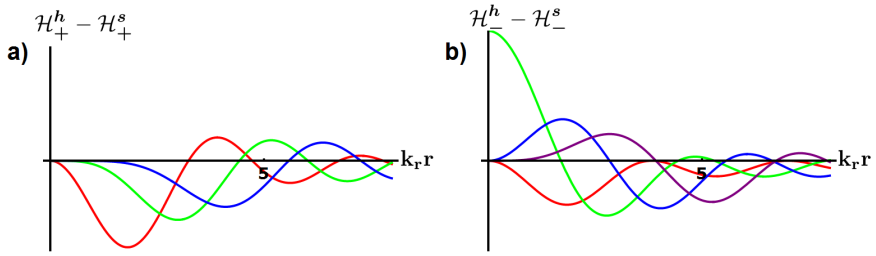

Figure 3.5: Difference between the helicity density of the helicity fields and the spin Bessel beams; a): the spin/helicity up fields, b): the spin/helicity down states. Red line $\ell = 1$, green $\ell = 2$, blue $\ell = 3$ and purple $\ell = 4$.

The radial dependence of this difference depends on the spin state. For the positive helicity or spin up states, of this function is first negative before oscillating around zero for larger radii; for higher values of ℓ the minimum shifts out of the centre of the beam, as shown in part a) of figure 3.5. For negative helicity or spin down, the analysis becomes more complicated. For $\ell = 1$ the difference between the helicity densities is negative, while for $\ell = 2$ it is positive for small radii. Both oscillate just below zero for larger radii. For $\ell \geq 3$ the difference starts out as positive before becoming negative, after which it starts to oscillate around zero, as shown in part b) of figure 3.5. For all values of ℓ, s and h the difference starts to oscillate for radii larger than $\sim 5\ k_r r$. The reason that the helicity density of the helical fields can be *smaller* than that of the spin fields is that the electric and magnetic fields of the helical fields are proportional to each other, making the helicity density *smaller* than that of the spin fields. The radial dependence of the helicity density for $\ell = 1$ is plotted in figure 3.6 for all four different fields.

Similarly as seen for electrons, a quantum core radius can be defined for the optical field. The large and small parts of the helicity density are:

$$\mathcal{H}^s_{\pm,1} = -\tfrac{1+\cos^2(\theta)}{k\cos(\theta)} J_1^2, \qquad \mathcal{H}^s_{\pm,2} = -\tfrac{\sin^2(\theta)}{k\cos(\theta)} J_0^2,$$

$$\mathcal{H}^h_{\pm,1} = -\tfrac{2}{k} J_1^2, \qquad \mathcal{H}^h_{\pm,2} = -\tfrac{4}{k}\tan^2(\theta/2) J_0^2 - \tfrac{2}{k}\tan^4(\theta/2) J_{-1}^2.$$

Equating $\mathcal{H}_1$ and $\mathcal{H}_2$ leads to the following expressions for the radii, at which the contributions are equal:

$$R_p^s = \frac{2}{k}\sqrt{\frac{1}{1+\cos^2(\theta)}} \underset{\theta\to 0}{\approx} \frac{\sqrt{2}}{k}\left(1+\frac{\theta^2}{4}\right),$$

$$R_p^h = \frac{2}{k}\frac{1}{\sin(\theta)}\sqrt{\frac{2\tan^2(\theta/2)}{1-\tan^4(\theta/2)}} \underset{\theta\to 0}{\approx} \frac{\sqrt{2}}{k}\left(1+\frac{\theta^2}{4}\right).$$

It can be concluded that for the optical fields the quantum core radius does not depend on the polarization in the paraxial limit. For a typical Bessel beam with a wavelength of $\lambda \sim 633$ nm [134, 135] and $\theta \sim \pi/90$, this radius will be of the order of 10^{-6} m, and possibly detectable in experiments. This is subject to the possibility of realising a scalar (i.e. fully polarized) optical field of which the helicity density is described by a single Bessel function.

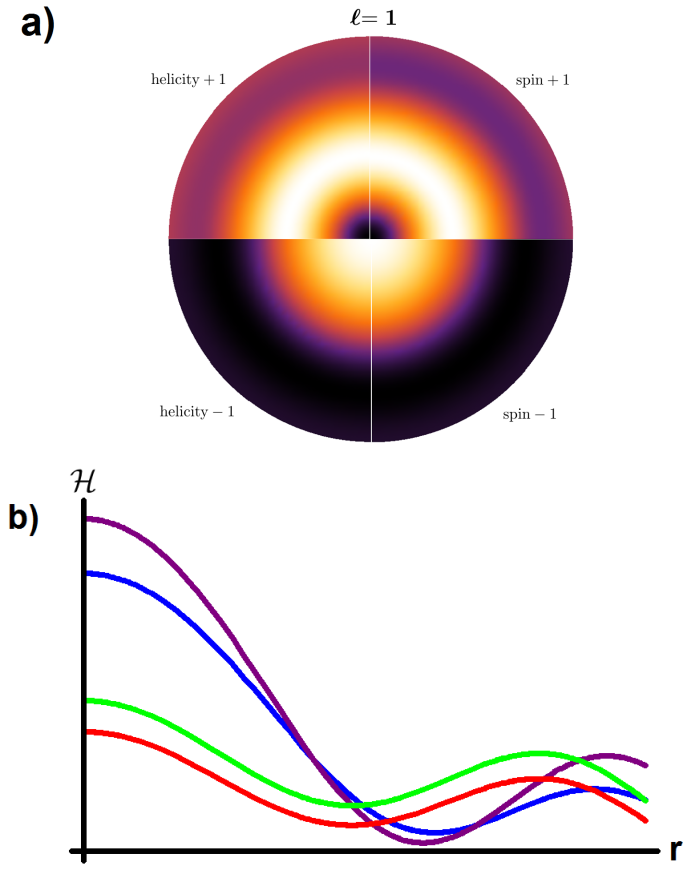

Figure 3.6: Helicity density of the right-handed and left-handed spin and helicity optical beams. a): Densityplot. b): Graph: Purple: helicity $+1$, Blue: spin $+1$, Green: spin -1, Red: helicity -1. For clarity $\theta = \pi/3$. As can be seen, the right-handed helicity state has a slightly larger helicity density than the right-handed spin state in its second maximum. The left-handed helicity and spin beams have a helicity distribution that varies similarly with the radial distance, keeping the ratio between the two approximately 1, with the helicity density of the helicity beam slightly smaller than that of the spin beam. The differences between spin and helicity ± 1 arise due to the presence of Bessel functions of the order 0, causing the helicity density to be non-zero on the beam axis. The small differences between the spin and helicity states can be explained by their different expressions.

The spin current densities are in the longitudinal direction given by:

$$\begin{aligned}\mathbf{S}_{\pm}^{z,s} &= \pm\frac{1}{2k}\left[J_\ell^2\left(\frac{1+9\cos^2(\theta)}{8\cos^2(\theta)}\right) - J_{\ell\pm2}^2\frac{\sin^4(\theta)}{4\cos^2(\theta)}\right] \\ &\approx \pm\frac{1}{k}\left[\left(1+\frac{\theta^4}{8}\right)J_\ell^2 - \frac{\theta^4}{8}J_{\ell\pm2}^2\right], \\ \mathbf{S}_{\pm}^{z,h} &= \frac{1}{k}\left[J_\ell^2 - J_{\ell\pm2}^2\tan^4(\theta/2)\right] \approx \pm\frac{1}{k}\left[J_\ell^2 - \frac{\theta^4}{16}J_{\ell\pm2}^2\right].\end{aligned} \tag{3.26a}$$

Similar to the helicity densities, the longitudinal spin densities of the two beams are the same for small powers of θ, and differences arise for θ^4, leading to a longitudinal spin density that is less (more) spread out for the right-(left-) handed spin states than for the right-(left-)handed helicity states. The difference is in fact given by the same expression as (3.25) up to orders of θ^4:

$$\mathbf{S}_{p,\pm}^{z,h} - \mathbf{S}_{p,\pm}^{z,s} \approx \frac{\theta^4}{16k}\left[J_{\ell\pm2}^2 - 2J_\ell^2\right].$$

However, there are no terms proportional to $J_{\ell\pm1}^2$.

The spin current densities in the azimuthal direction are given by:

$$\begin{aligned}\mathbf{S}_{p,\pm}^{\phi,s} &= \pm\frac{\tan(\theta)}{4k}J_{\ell\pm1}\left[J_\ell\left(3+\cos^2(\theta)\right) + J_{\ell\pm2}\sin^2(\theta)\right] \\ &\approx \pm\frac{\theta}{4k}J_{\ell\pm1}\left[4J_\ell + J_{\ell\pm2}\theta^2\right], \\ \mathbf{S}_{p,\pm}^{\phi,h} &= \pm\frac{2\tan(\theta/2)}{k}J_{\ell\pm1}\left[J_\ell + J_{\ell\pm2}\tan^2(\theta/2)\right] \\ &\approx \pm\frac{\theta}{4k}J_{\ell\pm1}\left[4J_\ell + J_{\ell\pm2}\theta^2\right].\end{aligned} \tag{3.27a}$$

These are the same for the spin and helicity beams, and vanish in the paraxial limit as desired.

It can be concluded that the helicity densities of the two beams are very similar to each other, and their quantum core radii are given by the same expressions in the paraxial limit. However, the helicity density of the helicity fields is smaller than the helicity density of the spin fields, as the electric and magnetic fields of the helical fields are proportional to each other.

The longitudinal currents are also very similar, with small differences arising for terms of $\mathcal{O}(\theta^4)$. The transverse spread depends on the handedness of the fields. The azimuthal currents of both fields are approximately the same, and reduce to zero in the paraxial limit.

3.4 The energy-momentum tensor components

In this section the components of the energy-momentum tensor of the optical and electron vortex beams will be discussed. The quantities of both the spin and helicity fields will be considered to identify specific contributions resulting from using in the spin or helicity representations. By applying the Belinfante symmetrization procedure (2.35) to the energy-momentum tensor a canonical part and spin part can be identified for all tensor components. For the spinor field these quantities are related to the gauge current, but this is not the case for the optical fields.

These symmetrized energy-momentum tensor components can be compared to the corresponding quantities for scalar Bessel beams (1.7) without the need for symmetrization, since the scalar energy-momentum tensor is symmetric. With the scalar Lagrangian density (2.18) given by

$$\mathcal{L} = \frac{1}{2}\left(\omega^2 - \frac{\ell^2}{r^2} - k_z^2 - m^2\right)|\varphi|^2 - \frac{1}{2}|\partial_r\varphi|^2 = \frac{1}{2}k_r^2\left(J_\ell^2 - \frac{1}{2}(J_{\ell-1}^2 + J_{\ell+1}^2)\right), \tag{3.28}$$

the energy-momentum tensor components are found to be

$$T^{00} = \omega^2 J_\ell^2 + \frac{k_r^2}{4}\left(J_{\ell-1}^2 - 2J_\ell^2 + J_{\ell+1}^2\right), \tag{3.29}$$

$$T^{0\phi} = \omega\frac{\ell}{r}J_\ell^2(k_r r), \tag{3.30}$$

$$T^{0z} = \omega k_z J_\ell^2(k_r r), \tag{3.31}$$

$$T^{rr} = \frac{k_r^2}{2}\left(J_\ell^2 - 2J_{\ell-1}J_{\ell+1}\right), \tag{3.32}$$

$$T^{\phi\phi} = \frac{\ell^2}{r^2}J_\ell^2 - \frac{k_r^2}{4r^2}\left(J_{\ell-1}^2 - 2J_\ell^2 + J_{\ell+1}^2\right), \tag{3.33}$$

$$T^{zz} = k_z^2 J_\ell^2 - \frac{k_r^2}{4}\left(J_{\ell-1}^2 - 2J_\ell^2 + J_{\ell+1}^2\right). \tag{3.34}$$

Comparing these expressions to the scalar gauge density (3.12) and current (3.13) shows that for a scalar field the momentum density is proportional to the gauge current; $T^{0j} = \frac{\omega}{2}J^j$. The T^{0r} component is zero. It can be concluded that the fields are indeed invariant under $\hat{\mathbf{z}}$ and $\widehat{\boldsymbol{\phi}}$ translations, but not under $\hat{\mathbf{r}}$ translations. The shear stresses are zero.

3.4.1 Energy-momentum tensor components of optical Bessel beams

The energy-momentum tensor of the optical field is given by equation (2.44). The energy density, momentum densities and stress densities will be discussed

separately, before considering the conservation of energy and momentum. Where appropriate the quantities of the spin and helicity beams can be compared with each other or with the scalar quantities.

Energy density

The energy density of a field is described by the Θ^{00} component of the energy-momentum tensor, for the electromagnetic field given by

$$\Theta^{00} = \frac{1}{2}(|E|^2 + |B|^2). \tag{3.35}$$

This can be separated in the canonical part and the spin part as summarized in table 2.1:

$$T^{00} = (-\partial_t \mathbf{A}) \cdot \mathbf{E}^* - \frac{1}{2}(|E|^2 - |B|^2), \qquad \Theta^{00} - T^{00} = -\mathbf{E}^* \cdot \nabla V.$$

Throughout this thesis the convention $V = 0$ will be adopted, and thus $T^{00} = \Theta^{00}$. The energy densities of the spin and helicity fields are:

$$(\Theta^{00})^s_\pm = J_\ell^2 \left(\frac{1 - 6\cos^2(\theta) + \cos^4(\theta)}{8\cos^2(\theta)} \right) + J_{\ell\pm1}^2 \left(\frac{1 + \cos^2(\theta)}{4} \right) + J_{\ell\pm2}^2 \left(\frac{\sin^4(\theta)}{64\cos^2(\theta)} \right),$$

$$(\Theta^{00})^h_\pm = J_\ell^2 + 2\tan^2(\theta/2) J_{\ell\pm1}^2 + \tan^4(\theta/2) J_{\ell\pm2}^2.$$

The energy density of the spin fields contains many different terms, while this is not the case for the helicity states. This can be explained by the fact that the magnetic field of the spin fields is not proportional to the electric field, and hence the product $|E|^2 + |B|^2$ contains different powers of cosines. Further, the Lagrangian density $\mathcal{L}$ is zero for the helicity fields but not for the spin fields. However, the extra contributions to the J_ℓ^2 term vanish in the paraxial limit since these are proportional to θ^4:

$$(\Theta^{00})^s_\pm \approx J_\ell^2 \left(1 + \frac{\theta^4}{8}\right) + J_{\ell\pm1}^2 \left(\frac{\theta^2}{2} + \frac{\theta^4}{12} \right) + \frac{\theta^4}{8} J_{\ell\pm2}^2,$$

$$(\Theta^{00})^h_\pm \approx J_\ell^2 + J_{\ell\pm1}^2 \left(\frac{\theta^2}{2} + \frac{\theta^4}{12} \right) + \frac{\theta^4}{16} J_{\ell\pm2}^2.$$

Up to low orders of θ, the two energy densities are the same, with differences of the order θ^4. The term proportional to $J_{\ell\pm2}^2$ comes solely from the magnetic field in the case of the spin fields, while both the electric and magnetic fields of the helicity beams contribute to this term.

Since the Lagrangian density of the scalar field is non-zero, it is not straightforward to compare the expressions of the energy density, as these contain a lot of different terms. The main conclusion from the comparison of the energy density between the helicity fields and the scalar field is that on the one hand, the helicity field has three components that all contribute, but on the other hand the Lagrangian density of the scalar field brings in Bessel functions of different orders.

Longitudinal momentum density

The momentum density of the electromagnetic field is given by the real part of the Poynting vector

$$\boldsymbol{\mathcal{S}} = \mathbf{E}^* \times \mathbf{B}. \tag{3.36}$$

This is the complex version of the expression as derived in (2.45)[5]. The canonical part of (3.36) is now given by $\mathbf{T} = \mathbf{E}^* \cdot \nabla \mathbf{A}$.

In the longitudinal direction, the momentum densities are given by the following expressions, and can be split in scalar, orbital and spin parts:

$$\begin{aligned}
(\mathcal{S}^z)^s &= \frac{1+\cos^2(\theta)}{\cos(\theta)} J_\ell^2, && \text{(3.37a)}\\
&= \cos(\theta) J_\ell^2 + \frac{\sin^2(\theta)}{2\cos(\theta)} J_{\ell\pm1}^2 + \frac{\sin^2(\theta)}{2\cos(\theta)} (J_\ell^2 - J_{\ell\pm1}^2),\\
(\mathcal{S}^z)^h &= J_\ell^2 - \tan^4(\theta/2) J_{\ell\pm2}^2, && \text{(3.37b)}\\
&= J_\ell^2 \cos(\theta) + \cos(\theta)\tan^2(\theta/2)[2J_{\ell\pm1}^2 + \tan^2(\theta/2) J_{\ell\pm2}^2]\\
&\qquad + 2\tan^2(\theta/2)\left[\cos^2(\theta/2) J_\ell^2 - \cos(\theta) J_{\ell\pm1}^2 - \sin^2(\theta/2) J_{\ell\pm2}^2\right].
\end{aligned}$$

For both fields the terms proportional to $J_{\ell\pm1}^2$ cancel each other. This is exactly the orbital contribution for the spin states. It is remarkable that the spin part of the spin fields also contains a term J_ℓ^2.

Approximating the expressions for small θ shows the similarities and differences:

$$\begin{aligned}
(\mathcal{S}^z)^s_\pm &\approx J_\ell^2 \left(1 - \frac{\theta^2}{2} + \frac{\theta^2}{2}\right) + J_{\ell\pm1}^2 \frac{\theta^2}{2} - J_{\ell\pm1}^2 \frac{\theta^2}{2},\\
(\mathcal{S}^z)^h_\pm &\approx J_\ell^2 \left(1 - \frac{\theta^2}{2} + \frac{\theta^2}{2}\right) + J_{\ell\pm1}^2 \frac{\theta^2}{2} - J_{\ell\pm1}^2 \frac{\theta^2}{2} + J_{\ell\pm2}^2 \frac{\theta^4}{16} - J_{\ell\pm2}^2(k_r r)\frac{\theta^4}{8}.
\end{aligned}$$

Differences arise in θ^4 terms, while for lower powers of θ the spin and orbital contributions cancel each other.

[5] As mentioned in section 1.6 the electromagnetic fields are real, but making them complex is a mathematical trick that simplifies calculations.

The difference between the Poynting vector and the scalar momentum density (3.31) rescaled by $k\omega$ is:

$$(\mathcal{S}^z)^s - \frac{T^{0z}}{k\omega} = \frac{\sin^2(\theta)}{2\cos(\theta)} J_\ell^2 \approx \left(\frac{\theta^2}{2} + \frac{\theta^4}{12}\right) J_\ell^2,$$
$$(\mathcal{S}^z)^h - \frac{T^{0z}}{k\omega} = (1-\cos(\theta)) J_\ell^2 - \tan^4(\theta/2) J_{\ell\pm2}^2 \approx \left(\frac{\theta^2}{2} - \frac{\theta^4}{24}\right) J_\ell^2 + \frac{\theta^4}{16} J_{\ell\pm1}^2,$$

where higher order terms of θ are ignored. This shows that differences in the longitudinal momentum arise with θ^4, where the difference between the momentum densities of the scalar and optical helicity fields is slightly smaller than that between the scalar and optical spin fields.

Azimuthal momentum density

The optical azimuthal momentum densities are decomposed as follows:

$$(\mathcal{S}^\phi)^s = \frac{\ell}{kr} J_\ell^2 + \frac{\ell \pm 1}{2kr} \tan^2(\theta) J_{\ell\pm1}^2 \pm \left(\frac{\ell-1}{kr} J_\ell^2 - J_\ell J_{\ell-1} \sin(\theta)\right), \tag{3.38a}$$

$$(\mathcal{S}^\phi)^h = \frac{\ell}{kr} J_\ell^2 + \tan^2(\theta/2) \left(\frac{2(\ell\pm1)}{kr} J_{\ell\pm1}^2 + \frac{\ell\pm2}{kr} \tan^2(\theta/2) J_{\ell\pm2}^2\right)$$
$$\pm \sin(\theta) \left(\frac{1}{2} J_\ell (J_{\ell+1} - J_{\ell-1}) \pm \tan^4(\theta/2) J_{\ell\pm1} J_{\ell\pm2} \mp \frac{\ell\pm2}{kr} \tan^4(\theta/2) J_{\ell\pm2}^2\right). \tag{3.38b}$$

The orbital part of the azimuthal momentum density is always dependent on the spin state, while the sign of the spin part depends on the spin state considered, in addition to the orders of the Bessel functions. Every term in the expression of the orbital part is weighted by its azimuthal winding number divided by the product of radius and wavenumber; $(\ell\pm1)/kr$ and $(\ell\pm2)/kr$. As expected, the azimuthal momentum vanishes in the paraxial limit, as in this limit all wave vectors are aligned with the $\hat{\mathbf{z}}$-axis.

The spin contribution to the azimuthal momentum of the spin fields has a term independent on θ, while for higher powers of θ the contributions of both the spin and helicity states are the same:

$$\pm\left(\frac{\ell-1}{kr} J_\ell^2 - J_\ell J_{\ell-1}\sin(\theta)\right) = \mp\frac{1}{kr} J_\ell^2 \pm \frac{1}{2}\sin(\theta) J_\ell (J_{\ell+1} - J_{\ell-1})$$
$$\approx \mp\frac{1}{kr} J_\ell^2 \pm \frac{1}{2} J_\ell (J_{\ell+1} - J_{\ell-1}) \left(\theta - \frac{1}{6}\theta^3\right) + \mathcal{O}(\theta^4),$$
$$\text{spin part}(\mathcal{S}^\phi)^h \approx \pm\frac{1}{2} J_\ell (J_{\ell+1} - J_{\ell-1}) \left(\theta - \frac{1}{6}\theta^3\right) + \mathcal{O}(\theta^4).$$

To compare the azimuthal momentum density with the scalar equivalent (3.30), the average of both states needs to be taken; $(\widetilde{\mathcal{S}}^{\phi}) = \frac{1}{2}((\mathcal{S}^{\phi})_{+} + (\mathcal{S}^{\phi})_{-})$. The differences between these quantities and the scalar momentum density are:

$$\begin{aligned}
(\widetilde{\mathcal{S}}^{\phi})^{s} - \frac{T^{0\phi}}{k\mathcal{E}} &= \left[\frac{\sin(\theta)}{4}\left(\frac{1}{\cos^2(\theta)} + 1\right)\right] J_{\ell}(J_{\ell-1} + J_{\ell+1}) + \dots \\
&\approx \left(\frac{\theta}{2} + \frac{\theta^3}{6}\right) J_{\ell}(J_{\ell-1} + J_{\ell+1}) + \frac{\theta^3}{4}\dots, \\
(\widetilde{\mathcal{S}}^{\phi})^{h} - \frac{T^{0\phi}}{k\mathcal{E}} &= \sin(\theta/2)\left(\frac{2}{\cos(\theta/2)} - \cos(\theta/2)\right) J_{\ell}(J_{\ell-1} + J_{\ell+1}) + \dots \\
&\approx \left(\frac{\theta}{2} + \frac{\theta^3}{6}\right) J_{\ell}(J_{\ell-1} + J_{\ell+1}) + \frac{\theta^3}{4}\dots.
\end{aligned}$$

Here the dots denote the extra terms of order $J_{\ell\pm2}$, that do not appear in the scalar expression. Perhaps remarkable is that the spin and helicity momentum densities are equal up to (the high power of) $\mathcal{O}(\theta^3)$ and differences only appear for $\mathcal{O}(\theta^5)$; $\frac{31}{240}$ for the spin fields compared to $\frac{1}{240}$ for the helicity fields. This is simply a result of the trigonometric identities.

The energy density and Poynting vector form a conserved four-current;

$$\partial_t \Theta^{00} - \partial_r \mathcal{S}_r - \frac{1}{r}\partial_\phi \mathcal{S}_\phi - \partial_z \mathcal{S}_z.$$

Since all quantities in this equation are the product of a field and the complex conjugated field, no quantity does depend on either t, ϕ or z. The only coordinate they depend on is the radial distance r. Since the radial component of the Poynting vector is zero, the conservation of energy is automatically fulfilled.

Stresses

The normal stresses of the optical field are given by $\Theta^{jj} = |E^j|^2 + |B^j|^2 + \eta^{jj}\frac{1}{2}(|E|^2 + |B|^2)$, and all three are non-zero. The zz-stress is given by:

$$\begin{aligned}
(\Theta^{zz})^{s}_{\pm} &= J_{\ell}^2\left[\frac{35 + 28\cos(2\theta) + \cos(4\theta)}{64\cos^2(\theta)}\right] - \frac{1}{8}\tan^2(\theta)\left[J^2_{\ell\pm1}(3 + \cos(2\theta)) - J^2_{\ell\pm2}\sin^2(\theta)\right] \\
&\approx J_{\ell}^2 - \frac{1}{2}J^2_{\ell\pm1}\theta^2 + \frac{1}{24}\left(3J_{\ell}^2 - 2J^2_{\ell\pm1} + 3J^2_{\ell\pm2}\right)\theta^4, \\
(\Theta^{zz})^{h}_{\pm} &= J_{\ell}^2 - 2J^2_{\ell\pm1}\tan^2(\theta/2) + J^2_{\ell\pm2}\tan^4(\theta/2) \\
&\approx J_{\ell}^2 - \frac{1}{2}J_{\ell\pm1}\theta^2 + \frac{1}{24}\left(-2J_{\ell\pm1} + 3J^2_{\ell\pm2}\right)\theta^4.
\end{aligned}$$

This normal stress is the same for helicity and spin fields for small θ. Differences arise in the term proportional to θ^4, similar to the energy density; the zz-stress of the helicity fields is proportional to J_{ℓ}^2, but the stress of the spin fields is

proportional to $J_\ell^2(1+\frac{1}{8}\theta^4)$. The explanation for this is that the stress can be written as $\Theta^{zz} = |E_z|^2 + |B_z|^2 - \Theta^{00}$, where the z-components of the fields are proportional to $J_{\ell\pm1}$. The $\phi\phi$- and rr-stresses are given by:

$$(\Theta^{\phi\phi})^s_\pm = \frac{3+\cos(2\theta)}{8}\tan^2(\theta)\left(J^2_{\ell\pm1} + J_\ell J_{\ell\pm2}\right) \tag{3.39}$$

$$\approx \left(\frac{\theta^2}{2} + \frac{\theta^4}{12}\right)(J^2_{\ell\pm1} + J_\ell J_{\ell\pm2}), \tag{3.40}$$

$$(\Theta^{\phi\phi})^h_\pm = 2\tan^2(\theta/2)\left(J^2_{\ell\pm1} + J_\ell J_{\ell\pm2}\right) \tag{3.41}$$

$$\approx \left(\frac{\theta^2}{2} + \frac{\theta^4}{12}\right)(J^2_{\ell\pm1} + J_\ell J_{\ell\pm2}), \tag{3.42}$$

$$(\Theta^{rr})^s_\pm = \frac{3+\cos(2\theta)}{8}\tan^2(\theta)\left(J^2_{\ell\pm1} - J_\ell J_{\ell\pm2}\right) \tag{3.43}$$

$$\approx \left(\frac{\theta^2}{2} + \frac{\theta^4}{12}\right)(J^2_{\ell\pm1} - J_\ell J_{\ell\pm2}), \tag{3.44}$$

$$(\Theta^{rr})^h_\pm = 2\tan^2(\theta/2)\left(J^2_{\ell\pm1} - J_\ell J_{\ell\pm2}\right) \tag{3.45}$$

$$\approx \left(\frac{\theta^2}{2} + \frac{\theta^4}{12}\right)(J^2_{\ell\pm1} - J_\ell J_{\ell\pm2}). \tag{3.46}$$

Remarkable is that there is a difference between the azimuthal and radial stresses proportional to θ^2; $J_{\ell\pm2}$ vs. $\frac{1}{2}J_\ell J_{\ell\pm2}$, but the terms proportional to θ^4 are equal. Further, both stresses are approximately the same for the spin and helicity fields.

The only shear stresses that are non-zero are the ϕz- and $z\phi$-stresses. These are the same for the spin and helicity fields in the paraxial limit:

$$(\Theta^{\phi z})^s_\pm = \frac{\tan(\theta)}{8}J_{\ell\pm1}\left((7+\cos(2\theta))J_\ell - 2\sin^2(\theta)J_{\ell\pm2}\right)$$

$$\approx J_\ell J_{\ell\pm1}\theta + \frac{1}{12}J_{\ell\pm1}(J_\ell - 3J_{\ell\pm2})\theta^3,$$

$$(\Theta^{\phi z})^h_\pm = 2\tan(\theta/2)J_{\ell\pm1}\left(J_\ell - J_{\ell\pm2}\tan^2(\theta/2)\right)$$

$$\approx J_\ell J_{\ell\pm1}\theta + \frac{1}{12}J_{\ell\pm1}\left(J_\ell - 3J_{\ell\pm2}\right)\theta^3.$$

However, for a scalar field this stress is zero.

Noteworthy is that the rr-stress does not vanish in the paraxial limit, while the scalar stress (3.32) does. A non-vanishing radial stress does not automatically pose a problem, as the momentum density can still be conserved. The divergence of the stress tensor is equal to the time derivative of the momentum density, forming a conserved 4-current;

$$\partial_t \mathcal{S}_j + \partial^i \Theta_{ij} = 0.$$

In cylindrical coordinates the divergence of the stress tensor is given by:

$$\partial^i \Theta_{ij} = \left(\partial_r \Theta_{rr} + \frac{1}{r}\Theta_{rr} + \frac{1}{r}\partial_\phi \Theta_{r\phi} + \partial_z \Theta_{rz} - \frac{1}{r}\Theta_{\phi\phi}\right)\hat{\mathbf{r}} + \left(\partial_r \Theta_{r\phi} + \frac{1}{r}\Theta_{r\phi} + \frac{1}{r}\partial_\phi \Theta_{\phi\phi} + \partial_z \Theta_{\phi z} + \frac{1}{r}\Theta_{r\phi}\right)\hat{\boldsymbol{\phi}} + \left(\partial_r \Theta_{rz} + \frac{1}{r}\Theta_{rz} + \frac{1}{r}\partial_\phi \Theta_{\phi z} + \partial_z \Theta_{zz}\right)\hat{\mathbf{z}}. \quad (3.47)$$

Considering the components of the Poynting vector individually, this leads to the following conditions:

$$\left(\partial_r \Theta_{rr} + \frac{1}{r}\Theta_{rr} - \frac{1}{r}\Theta_{\phi\phi}\right) = 0, \quad (3.48)$$

$$\left(\frac{1}{r}\partial_\phi \Theta_{\phi\phi} + \partial_z \Theta_{\phi z}\right) = \frac{1}{r}\partial_t \mathcal{S}^\phi = 0, \quad (3.49)$$

$$\left(\frac{1}{r}\partial_\phi \Theta_{\phi z} + \partial_z \Theta_{zz}\right) = \frac{1}{r}\partial_t \mathcal{S}^z = 0. \quad (3.50)$$

The only condition that is not trivially satisfied is (3.48). However, the expressions (3.39), (3.41), (3.43) and (3.45) do satisfy this condition.

Discussion

It can be concluded that differences between the energy densities of the spin and helicity states come from two parts; the fact that the electric field has multiple components and that these all contribute, and the Lagrangian density which is zero for the helicity fields, but non-zero for the scalar and the spin-polarized electric fields. The orbital part of the longitudinal momentum density is totally (spin) or partially (helicity) cancelled by the spin part. This spin part has terms that are independent of the spin state. Differences between the longitudinal momentum densities of both fields are of the order θ^4. The difference between the longitudinal momentum densities of the scalar field and the helicity fields is slightly smaller than between the scalar and spin fields, although there is a term proportional to $J_{\ell\pm1}$. This term is small in the paraxial limit.

The radial behaviour of the orbital part of the momentum densities depends on the spin state (up/down or right-/left-handed), while the spin part of the spin fields contains a term independent of the spin. Here it is the overall sign of the spin part that depends on the spin state. All terms of the scalar and orbital part are weighted by their azimuthal quantum number. Differences with the scalar azimuthal momentum density are the same for both the spin and helicity fields and of order θ.

The different contributions to the energy and momentum densities are summarized in the following table, with $n = 1, 2$:

		Orbital J^2_ℓ	Orbital $J^2_{\ell\pm n}$	Spin J^2_ℓ	Spin $J^2_{\ell\pm n}$	Spin $\pm$
Spin	energy	✓	✓	n/a	n/a	n/a
	$\mathcal{S}^z$	x	✓	✓	✓	x
	$\mathcal{S}^\phi$	x	✓	✓	✓	✓
Helicity	energy	✓	✓	n/a	n/a	n/a
	$\mathcal{S}^z$	x	✓	✓	✓	x
	$\mathcal{S}^\phi$	x	✓	x	✓	✓

Table 3.2: Contributions to the energy and momentum densities of the optical spin and helicity Bessel beams

3.4.2 Energy-momentum tensor components of spinor Bessel beams

Similarly to the optical Bessel beams, the energy-momentum components of the electron Bessel beams will be discussed for both the helicity and spin states. The energy-momentum tensor of the Dirac field is given by (2.42). Components of this tensor are related to the gauge current that can be separated into a scalar-like part and spin part as a consequence of the Gordon decomposition.

Energy density

The energy density of the fermion field is given by $\Theta^{00} = \frac{i}{2}(\psi^\dagger \partial_t \psi - (\partial_t \psi^\dagger)\psi)$. The Lagrangian density does not play a role here as it is zero for the Dirac field. Since the spinor ψ depends only on time as $e^{-i\mathcal{E}t}$, the energy density is proportional to the probability densities (3.14) and (3.15):

$$(\Theta^{00}_e)^{s,h}_\pm = \mathcal{E}(\rho_e)^{s,h}_\pm.$$

This is comparable to the scalar energy density, although this energy density is quadratic in energy instead of linear: $\mathcal{E}^2\rho$. Further, the symmetrized energy density is equal to the canonical energy density; $\Theta^{00}_e = T^{00}_e$.

The scalar energy density can compactly be written as $T^{00} = \omega^2\rho - \mathcal{L}$ and hence there are two reasons for the difference between the spinor and scalar energy densities; the multicomponent nature of the spinor field and the non-zero Lagrangian density of the scalar field;

$$\frac{1}{\mathcal{E}}\Theta^{00}_e - \frac{1}{\omega^2}T^{00} = \rho_e - \rho + \frac{1}{\omega^2}\mathcal{L}.$$

Momentum density

The symmetrized momentum density can be split into a canonical momentum density and a spin part as in (2.41). However, another useful separation is to split the momentum density into a part proportional to the canonical momentum density and a part proportional to the probability density;

$$\Theta^{0j} = \frac{1}{2}T_e^{0j} + \frac{\mathcal{E}}{2}\mathbf{J}_e^j. \tag{3.51}$$

In general, the scalar, orbital and spin contributions can be identified as the respective parts of the gauge current and canonical momentum density. The canonical longitudinal momentum density is proportional to the probability density, both for spin (3.14) and helicity (3.15) EVBs:

$$(T_e^{0z})_\pm^{s,h} = k\cos(\theta)(\rho_e)_\pm^{s,h}.$$

This momentum density resembles the scalar momentum density $T^{0z} = k_z\mathcal{E}\rho$ (3.31). Combining this with the longitudinal probability currents (3.18) and (3.19), the symmetrized longitudinal momentum density becomes

$$(\Theta_e^{0z})_\pm^s = \frac{k}{2}\cos(\theta)J_\ell^2 + k\cos(\theta)\left(\frac{\mathcal{E}+m}{4\mathcal{E}}J_\ell^2 + \frac{\mathcal{E}-m}{4\mathcal{E}}\left(\cos^2(\theta)J_\ell^2 + \sin^2(\theta)J_{\ell\pm1}^2\right)\right),$$
$$(\Theta_e^{0z})_\pm^h = k\left(\cos^4(\theta/2)J_\ell^2 - \sin^4(\theta/2)J_{\ell\pm1}^2\right).$$

Moving on to the canonical azimuthal momentum density, this quantity is not proportional to the probability density, as every term is weighted by the order of the Bessel function divided by the radius:

$$(T_e^{0\phi})_\pm^s = \frac{\mathcal{E}+m}{2\mathcal{E}}\left(\frac{\ell}{r}[1+\varepsilon^2\cos^2(\theta)]J_\ell^2 + \frac{\ell\pm1}{r}\varepsilon^2\sin^2(\theta)J_{\ell\pm1}^2\right),$$
$$(T_e^{0\phi})_\pm^h = \frac{\ell}{r}\cos^2(\theta/2)J_\ell^2 + \frac{\ell\pm1}{r}\sin^2(\theta/2)J_{\ell\pm1}^2.$$

As the azimuthal probability current (3.20) is the same for both the spin and helicity fields, the symmetrized momentum densities become:

$$(\Theta_e^{0\phi})_\pm^s = \frac{1}{2}(T_e^{0\phi})_\pm^s + \frac{1}{2}k\sin(\theta)J_\ell J_{\ell\pm1},$$
$$(\Theta_e^{0\phi})_\pm^h = \frac{1}{2}(T_e^{0\phi})_\pm^h + \frac{1}{2}k\sin(\theta)J_\ell J_{\ell\pm1}.$$

It can be concluded that the expressions for the energy density and symmetrized momentum densities are all related to the gauge density and currents. Hence the orbital and spin effects of the energy-momentum tensor are directly related to the orbital and spin effects of the conserved gauge current.

Stresses

The normal stress components of the Dirac energy-momentum tensor (2.42) are given by:

$$\Theta^{jj} = \frac{i}{2}\left(\bar{\psi}\gamma^j\partial_j\psi - (\partial_j\bar{\psi})\gamma^j\psi\right) = T^{jj}.$$

The zz component can be simplified in terms of the probability current, as $\partial_z\psi = ik_z\psi$:

$$\Theta^{zz} = -k_z\left(\bar{\psi}\gamma^z\psi\right) = -k_z(\mathbf{J}_e^z)_\pm.$$

Hence the separation into a canonical and spin part is the same as for the longitudinal probability current. For completeness, the stresses for the spin and helicity states are given by:

$$(\Theta^{zz})^s_\pm = -\frac{k^2}{\mathcal{E}}\cos^2(\theta)J_\ell^2,$$
$$(\Theta^{zz})^s_\pm = -\frac{k^2}{\mathcal{E}}\cos(\theta)\left[\cos^2(\theta/2)J_\ell^2 - \sin^2(\theta/2)J_{\ell\pm1}^2\right].$$

Similar to the stresses for the electromagnetic field, these expressions are difficult to compare with the scalar quantities as the Dirac Lagrangian is zero, but the scalar Lagrangian is not.

The $\phi\phi$-stress is also proportional to the azimuthal probability density, although this might not be expected since not all components of the spinor have the same azimuthal winding number. This is explained by the fact that γ^ϕ is anti-diagonal, and hence the stress is calculated by the following matrix multiplication:

$$\Theta^{\phi\phi} = \frac{i}{2}\left[(\psi_1^*,\psi_2^*,-\psi_3^*,-\psi_4^*)\begin{pmatrix} & & & -ie^{-i\phi} \\ & & ie^{i\phi} & \\ & -ie^{-i\phi} & & \\ ie^{i\phi} & & & \end{pmatrix}\partial_\phi\begin{pmatrix}\psi_1\\ \psi_2\\ \psi_3\\ \psi_4\end{pmatrix} + \psi \leftrightarrow \bar{\psi}\right].$$

Every product of terms, for example $\psi_1^*\psi_4$, occurs twice. Once the derivative ∂_ϕ gives a factor ℓ, the other time $\ell \pm 1$. This averages out to $\ell \pm 1/2$. Consequently the $\phi\phi$-stress is given by:

$$\Theta^{\phi\phi} = -\frac{\ell \pm 1/2}{r}(\bar{\psi}\gamma^\phi\psi) = -\frac{\ell \pm 1/2}{r}(\mathbf{J}_e^\phi)_\pm = -\frac{k}{\mathcal{E}}\frac{\ell \pm 1/2}{r}J_\ell J_{\ell\pm1}. \tag{3.52}$$

A similar effect can be seen for the ϕz-component of the stress tensor, given by:

$$\Theta^{\phi z} = \frac{1}{2}(T^{\phi z} + T^{z\phi}) = \frac{i}{4}\left(\bar{\psi}\gamma^\phi\partial_z\psi - (\partial_z\bar{\psi})\gamma^\phi\psi + \frac{1}{r}\bar{\psi}\gamma^z\partial_\phi\psi - \frac{1}{r}(\partial_\phi\bar{\psi})\gamma^z\psi\right).$$

The term $\frac{1}{2}T^{\phi z}$ is for both the helicity and spin states equal to $-\frac{k_z}{4}\bar{\psi}\gamma^\phi\psi = -\frac{k_z}{4}\mathbf{J}_e^\phi$. However, the term $\frac{1}{2}T^{z\phi}$ can be written in terms of the longitudinal probability

current for the spin states, but not for the helicity states. This is because the longitudinal probability current only contains one order of Bessel functions for the spin states, while both orders are present for the helicity states:

$$\begin{aligned}\frac{1}{2}(T^{z\phi})^s_\pm &= -\frac{1}{4}\frac{\ell}{r}(\bar\psi\gamma^z\psi) = -\frac{\ell}{4r}(\mathbf{J}^z_e)^s_\pm,\\ \frac{1}{2}(T^{z\phi})^h_\pm &= -\frac{k}{4\mathcal{E}}\left[\frac{\ell}{r}\cos^2(\theta/2)J^2_\ell - \frac{\ell\pm1}{r}\sin^2(\theta/2)J^2_{\ell\pm1}\right]\\ &= -\frac{\ell}{4r}(\mathbf{J}^z_e)^h_\pm \pm \frac{k}{2\mathcal{E}r}\sin^2(\theta/2)J^2_{\ell\pm1}.\end{aligned}$$

The total ϕz-stress now becomes:

$$\begin{aligned}(\Theta^{\phi z})^s_\pm &= -\frac{1}{4}\left(k_z(\mathbf{J}^\phi_e)^s_\pm + \frac{\ell}{r}(\mathbf{J}^z_e)^s_\pm\right),\\ &= -\frac{k}{2\mathcal{E}}\frac{\ell}{r}\cos(\theta)J^2_\ell - \frac{k^2}{2\mathcal{E}}\cos(\theta)\sin(\theta)J_\ell J_{\ell\pm1},\\ (\Theta^{\phi z})^h_\pm &= -\frac{1}{4}\left(k_z(\mathbf{J}^\phi_e)^h_\pm + \frac{\ell}{r}(\mathbf{J}^z_e)^h_\pm\right) \pm \frac{k}{2\mathcal{E}r}\sin^2(\theta/2)J^2_{\ell\pm1},\\ &= -\frac{k}{2\mathcal{E}}\left(\frac{\ell}{r}\cos^2(\theta/2)J^2_\ell - \frac{\ell\pm1}{r}\sin^2(\theta/2)J^2_{\ell\pm1}\right) \pm \frac{k^2}{2\mathcal{E}}\cos(\theta)\sin(\theta)J_\ell J_{\ell\pm1}.\end{aligned}$$

The only component that cannot be expressed in terms of the probability current is the rr-stress:

$$\Theta^{rr} = T^{rr} = \frac{i}{2}\left(\bar\psi\gamma^r\partial_r\psi - (\partial_r\bar\psi)\gamma^r\psi\right).$$

These stress components for the spin and helicity states are equal to each other, and given by:

$$\Theta^{rr} = -\frac{k_r^2}{4\mathcal{E}}\left(J^2_\ell + J^2_{\ell\pm1} - J_{\ell+1}J_{\ell-1} - J_\ell J_{\ell\pm2}\right). \tag{3.53}$$

The other components, $\Theta^{r\phi}$ and Θ^{rz} are zero for both fields. Considering the conservation of momentum, the only condition that is not automatically satisfied is (3.48) since all stress components only depend on the radial distance r. However, with the expressions (3.52) and (3.53) this condition is fulfilled.

3.5 Discussion

The overall conclusion of this chapter is that differences between the helicity and spin states are in general small and disappear in the paraxial limit, $\theta \to 0$, for both the optical and spinor field.

Gauge quantities The spinor quantities related to the $U(1)$ gauge symmetry can be separated in a scalar, orbital and spin part. The orbital and spin parts are proportional to $\sin(\theta)$ for the spin states and $\sin(\theta/2)$ for the helicity states.

The orbital and spin parts of the gauge quantities of the helicity beams are proportional to the *difference* $J_\ell^2 - J_{\ell\pm1}^2$, which will vanish for small radii, while for larger radii this becomes equal to a periodically oscillating function of amplitude $\frac{1}{k_r r}$. The density distribution of the helicity beams does not have a spin contribution. For the spin beams, some contributions are proportional to this same factor, but others are proportional to the *sum* $J_\ell^2 + J_{\ell\pm1}^2$, which approximates to a constant value $\frac{1}{k_r r}$.

The azimuthal current can be completely contributed to the spin contribution. The scalar current can be found by taking the average of the two azimuthal currents for both the spin or helicity states.

The helicity densities of the electromagnetic beams cannot be compared with the scalar quantities as there is no scalar equivalent. There is no distinction between the spin and helicity beams for small powers of θ, while differences arise in terms of order θ^4. This difference starts out as either positive or negative at small distances from the beam axis, but will end up oscillating close to zero for larger radii. The helicity density of the helical fields is *smaller* than that of the spin fields.

Energy and momentum densities The energy and momentum densities of the spinor field can be directly traced back to the gauge quantities. Differences between the optical and scalar quantities come from two parts; the fact that the electric field has multiple components that all contribute, and the Belinfante symmetrization accounting for the spin current.

Differences in the energy density between the spin and helicity fields can also be explained by the fact that the Lagrangian density of the spin polarized fields is non-zero, while this is zero for the helicity polarized fields.

The spin part of the longitudinal momentum has a term that is not dependent on the polarization of the fields. The orbital part of the momentum densities always depends on the spin state (up/down, right-/left-handed), while the spin part of the spin fields contains a term independent of the spin, with only the overall sign depending on the spin state. All terms of the scalar and orbital part are weighted by their azimuthal quantum number.

Differences between scalar and spinor or vector fields The largest corrections to the spinor (electron) quantities relative to the scalar ones are found in the probability density; these are of the order of 10^{-4} in magnitude. This results in a quantum core radius that is too small ($\sim 10^{-13}$ m) to be observed. Other corrections, for example on the spinor longitudinal current, are orders of magnitude smaller; these are 10^{-9} of the total current density. However, the azimuthal current could prove helpful to distinguish between a spinor and scalar beam, for example when the energy of the beam becomes very large and spin effects cannot be ignored, as the superposition of the azimuthal currents of two oppositely polarized beams is proportional to the scalar current.

The optical quantities contain a scalar term and further corrections that all disappear in the paraxial limit. The way to distinguish between a vector and scalar beam is hence not in the measurement of these quantities, but in the polarization direction. As the components are described by different orders of Bessel functions, the polarization changes with the radial distance. Differences between helicity beams and spin beams are also very small and unlikely to be measured. However, if an optical field could be constructed for which the helicity density was described by a single Bessel function, there would be a difference measurable; the quantum core radius for the optical beams is of the order of 10^{-6} m.

This chapter focused on the distinction between helical beams and beams that were spin-polarized in the longitudinal direction. This corresponds to circular polarization for both the optical field and electron field, as these fields have only two spin degrees of freedom. However, beams can also be polarized in either of the transverse directions. These polarization states are superpositions of the two circular polarization states, while superpositions of the two helicity states also exist. The differences between these beams will be the focus of chapter 4.

4 Linear polarization and the Majorana representation

Light in free space can be described in either the linear or circular polarization basis[1]. These two descriptions are both equally valid, as a linearly polarized wave is a superposition of both a left- and right-handed circularly polarized wave and a circularly polarized wave is a superposition of two waves that are linearly polarized in the transverse directions [75].

Helicity and circular polarization are indistinguishable for *plane waves*, with differences arising when the polarization of light beams is considered. These differences were discussed in chapter 3. Similarly, a linearly polarized wave is comparable to a TE or TM mode. These modes arise in waveguides, when due to the boundary conditions either the electric or magnetic field is transverse, while the other field is allowed to have a longitudinal component [75]. However, a plane wave in vacuum is completely transverse. Moreover, linearly polarized optical beams are considerably different from TE and TM optical beams. The discrepancies between these modes will be the focus of this chapter.

Fermionic states that are polarized in the transverse plane (similar to linearly polarized light) can be derived from superpositions of the spin-polarized states [52] that were discussed in chapter 3. However, these differ from superpositions of helical spinor beams that are more similar to Majorana states. These will henceforth be called quasi-Majorana, and this chapter will conclude with a comparison between these states and the actual Majorana states.

4.1 Linearly polarized and TE/TM optical Bessel beams

A short review of the research performed on vector Bessel beams was given in section 3.1. The experiments mentioned here focused each on a vortex beam that

[1] Or, for that matter, by any two points that are opposite to each other on the Poincaré sphere.

was polarized in a unique way. In addition, there have been a number of studies into the effects of the polarization on the properties of these beams, such as the ability for self-healing. For example [140, 134], that studied the self-healing of the *polarization* state of radially and azimuthally polarized Bessel beams; whether the obstructed beam has the same polarization as the initial beam. Radially and linearly polarized Bessel-Gauss beams were compared in [141]. It was found that the radially polarized beam has a better self-healing ability than the linearly polarized beam, and that the polarization state of the radially polarized beam was modified by the obstacle.

In 2002 it was predicted that radially and azimuthally polarized Bessel beams do not carry OAM when the OAM density is integrated over all space [151]. This was experimentally confirmed in 2006 [152]. These beams were created from LG beams converted by an axicon. Similar beams can also be created using an optical element, that creates a phase difference from local changes in the polarization [153].

The differences between spin and helicity Bessel beams vanish in the paraxial limit. One can wonder if this is also the case for differences between the linearly polarized states and the TE and TM modes for light, and the quasi-Majorana states for electrons. Using the knowledge that the lowest order TM and TE beams are radially and azimuthally polarized [152], can the observation of a vanishing OAM be confirmed?

In the next section the linearly polarized Bessel beams will be derived, followed by the derivation of the TE and TM modes for optical Bessel beams.

4.1.1 Linearly polarized Bessel beams

Linearly polarized plane waves are related to circularly polarized plane waves by the relationships:

$$\mathbf{E}_X = \frac{1}{\sqrt{2}}(\mathbf{E}_+ + \mathbf{E}_-), \qquad \mathbf{E}_Y = -\frac{i}{\sqrt{2}}(\mathbf{E}_+ - \mathbf{E}_-). \tag{4.1}$$

Linearly polarized Bessel beams can be constructed in the same way. However, the circularly polarized beams (3.6) need to have the same OAM value; $\mathbf{E}_X^\ell = \frac{1}{\sqrt{2}}(\mathbf{E}_+^\ell + \mathbf{E}_-^\ell)$ and $\mathbf{E}_Y^\ell = -\frac{i}{\sqrt{2}}(\mathbf{E}_+^\ell - \mathbf{E}_-^\ell)$, as this will create beams with one transverse field component in the Cartesian basis:

$$\mathbf{E}_X^\ell(t,\mathbf{r}) = \begin{pmatrix} J_\ell \\ 0 \\ \frac{i}{2}\tan(\theta)(J_{\ell-1}e^{-i\phi} - J_{\ell+1}e^{i\phi}) \end{pmatrix} e^{-i\omega t + ik_z z + i\ell\phi},$$

$$\mathbf{E}_Y^\ell(t,\mathbf{r}) = \begin{pmatrix} 0 \\ J_\ell \\ -\frac{1}{2}\tan(\theta)(J_{\ell-1}e^{-i\phi} + J_{\ell+1}e^{i\phi}) \end{pmatrix} e^{-i\omega t + ik_z z + i\ell\phi},$$

with the capital subscript denoting the polarization direction. In the helical basis (1.14) these fields are:

$$\mathbf{E}_X^\ell(t,\mathbf{r}) = \frac{1}{\sqrt{2}} \begin{pmatrix} J_\ell \\ J_\ell \\ \frac{i}{\sqrt{2}}\tan(\theta)(J_{\ell-1}e^{-i\phi} - J_{\ell+1}e^{i\phi}) \end{pmatrix} e^{-i\omega t + ik_z z + i\ell\phi}, \tag{4.2a}$$

$$\mathbf{E}_Y^\ell(t,\mathbf{r}) = -\frac{i}{\sqrt{2}} \begin{pmatrix} J_\ell \\ -J_\ell \\ -\frac{i}{\sqrt{2}}\tan(\theta)(J_{\ell-1}e^{-i\phi} + J_{\ell+1}e^{i\phi}) \end{pmatrix} e^{-i\omega t + ik_z z + i\ell\phi}. \tag{4.2b}$$

Using these conventions, the longitudinal component is described by Bessel functions of order $\ell \pm 1$, while the transverse components are given by Bessel functions of only order ℓ. The corresponding magnetic fields are in the Cartesian basis:

$$\mathbf{B}_X^\ell(t,\mathbf{r}) = \frac{e^{-i\omega t + ik_z z + i\ell\phi}}{4\sqrt{2}\cos(\theta)} \begin{pmatrix} i\sin^2(\theta)(J_{\ell-2}e^{-2i\phi} - J_{\ell+2}e^{2i\phi}) \\ 2(1+\cos^2(\theta))J_\ell - \sin^2(\theta)(J_{\ell-2}e^{-2i\phi} + J_{\ell+2}e^{2i\phi}) \\ -\sqrt{8}\cos(\theta)\sin(\theta)(J_{\ell-1}e^{-i\phi} + J_{\ell+1}e^{i\phi}) \end{pmatrix},$$

$$\mathbf{B}_Y^\ell(t,\mathbf{r}) = \frac{-e^{-i\omega t + ik_z z + i\ell\phi}}{4\sqrt{2}\cos(\theta)} \begin{pmatrix} 2(1+\cos^2(\theta))J_\ell + \sin^2(\theta)(J_{\ell-2}e^{-2i\phi} + J_{\ell+2}e^{2i\phi}) \\ i\sin^2(\theta)(J_{\ell-2}e^{-2i\phi} - J_{\ell+2}e^{2i\phi}) \\ i\sqrt{8}\cos(\theta)\sin(\theta)(J_{\ell-1}e^{-i\phi} - J_{\ell+1}e^{i\phi}) \end{pmatrix},$$

and in the helical basis:

$$\mathbf{B}_X^\ell(t,\mathbf{r}) = \frac{i}{2\sqrt{2}\cos(\theta)} \begin{pmatrix} -(1+\cos^2(\theta))J_\ell + \sin^2(\theta)J_{\ell-2}e^{-2i\phi} \\ (1+\cos^2(\theta))J_\ell - \sin^2(\theta)J_{\ell+2}e^{2i\phi} \\ i\sqrt{2}\cos(\theta)\sin(\theta)(J_{\ell-1}e^{-i\phi} + J_{\ell+1}e^{i\phi}) \end{pmatrix} e^{-i\omega t + ik_z z + i\ell\phi}, \tag{4.3a}$$

$$\mathbf{B}_Y^\ell(t,\mathbf{r}) = \frac{-1}{2\sqrt{2}\cos(\theta)} \begin{pmatrix} (1+\cos^2(\theta))J_\ell + \sin^2(\theta)J_{\ell-2}e^{-2i\phi} \\ (1+\cos^2(\theta))J_\ell + \sin^2(\theta)J_{\ell+2}e^{2i\phi} \\ i\sqrt{2}\cos(\theta)\sin(\theta)(J_{\ell-1}e^{-i\phi} - J_{\ell+1}e^{i\phi}) \end{pmatrix} e^{-i\omega t + ik_z z + i\ell\phi}. \tag{4.3b}$$

The subscript denotes the polarization of the corresponding *electric* field. In contrast to the electric fields, both transverse components of the magnetic field have Bessel functions of the order ℓ and $\ell \pm 2$. However, the terms $J_{\ell\pm2}$ are proportional to $\sin^2(\theta)$ and small in the paraxial limit. As can be seen from the field expressions in the Cartesian basis, the transverse component of the magnetic field perpendicular to the polarization direction of the electric field is the largest component; the x-component of $\mathbf{B}_X$ is proportional to $\sin^2(\theta)$ while the y-component has a term proportional to $(1+\cos^2(\theta))J_\ell^2$. Hence the electric and magnetic fields are perpendicular to each other, similar to the fields of a plane wave.

Whether these beams are indeed linearly polarized can be checked by considering the expectation value of the SAM operator

$$\langle \mathbf{E}^\ell_{X/Y} | S_z | \mathbf{E}^\ell_{X/Y} \rangle = 0.$$

This confirms that the linearly polarized beams are superpositions of beams with opposite polarization. Further, the expectation value of the OAM operator for the linearly polarized beams is given by:

$$\langle \mathbf{E}^\ell_{X/Y} | L_z | \mathbf{E}^\ell_{X/Y} \rangle = \ell \langle \mathbf{E}^\ell_X | \mathbf{E}^\ell_X \rangle + \frac{\tan^2(\theta)}{4} \left(J_{\ell-1} - J_{\ell+1} \right)^2 .$$

This reduces to $\ell |\mathbf{E}^\ell_{X/Y}|^2$ in the paraxial limit, when $\tan^2(\theta) \to 0$.

Conserved quantities of linearly polarized optical Bessel beams

From the derivation of the linearly polarized Bessel beams it becomes clear that there are two "extra" contributions to the fields compared to plane waves. These contributions can be singled out when considering the conserved quantities, as they are the Bessel functions of order $\ell \pm 1$ from the longitudinal components (shown in red) of both the electric and magnetic fields, and of order $\ell \pm 2$ from the transverse components of the magnetic field (shown in blue). Unless specified, the quantity for the $\hat{\mathbf{x}}$-polarized fields is described by the top line of the expression.

The helicity densities (3.23a) of the linearly polarized fields are:

$$\mathcal{H}_{X/Y} = \frac{\sin^2(\theta)}{8k\cos(\theta)} \left[J^2_{\ell+1} \mp J^2_{\ell-1} \pm \cos(2\phi) J_\ell (-J_{\ell-2} + J_{\ell+2}) \right].$$

There is no contribution from the "scalar" parts of the fields, since a linearly polarized plane wave has helicity 0. This is also in agreement with the observation that the helicity density vanishes in the paraxial limit.

The longitudinal spin currents (the $\hat{\mathbf{z}}$-component of (3.23b)) of the linearly polarized Bessel beams are:

$$(S_z)_{X/Y} = \frac{\tan^2(\theta)}{32k}(J_{\ell-2} - J_{\ell+2})\times \\ \left[\pm\sin^2(\theta)(J_{\ell-2} + J_{\ell+2}) - 2\cos(2\phi)(1+\cos^2(\theta))J_\ell\right]. \quad (4.4)$$

There is no term proportional to J_ℓ^2 as the contribution from the $\mathbf{E}\times\mathbf{A}^*$ part is zero and the only contribution comes from the $\mathbf{B}\times\mathbf{C}^*$ part. This also explains why the overall proportionality factor is $\tan^2(\theta)$; this current will vanish in the paraxial limit, in contrast to the longitudinal current of the spin and helicity Bessel beams. The transverse spin currents of the linearly polarized fields are:

$$(S_x)_Y = (S_y)_X = \frac{\tan(\theta)}{16k}A_{X/Y}\Big\{4J_\ell(J_{\ell+1} - J_{\ell-1}) \\ +\sin^2(\theta)\left[(J_{\ell+1}J_{\ell+2} - J_{\ell-1}J_{\ell-2}) + B_{X/Y}(J_{\ell-2}J_{\ell+1} - J_{\ell-1}J_{\ell+2})\right]\Big\},$$
$$(S_x)_X = (S_y)_Y = \frac{\tan(\theta)}{16k}C_{X/Y}\Big\{(3+\cos(2\theta))J_\ell(J_{\ell-1} - J_{\ell+1}) \\ +\sin^2(\theta)\left[(J_{\ell-2}J_{\ell-1} - J_{\ell+1}J_{\ell+2}) + D_{X/Y}(J_{\ell-2}J_{\ell+1} - J_{\ell-1}J_{\ell+2})\right]\Big\}.$$

In these expressions the constants are given by:

$$A_X = C_Y = \cos(\phi), \qquad B_X = D_Y = 1 - 2\cos(2\phi) = 3\sin^2(\phi) - \cos^2(\phi),$$
$$A_Y = C_X = \sin(\phi), \qquad B_Y = D_X = 1 + 2\cos(2\phi) = 3\cos^2(\phi) - \sin^2(\phi).$$

It can be concluded that the spin currents parallel to the polarization direction are described by the same expression, and similarly for the spin currents perpendicular to the polarization direction. The main difference between the parallel and perpendicular currents is the first term that is proportional to $J_\ell J_{\ell\pm1}$; the current perpendicular to the polarization direction is multiplied by a factor 4 while the parallel current is multiplied by $3+\cos(2\theta) = 2(1+\cos^2(\theta))$. This shows that the parallel current is smaller than the perpendicular current, and can be explained by the fact that the perpendicular transverse components of these linearly polarized field are approximately zero. The contribution to the spin current that remains is from the parallel transverse and longitudinal components, and will be in the direction perpendicular to the polarization. This phenomenon is also observed in evanescent waves [154]. The spin currents in the transverse plane are larger than the longitudinal current, in contrast to the spin currents of the longitudinally polarized Bessel beams (3.26a) and (3.27a).

The optical energy density (2.45) can be split into different terms corresponding to the field components:

$$\mathcal{E} = \frac{1}{2}\left(E_{\parallel}^2 + E_z^2 + B_{\parallel}^2 + B_{\perp}^2 + B_z^2\right).$$

Here $E_{\parallel}$ is the electric field component parallel to the polarization direction, and $B_{\perp}$ is the component of the magnetic field perpendicular to the polarization direction, i.e. the largest component of the magnetic field. Adopting these colours, the energy density is given by:

$$\begin{aligned}\mathcal{E}_{X/Y} = &\left(\frac{1}{4} + \frac{(1+\cos^2(\theta))^2}{16\cos^2(\theta)}\right) J_\ell^2 \\ &+ \frac{\tan^2(\theta)}{16}\Big\{ -(1+\cos^2(\theta))\cos(2\phi) J_\ell (J_{\ell-2} + J_{\ell+2}) \\ &+ [1 \pm \cos^2(\theta)]\left(J_{\ell+1}^2 + J_{\ell-1}^2 + 2\cos^2(\theta)\cos(\phi) J_{\ell-1} J_{\ell+1}\right) \\ &\pm \frac{\sin^2(\theta)}{2}(J_{\ell-2}^2 + J_{\ell+2}^2)\Big\}.\end{aligned}$$

The second term, in blue, is the result of the $J_{\ell\pm2}$ terms in the $B_\perp$ component and varies with ϕ. For plane waves the components E_z, B_z and $B_\parallel$ vanish, and only the terms in black remain.

The components of the Poynting vector become:

$$\begin{aligned}\mathcal{S}_{X/Y}^z &= \frac{1}{8\cos(\theta)} J_\ell \left[(3+\cos(2\theta)) J_\ell \mp \sin^2(\theta)\cos(2\phi)(J_{\ell-2} + J_{\ell+2})\right], \\ \mathcal{S}_X^x = \mathcal{S}_Y^y &= \frac{\tan(\theta)}{16}\left\{\frac{3+\cos(2\theta)}{\cos(\theta)} A_{X/Y} J_\ell (J_{\ell-1} + J_{\ell+1})\right. \\ &\left. + \frac{\sin^2(\theta)}{\cos(\theta)}\left[A_{X/Y}\left(J_{\ell+2}J_{\ell+1} + J_{\ell-2}J_{\ell-1}\right) + B_{X/Y}\left(J_{\ell+2}J_{\ell-1} + J_{\ell-2}J_{\ell+1}\right)\right]\right\}, \\ \mathcal{S}_Y^x = \mathcal{S}_X^y &= \frac{\sin(\theta)}{8} C_{X/Y}\left\{J_\ell\left[2(J_{\ell-1} + J_{\ell+1}) + \frac{\ell}{k_r r}(J_{\ell-2} + J_{\ell+2})\right]\right. \\ &\left. \mp \tan^2(\theta)\cos(2\phi)\left[J_{\ell-2}J_{\ell+1} + J_{\ell-1}J_{\ell+2}\right]\right\}.\end{aligned}$$

The superscript denotes the component of the Poynting vector, while the capital subscript stands for the polarization of the (electric) fields. The terms in purple are a product of the blue terms from the magnetic field and red terms from the longitudinal components of the electric field, for example for $\mathcal{S}_Y^x = E_Y^y B_Y^z - E_Y^z B_Y^y = \mathcal{O}(J_\ell J_{\ell\pm1}) + \mathcal{O}(J_{\ell\pm1}J_{\ell\pm2})$. The constants are given by

$$A_X = C_Y = -\sin(\phi),\ A_Y = C_X = \cos(\phi),\ B_X = \sin(3\phi),\ B_Y = \cos(3\phi),$$

which shows that the momentum density depends on the angle ϕ, as expected.

Similar to the spin currents, the Poynting vector parallel to the direction of the polarization is different from the perpendicular direction. Considering the momentum density parallel to the polarization, the first term can be rewritten as

$$\frac{\tan(\theta)}{16}\left(\frac{3+\cos(2\theta)}{\cos(\theta)}\right) = \frac{\sin(\theta)}{8} + \frac{\sin(\theta)}{8\cos^2(\theta)}.$$

The first part is exactly half of the constant in the expression of the perpendicular momentum density; the perpendicular momentum density is larger than the parallel momentum density in the paraxial limit. However, from its expansion in θ it can be concluded that the longitudinal momentum is the largest component of the Poynting vector since the transverse components are proportional to $\sin(\theta)$:

$$\mathcal{S}^z_{X/Y} \approx \left(\frac{1}{2} + \frac{\theta^4}{16}\right) J_\ell^2 + \frac{\theta^2}{8} J_\ell J_{\ell\pm 2}.$$

4.1.2 TE and TM Bessel beams

Linearly polarized light beams are a superpositions of circularly polarized beams. What about the superpositions of helical beams? These superpositions turn out to be related to the TE and TM modes. These modes are used to describe light confined in wave guides, where it will develop specific modes to comply with the boundary conditions. For example, if the wave guide is a perfect conductor the boundary conditions require the parallel component of $\mathbf{E}$ and the perpendicular components of $\mathbf{B}$ to be zero. As a result, the magnetic field can be longitudinal but the electric field is transverse; this is a TE (transverse electric) mode. The complementary field is called a TM (transverse magnetic) mode. If both fields are transverse the mode is called a TEM mode.

A general electric field propagating in the $\hat{\mathbf{z}}$-direction in vacuum is described by the superposition of two basis states (1.39). The first state is clearly a transverse mode, as the longitudinal component is zero [55]:

$$\text{Transverse mode: } \mathbf{F}_T(t,\mathbf{r}) = \begin{pmatrix} J_{\ell-1}e^{-i\phi} \\ J_{\ell+1}e^{i\phi} \\ 0 \end{pmatrix} e^{-i\omega t + ik_z z + i\ell\phi}. \tag{4.5}$$

As mentioned in section 1.4.2, the basis states transform into each other under the curl operator, and hence the curl of (4.5) is proportional to the second basis state in (1.39):

$$\nabla \times \mathbf{F}_T(t,\mathbf{r}) = \begin{pmatrix} \cos(\theta)J_{\ell-1}e^{-i\phi} \\ -\cos(\theta)J_{\ell+1}e^{i\phi} \\ -i\sqrt{2}\sin(\theta)J_\ell \end{pmatrix} e^{-i\omega t + ik_z z + i\ell\phi}. \tag{4.6}$$

If the electric field is a TE mode similar to (4.5), the magnetic field will be proportional to (4.6). Vice versa, if the magnetic field is transverse, the electric field will be of the form (4.6). Thus the TE and TM electric fields can be defined as

$$\mathbf{E}^{\ell}_{TE}(t,\mathbf{r}) = \begin{pmatrix} J_{\ell-1}e^{-i\phi} \\ J_{\ell+1}e^{i\phi} \\ 0 \end{pmatrix} e^{-i\omega t+ik_z z+i\ell\phi}, \tag{4.7}$$

$$\mathbf{E}^{\ell}_{TM}(t,\mathbf{r}) = \begin{pmatrix} \cos(\theta)J_{\ell-1}e^{-i\phi} \\ -\cos(\theta)J_{\ell+1}e^{i\phi} \\ -i\sqrt{2}\sin(\theta)J_{\ell} \end{pmatrix} e^{-i\omega t+ik_z z+i\ell\phi}. \tag{4.8}$$

These field expressions have been derived before [55], but have not been compared to linearly polarized beams from the perspective of their mechanical properties. The relation between the electric and magnetic fields is given by the equations

$$\mathbf{B}^{\ell}_{TE} = -i\frac{k}{\omega}\mathbf{E}^{\ell}_{TM} = -i\mathbf{E}^{\ell}_{TM}, \qquad \mathbf{B}^{\ell}_{TM} = -i\frac{k}{\omega}\mathbf{E}^{\ell}_{TE} = -i\mathbf{E}^{\ell}_{TE}.$$

Comparing the TE/TM modes with the helicity Bessel beams (3.3) shows that these modes are superpositions of the helical Bessel beams, but with a shift in the OAM value:

$$\mathbf{E}^{\ell}_{TE} = \cos^2(\theta/2)\left(\mathbf{E}^{h,\ell-1}_{+} + \mathbf{E}^{h,\ell+1}_{-}\right), \tag{4.9a}$$

$$\mathbf{E}^{\ell}_{TM} = \cos^2(\theta/2)\left(\mathbf{E}^{h,\ell-1}_{+} - \mathbf{E}^{h,\ell+1}_{-}\right). \tag{4.9b}$$

This shift in $\ell \pm 1$ is to ensure that the angular momentum of the components of the two fields is the same when they are superposed. As a result the expectation values of the angular momentum operators of the TE mode are given by

$$\begin{aligned} \langle \mathbf{E}^{\ell}_{TE}|L_z|\mathbf{E}^{\ell}_{TE}\rangle &= \ell\langle \mathbf{E}^{\ell}_{TE}|\mathbf{E}^{\ell}_{TE}\rangle - \langle \mathbf{E}^{\ell}_{TE}|S_z|\mathbf{E}^{\ell}_{TE}\rangle, \\ \langle \mathbf{E}^{\ell}_{TE}|S_z|\mathbf{E}^{\ell}_{TE}\rangle &= J^2_{\ell-1} - J^2_{\ell+1}. \end{aligned}$$

This shows that the total angular momentum is of magnitude ℓ and the helicities cancel. The only angular momentum left is the OAM. Similarly, the total angular momentum of the TM mode has a magnitude ℓ:

$$\begin{aligned} \langle \mathbf{E}^{\ell}_{TM}|L_z|\mathbf{E}^{\ell}_{TM}\rangle &= \ell\langle \mathbf{E}^{\ell}_{TM}|\mathbf{E}^{\ell}_{TM}\rangle - \langle \mathbf{E}^{\ell}_{TM}|S_z|\mathbf{E}^{\ell}_{TM}\rangle, \\ \langle \mathbf{E}^{\ell}_{TM}|S_z|\mathbf{E}^{\ell}_{TM}\rangle &= \cos^2(\theta)\left(J^2_{\ell-1} - J^2_{\ell+1}\right), \end{aligned}$$

Following [151], an azimuthally polarized Bessel beam corresponds to a TE mode and a radially polarized Bessel beam corresponds to a TM mode, both with $\ell = 0$. The expectation values of L_z are thus

$$\begin{aligned}\langle \mathbf{E}^0_{TE}|L_z|\mathbf{E}^0_{TE}\rangle &= -J^2_{-1} + J^2_{+1} = 0,\\ \langle \mathbf{E}^0_{TM}|L_z|\mathbf{E}^0_{TM}\rangle &= -\cos^2(\theta)\left(J^2_{-1} + J^2_{+1}\right) = 0.\end{aligned}$$

which is in agreement with the prediction that the total OAM of radially and azimuthally polarized Bessel beams vanish.

The TE and TM fields are clearly different from the linearly polarized Bessel beams (4.2) and (4.3). This can also be concluded from the conserved quantities of both beams.

Conserved quantities of electromagnetic TE/TM Bessel beams

A quick inspection of the definition of the conserved quantities of the optical field, (3.35), (3.36), (3.23a) and (3.23b), shows that, since the magnetic field of the TE mode is proportional to the electric field of the TM mode and vice versa, the calculations can be simplified as the conserved quantities for the TE and TM modes are equal to each other. However, the separation of the Poynting vector into a canonical and spin part, as shown in table 2.1, does depend on the mode.

The helicity density and spin currents are as follows:

$$\begin{aligned}\mathcal{H}^{TE/TM} &= \frac{\cos(\theta)}{4k\cos^2(\theta/2)}\left(J^2_{\ell-1} - J^2_{\ell+1}\right),\\ \mathbf{S}^{TE/TM} &= \frac{1}{8k\cos^4(\theta/2)}\Big\{\left[1+\cos^2(\theta/2)\right]\left(J^2_{\ell-1} - J^2_{\ell+1}\right)\hat{\mathbf{z}}\\ &\qquad +2\sin(\theta)\cos(\theta)J_\ell\left(J_{\ell-1} - J_{\ell+1}\right)\hat{\boldsymbol{\phi}}\Big\}.\end{aligned}$$

The helicity density does not have a term proportional to J_ℓ as this only appears in the longitudinal component of a TM-field, and vanishes in the dot product. Similar to the spin and helicity Bessel beams, the helicity density does not vanish in the paraxial limit for $\ell = 1$, since it can be approximated by $\mathcal{H}^{TE/TM} \approx \frac{1}{4} - \frac{\theta^2}{16}$. This can be explained by the relation between the TE/TM fields and the helicity Bessel beams, equation (4.9); both helical beams with $\ell = 0$ and $\ell = 2$ are present, but they carry different amounts of helicity density as their OAM is different, see equation (3.24b).

Since the TE and TM fields are the superposition of right- and left-handed fields, one could expect that the helicity density is the sum of the two (3.24b),

while having opposite signs, i.e. it vanishes. However, the TE and TM modes are superpositions of the helicity beams with their OAM values *shifted* as in equation (4.9). The helicity density is hence proportional to $J_{\ell-1}^2 - J_{\ell+1}^2$, which reduces to zero for large radii. The azimuthal spin current vanishes on the beam axis and in the paraxial limit as required, while the longitudinal component does not.

The energy density and the longitudinal and azimuthal components of the Poynting vector and the canonical energy momentum tensor are given by:

$$\begin{aligned}
\mathcal{E} &= \frac{1}{8\cos^4(\theta/2)}\left[(1+\cos^2(\theta))\left(J_{\ell-1}^2 + J_{\ell+1}^2\right) + 2\sin^2(\theta)J_\ell^2\right], \\
\boldsymbol{S} &= \frac{1}{\cos^4(\theta/2)}\left[\frac{\cos(\theta)}{4}\left(J_{\ell-1}^2 + J_{\ell+1}^2\right)\hat{\mathbf{z}} + \frac{\ell}{2kr}J_\ell^2\hat{\boldsymbol{\phi}}\right], \\
(T^{0z})^{TE} &= \mathcal{S}_z^{TE}, \\
(T^{0z})^{TM} &= \frac{1}{\cos^4(\theta/2)}\frac{\cos^3(\theta)}{4}\left(J_{\ell-1}^2 + J_{\ell+1}^2\right) + 2\cos(\theta)\tan^2(\theta/2)J_\ell^2, \\
(T^{0\phi})^{TE} &= \frac{1}{\cos^4(\theta/2)}\left(\frac{\ell-1}{4kr}J_{\ell-1}^2 + \frac{\ell+1}{4kr}J_{\ell+1}^2\right), \\
(T^{0\phi})^{TM} &= \frac{\cos^2(\theta)}{\cos^4(\theta/2)}\left(\frac{\ell-1}{4kr}J_{\ell-1}^2 + \frac{\ell+1}{4kr}J_{\ell+1}^2\right) + \tan^2(\theta/2)\frac{2\ell}{kr}J_\ell^2.
\end{aligned}$$

The terms in red come from the longitudinal component of either the electric or magnetic field. The energy density is equal for both modes, since both the electric and magnetic field contribute. However, the canonical momentum density of the TM mode has an extra term compared to the TE mode, as the longitudinal component of the electric field is non-zero, $T^{0j} \sim \mathbf{E}^* \cdot \partial^j \mathbf{E}$. This also explains the difference between the TE and TM mode in the canonical azimuthal momentum density; the factors $\cos(\theta)$ reflect the factors in the field expressions themselves. However, the contribution from the spin current compensates for this. With a little manipulation of these expressions, it can be seen that these quantities are the sum of the individual quantities of the right- and left-handed fields as found in chapter 3, equations (3.37b) and (3.38b).

4.1.3 Comparisons between linearly polarized and TE/TM optical Bessel beams

The linearly polarized beams are clearly very different from the TE and TM Bessel beams, as can be seen from the expressions of the helicity densities and spin currents. The helicity density of the linearly polarized beams vanishes in the paraxial limit, while the helicity density of the TE/TM fields does not. This is

because the TE/TM modes are superpositions of helicity beams with different values of OAM, while the linearly polarized beams are superpositions of beams with the same value. Further, the longitudinal spin current of the TE/TM modes is dominating the other spin current components, but it is the smallest component of the spin current for the linearly polarized fields. For these fields the transverse component perpendicular to the polarization direction is the largest component.

According to [141], a linearly polarized Bessel beam is less able to perform self-healing than a radially polarized one (corresponding to a 0^{th} order TM mode). This is explained by the authors by considering the transverse Poynting vector components; the momentum flow of the radially polarized beam is radial, while for the linearly polarized beam the flow is azimuthal. Considering the transverse components of the Poynting vector of the beam polarized in the $\hat{\mathbf{x}}$ direction, the leading terms of $\mathcal{S}_X^x$ and $\mathcal{S}_X^y$ are proportional to $-\sin(\phi)$ and $\cos(\phi)$ respectively, i.e. the momentum flows in the azimuthal direction. However, the Poynting vector of the TM mode only has a longitudinal component for $\ell = 0$, which seems to be in contradiction with the observations. One reason for this could be that the experiment was performed with Bessel-Gauss beams. These beams diffract, giving rise to a radial momentum flow.

Comparing the quantities of the linearly polarized and TE/TM beams with each other is complicated by the fact that the OAM values of the constituent helicity polarized beams are shifted. However, this is also the main difference between the two beams. Since spin and helicity polarized beams are indistinguishable in the paraxial limit, one would expect that this is also true for their superpositions. Clearly, this is not the case.

4.2 Fermionic analogues

Having found the different optical Bessel beams that correspond to linear polarization and the TE and TM modes, this section will consider the fermionic analogues. Up to now, no experiments have been performed that considered the polarization of electron vortex beams.

4.2.1 Electron Bessel beams polarized in the transverse plane

When the plane wave solutions of the Dirac equation were derived (1.34), there was a freedom of choice in the polarization spinor w. This spinor was chosen to be an eigenstate of σ_z, (1.21), polarizing the electrons in the $\hat{\mathbf{z}}$ direction (3.9), or

an eigenstate of the helicity operator, yielding helical EVBs. However, the plane wave solutions can also be polarized in the transverse directions, by choosing w as an eigenspinor of σ_x or σ_y;

$$\sigma_x = \begin{pmatrix} 0 & 1 \\ 1 & 0 \end{pmatrix} \quad \rightarrow \quad w_+^{(x)} = \tfrac{1}{\sqrt{2}} \begin{pmatrix} 1 \\ 1 \end{pmatrix}, \quad w_-^{(x)} = \tfrac{1}{\sqrt{2}} \begin{pmatrix} 1 \\ -1 \end{pmatrix},$$

$$\sigma_y = \begin{pmatrix} 0 & -i \\ i & 0 \end{pmatrix} \quad \rightarrow \quad w_+^{(y)} = \tfrac{1}{\sqrt{2}} \begin{pmatrix} 1 \\ i \end{pmatrix}, \quad w_-^{(y)} = \tfrac{1}{\sqrt{2}} \begin{pmatrix} 1 \\ -i \end{pmatrix}.$$

The eigenspinors of σ_x and σ_y are superpositions of the eigenspinors of σ_z;

$$w_\pm^{(x)} = \frac{1}{\sqrt{2}} \left(w_+^{(z)} \pm w_-^{(z)} \right), \qquad w_\pm^{(y)} = \frac{1}{\sqrt{2}} \left(w_+^{(z)} \pm i w_-^{(z)} \right).$$

This shows that choosing the $w_\pm^{(x)}$ spinor instead of the $w_\pm^z$ is the fermionic analogue of choosing linear polarization over circular polarization; the spin eigenstates are combined in the same way as the electric fields (4.1). The spinor $w_+^{(x)}$ corresponds to $\mathbf{E}_x$ and $w_-^{(x)}$ to $i\mathbf{E}_y$. These are the ones that will be considered in the following sections, as the eigenstates of σ_y correspond to *diagonal* polarization of the electric fields;

$$\frac{1}{\sqrt{2}}(\mathbf{E}_+ + i\mathbf{E}_-) = \frac{1+i}{\sqrt{2}}(\mathbf{E}_x - \mathbf{E}_y) = e^{i\pi/4}(\mathbf{E}_x - \mathbf{E}_y),$$
$$\frac{1}{\sqrt{2}}(\mathbf{E}_+ - i\mathbf{E}_-) = \frac{1-i}{\sqrt{2}}(\mathbf{E}_x + \mathbf{E}_y) = e^{-i\pi/4}(\mathbf{E}_x + \mathbf{E}_y).$$

The states with the spinor w_+^x will be called x-polarized and with w_-^x y-polarized from now on. The electron Bessel beams are with these conventions given by

$$\psi_{x/y}^\ell(t, \mathbf{r}) = e^{-i\mathcal{E}t + ip_z z + i\ell\phi} \sqrt{\frac{\mathcal{E}+m}{4\mathcal{E}}} \left\{ J_\ell \begin{pmatrix} \alpha+\beta \\ \alpha-\beta \\ 0 \\ 0 \end{pmatrix} + \right.$$
$$\left. + \varepsilon \cos(\theta) J_\ell \begin{pmatrix} 0 \\ 0 \\ \alpha+\beta \\ -\alpha+\beta \end{pmatrix} + i\varepsilon \sin(\theta) \begin{pmatrix} 0 \\ 0 \\ (-\alpha+\beta) J_{\ell-1} e^{-i\phi} \\ (\alpha+\beta) J_{\ell+1} e^{i\phi} \end{pmatrix} \right\}. \tag{4.10}$$

Here $\alpha = 1$ corresponds to x-polarization and $\beta = 1$ to y-polarization, and $|\alpha|^2 + |\beta|^2 = 1$. Polarizing EVBs in the transverse plane instead of the longitudinal direction has significant consequences for the conserved quantities.

Conserved quantities of fermionic x/y polarized Bessel beams

The gauge density and currents for the x/y polarized Bessel beams are calculated to be:

$$\begin{aligned}
\rho_{X/Y} &= \frac{1}{\mathcal{E}} J_\ell^2 \left[(\mathcal{E}+m) + (\mathcal{E}-m)\cos^2(\theta)\right] + \frac{\mathcal{E}-m}{2\mathcal{E}} \sin^2(\theta)(J_{\ell-1}^2 + J_{\ell+1}^2) \\
&\quad \mp \frac{\mathcal{E}-m}{2\mathcal{E}} \sin(2\theta)\sin(\phi) J_\ell (J_{\ell-1} - J_{\ell+1}), \\
J_z &= \frac{2k}{\mathcal{E}} \cos(\theta) J_\ell^2 - \frac{k}{\mathcal{E}} \sin(\theta)\sin(\phi) J_\ell (J_{\ell-1} - J_{\ell+1}), \\
J_\phi &= \frac{k}{\mathcal{E}} \sin(\theta) J_\ell (J_{\ell-1} + J_{\ell+1}) = \frac{2}{\mathcal{E}} \frac{\ell}{r} J_\ell^2 \qquad \rightarrow \begin{cases} J_x = -\sin(\phi) \frac{2}{\mathcal{E}} \frac{\ell}{r} J_\ell^2, \\ \\ J_y = \cos(\phi) \frac{2}{\mathcal{E}} \frac{\ell}{r} J_\ell^2. \end{cases}
\end{aligned}$$

Clearly, the gauge density does resemble the gauge density of the spin polarized beams (3.14), but there is an additional term of Bessel functions of mixed orders. This term arises from the red and blue parts of the spinor and is the purple term. A similar term also appears in the expressions of the longitudinal and azimuthal gauge currents, but here the terms are products of the scalar (black) part and the blue terms. These terms contain both Bessel functions of order $\ell \pm 1$, emerging from the eigenspinors of σ_x that are superpositions of the eigenspinors of σ_z.

Due to form of $\gamma^0\gamma^\phi$, which is anti-diagonal and symmetric, the products of the red terms with the scalar (black) terms cancel and only the products of the blue with black terms survive. However, for the longitudinal current this is not the case, as due to the form of $\gamma^0\gamma^z$ the $\cos(\theta)$ terms survive. Another important observation is that the gauge current does not depend on the polarization direction.

Similar to the spin and helical electron beams, the energy density and canonical longitudinal momentum density are proportional to the gauge density; $\mathcal{E} = \mathcal{E}\rho$ and $T^{0z} = k\cos(\theta)\rho$. However, the canonical azimuthal momentum density is given by:

$$\begin{aligned}
T^{0\phi} = \frac{1}{\mathcal{E}} \frac{\ell}{r} J_\ell^2 &\left[(\mathcal{E}+m) + (\mathcal{E}-m)\cos^2(\theta)\right] \\
&+ \frac{\mathcal{E}-m}{2\mathcal{E}} \sin^2(\theta) \left(\frac{\ell-1}{r} J_{\ell-1}^2 + \frac{\ell+1}{r} J_{\ell+1}^2 \right) \\
&\mp \frac{(\mathcal{E}-m)}{2\mathcal{E}} \sin(\phi)\sin(2\theta) J_\ell \left[\frac{\ell-\frac{1}{2}}{r} J_{\ell-1} - \frac{\ell+\frac{1}{2}}{r} J_{\ell+1} \right].
\end{aligned} \tag{4.11}$$

This is clearly a modified density distribution with every term multiplied by its winding number. Remarkable is that the product $J_\ell J_{\ell\pm1}$ is multiplied by $\ell \pm \frac{1}{2}$, the

average of ℓ and $\ell \pm 1$. This was seen before in the calculation of the azimuthal normal stress (3.52).

The symmetrized momentum density can be found from (3.51). Remarkable is that the canonical radial momentum density is non-zero, and since the gauge current *is* zero, the symmetrized momentum density does not vanish:

$$\begin{aligned} T^{0r} &= \pm\frac{\mathcal{E}-m}{2\mathcal{E}}\cos(\phi)\sin(2\theta)\frac{1}{2r}J_\ell(J_{\ell-1}+J_{\ell+1}), \\ &= \pm\frac{\mathcal{E}-m}{2\mathcal{E}}\cos(\phi)\sin(2\theta)\frac{\ell}{k_r r^2}J_\ell^2, \\ \Theta^{0r} &= \frac{1}{2}T^{0r}. \end{aligned}$$

This is a result of the different orders of Bessel functions in the red and blue components of (4.10); the product $\psi^\dagger(\partial_r\psi)$ is not equal to $(\partial_r\psi^\dagger)\psi$ due to the crossterms that appear. Since the radial momentum density is proportional to J_ℓ^2/r^2, the integral over the transverse plane is finite.

It can be concluded that the gauge densities of the linearly polarized fermionic fields resemble those of the spin-polarized fields, with extra mixing terms. The azimuthal gauge current is clearly the sum of the two currents of the spin-polarized fields separately. The longitudinal current gets an extra term proportional to $\sin(\theta)$. The relationships between the energy and momentum densities and the gauge currents is unchanged. Although the radial momentum density is not zero, the integral of this density over all space vanishes.

4.2.2 Superpositions of helical electron Bessel beams

In analogy to the optical TE and TM modes, it is also possible to define superpositions of the helical electron beams (3.10). However, since the choice in representation does not have a physical effect or change the conserved quantities, superpositions of the Bessel beams derived from the Weyl spinors (2.3) can be considered. These are more straightforward to work with as they only have two non-zero components.

In analogy with the optical TE and TM Bessel beams, the OAM values of the two electron beams need to be the same when they are superposed, as in (4.9). However, since the SAM of electrons is $\pm\frac{1}{2}$, only the OAM of the right-handed beam needs to be lowered or the OAM of the left-handed beam needs to be raised, but not both at the same time:

$$\psi^A_\pm(t,\mathbf{r}) = \frac{1}{\sqrt{2}}\left(\psi^{\ell-1,h}_+(t,\mathbf{r}) \pm \psi^{\ell,h}_-(t,\mathbf{r})\right),$$
$$\psi^B_\pm(t,\mathbf{r}) = \frac{1}{\sqrt{2}}\left(\psi^{\ell,h}_+(t,\mathbf{r}) \pm \psi^{\ell+1,h}_-(t,\mathbf{r})\right).$$

The notation from the optical beams will be adopted, calling ψ_+ the "TE" mode and ψ_- the "TM" mode. The choice in states $\psi^{A/B}$ shifts every ℓ to $\ell \pm 1$, but has no actual consequence for the conserved quantities of the fields. Using ψ^A from now on, these states become in full form:

$$\psi^A_{TE}(t,\mathbf{r}) = \frac{1}{\sqrt{2}}\begin{pmatrix} \cos(\theta/2)J_\ell \\ i\sin(\theta/2)J_{\ell+1}e^{i\phi} \\ \sin(\theta/2)J_\ell \\ -i\cos(\theta/2)J_{\ell+1}e^{i\phi} \end{pmatrix} e^{-i\mathcal{E}t+ip_z z+i\ell\phi}, \tag{4.12a}$$

$$\psi^A_{TM}(t,\mathbf{r}) = \frac{1}{\sqrt{2}}\begin{pmatrix} \cos(\theta/2)J_\ell \\ i\sin(\theta/2)J_{\ell+1}e^{i\phi} \\ -\sin(\theta/2)J_\ell \\ i\cos(\theta/2)J_{\ell+1}e^{i\phi} \end{pmatrix} e^{-i\mathcal{E}t+ip_z z+i\ell\phi}. \tag{4.12b}$$

These states are eigenstates of the total angular momentum operator with expectation value $\langle J_z\rangle = \ell + \frac{1}{2}$, but they are not eigenstates of the helicity operator, as they involve two states with opposite helicity.

The conserved gauge quantities (2.21) of these states take the simple forms:

$$\rho = \frac{1}{2}\left(J^2_\ell + J^2_{\ell+1}\right), \tag{4.13a}$$
$$J_z = \pm\frac{\sin(\theta)}{2}\left(J^2_\ell + J^2_{\ell+1}\right), \tag{4.13b}$$
$$J_\phi = \mp J_\ell J_{\ell+1}\cos(\theta). \tag{4.13c}$$

The top line describes the TE mode, the bottom line the TM mode. The currents are oppositely directed for the two modes. Similar to the spin currents of the linearly polarized optical beams, the longitudinal current is actually smaller than the azimuthal current. As observed before for the spin-polarized and helical electron Bessel beams, the energy and momentum densities are related to the gauge quantities, hence a discussion of these will be omitted here. These modes are similar to Majorana Bessel beams, that will be derived next.

4.3 Majorana Bessel beams

The superposition of two electron states with well-defined and opposite helicity was encountered before in the construction of Majorana fermions from Weyl spinors (2.6). These plane wave solutions are in full form, with $\Phi = \mathcal{E}t - \mathbf{p}\cdot\mathbf{r}$:

$$\psi_a(t,\mathbf{r}) = \begin{pmatrix} u_+ \\ i\sigma^2 u_+^* \end{pmatrix} = \frac{1}{\sqrt{2}} \begin{pmatrix} \cos(\theta/2)e^{-i\Phi} \\ \sin(\theta/2)e^{i\phi}e^{-i\Phi} \\ \sin(\theta/2)e^{-i\phi}e^{i\Phi} \\ -\cos(\theta/2)e^{i\Phi} \end{pmatrix}, \tag{4.14a}$$

$$\psi_b(t,\mathbf{r}) = \begin{pmatrix} -i\sigma^2 u_-^* \\ u_- \end{pmatrix} = \frac{1}{\sqrt{2}} \begin{pmatrix} -\cos(\theta/2)e^{i\Phi} \\ -\sin(\theta/2)e^{i\phi}e^{i\Phi} \\ -\sin(\theta/2)e^{-i\phi}e^{-i\Phi} \\ \cos(\theta/2)e^{-i\Phi} \end{pmatrix}. \tag{4.14b}$$

These solutions are clearly superpositions of particles and antiparticles, as both the exponentials $e^{\pm i\Phi}$ appear. As explained on page 33, a particle moving forward in time can be considered as an antiparticle moving backwards in time.

These plane wave solutions can be converted to Bessel beams by means of the integral (1.41) as explained in section 1.2.1. The terms in $\widehat{\psi}(\mathbf{k})$ that contain a term $e^{\pm i\phi}$ shift the order of the Bessel function:

$$\widehat{\psi}(\mathbf{k}) = \begin{cases} \text{const.} & \\ & \to \\ \text{const. } e^{\pm i\phi_k} & \end{cases} \begin{matrix} J_n(k_r r)e^{in\phi_r}e^{-i\mathcal{E}t+ik_z z}, \\ \\ \pm iJ_{n\pm1}(k_r r)e^{i(n\pm1)\phi_r}e^{-i\mathcal{E}t+ik_z z}. \end{matrix}$$

The Majorana states (4.14) also contain the complex conjugated wavefunctions. Since the Fourier exponential changes sign when taking the Fourier transform of a complex conjugated wavefunction, the phase shift is exactly opposite for $\widehat{\psi}^*$;

$$\widehat{\psi}(\mathbf{k})^* = \begin{cases} \text{const.} & \\ & \to \\ \text{const. } e^{\pm i\phi_k} & \end{cases} \begin{matrix} J_n(k_r r)e^{-in\phi_r}e^{i\mathcal{E}t-ik_z z}, \\ \\ \pm iJ_{n\mp1}(k_r r)e^{-i(n\mp1)\phi_r}e^{i\mathcal{E}t-ik_z z}. \end{matrix}$$

It is not the sign in $e^{\pm i\phi_k}$ that determines the shift, but the sign relative to $e^{\pm i\widetilde{\Phi}}$. An important observation here is that also the complex conjugate of the factor $(-i)^n$ in front of the integral needs to be taken, as it comes from the wave spectrum of the field.

Performing the Fourier transform on the plane wave Majorana states (4.14) gives the following fermionic Majorana Bessel beams:

$$\psi_a^\ell(t,\mathbf{r}) = \frac{1}{\sqrt{2}} \begin{pmatrix} \cos(\theta/2) J_\ell \, e^{-i\widetilde{\Phi}} \\ i\sin(\theta/2) J_{\ell+1} \, e^{i\phi} e^{-i\widetilde{\Phi}} \\ -i\sin(\theta/2) J_{\ell+1} \, e^{-i\phi} e^{i\widetilde{\Phi}} \\ -\cos(\theta/2) J_\ell \, e^{i\widetilde{\Phi}} \end{pmatrix}, \tag{4.15a}$$

$$\psi_b^\ell(t,\mathbf{r}) = \frac{1}{\sqrt{2}} \begin{pmatrix} -\cos(\theta/2) J_\ell \, e^{i\widetilde{\Phi}} \\ -i\sin(\theta/2) J_{\ell-1} \, e^{i\phi} e^{i\widetilde{\Phi}} \\ i\sin(\theta/2) J_{\ell-1} \, e^{-i\phi} e^{-i\widetilde{\Phi}} \\ \cos(\theta/2) J_\ell \, e^{-i\widetilde{\Phi}} \end{pmatrix}. \tag{4.15b}$$

These states are neither eigenstates of the total angular momentum operator J_z nor helicity. The components of the conserved vector gauge current of the states (4.15) are given by the same expressions as the quantities of the helicity fields; the gauge density (3.15), longitudinal gauge current (3.19) and azimuthal gauge current (3.20). This reflects the fact that the Majorana states are superpositions of helicity (Weyl) states, but is in contradiction with the theory that the vector gauge current of Majorana fermions should vanish, as explained in section 2.3.1. However, all components of the energy-momentum tensor are zero; the fermion and anti-fermion part both have the same energy and wavevector, but with opposite signs.

4.3.1 Comparison between fermionic TE/TM and Majorana states

The fermionic TE/TM analogues (4.12) are clearly different from the Majorana states (4.15). Due to the shift in OAM, the Bessel functions of order $\ell + 1$ are found in the second and fourth component of the TE/TM fields, instead of the second and third component of the Majorana states. This results in one term J_ℓ that is multiplied by $\cos(\theta/2)$ and one by $\sin(\theta/2)$, which will add up to 1 when calculating the probability density, for example, explaining the simple form of the expressions (4.13).

Another important difference is the sign of the exponential $e^{\pm i\widetilde{\Phi}}$. Since Majorana fermions are the superpositions of a particle and antiparticle, both signs occur. This explains why the energy and momentum densities of the Majorana fermions are zero.

It can be concluded that Majorana states are *not* equal to a superposition of opposite helicity states, as this does not take the charge conjugation into account.

4.3.2 Standing waves and the Majorana states

The Majorana solutions (4.15) are defined in the Weyl representation. They can be transformed into the Majorana representation by multiplication by the matrix $U^{(2)}$; $\psi_M = U\psi_W$. This transformation does not change the physical properties of the fields. However, doing this demonstrates an important property of the Majorana fermions; they are *real* solutions as the complex exponentials $e^{\pm i\Phi}$ are converted into sines and cosines:

$$\psi_a^{\ell,M}(t,\mathbf{r}) = \begin{pmatrix} -\cos(\theta/2)J_\ell \sin(\Phi) + \sin(\theta/2)J_{\ell+1}\sin(\phi-\Phi) \\ \cos(\theta/2)J_\ell \cos(\Phi) + \sin(\theta/2)J_{\ell+1}\cos(\phi-\Phi) \\ \cos(\theta/2)J_\ell \sin(\Phi) + \sin(\theta/2)J_{\ell+1}\sin(\phi-\Phi) \\ \cos(\theta/2)J_\ell \cos(\Phi) - \sin(\theta/2)J_{\ell+1}\cos(\phi-\Phi) \end{pmatrix}, \tag{4.16a}$$

$$\psi_b^{\ell,M}(t,\mathbf{r}) = \begin{pmatrix} -\cos(\theta/2)J_\ell \cos(\Phi) - \sin(\theta/2)J_{\ell-1}\cos(\phi+\Phi) \\ \cos(\theta/2)J_\ell \sin(\Phi) + \sin(\theta/2)J_{\ell-1}\sin(\phi+\Phi) \\ \cos(\theta/2)J_\ell \cos(\Phi) - \sin(\theta/2)J_{\ell-1}\cos(\phi+\Phi) \\ \cos(\theta/2)J_\ell \sin(\Phi) - \sin(\theta/2)J_{\ell-1}\sin(\phi+\Phi) \end{pmatrix}. \tag{4.16b}$$

As a result, these states describe *standing* waves instead of the propagating waves of their constituents (4.14). This principle was mentioned in section 1.6; the distinction between a real and complex description is analogous to either using travelling or standing waves to describe particle states.

4.4 Discussion

Several different superpositions of spin- and helicity polarized Bessel beams have been discussed in this chapter. Superpositions of optical spin-polarized beams give linearly polarized beams, while the superposition of helicity beams that are shifted in OAM values gives TE and TM modes. As a result, these beams do not reduce to each other in the paraxial limit, while the spin- and helicity polarized beams do.

[2]The matrix U relates the Weyl representation to the Majorana representation; $\gamma_M^\mu = U\gamma_W^\mu U^\dagger$, with

$$U = \frac{i}{2}\begin{pmatrix} -\mathbb{1}-\sigma^2 & \mathbb{1}-\sigma^2 \\ \mathbb{1}-\sigma^2 & \mathbb{1}+\sigma^2 \end{pmatrix}.$$

This is a product of the inverse of the transformation matrix from the Dirac to the Weyl representation (2.2) and the transformation from the Dirac to the Majorana representation (1.51).

Superpositions of oppositely spin-polarized electron beams can be considered as the analogue of linearly polarized optical beams, as their conserved quantities reflect the conserved quantities of their constituent counterparts. Constructing the fermionic analogues of the optical TE and TM beams, the OAM value of one beam needs to be shifted. Due to this shift, some factors of i are picked up, and sines and cosines are interchanged. This results in oppositely directed currents and the conserved quantities are not the sum of their constituent parts.

Although these "fermionic TE/TM" modes resemble the fermionic Majorana modes, they are clearly different as Majorana modes incorporate both particle states and their complex conjugated counterparts (antiparticle states).

These Majorana states are described by standing waves in the Majorana representation, an important indication that the Majorana representation is a real representation instead of a complex one. Since the optical field is real, there is no Majorana construction necessary to describe an optical field that is its own charge conjugate.

The question now arises if there is a more fundamental reasoning that will lead to the conclusion that invariance under charge conjugation implies a description in terms of standing waves. For this purpose a "charge conjugation" operator needs to be defined for the optical field. This operator can be related to other spacetime symmetries and will be discussed in chapter 5.

5 The optical Dirac equation and Majorana states

The previous chapter concluded with the observation that the Majorana representation describes *real* fermionic states in terms of *standing* waves. This is in contrast with the more common description of *complex* fermionic states in terms of *travelling* waves. These descriptions are interchangeable; standing waves are superpositions of travelling waves and vice versa [75]. A complex field, that has two degrees of freedom, can also be described by two real fields.

As explained in section 2.1.3, describing fermions in the Majorana representation restricts the fields to being real instead of complex. As a consequence, they are invariant under charge conjugation. This can be realized by making a superposition of a fermionic field and its charge conjugate; it is a pseudo-particle that behaves as a Majorana particle, while the physical particle is an electron. Majorana fermions can therefore be considered as the superposition of a fermion and an anti-fermion with opposite helicity or spin. Up to now, it has only been possible to create these Majorana-like excitations in superconductors [89].

This is in stark contrast to the observation that Majorana bosons exist in abundance: photons are described by the real optical field, making charge conjugation a trivial operation. Ettore Majorana himself, when he developed his theory, already noticed this; the quantization of Majorana fermions is similar to the quantization of the optical field, but with finite mass and different statistics (fermionic instead of bosonic) [84]. However, the charge conjugation transformation can be related to the discrete spacetime transformations parity ($\mathcal{P}$, equation (2.12)) and time ($\mathcal{T}$, equation (2.14)) reversal [50]. This relationship can be exploited to define an analogous "charge-conjugation" operator for the optical field. Similar conclusions about optical "charge conjugation" can also be drawn from adopting a Dirac-like description of Maxwell's equations.

It turns out that a key property of these optical waves is *linear* polarization.

There is no constraint on whether these waves are propagating or standing waves, similar to the freedom of describing Majorana particles in either the Weyl or Majorana representation of the Dirac equation.

It can be concluded that optical Majorana states appear in great abundance, and these are not exceptional states. The only distinction between Majorana states and "normal" optical states is the choice in polarization. However, linear and circular polarization are fully equivalent bases to describe the direction of oscillation of the electric field in. Linear polarization simply means that there are equal amounts of right- and left-handed circular polarization present [75]. This is exactly analogous to constructing a complex field from two real fields or a real field from two complex fields.

Optical systems that favour linear polarization can be compared to fermionic systems that give rise to Majorana states, showing a cunning similarity; optical Majorana states typically appear as edge states. As the optical field is less restricted than the fermionic field, Majorana modes can also appear in the bulk of a 3-dimensional system.

This chapter is structured as follows. First, by considering parity and time reversal symmetries, an analogue for complex conjugation can be defined for the optical field. Secondly a spinor description of Maxwell's equations will be considered, which allows for the derivation of the Majorana representation of the optical Dirac equation. Both discussions lead to the conclusion that the optical eigenstates of charge conjugation are linearly polarized waves. This is followed by a discussion of the optical equivalent of particle-hole symmetry and fermionic Majorana excitations, and examples of optical systems that favour linear over circular polarization. These linearly polarized waves share many similarities with the fermionic Majorana excitations, leading to the conclusion that these are the optical analogue of the Majorana modes.

5.1 Symmetry considerations

The defining property of a Majorana particle, being invariant under charge conjugation, is trivially satisfied by the optical field. This implies that there needs to be another symmetry operator involved to deduce the form of an optical Majorana state. This operator can be derived from different considerations. Firstly, fermionic systems with Majorana-like excitations share similarities with systems described by Hamiltonians that are symmetric under the combined action of parity (2.12) and

time (2.14) reversal. Moreover, considering the action of $\mathcal{CPT}$ transformations on the optical field leads to the same conclusion that Majorana modes are eigenstates of $\mathcal{PT}-$reversal.

Eigenstates of the $\mathcal{PT}$ transformation can be found by considering the action of these transformations on the electromagnetic field components separately, and by studying the effect of Lorentz boosts.

5.1.1 $\mathcal{PT}$-symmetric Hamiltonian

Fermionic Majorana states are a superposition of two particle states with different (effective) masses, as explained in section 2.1.2. The superposition of two states with different masses, or even positive and negative mass, has also been observed in the study of $\mathcal{PT}$-symmetric systems describing fermionic systems. The Hamiltonian describing such a system is conserved under the combined action of $\mathcal{PT}$-reversal, but not under time or parity reversal separately. This allows for real energy values, even though the Hamiltonian is not necessarily Hermitian [155, 156, 157]. An example is the following Hamiltonian:

$$H = \boldsymbol{\alpha} \cdot \mathbf{p} + m_1 + \gamma^5 m_2.$$

This is the normal Dirac Hamiltonian extended with a mass term proportional to γ^5. As explained in section 2.2, multiplying the field by γ^5 changes the sign of the mass, hence a $\mathcal{PT}$-symmetric Hamiltonian is the perfect candidate to describe a Majorana particle.

5.1.2 Discrete spacetime symmetries

This observation suggests that the action of charge conjugation is related to that of $\mathcal{PT}$ reversal. Electromagnetic fields are invariant under the combined action of $\mathcal{CPT}$, since Maxwell's equations are invariant under this operator[1]. This leads to the prediction that the action of $\mathcal{C}$ is equivalent to the inverse actions of $\mathcal{P}$ and $\mathcal{T}$ combined. The electric field, induced by static charges, transforms as a vector, while the magnetic field, induced by charge currents, transforms as a pseudo-vector. A pseudo-vector transforms as a vector under rotations, but

[1] Under the combined action of $\mathcal{CPT}$, the electromagnetic 4-potential transforms as [57]

$$A^\mu(t, \mathbf{r}) \rightarrow -A^\mu(-t, -\mathbf{r}).$$

However, since both $\mathbf{E}$ and $\mathbf{B}$ are related to this potential by derivatives, the minus signs cancel and the fields are unchanged.

changes sign under reflections. The wave-vector changes sign both under time and parity reversal, since it denotes the direction of propagation of a travelling wave. These transformations can be summarized as:

$$\begin{aligned} \mathcal{P} &: \mathbf{E} \to -\mathbf{E} \qquad \mathcal{T} : \mathbf{E} \to \mathbf{E}, \\ \mathcal{P} &: \mathbf{B} \to \mathbf{B} \qquad \mathcal{T} : \mathbf{B} \to -\mathbf{B}, \\ \mathcal{P} &: \mathbf{k} \to -\mathbf{k} \qquad \mathcal{T} : \mathbf{k} \to -\mathbf{k}. \end{aligned}$$

As a result, under the combined action of $\mathcal{P}$ and $\mathcal{T}$ both the electric and magnetic fields reverse direction but the wave vector remains unchanged:

$$\mathcal{PT} : \mathbf{E} \to -\mathbf{E},\ \mathbf{B} \to -\mathbf{B},\ \mathbf{k} \to \mathbf{k}. \tag{5.1}$$

From the invariance of the optical field under $\mathcal{CPT}$, it can be concluded that the effective action of $\mathcal{C}$ on the electromagnetic field is given by the inverse of (5.1):

$$\mathcal{C} : \mathbf{E} \to -\mathbf{E},\ \mathbf{B} \to -\mathbf{B},\ \mathbf{k} \to \mathbf{k}. \tag{5.2}$$

However, since $\mathcal{P}^2 = \mathcal{T}^2 = \mathbb{1}$, this operation is the same as $\mathcal{PT}$-reversal. In the rest of this chapter there will therefore be made no distinction made the action of $(\mathcal{PT})^{-1}$ or $\mathcal{PT}$.

An important consequence of the relationship (5.2) is that eigenstates of $\mathcal{C}$- or $\mathcal{PT}$-reversal cannot be circularly polarized, since the handedness of the field is inverted by $\mathcal{T}$, which involves complex conjugation. The total transformation of a circularly polarized electromagnetic field is thus described by

$$\mathcal{PT}(\mathbf{E} \pm i\mathbf{B}) \to -\mathbf{E} \pm i\mathbf{B} \sim \mathbf{E} \mp i\mathbf{B}.$$

It can be concluded that linearly polarized fields are the only eigenstates of $\mathcal{C}$-conjugation.

5.1.3 Invariance under Lorentz boosts

Eigenstates of $\mathcal{PT}$ (or $\mathcal{C}$) reversal can also be found by considering the eigenstates of operators that commute with $\mathcal{PT}$ reversal, as commuting operators share a set of eigenstates. For example Lorentz boosts, as these are determined by the velocity vector and velocity does not change direction under $\mathcal{PT}$ reversal. The action of a Lorentz boost on electric and magnetic fields leaves the field components parallel to the boosting direction unchanged, but mixes the perpendicular components:

$$\mathbf{E}'_{\parallel} = \mathbf{E}_{\parallel}, \qquad \mathbf{B}'_{\parallel} = \mathbf{B}_{\parallel},$$

$$\mathbf{E}'_{\perp} = \gamma(\mathbf{E} + \boldsymbol{\beta} \times \mathbf{B})_{\perp}, \qquad \mathbf{B}'_{\perp} = \gamma(\mathbf{B} - \boldsymbol{\beta} \times \mathbf{E})_{\perp}.$$

Considering a boost in the $\hat{\mathbf{z}}$-direction, the following combinations of field components are thus eigenstates of these Lorentz boosts:

$$\begin{pmatrix} E'_x - B'_y \\ E'_y + B'_x \end{pmatrix} = \gamma(1+\beta) \begin{pmatrix} E_x - B_y \\ E_y + B_x \end{pmatrix}, \tag{5.3a}$$

$$\begin{pmatrix} E'_x + B'_y \\ E'_y - B'_x \end{pmatrix} = \gamma(1-\beta) \begin{pmatrix} E_x + B_y \\ E_y - B_x \end{pmatrix}. \tag{5.3b}$$

The combinations of field components with eigenvalue $\gamma(1 \pm \beta)$ correspond to a linearly polarized wave travelling in the negative (positive) $\hat{\mathbf{z}}$-direction. It can be concluded that linear polarization is an *eigenpolarization* of a Lorentz boost parallel to the propagation direction. Linearly polarized waves are not *invariant* under Lorentz boosts, but keep their form; a boost is *form-preserving*.

From the observation that $\mathcal{PT}-$symmetric systems allow for negative mass terms in their Hamiltonian and that the optical field is invariant under $\mathcal{CPT}$ transformations, it can be concluded that the optical analogue of charge conjugation is $\mathcal{PT}$ reversal. Eigenstates of this operator are linearly polarized waves.

5.2 A spinor formalism for Maxwell's equations

The optical equivalents of Majorana spinors can also be found by using the optical Dirac equation. To wit, Maxwell's equations can be cast in a form similar to the Weyl equation for massless electrons, exploiting the fact that both the optical field and the Dirac field have two degrees of freedom. This idea has been around for several years and various papers about a *spinor formalism* for Maxwell's equations have been published; Oppenheimer [158] developed a 4-component spinor theory for electromagnetism that is Lorentz invariant, Laporte and Uhlenbeck [159] applied a spinor analysis to both Maxwell's equations and the Dirac equation and drew parallels between them, and Berry published notes about the spinor formalism for Maxwell's equations in matter [160]. Describing the optical field in a Dirac-like way shows that its mechanical properties and conservation laws arise naturally from the Dirac formalism, similarly to the separation of angular momentum in an orbital part and a spin part [161].

This optical Dirac equation is helpful in deriving the form of the optical Majorana states, as the different representations appear to be related to the polarization states of the optical field. In the next subsection the derivation of the optical Dirac equation will be discussed, followed by a consideration of the different representations of this equation.

5.2.1 Derivation of the optical Dirac equation

The main difference between the optical field and the Dirac field is that the optical field is real while the Dirac field is complex. This can be overcome by defining the electric and magnetic fields as the real and imaginary part of one complex field. This is the Riemann-Silberstein vector [162, 163][2]:

$$\mathbf{F} = \mathbf{E} + i\mathbf{B}. \tag{5.4}$$

In terms of this vector, the four Maxwell's equations (1.35) are reduced to two equations [162, 163]:

$$\nabla \cdot \mathbf{F} = 0, \tag{5.5}$$

$$\nabla \times \mathbf{F} = i\partial_t \mathbf{F}. \tag{5.6}$$

The first equation is a constraint on the components of $\mathbf{F}$, a vanishing divergence. The second one describes the dynamics of the fields. This is the equation that will be considered when deriving the optical Dirac equation. It can be written in a

[2]This vector is conserved under the duality transformation (2.47) between the electric and magnetic fields. The similarity between the duality rotations of the fields and potentials (2.48) suggests that not only the fields, but also the potentials and field tensors can be combined into a complex vector potential and tensor respectively:

$$X^\alpha = A^\alpha + iC^\alpha,$$
$$D^{\alpha\beta} = F^{\alpha\beta} + iG^{\alpha\beta}.$$

In terms of these complex field tensors the Lagrangian acquires the following form

$$\mathcal{L} = -\frac{1}{8} D^{\alpha\beta} D^*_{\alpha\beta}.$$

The dual transformations (2.47) now become gauge transformations;

$$\mathbf{D} \to e^{-i\theta}\mathbf{D},\ X^\alpha \to e^{-i\theta}X^\alpha,\ D^{\alpha\beta} \to e^{-i\theta}D^{\alpha\beta},$$

with associated conserved current

$$J^\alpha = \frac{1}{2}\mathrm{Im}(D^{\alpha\beta}X^*_\beta).$$

Components of this current are exactly the helicity density (3.23a) and spin currents (3.23b). This shows that the $U(1)$ symmetry of the Riemann-Silberstein vector is equivalent to the Heaviside-Larmor symmetry between the electric and magnetic fields.

different form, by using the identity $\mathbf{A} \times \mathbf{B} = -i(\mathbf{A} \cdot \mathbf{S})\mathbf{B}$, where $\mathbf{S}$ are the spin-1 matrices (1.19):

$$i\partial_t \mathbf{F} = -i(\mathbf{S} \cdot \nabla)\mathbf{F} = (\mathbf{p} \cdot \mathbf{S})\mathbf{F}. \tag{5.7}$$

This equation is similar in form to the Weyl Hamiltonian for fermions (2.5), up to a minus sign:

$$i\partial_t \psi = \begin{pmatrix} \boldsymbol{\sigma} \cdot \mathbf{p} & 0 \\ 0 & -\boldsymbol{\sigma} \cdot \mathbf{p} \end{pmatrix} \psi, \tag{5.8}$$

when $\mathbf{F}$ is replaced by the spinor ψ and the spin matrices $\mathbf{S}$ by $\boldsymbol{\sigma}$. This equation shows that the vector $\mathbf{F}$ is necessarily a 6-component vector. Further, the sign of the energy is related to the handedness of the field. A positive energy corresponds to the spin aligned with the momentum, $\mathbf{p} \cdot \hat{\mathbf{S}} = |\mathbf{p}|$.

However, different papers have been published about the spinor-like photon wave function [161, 164, 165], using different choices for the components of the vector $\mathbf{F}$. These choices turn out to correspond to different representations of the Dirac equation.

Weyl representation One choice for the Riemann-Silberstein vector components is $\mathbf{F} = (\mathbf{E} + i\mathbf{B}, \mathbf{E} - i\mathbf{B})^T$, as in [164]. This transforms (5.7) to the following matrix equation:

$$i\partial_t \begin{pmatrix} \mathbf{E} + i\mathbf{B} \\ \mathbf{E} - i\mathbf{B} \end{pmatrix} = \begin{pmatrix} \hat{\mathbf{S}} \cdot \mathbf{p} & 0 \\ 0 & -\hat{\mathbf{S}} \cdot \mathbf{p} \end{pmatrix} \begin{pmatrix} \mathbf{E} + i\mathbf{B} \\ \mathbf{E} - i\mathbf{B} \end{pmatrix}. \tag{5.9}$$

This matrix is of the same form as the Weyl Hamiltonian (2.5). The electric and magnetic fields are combined in a helical way, such that eigenstates are circularly polarized. This shows that helicity states of light indeed are circularly polarized.

Dirac representation Choosing the vector components as $\mathbf{F} = (\mathbf{E}, i\mathbf{B})^T$ (as in [161]) transforms (5.7) to the equation

$$i\partial_t \begin{pmatrix} \mathbf{E} \\ i\mathbf{B} \end{pmatrix} = \begin{pmatrix} 0 & \hat{\mathbf{S}} \cdot \mathbf{p} \\ \hat{\mathbf{S}} \cdot \mathbf{p} & 0 \end{pmatrix} \begin{pmatrix} \mathbf{E} \\ i\mathbf{B} \end{pmatrix}. \tag{5.10}$$

This equation is of the same form as the Hamiltonian in the Dirac representation (1.43) with zero mass, as the matrix $\boldsymbol{\alpha}$ in the Dirac representation is of the form $\boldsymbol{\alpha} = \begin{pmatrix} 0 & \boldsymbol{\sigma} \\ \boldsymbol{\sigma} & 0 \end{pmatrix}$. In this basis the electric and magnetic field components are decoupled, and the polarization direction can be chosen freely. However, since the fields need to be transverse and perpendicular to each other, there are only two different polarization states allowed.

5.2.2 Majorana representation

Choosing $\mathbf{F}$ suitably, the optical Dirac equation can thus be written in exactly the same form as the Dirac equation in the Dirac or Weyl representations. The form of $\mathbf{F}$ suggests that different polarization states are favoured by different representations. There is also a choice possible for $\mathbf{F}$ that gives the equivalent of the Hamiltonian in the Majorana representation. Since this representation is not encountered before, the corresponding form of $\mathbf{F}$ will be derived here. This leads to conclusions about the preferred polarization states of this representation. However, the Majorana representation that will be used here is slightly different from the standard representation (1.50).

In the standard Majorana representation (1.50), the generator of the boost in the $\hat{\mathbf{y}}$-direction is diagonal:

$$S^{02} = \frac{i}{4}[\gamma^0, \gamma^2] = \frac{i}{2}\begin{pmatrix} \mathbb{1} & 0 \\ 0 & -\mathbb{1} \end{pmatrix}. \qquad \text{(Majorana representation)}$$

As seen before, optical Majorana states are eigenstates of Lorentz boosts *along* the propagation direction, which has been the $\hat{\mathbf{z}}$-direction throughout this thesis. It would therefore be convenient if there was a Majorana representation that diagonalises the boost in the $\hat{\mathbf{z}}$ direction instead.

Since the generators of Lorentz transformations acting on spinors are given by $\Sigma^{0j} = \frac{i}{4}[\gamma^0, \gamma^j]$, equation (1.31), the form of these generators depends on the choice of representation of the Dirac equation. Different representations diagonalise different generators. The generator Σ^{03} can be transformed into a diagonal form by performing a cyclic rotation on the spatial γ-matrices:

$$\gamma^0 \to \gamma^0 \qquad\qquad \gamma^1 \to \gamma^2 \to \gamma^3 \to \gamma^1 \tag{5.11}$$

as now the generator S^{02} is transformed to S^{03}:

$$S^{02} \mapsto S^{03} = \frac{i}{2}\begin{pmatrix} \mathbb{1} & 0 \\ 0 & -\mathbb{1} \end{pmatrix}. \qquad \text{(modified Majorana representation)}$$

This permutation leaves the Clifford algebra (1.30) invariant and is therefore also a physically allowed representation of the Dirac equation.

Using this cyclic permuted Majorana representation (5.11), the Hamiltonian (5.8) is written in the following form:

$$i\partial_t \psi = \begin{pmatrix} p_z & -\sigma^3 p_x - \sigma^1 p_y \\ -\sigma^3 p_x - \sigma^1 p_y & -p_z \end{pmatrix} \psi.$$

Analogous to the Dirac and Weyl representations, it can be predicted that the Hamiltonian for the optical field has the same structure as the fermionic Hamiltonian. Replacing the Pauli spin matrices by the spin-1 matrices (1.19) gives the following 6×6 matrix:

$$i\partial_t \mathbf{F} = \begin{pmatrix} p_z & 0 & 0 & 0 & ip_x & 0 \\ 0 & p_z & 0 & -ip_x & 0 & ip_y \\ 0 & 0 & p_z & 0 & -ip_y & 0 \\ 0 & ip_x & 0 & -p_z & 0 & 0 \\ -ip_x & 0 & ip_y & 0 & -p_z & 0 \\ 0 & -ip_y & 0 & 0 & 0 & -p_z \end{pmatrix} \mathbf{F}. \tag{5.12}$$

From this equation the components of $\mathbf{F}$ can be derived. The time derivative of the electric field can be expressed in spatial derivatives of the magnetic field, and vice versa, by Maxwell's equations (1.35b). These derivatives are transformed into components of the momentum by a Fourier transformation. Since p_z appears on the diagonal, specific combinations of the field components fit this criterium:

$$\partial_t \begin{pmatrix} E_x + B_y \\ E_y - B_x \end{pmatrix} = p_z \begin{pmatrix} E_x + B_y \\ E_y - B_x \end{pmatrix} - p_x \begin{pmatrix} E_z \\ -B_z \end{pmatrix} - p_y \begin{pmatrix} B_z \\ E_z \end{pmatrix} \tag{5.13}$$

$$\partial_t \begin{pmatrix} E_x - B_y \\ E_y + B_x \end{pmatrix} = -p_z \begin{pmatrix} E_x - B_y \\ E_y + B_x \end{pmatrix} + p_x \begin{pmatrix} B_z \\ E_z \end{pmatrix} + p_y \begin{pmatrix} E_z \\ -B_z \end{pmatrix} \tag{5.14}$$

Taking superpositions of these combinations gives the two vectors that satisfy equation (5.12), with specific constraints:

$$\mathbf{F}_1 = \begin{pmatrix} (E_x + B_y) + (E_y - B_x) \\ i(E_z - B_z) \\ (E_x + B_y) - (E_y - B_x) \\ -(E_x - B_y) + (E_y + B_x) \\ i(E_z - B_z) \\ -(E_x - B_y) - (B_x + E_y) \end{pmatrix} \; ; \; E_z = -B_z,$$

$$\mathbf{F}_2 = \begin{pmatrix} (E_x + B_y) - (E_y - B_x) \\ -i(E_z + B_z) \\ -(E_x + B_y) - (E_y - B_x) \\ (E_x - B_y) + (E_y + B_x) \\ i(E_z + B_z) \\ (E_x - B_y) - (E_y + B_x) \end{pmatrix} \; ; \; E_z = B_z.$$

The upper three components of the vectors $\mathbf{F}_{1,2}$ correspond to components of a linearly polarized electromagnetic wave travelling in the positive $\hat{\mathbf{z}}$ direction, and the lower three correspond to a wave travelling in the negative $\hat{\mathbf{z}}$ direction. These combinations are exactly the combinations found in (5.3), the eigenstates of Lorentz transformations. The vectors can be simplified by taking linear combinations of $\mathbf{F}_1$ and $\mathbf{F}_2$, that are also solutions of (5.12). The sum and difference of $\mathbf{F}_1$ and $\mathbf{F}_2$ are the vectors:

$$\mathbf{F}_a = \frac{1}{2}(\mathbf{F}_1 + \mathbf{F}_2) = \begin{pmatrix} E_x + B_y \\ -iB_z \\ -E_y + B_x \\ E_y + B_x \\ iE_z \\ E_x - B_y \end{pmatrix}, \quad \mathbf{F}_b = \frac{1}{2}(\mathbf{F}_1 - \mathbf{F}_2) = \begin{pmatrix} E_y - B_x \\ iE_z \\ E_x + B_y \\ -E_x + B_y \\ -iB_z \\ E_y + B_x \end{pmatrix}. \tag{5.15}$$

However, by combining $\mathbf{F}_1$ and $\mathbf{F}_2$ the two constraints are also combined; $E_z = B_z = -B_z$, which can only be satisfied if $E_z = B_z = 0$, consistent with a plane wave travelling in the $\hat{\mathbf{z}}$-direction. This condition is a consequence of the definition of the gamma matrices. In the standard Majorana representation the condition would have been $E_y = B_y = 0$, which reflects that the direction of propagation was here the $\hat{\mathbf{y}}$-direction. The modified representation favours the $\hat{\mathbf{z}}$-direction as direction of propagation. The two vectors $\mathbf{F}_a, \mathbf{F}_b$ are related to each other by a rotation over ϕ in the (x, y)-plane; $\mathbf{F}_a(\phi + \pi/2) = \mathbf{F}_b$.

It can be concluded that the eigenstates of the Hamiltonian (5.12) are linearly polarized waves. This is in contrast with the solutions in the Dirac representation, where the polarization was unspecified and could be chosen freely. It is in agreement with the observation that the optical analogue of charge conjugation is the combined reversal of parity and time, of which eigenstates are linearly polarized waves.

The quest for finding optical Majorana states can now be divided into two parts. On the one hand, there are systems possible that mimic the superconducting systems where Majorana excitations occur. On the other hand, there are optical systems possible that *favour* linear polarization, but where the analogue with a fermionic systems is not clear or not even present. Both types of systems will be discussed in the next two sections, starting with the construction of optical modes that are the analogy of fermionic Majorana-like excitations.

5.3 Construction of optical Majorana excitations

In section 2.1.3 the fermionic Majorana excitations in solid-state systems were discussed. It was possible to create these excitations because of the particle-hole symmetry in superconducting systems; these excitations are their own antiparticle, hence invariant under charge conjugation. This Majorana physics has been *simulated* with light instead of fermions in various optical experiments.

An example of these experiments is the design of an optical system that shows the same characteristics as Kitaev's 1D chain (section 2.1.3); this can be realized with photons in a 1D array of optical cavities [166]. These cavities support a single photon mode each, which implies that the photons behave effectively as if they were spinless fermions; fermions in the presence of a magnetic field, such that only one spin state is allowed. The cavities are coupled through nearest-neighbour tunnelling as the photon modes overlap slightly. Under specific conditions[3] the Hamiltonian can be written in a way similar to the modified Kitaev Hamiltonian (2.11).

Other experiments that simulate the Majorana physics include [167] that studied the non-Abelian statistics of Majorana modes with an optical quantum simulator, and [168] that coupled two photonic crystals to simulate the Majorana equation decoupled into two Dirac equations. A different experiment, based on optically simulating the particle-hole symmetry mechanism by considering the effect of different transformations on the polarization states [169], will be discussed next.

5.3.1 Optical simulation of particle-hole symmetry

The simulation of the particle-hole symmetry with light as described in [169] confirms the prediction that optical Majorana states are linearly polarized waves. The analogy is as follows. Propagating waves in two dimensions can be classified as either TE or TM modes. These modes can be transformed into each other by the dual-symmetry of Maxwell's equations (2.47) and can be used to simulate the particle-hole symmetry. However, since particles and holes have positive and negative energies (with respect to the Fermi energy) respectively, the dual-symmetry alone is not sufficient.

[3] The energy to add a photon needs to be very large compared to the energy cost to tunnel from one cavity to another.

From equation (5.7) it can be deduced that the sign of the energy is related to the handedness (helicity)of the field; handedness inversion can be used as an alternative for changing positive to negative energies. For this purpose metamaterials with positive and negative refractive index can be used, as this effectively changes the handedness of the light. However, handedness inversion also effectively inverts the momentum direction $\mathbf{k}$. It was concluded [169] that the particle-hole symmetry can be simulated by the dual-symmetry and handedness inversion combined; a right-handed TE mode representing a particle can be transformed to a left-handed TM mode representing a hole.

The effect of this transformation on the fields can be found by considering the following example. A TE mode is propagating in the $\hat{\mathbf{z}}$-direction, with the electric field pointing in the $\hat{\mathbf{x}}$-direction and the magnetic field in both the $\hat{\mathbf{y}}$ and $\hat{\mathbf{z}}$ directions. Consequently performing a duality transformation and handedness inversion gives:

$$\begin{array}{lcll} \mathbf{k} = +k_z & & \mathbf{k} = +k_z & \mathbf{k} = -k_z \\ \mathbf{E} = E_x & \underset{\text{duality}}{\rightarrow} & \mathbf{E} = -E_{yz} & \underset{\text{handedness}}{\rightarrow} \quad \mathbf{E} = -E_{yz} \\ \mathbf{B} = B_{yz} & & \mathbf{B} = B_x & \mathbf{B} = B_x \end{array} . \tag{5.16}$$

The effect of this transformation is also shown in the following diagram:

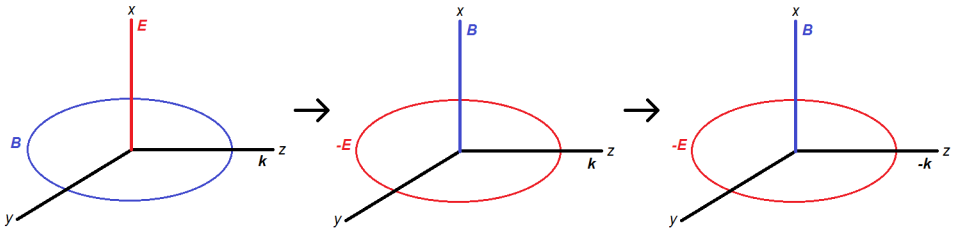

Figure 5.1: Particle-hole symmetry simulated with light modes

It can be concluded that the total transformation interchanges the directions of the electric and magnetic fields, and inverts the propagation direction. This concept can be extended from light in a metamaterial to plane waves in vacuum, yielding the polarization states of plane waves that are invariant under this optical analogue of particle-hole inversion.

5.3.2 Free space modes

If a plane wave of light in vacuum is linearly polarized in either the $\hat{\mathbf{x}}$ or $\hat{\mathbf{y}}$ direction, the transformation (5.16) simplifies to[4]

$$\{\mathbf{k} = k_z, \mathbf{E} = E_x, \mathbf{B} = B_y\} \rightarrow \{\mathbf{k} = -k_z, \mathbf{E} = E_y, \mathbf{B} = -B_x\}, \tag{5.17a}$$

$$\{\mathbf{k} = k_z, \mathbf{E} = E_y, \mathbf{B} = -B_x\} \rightarrow \{\mathbf{k} = -k_z, \mathbf{E} = -E_x, \mathbf{B} = -B_y\}. \tag{5.17b}$$

Under this total transformation the direction of propagation is inverted and the polarization direction is rotated over $\pi/2$ about the momentum vector. A rotation like this does not have an effect on the polarization of a circularly polarized wave, as can be seen from adding the two transformations (5.17):

$$\{\mathbf{k} = k_z, \mathbf{E} = E_x + iE_y\} \rightarrow \{\mathbf{k} = -k_z, \mathbf{E} = E_y - iE_x\} = \{\mathbf{k} = -k_z, \mathbf{E} = -i(E_x + iE_y)\}.$$

The only change between the initial and final state is the direction of propagation, which is reversed.

However, the helicity of the field *is* inherently related to the direction of propagation; it is the projection of the spin onto the momentum direction. Therefore, there are two different interpretations of this transformation possible. A right-handed wave travelling in the $+\hat{\mathbf{z}}$ direction can be transformed to a right-handed wave travelling in the opposite direction, or a left-handed wave travelling in the same direction;

$$\gamma = \{\mathrm{RH}, +\mathbf{k}\} \rightarrow \gamma^\dagger = \begin{cases} \{\mathrm{RH}, -\mathbf{k}\} \\ \{\mathrm{LH}, +\mathbf{k}\} \end{cases}. \tag{5.18}$$

From this observation it can be concluded that the action of the charge conjugation operator (5.2), changing the field directions but keeping the propagation direction unchanged, is equivalent to keeping the field directions unchanged and reversing the propagation direction.

Depending on the choice of "antiphoton-state" (5.18), the superposition of a photon and "antiphoton" can be interpreted in two ways: either two right-handed waves travelling in opposite directions, which gives a standing wave (necessarily linearly polarized), or one right- and one left-handed wave travelling in the same direction; this gives a travelling wave but it is also linearly polarized[5].

[4] Although this agrees with [169], it might not be appropriate to take the analogy from optical modes in metamaterials to vacuum.

[5] To distinguish between the two situations the *flux* of the chirality density, which is an appropriate measure for the helicity locally [117], might be worth considering.

However, whether a standing or travelling wave is observed depends merely on the choice of reference frame. Moving along with a travelling wave a standing wave is observed and vice versa. This is comparable to the choice in representation of the Dirac equation; transforming the states from the Weyl representation to the Majorana representation transforms propagating waves to standing waves but does not physically change the states. This is in agreement with the observation that the wave modes derived from the optical Dirac equation (5.15) are linearly polarized, but there is no way to distinguish whether these are travelling or standing waves, as light waves move with the speed of light. There is no reference frame possible in which the wave is a standing wave.

The superposition of two waves with opposite helicity propagating in the same direction resembles the TE and TM modes of the Bessel beams. The superposition of two waves with the same handedness travelling in opposite directions was not considered for Bessel beams, but there is no physical distinction possible between these and the optical TE/TM modes. Hence it can be concluded that the TE and TM modes for Bessel beams behave as optical Majorana modes; these are the closest analogue of fermionic Majorana Bessel beams. The next section will make this correspondence even more clear by considering optical systems that favour linear polarization. These optical states that appear are either TE or TM modes, and appear on the edges of the system. Further, the number of degrees is halved as either mode is allowed on one edge only.

5.4 Optical systems that favour linear polarization

The previous subsection considered how to optically simulate the particle-hole symmetry that is necessary to create Majorana-like excitations in superconductors. However, there are also optical states that demonstrate the Majorana physics while they are not designed to do so in any way, but appear so naturally. A distinction can be made between free space modes, surface states and bulk modes.

The optical Majorana modes in free space are simply linearly polarized waves. In contrast, Majorana fermions in free space have been unconfirmed up to now. All known particles in the Standard Model behave as Dirac fermions except the neutrino; it is still unknown whether this is a Dirac or Majorana fermion [88].

Optical surface modes appear in different forms, and are the analogue of the fermionic Majorana excitations in solid state systems. However, there are also modes in the bulk of optical crystals that are restricted to linear polarization.

There are no fermionic analogues of these modes. Two examples of surface modes and one example of a bulk mode will be discussed in the next subsections.

5.4.1 Reflection and refraction

The first example of an optical surface mode considers light that is incident on a boundary between two media. It can be reflected back into the first medium or transmitted into the second. The fraction of the light that is reflected is determined by the Fresnel coefficients. These coefficients depend on a number of parameters; the angle of incidence, the ratio between ϵ and μ of the two media and, but most importantly, the polarization direction of the light, that can be either s-polarized or p-polarized. The wave is s-polarized if the electric field lies in the plane perpendicular to the plane of incidence (i.e. parallel to the surface), or p-polarized if the electric field is parallel to the plane of incidence (parallel to the normal plane and perpendicular to the interface).

The Fresnel coefficients for s- and p-polarization are given by the expressions

$$R_s = \left| \frac{\sqrt{\frac{\mu_2}{\epsilon_2}}\cos(\theta_i) - \sqrt{\frac{\mu_1}{\epsilon_1}}\cos(\theta_t)}{\sqrt{\frac{\mu_2}{\epsilon_2}}\cos(\theta_i) + \sqrt{\frac{\mu_1}{\epsilon_1}}\cos(\theta_t)} \right|^2, \qquad R_p = \left| \frac{\sqrt{\frac{\mu_2}{\epsilon_2}}\cos(\theta_t) - \sqrt{\frac{\mu_1}{\epsilon_1}}\cos(\theta_i)}{\sqrt{\frac{\mu_2}{\epsilon_2}}\cos(\theta_t) + \sqrt{\frac{\mu_1}{\epsilon_1}}\cos(\theta_i)} \right|^2.$$

The coefficients R_s and R_p are in general not equal to each other and field components will be refracted in different amounts. For example an incident circularly polarized wave, with both polarizations present in equal amounts, will not be circularly polarized any more when reflected or transmitted but elliptically. However, linearly polarized light will always remain linearly polarized.

However, if the interface is between two media that have the same ratio $\frac{\epsilon}{\mu}$, the Fresnel coefficients reduce to

$$R_s = \frac{\mu}{\epsilon}\left| \frac{\cos(\theta_i) - \cos(\theta_t)}{\cos(\theta_i) + \cos(\theta_t)} \right|^2, \qquad R_p = \frac{\mu}{\epsilon}\left| \frac{\cos(\theta_t) - \cos(\theta_i)}{\cos(\theta_t) + \cos(\theta_i)} \right|^2.$$

These coefficients are equal to each other. If the electric field corresponds to one polarization direction, the magnetic field is aligned with the other direction and both fields will be refracted equally. This process conserves the dual-symmetry (2.47) [120].

If the interface does not conserve dual-symmetry, evanescent waves appear that propagate along and decay away from the interface. These evanescent waves are either TE or TM modes, but cannot appear at the same time. This reduces the four modes (two polarizations for both propagation directions) that are accessible

in free space to two; this is the photonic quantum spin Hall effect [170]. The momentum direction and transverse spin direction of these modes are coupled to each other.

5.4.2 Surface plasmon polaritons

Another example of an optical wave that propagates along a surface is the surface plasmon polariton (SPP). SPPs propagate along the surface between a conductor and a dielectric (or vacuum). They are trapped on this surface due to their interaction with the free charges in the conductor [171]; the electrons on the surface resonate with the light wave. This explains the name SPP; an electromagnetic wave (*polariton*) moves along a *surface* and causes charges to move collectively in the conductor (*plasmon*).

The interaction between the surface charges and electromagnetic wave increases the momentum of the wave k_{SPP} compared to the momentum k_0 of a wave in free space with the same frequency; the velocity of propagation decreases. These wavenumbers are related by [171]:

$$k_{\text{SPP}} = k_0 \sqrt{\frac{\epsilon_d \epsilon_c}{\epsilon_d + \epsilon_c}}. \tag{5.19}$$

with ϵ_d the electric permittivity of the dielectric and ϵ_c of the conductor. The condition $k_{\text{SPP}} > k_0$ is satisfied for metals, as ϵ_c is negative. This increase in momentum has an important consequence; the field component perpendicular to the surface decays exponentially as it cannot radiate. As a result an SPP cannot be directly excited by shining light on the conductor surface. It can only be generated by incident light that is totally internally reflected at the surface, approaching the boundary from the conductor side. The momentum is large enough in the conductor to excite an SPP.

Taking the transition from conductor to dielectric in the $\hat{\mathbf{z}}$-direction, the SPP propagates along the surface in the $\hat{\mathbf{x}}$-direction and decays in the $\hat{\mathbf{z}}$-direction. It has electric field components in both these directions, that relate to each other through [172]:

$$E_z = i \frac{k_{\text{SPP}}}{k_z} E_x.$$

It can be concluded that the transverse component is in general larger than the longitudinal component. The accompanying magnetic field is necessarily polarized in the $\hat{\mathbf{y}}$-direction; parallel to the surface and perpendicular to the propagation direction. This is a TM mode, and due the boundary conditions there is no TE mode allowed.

Both of the edge states considered here (the evanescent waves and the SPP modes) demonstrate two important properties in the context of Majorana surface modes; a unique wavenumber and a halving of the number of accessible modes. For a transmitted evanescent wave the wavenumber is determined by the incident light, and the number of states is halved by the photonic quantum spin Hall effect. When exciting an SPP, there is a unique wavevector $\mathbf{k}$ for every wavelength of the light involved as a consequence of (5.19) [173], and every SPP is a TM mode, halving the number of accessible modes.

These optical surface modes are comparable to the Majorana states in p-wave superconductors, that allow for only one mode for each wavevector, with the momentum direction and sign of the energy coupled to each other and oppositely polarized modes localized on opposite boundaries of the superconductor. However, the main difference with the optical boundary modes is that the propagation direction depends on the propagation direction of the incident light. The spin direction is then determined by coupling to the momentum.

5.4.3 Optical Majorana bulk modes

To conclude this chapter, a special class of optical Majorana states will be considered that appear in the bulk of a system, in this case a photonic crystal. There are no analogous fermionic Majorana modes, as a fermionic Majorana mode is always spatially separated in two parts. This makes the modes appear at the edges of the system. Optical Majorana modes do not have to be spatially separated, but they do need to conserve specific symmetries.

A photonic crystal can be created by stacking (alternating) layers of two media with different refractive indices on top of each other, or by using one uniform medium with a two-dimensional array of holes. A result of this periodicity is that the photon states are described by Bloch functions, similar to the electron wavefunctions in solid state systems. The wavenumber is bounded from below by the inverse length of the Brillouin zone, k_{min}.

These photonic crystals can be used to slow down light. Slow light has many practical applications in optical signal processing, as the arrival of the optical signals can be controlled. Further, slowing down light increases the energy density of the light, enhancing interactions between light and matter. It depends on the medium characteristics how the slowing down is achieved. One example is by dispersion; the group velocity can be designed to strongly depend on the frequency and be much smaller than c. Moreover, the photonic crystal can be engineered to

have a photonic bandgap in which it acts as an insulator and does not transmit light of certain frequencies [174]. This is caused by backscattering at the edges of the unit cell, creating counterpropagating waves[6]. If the wavenumber is close to k_{min}, where the group velocity $d\omega/dk$ vanishes [175], the resulting wave is propagating very slowly. The light can even be stopped completely when the wavenumber is exactly equal to k_{min}.

The concept of slow light is not in contradiction with the conservation of energy. When the group velocity gets close to zero the energy density increases, keeping the rate of energy transfer constant [176].

Light propagating in a photonic crystal does not necessarily have to be transversely polarized as in vacuum, but can have longitudinal components, just like the TE and TM modes in an optical waveguide. The light will generally be elliptically polarized [177] but there are also points at which the light is perfectly circularly polarized. These points are called C-points, and the electric and magnetic field components are exactly out of phase by $\pi/2$.

This circular polarization is *transverse* circular polarization, in contrast to longitudinal circular polarization for plane waves in vacuum. Transverse circular polarization is comparable to the transverse spin momentum in evanescent waves [170] and reverses sign under $\mathcal{T}$-reversal. Longitudinal circular polarization (i.e. helicity) does not, as both the sense of rotation and the propagation direction are reversed. However, for both transverse and longitudinal circular polarization the directions of propagation and the spin momentum are coupled to each other; a wave travelling in the opposite direction also reverses its spin direction.

C-points are surrounded by an area where the light is elliptically polarized, with the polarization direction rotating around the C-points. This defines the charge of the C-points: the direction of rotation of the polarization ellipses, as shown in figure 5.2. It is shown that C-points occur in pairs of the same charge but in regions where the polarization is of opposite handedness. As a result they are separated by an L-line, where the polarization is purely linear [177].

[6] See Appendix B for a more detailed discussion about wave modes in stratified media.

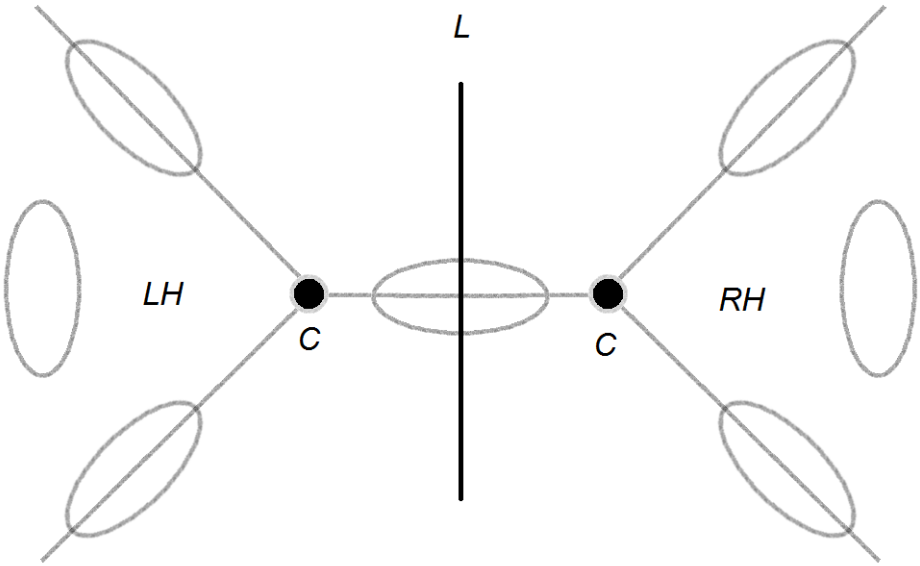

Figure 5.2: Simplification of a figure from [177] showing the polarization direction of light in an optical crystal. RH and LH denote the handedness of the polarization ellipses. They are separated by a L-line; a line of linear polarization. The area shown here is one unit cell.

If the wavenumber has the right value, the light can be stopped completely by the interference of counterpropagating waves. This corresponds to the conservation of time reversal and hence any circular polarization must vanish. This is confirmed in simulations [175]: when the wavenumber approaches the edge value of the Brillouin zone the C-points approach and annihilate each other on the L-line separating the two. This is caused by the interference of the counterpropagating waves, which makes the longitudinal electric field component vanish; there is no overall transverse circular polarization.

This observation can be illustrated by considering a transversely circularly polarized plane wave in a photonic crystal, travelling in the $\hat{\mathbf{z}}$ direction with field components $\mathbf{E}_x, \mathbf{E}_z$ and $\mathbf{B}_y$, and the spin pointing in the $\hat{\mathbf{y}}$ direction. Reflection at the edge of a unit cell gives rise to the time-reversed wave

$$\mathcal{T} : \{\mathbf{E}_x - i\mathbf{E}_z, \mathbf{B}_y, \mathbf{S}_y, \mathbf{k}_z\} \to \{\mathbf{E}_x + i\mathbf{E}_z, -\mathbf{B}_y, -\mathbf{S}_y, -\mathbf{k}_z\}.$$

Taking the superposition of these two waves, the only non-zero field component is $\mathbf{E}_x$, hence the field is linearly polarized. It can thus be concluded that in a photonic crystal, when the wavenumber is on the edge of the Brillouin zone, the

reflected, time-reversed, wave interferes with the propagating wave and creates a standing wave. This standing wave is necessarily linearly polarized, conserving time-reversal symmetry.

5.5 Conclusions

In this chapter the optical analogue of charge conjugation was derived as the composite of time and parity reversal. Eigenstates of this operation are linearly polarized waves. The same conclusion can be drawn from considering the optical Dirac equation in the Majorana representation.

Fermionic Majorana excitations are created in superconductors, systems that respect the particle-hole symmetry. It is possible to engineer a system with photons described by the same Hamiltonian as a one-dimensional p-wave superconductor. Further, the particle-hole symmetry can be optically simulated by the combined action of duality symmetry and helicity inversion. States that are symmetric under this transformation are linearly polarized, either travelling or standing waves.

However, there also exist systems where light is *confined* to linear polarization; these systems involve a boundary that breaks the dual-symmetry between the electric and magnetic field, halving the number of accessible states. This is comparable to the halving of states in fermionic systems due to the breaking of time-reversal symmetry. The wavenumber of the optical boundary modes (evanescent waves) that appear depends on the wavenumber of the incident light.

Finally, there are also Majorana-like modes possible in the bulk of photonic crystals. There does not exist a fermionic analogue of these bulk modes, as fermionic Majorana modes need to be spatially separated and hence always appear on the boundaries of a system. The periodicity of the system makes waves appear in counterpropagating pairs, conserving time-reversal symmetry and giving rise to standing waves.

6 Angular momentum in parabolic coordinates

In section 1.2 it was mentioned that the transverse Helmholtz equation is separable in different coordinate systems. These include Cartesian and cylindrical polar coordinates, but also cylindrical parabolic and elliptic coordinates. All these coordinate systems are cylindrical systems; the longitudinal ($\hat{\mathbf{z}}$) axis is the same while only the definition of the transverse coordinates is changed.

Propagation invariant fields are defined by their angular spectrum as expressed by the Whittaker integral (1.9b). This angular spectrum is defined on a circle with constant radius $k_\perp$ and only a function of the azimuthal angle ϕ_k. As a result, the longitudinal and transverse wavenumbers are constant and the beam retains its shape upon propagation [178]. The spectrum of a Bessel beam (1.8) has a uniform amplitude over ϕ_k, reflecting the invariance of Bessel beams under rotations about the $\hat{\mathbf{z}}$-axis. However, this is not a necessary condition and spectra in other cylindrical coordinate systems can vary in amplitude as a function of ϕ_k. This creates beams with various intensity patterns, reflecting the symmetries of the corresponding coordinate system.

The basis states in cylindrical elliptic and parabolic coordinates are Mathieu and Weber beams respectively. In the rest of this chapter the name Weber beam will not be used to avoid confusion with the Weber functions, special solutions of the wave equation in parabolic coordinates. The beams will be called *parabolic harmonics* instead. Different beams conserve different mechanical quantities depending on the specific symmetries of the coordinate system.

Parabolic coordinates (u, v) are defined as $x + iy = \frac{1}{2}(u + iv)^2$;

$$x = \frac{1}{2}(u^2 - v^2), \qquad y = uv. \tag{6.1}$$

The parabolic coordinate system is shown in figure 6.1. The surfaces of constant coordinates u and v describe parabolae that open to the negative and

positive x-direction respectively. Close to the focal point of these parabolae the system resembles the cylindrical polar coordinate system, but only in one half of the plane; the parabolae describe an almost circular path around one side of the focus but become elongated on the other side. Expressing the parabolic coordinates (6.1) in polar cylindrical coordinates shows this explicitly[1]:

$$u = h\cos(\beta), \qquad v = h\sin(\beta). \tag{6.2}$$

This is similar to expressing Cartesian coordinates in cylindrical coordinates, $x = r\cos(\phi),\ y = r\sin(\phi)$, but with $h = \sqrt{2r}$ and $\beta = \phi/2$. Because the azimuthal dependence of parabolic coordinates is described by β instead of ϕ, the parabolic system can be considered as a "half-a-polar"-system.

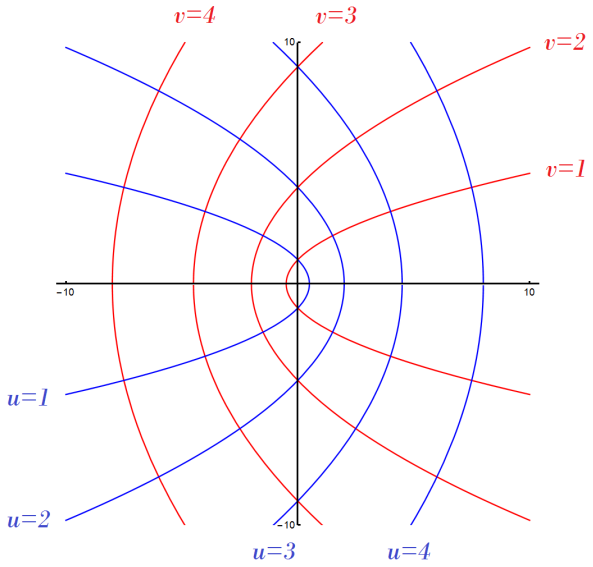

Figure 6.1: The parabolic coordinate system. Contours of constant coordinate u and v, both for values $1, 2, 3, 4$ are shown in the region $x, y \in [-10, 10]$. Lines of constant u open to the negative x-axis, lines of constant v open to the positive x axis.

This is exactly where the difficulty of working with parabolic coordinates lies: the coordinates are not continuously defined everywhere on the transverse plane as the coordinate v is discontinuous on the negative x-axis[2] [179].

[1] See Appendix C for all relationships and transformations for parabolic coordinates.

[2] This can be deduced from expressing the parabolic coordinates in Cartesian coordinates, equation (C.1). For negative x, taking the limit $y \to 0$ depends on the sign of y.

This has as a consequence that, although the parabolic coordinate system resembles the cylindrical polar coordinate system, it does not conserve OAM. It does conserve another mechanical quantity called parabolic momentum. The question is now how this parabolic momentum is different from OAM, and how OAM manifests itself in parabolic coordinates. Is there a coupling possible between spin and orbital angular momentum in parabolic coordinates? Or is there a coupling between the SAM and parabolic momentum instead?

First some characteristics of parabolic coordinates will be discussed, in particular the conserved quantity associated with the symmetry of this coordinate system. This will be followed by the derivation of the field solutions, and an investigation into the spin-orbit coupling effects.

6.1 Characteristics of parabolic coordinates

Cylindrical polar and parabolic coordinates are both related to cylindrical elliptic coordinates, that can be regarded as the most general coordinate system. The Cartesian, cylindrical polar and parabolic coordinate systems can be retrieved from this system by taking suitable limits.

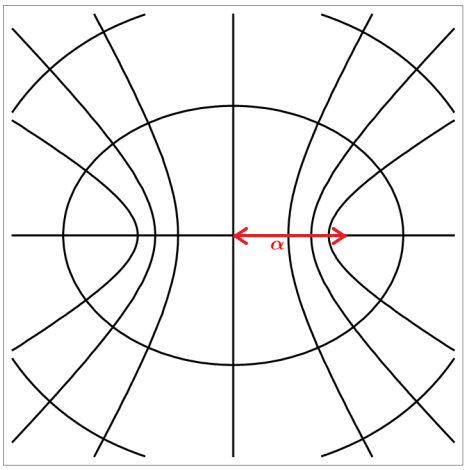

Figure 6.2: The elliptic coordinate system. Contours are shown for $\xi = \{1, 1.5, 2\}$ and $\eta = \{\pi/3, \pi/4, \pi/6\}$ with $\alpha = 1$. The region $x, y \in [-2, 2]$ is shown.

The Cartesian coordinates are in terms of elliptic coordinates η, ξ given by

$$x = \alpha \cosh(\xi)\cos(\eta), \qquad y = \alpha \sinh(\xi)\sin(\eta),$$

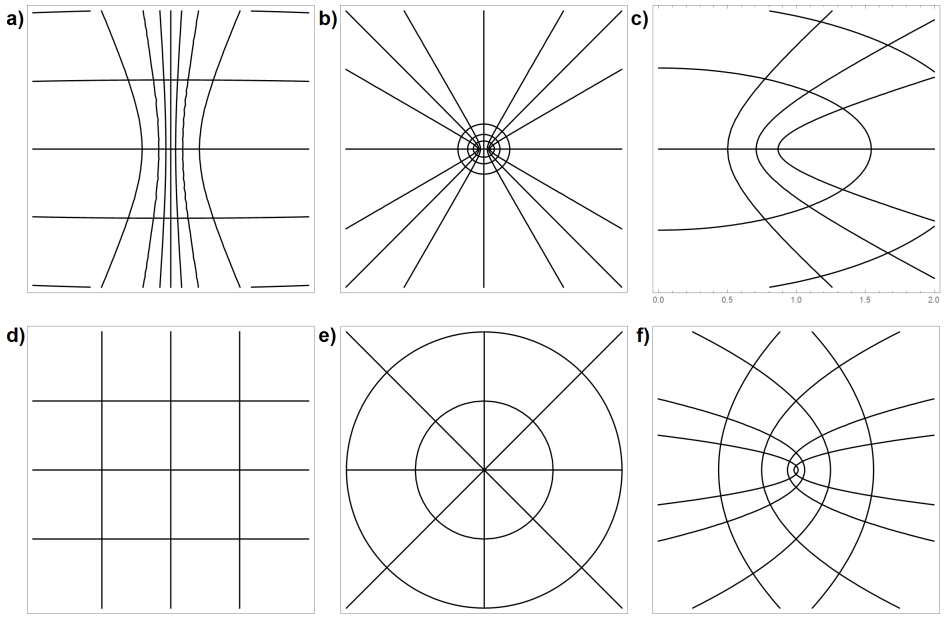

Figure 6.3: Comparison between the different coordinate systems. Top: the transformation of the elliptic coordinate system when taking different limits of α. a): $\alpha \to \infty$; b): $\alpha \to 0$; c): considering an area close to $x = +\alpha$. Bottom: the corresponding coordinate systems; d): Cartesian; e): polar; f): parabolic. The range of all coordinate axes is $[-2, 2]$ except for the x-axis in c) which is $[0, 2]$.

with α the focal distance: the distance between the focus and the origin of the coordinate system. This is shown in figure 6.2.

Taking suitable limits of α reduces the elliptical coordinate system to the other coordinate systems; in the limit $\alpha \to \infty$ the system looks like the Cartesian coordinate system, while in the limit $\alpha \to 0$ the foci come very close together and the cylindrical polar coordinate system is retrieved. Close to one focus, with the other one at infinity, the coordinate system resembles the cylindrical parabolic coordinate system. This explains the shape of the parabolae: they only resemble circular lines on one side of the focus and become elongated on the other side, and a discontinuity appears along the elongation direction. Approximations of these coordinate systems and their actual forms are shown in figure 6.1. Each coordinate system has different associated conserved quantities; the constants of motion.

6.1.1 Constants of motion

Constants of motion are the mechanical quantities that characterize the trajectories of a particle. The derivation of these conserved quantities by the Euler-Lagrange equations (2.16) was discussed in chapter 2. Here the different fields (scalar, spinor and vector) were described without specifying the coordinate system that was used. Another approach is to first derive a general expression for the conserved quantities of a scalar particle, and then vary the coordinate system in which the particle is described. This will demonstrate which quantities are conserved by the basis solutions in that coordinate system. This method will be used to derive the constants of motion of the parabolic coordinate system.

In a general curvilinear coordinate system, described by the transverse coordinates (p, q), the Lagrangian of a scalar particle can be written in the following form [180]:

$$\mathcal{L} = \frac{1}{2}[f_1(p) + f_2(q)](\dot{p}^2 + \dot{q}^2) + \frac{g_1(p) + g_2(q)}{f_1(p) + f_2(q)}, \tag{6.3}$$

where f_1, f_2, g_1, g_2 are functions of the coordinates and depend on the system considered. Solving the Euler-Lagrange equations in both coordinates p and q gives two coupled equations with a separation constant G:

$$G = -\frac{1}{2}\frac{1}{f_1(p) + f_2(q)}\left\{\left[f_2(q)\dot{p}^2 - f_1(p)\dot{q}^2\right] - 2\left[f_2(q)g_1(p) - f_1(p)g_2(q)\right]\right\}. \tag{6.4}$$

This constant G is the constant of motion, that can be written in terms of three operators; the Hamiltonian, the angular momentum in the $\hat{\mathbf{z}}$ direction L_z and the Runge-Lenz vector. The Hamiltonian operator is in general terms given by [180]

$$\langle H \rangle = \mathcal{E} = \frac{1}{2}[f_1(p) + f_2(q)](\dot{p}^2 + \dot{q}^2) - \frac{g_1(p) + g_2(q)}{f_1(p) + f_2(q)}, \tag{6.5}$$

and the Runge-Lenz vector is defined as

$$\mathbf{K} = \frac{1}{m}(\mathbf{p} \times \mathbf{L}). \tag{6.6}$$

This vector is clearly perpendicular to the angular momentum. Only one transverse component of this vector needs to be considered, as under rotations in the transverse plane $p_x \to p_y \to -p_x$ the components transform into each other $K_x \to K_y$. In this chapter only the $\hat{\mathbf{x}}$-component will be considered:

$$K_x = \frac{1}{m}p_y L_z.$$

Comparing the expression of (6.4) to the expressions of H, L_z and K_x in elliptical coordinates[3] gives the relationship [180]

$$G = m\alpha^2 H + m\alpha K_x + \frac{1}{2}L_z^2. \tag{6.7}$$

Taking the same limits as shown in figure 6.1 of (6.7) gives the following constants of motion associated with Cartesian and cylindrical polar coordinates:

Cartesian:	$\alpha \to \infty$	$G \approx H,$
Cylindrical polar:	$\alpha \to 0$	$G \approx L_z^2.$

This shows that cylindrical polar coordinates conserve the *square* of the OAM. This is because separable solutions of differential equations are real functions [178]. A Bessel beam, as a limiting case of a Mathieu beam, is a standing wave in the azimuthal direction. It is described by $\cos(\phi)$ or $\sin(\phi)$ and is hence not an eigenstate of the L_z operator but of L_z^2. However, creating a superposition $\cos(\phi) \pm i\sin(\phi)$ yields a helical beam, and this is an eigenstate of L_z. The phase *winds* around the propagation axis upon propagation. This gives the Bessel beam expression (1.7), with the order ℓ both the eigenvalue of the OAM and the separation constant found when solving the wave equation (1.6).

Writing the Lagrangian in parabolic coordinates (C.6a) and using the expressions for the Hamiltonian (C.6b) and OAM operator (C.6c) shows that the conserved quantity (6.4) is found to be proportional to the Runge-Lenz vector:

$$G = \frac{1}{2(\mu^2 + v^2)}\left[(u^2 p_v^2 - v^2 p_u^2) - 2mk(u^2 - v^2)\right] = mK_x.$$

The conjugate momenta are $p_u = m(u^2 + v^2)\dot{u}$ and $p_v = m(u^2 + v^2)\dot{v}$. This constant turns out to be *related* to the separation constant found when solving the Helmholtz equation in parabolic cylinder coordinates, similar to the appearance of the quantum number ℓ in the derivation of Bessel beams.

[3]The quantities are in elliptical coordinates given by

$$\begin{aligned}
H &= \frac{1}{2ma^2}\left(\frac{p_\xi^2 + p_\eta^2}{\cosh^2(\xi) - \cos^2(\eta)}\right) - \frac{k}{a}\frac{1}{\cosh(\xi) - \cos(\eta)} \\
L_z &= -\frac{p_\xi \sin(\eta)}{\cosh(\xi) + \cos(\eta)} + \frac{p_\eta \sinh(\xi)}{\cosh(\xi) + \cos(\eta)} \\
K_x &= \left[\frac{-1}{\cosh^2(\xi) - \cos^2(\eta)}\left(p_\xi \cosh(\xi)\sin(\eta) + p_\eta \sinh(\xi)\cos(\eta)\right)\right] \times \\
&\qquad \left\{\frac{p_\xi \sin(\eta)}{\cosh(\xi) + \cos(\eta)} - \frac{p_\eta \sinh(\xi)}{\cosh(\xi) + \cos(\eta)}\right\} - kma\frac{\cosh(\xi)\cos(\eta) - 1}{\cosh(\xi) - \cos(\eta)}
\end{aligned}$$

6.1.2 Separation of variables

Applying the separation of variables procedure as explained in section 1.2 to parabolic cylindrical coordinates transforms the transverse part of the Helmholtz equation (1.5a) to

$$\frac{1}{u^2+v^2}(\partial_u^2+\partial_v^2)A(u,v) = -k_\perp^2 A(u,v). \tag{6.8}$$

The solution $A(u,v)$ can be separated in two parts, each dependent on one coordinate $A(u,v) = M(u)N(v)$. Inserting this in (6.8) gives two equations, with separation constant $2k_\perp a$:

$$M'' = (2k_\perp a - u^2 k_\perp^2)M, \tag{6.9}$$

$$N'' = -(2k_\perp a + v^2 k_\perp^2)N. \tag{6.10}$$

Now making a linear combination $v^2M''+u^2N''$ shows that $2k_\perp a$ is the eigenvalue of the following operator:

$$\left(\frac{v^2\partial_u^2 - u^2\partial_v^2}{u^2+v^2}\right)MN = 2k_\perp aMN. \tag{6.11}$$

This operator is the parabolic momentum K, in Cartesian coordinates given by the anticommutator of the momentum in the $\hat{\mathbf{y}}$-direction and the angular momentum: $\{L_z, p_y\}$ [181]. This parabolic momentum is *related* to the $\hat{\mathbf{x}}$-component of the Runge-Lenz vector [55];

$$mK_x = p_y L_z = L_z p_y - p_x = \frac{1}{2}\{L_z, p_y\} - \frac{1}{2}p_x.$$

From the comparison between cylindrical polar and parabolic coordinates it was concluded that the parabolic system resembles "half-a-polar" system, as it is elongated in one direction. It is therefore expected that its conserved quantity is that of the cylindrical polar coordinate system (OAM) modified with a translation. This is in agreement with the definition of the parabolic momentum as the anticommutator of the OAM operator and the momentum operator in the $\hat{\mathbf{y}}$-direction. It interpolates between angular and linear momentum, similar to the limit of elliptical coordinates that gives rise to the parabolic coordinates: close to one focus instead of decreasing the focal distance (polar), while the other focus is at infinity instead of having both infinitely far apart (Cartesian).

6.2 Parabolic field solutions

The differential equations (6.9) and (6.10), sometimes called the radial and angular equations, are related to each other by the substitution $u \to iv$. They can

be brought in the standard form by making the transformation $z = \sqrt{2k_\perp}u$:

$$P''(z;a) = -2k_\perp \left(\frac{1}{4}z^2 - a\right) P(z;a). \tag{6.12}$$

Writing the solution $P(z;a)$ as a power series and inserting this into (6.12) gives a recurrence relationship for the coefficients [179]:

$$P(z;a) = \sum_{n=0} c_n \frac{z^n}{n!}, \qquad\qquad c_{n+2} = ac_n - \frac{n(n-1)}{4}c_{n-2}.$$

For the even solutions P_e the first coefficients are $\{c_0 = 1,\ c_1 = 0\}$, while for the odd solutions P_o, the zeroth coefficient is zero $\{c_0 = 0,\ c_1 = 1\}$[4].

The notation as used in [179] is adopted here, but these functions are also described in [182], where the functions $P(z;a)$ correspond to the functions $W(a,x)$. Similarly, the functions $P_e(z;a) = w_1(a,x)$ and $P_o(z;a) = w_2(a,x)$ are defined in (12.14.9) and (12.14.10), and $W(a,x)$ can be expanded in terms of $w_1(a,x)$ and $w_2(a,x)$ as described in (12.14.8). The functions w_1, w_2 are related to Kummer functions, see (12.14.15) and (12.14.16) in [182].

Since the coordinate v is discontinuous for negative x, a continuous solution is always a product of two odd or even functions [179][5]

$$U_{e,k,a}(u,v) \propto P_e(\sqrt{2k_\perp}u;a)P_e(\sqrt{2k_\perp}v;-a), \tag{6.16a}$$

$$U_{o,k,a}(u,v) \propto P_o(\sqrt{2k_\perp}u;a)P_o(\sqrt{2k_\perp}v;-a). \tag{6.16b}$$

[4]There also exist solutions of (6.12) that can be found by making the replacement $z \to \sqrt{i}z$. This gives the following differential equation:

$$\partial_z^2 f(z) = \kappa^2 \left(\frac{\kappa^2}{4}z^2 - (in + \frac{1}{2})\right) f(z), \tag{6.13}$$

where the solutions $f(z) = D_{in}(\kappa z)$ are so-called Weber functions, with $\kappa = \sqrt{2ik_\perp}$. Solutions of the transverse Helmholtz equation (6.8) are given by the product of two Weber functions:

$$M(u)N(v) = D_{in}(\kappa u)D_{im}(\kappa v), \tag{6.14}$$

under the condition that the integers m and n are related to each other by $m + n = -1$. However, these solutions do not describe physical fields correctly, as they are not continuous on the transverse plane. Further, the integer n is related to the parabolic momentum by

$$-\left(in + \frac{1}{2}\right) = a\kappa^2 = \frac{\langle K\rangle}{2k_\perp} \leftrightarrow \langle K\rangle = in + \frac{1}{2}. \tag{6.15}$$

Due to the transformation $z \to \sqrt{i}z$, the integer n is multiplied by a factor of i, making the expectation value of the parabolic momentum operator complex. Expectation values that correspond to measurable quantities need to be real. This makes that the solutions (6.14) are not physically allowed.

[5]The products of one odd and one even function are double-valued in (vector) space. However, in space with a spinor structure, the requirement of single-valuedness does not imply that the values of the wavefunctions are equal at every point. Hence these (odd-even and even-odd) wavefunctions are also valid solutions in spinor space [183].

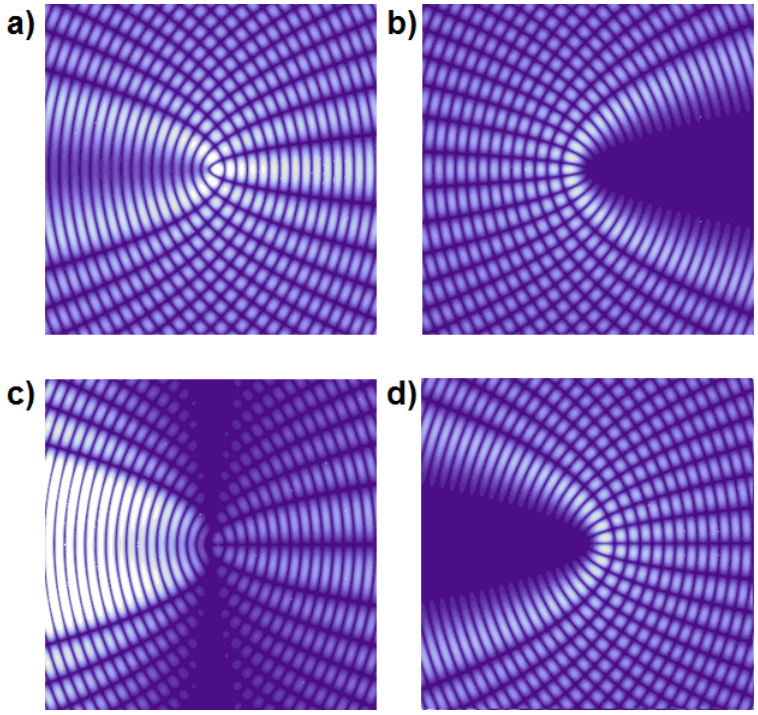

Figure 6.4: Intensity patterns of stationary parabolic beams described by (6.16). a): $U_{e,k,1}$, b): $U_{e,k,-4}$, c): $U_{o,k,1}$, d): $U_{o,k,4}$. These plots show that the solutions $U_{e,k,a}$ are even with respect to the x-axis, clearly visible for $x > 0$, while the odd solutions have a node. Changing the sign of a creates the pattern reflected in the y-axis.

A couple of stationary solutions are shown in figure 6.4. These solutions are perpendicular to each other with respect to a [179]:

$$\int d^2S\, U_{e/o,k,a}(u,v)U^*_{e/o,k,a'}(u,v) = \delta(a-a'), \tag{6.17}$$

where the integral is taken over the infinite transverse plane. They form a complete set of functions and any diffraction-free optical field can be expressed in them. These functions are specified by their eigenvalue of the parabolic momentum K, similar to the order of the Bessel beams (1.7) that is the eigenvalue of the OAM operator. The orthogonality of the parabolic harmonics follows from the orthogonality of the corresponding angular *spectra*, as discussed in the next section.

6.2.1 The angular spectrum

The spatial field distribution of a propagation invariant beam can be found from its angular spectrum, as earlier explained in section 1.2.1. The angular spectrum

of Bessel beams is given by (1.8): $A(\phi) = e^{im\phi}$, and has as result that the intensity pattern is independent of ϕ. This property enabled Durnin [25] to generate a Bessel beam by using an annular slit. For other types of beams the slit needs to modulated as described by the amplitude of the angular spectrum. This spectrum is for parabolic cylinder harmonics calculated to be [184]:

$$A_e(\phi; a) = \frac{1}{2\sqrt{\pi|\sin(\phi)|}} \exp\left(ia \ln|\tan(\phi/2)|\right), \tag{6.18a}$$

$$A_o(\phi; a) = -i \begin{cases} -A_e(\phi; a) & \phi \in (-\pi, 0), \\ A_e(\phi; a) & \phi \in (0, \pi), \end{cases} \tag{6.18b}$$

where the subscripts correspond to the subscripts of (6.16). The spectrum $A(\phi)$ is only defined on one half of the plane, $\phi \in (0, \pi)$, due to the branch cut on the negative x-axis. Field solutions on the full transverse plane can be defined by extending the spectrum to the other half of the plane in an odd or even way. This creates the stationary parabolic beams as shown in figure 6.4. The spectrum (6.18) was used in 2005 [185] to experimentally realize the first parabolic optical beams of zeroth order with the aid of an annular slit. Computer generated holograms were used to generate higher order beams. The intensity pattern observed showed the characteristics of even and odd modes, where the intensity followed parabolic lines [185].

The identity (6.17) is a result of the orthogonality of the corresponding spectra of the parabolic harmonics [181]. This is shown by taking the inner product of the two spectra:

$$\begin{aligned} \langle A(\phi; a)|A(\phi; a')\rangle &= \int_0^\pi \frac{1}{2\pi \sin(\phi)} \exp\left\{ i(a - a') \ln\left[\tan\left(\frac{\phi}{2}\right)\right]\right\} d\phi, \\ &= \int \frac{1}{2\pi} \exp\left[i(a' - a)t\right] dt, \\ &= \delta(a' - a). \end{aligned}$$

In the regime $\phi \in (0, \pi)$ both $\sin(\phi)$ and $\tan\left(\frac{\phi}{2}\right)$ are positive, hence the absolute value signs can be ignored. The variable ϕ is replaced by $t = \ln\left[\tan\left(\frac{\phi}{2}\right)\right]$ to go from the first to the second line, changing the limits of the integral to $(-\infty, \infty)$ and yielding the Jacobian factor $\sin(\phi)$. This is followed by implementing the definition of the Dirac delta function.

Similar to Bessel beams, parabolic beams stretch out to infinity in the transverse plane and therefore need to be regularized by a Gaussian envelope. The parabolic-

Gauss beams are described by [186] (where they are called Weber-Gauss beams):

$$E_a^{WG}(u,v,z) = \frac{1}{u(z)} \exp\left[i\left(k - \frac{k_\perp^2}{2ku(z)}\right)z\right] \exp\left(-\frac{r_\perp^2}{w_0^2 u(z)}\right) U_{e/o,k,a}(u,v).$$

Here $u(z) = 1 + iz/z_R$ with z_R the Rayleigh length, see Appendix A. There is only one parameter a, comparable to the parameter ℓ of the Bessel beams.

6.2.2 Accelerating beams

Travelling waves, as opposed to stationary waves, can be described by superpositions of even and odd modes, $U_{e,k,a}(u,v) \pm i\, U_{o,k,a}(u,v)$. An example is shown in 6.5. From (6.18) it can be concluded that the spectrum of these beams is only defined on half of the plane. These beams can be interpreted in two different ways; they are non-diffracting and propagating in a straight line (in the $\hat{\mathbf{z}}$-direction), or they are accelerating along a parabolic curve [181]. These beams are said to be *accelerating* as their intensity pattern shifts in the transverse direction ($\hat{\mathbf{x}}$) with an increasing velocity upon propagating (along $\hat{\mathbf{y}}$). Important to note here is that the propagation direction is changed from the $\hat{\mathbf{z}}$-direction to the $\hat{\mathbf{y}}$-direction!

Accelerating beams can even break the paraxial limit when they bend far enough, but do retain their self-healing and non-diffractive nature [187]. They can be constructed in different ways, based on creating a suitable superposition of rays in phase space that gives the desired bending behaviour [188]. By superimposing two beams that bend in different directions, two-dimensionally accelerating beams can be designed that follow an elliptic trajectory [189]. Parabolic accelerating beams have been created as superpositions of even and odd parabolic harmonics [181], showing that the linear momentum flows in parabolic lines. This allows for the transfer of parabolic momentum.

Accelerating beams can also be created from Bessel beams by taking only half of the spectrum $A(\phi)$ with $\phi \in [0, \pi]$; this gives forward propagating beams [190]. Taking the spectrum $\phi \in [-\pi, 0]$ creates a backwards propagating beam. These beams are also called "half-a-Bessel" beams as each one only describes half of the intensity pattern of concentric circles that is characteristic for Bessel beams. It was found that the "half-a-Bessel" beams shift faster in the transverse direction than accelerating parabolic beams [181].

Accelerating electron beams, numerically constructed by taking half of the Bessel spectrum, showed that electrons can also exhibit nonparaxial accelerating properties and self-healing [192]. These properties can be applied to improve the resolution of electron microscopes.

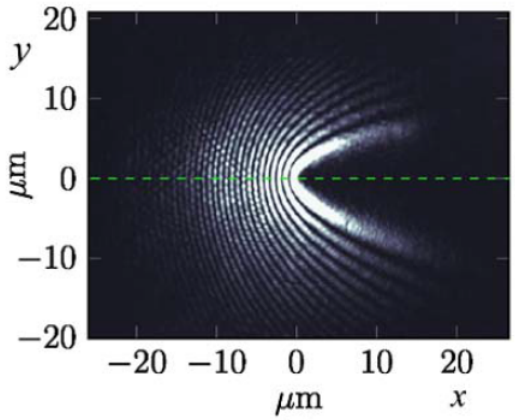

Figure 6.5: Transverse intensity pattern of an accelerating parabolic beam described by the superposition $U_{e,k,a}(u,v) + i\, U_{o,k,a}(u,v)$ with $a = 3$ and wavelength 532 nm [191].

Other examples of beams that are defined by spectra breaking the circular symmetry are pendulum beams as described in [178]. Their propagation invariant intensity pattern can take all kinds of shapes, for example a "Gaussian profile", while they also diffract upon propagation.

It can be concluded that parabolic harmonics are characterized by their parabolic momentum. The spectrum is defined on only half of the transverse plane. With the aid of this spectrum both stationary and travelling beams can be created. Travelling beams can also be interpreted as beams accelerating in the transverse direction.

6.3 OAM in parabolic coordinates

Knowing the field solutions, the manifestation of OAM and spin-orbit coupling effects in parabolic coordinates can be studied. From the comparison between the cylindrical polar and parabolic coordinate systems it was concluded that the parabolic coordinates resemble the cylindrical polar coordinates in only one half of the plane. The field solutions (6.16) are not eigenstates of the OAM operator but of the parabolic momentum K. However, the spectrum (6.18) can be compared with the angular spectrum of the Bessel beams $e^{i\ell\phi}$ to conclude to what extend the parabolic field solutions can be approximated as OAM eigenstates.

Further, it was explained in section 1.4 that the spinor and vector solutions

of the Helmholtz equation can be derived from the scalar solution, independent of the choice of transverse cylindrical coordinates. When the fields are described in polarization coordinates (1.14) the spin and orbital angular momentum are coupled to each other. This is the result of the action of the OAM ladder operators $U^{\pm}$ (1.16). The effect of these ladder operators on the parabolic harmonics can be studied to draw conclusions about the manifestation of OAM and spin-orbit coupling in parabolic coordinates.

6.3.1 Analysis of the angular spectrum

The angular spectrum of a Bessel beam is given by $A(\phi) = e^{i\ell\phi}$: the amplitude is constant while the phase increases linearly with ϕ. As a result, the OAM *density* of a field φ is constant:

$$\langle \widetilde{L}_z \rangle = \frac{\langle \varphi | L_z | \varphi \rangle}{\langle \varphi | \varphi \rangle} = -i \, \frac{e^{-i\ell\phi} \left(\partial_\phi e^{i\ell\phi} \right)}{1} = \ell.$$

Since the expectation value $\langle \widetilde{L}_z \rangle$ is a real number, its argument is equal to zero. The same calculation can be performed on the parabolic spectrum (6.18). The amplitude and argument of this spectrum are shown in figure 6.6, with the Bessel beam spectrum also shown for comparison. These plots show that for $\phi = \pi/2$ the amplitude of the spectrum becomes constant and the argument increases linearly. This is a necessary condition for an OAM eigenstate.

Using the fact that for this spectrum the derivative with respect to ϕ can be related to the spectrum itself through

$$\frac{dA(\phi)}{A d\phi} = \frac{2ia - \cos(\phi)}{2\sin(\phi)},$$

the expectation value of the angular momentum density is given by

$$\langle \widetilde{L}_z \rangle = \frac{\langle A(\phi) | L_z | A(\phi) \rangle}{\langle A(\phi) | A(\phi) \rangle} = \frac{2a + i\cos(\phi)}{2\sin(\phi)}. \tag{6.20}$$

The argument of this expectation value is zero for $\phi = \pi/2$, where $\langle L_z \rangle = a$. This leads to the conclusion that around $\phi = \pi/2$ the field resembles an OAM eigenstate. This is exactly the direction of propagation (the $\hat{\mathbf{y}}$-direction) for a forward propagating accelerating beam.

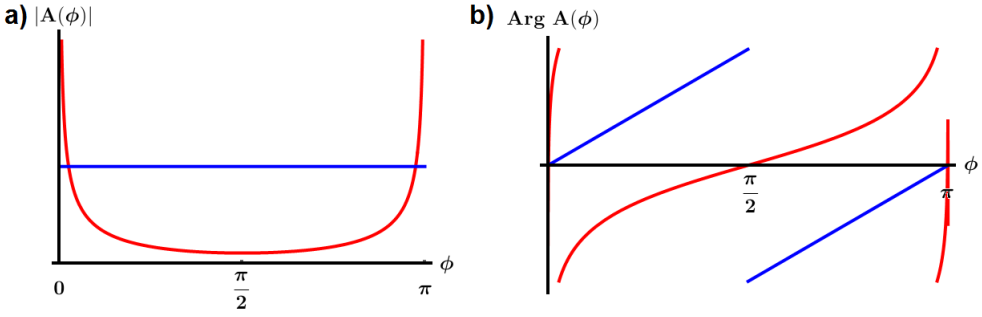

Figure 6.6: The amplitude and argument of the spectra of a Bessel beam ($\ell = 1$) and a parabolic beam ($a = 1$). a): amplitude, b): argument. The Bessel beam spectrum $e^{i\ell\phi}$ is shown in blue; the amplitude is constant and the argument increases linearly with ϕ. The parabolic spectrum has a minimum in amplitude and the phase increases linearly at $\phi = \pi/2$.

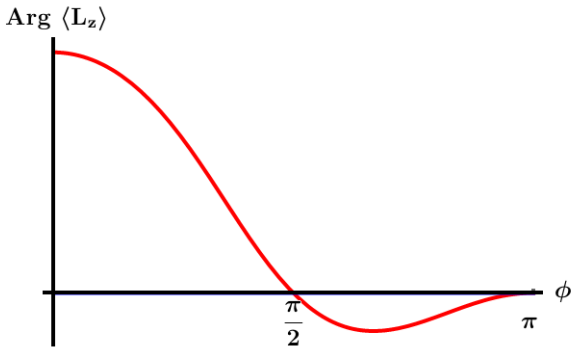

Figure 6.7: The argument of the expectation value of the OAM (6.20). The argument becomes 0 at $\phi = \pi/2$; the expectation value is real.

6.3.2 Vector and spinor fields in parabolic coordinates

As explained in sections 1.4.2 and 1.4.3, vector and spinor field solutions can be derived from the scalar field solutions as in (1.38) and (1.40). It was found that the field components were related to each other through the ladder operators for the OAM, $U^{\pm}$ (1.16).

Vector parabolic harmonics The general method to derive vector fields from a scalar solution is given by (1.37). With the definition of the curl operator in parabolic coordinates (C.5b) the fields (1.37) are found to be:

$$\mathbf{T} = \tfrac{1}{h}\begin{pmatrix} \partial_v \\ -\partial_u \\ 0 \end{pmatrix}\varphi, \qquad \mathbf{S} = \tfrac{1}{h}\begin{pmatrix} \partial_z\partial_u \\ \partial_z\partial_v \\ -\frac{1}{h^2}(\partial_u^2+\partial_v^2) \end{pmatrix}\varphi. \tag{6.21}$$

It can be verified that the divergence (C.5a) of these fields vanishes. The longitudinal component of $\mathbf{S}$ can be simplified as this is equal to the transverse part of the Laplacian $\nabla^2\varphi$ (C.5c). These general expressions for vector parabolic harmonics are similar to those found in [193]. However, parabolic vector harmonics can also be derived in the polarization basis. These fields are in general terms given by (1.38) and expressed in terms of the ladder operators $U^{\pm}$. These are in parabolic coordinates transformed to [55]

$$U^{\pm} = \frac{1}{\sqrt{2}h}e^{\pm i\beta}\left(\partial_u \pm i\partial_v\right). \tag{6.22}$$

These operators also appear in the derivation of spinor parabolic harmonics, as will be shown next. This will be followed by a discussion of the effects of these operators on the field solutions in the context of spin-orbit coupling.

Spinor parabolic harmonics To derive spinor parabolic harmonics, it is necessary to write the Dirac equation in parabolic coordinates. The divergence $\gamma^\mu\partial_\mu$ can be written in parabolic coordinates as

$$\gamma^\mu\partial_\mu = \gamma^0\partial_t - \gamma^x\partial_x - \gamma^y\partial_y - \gamma^z\partial_z = \gamma^0\partial_t - \gamma^u\partial_u - \gamma^v\partial_v - \gamma^z\partial_z.$$

By using the transformation rules $\partial_x = \frac{\partial u}{\partial x}\partial_u + \frac{\partial v}{\partial x}\partial_v$ and similar for ∂_y, the following γ-matrices are obtained:

$$\gamma^u = \frac{1}{h^2}\begin{pmatrix} 0 & 0 & 0 & u-iv \\ 0 & 0 & u+iv & 0 \\ 0 & -(u-iv) & 0 & 0 \\ -(u+iv) & 0 & 0 & 0 \end{pmatrix},$$

$$\gamma^v = \frac{1}{h^2}\begin{pmatrix} 0 & 0 & 0 & -i(u-iv) \\ 0 & 0 & i(u+iv) & 0 \\ 0 & i(u-iv) & 0 & 0 \\ -i(u+iv) & 0 & 0 & 0 \end{pmatrix}.$$

With these definitions, a general spinor field can be expressed in terms of scalar fields multiplied by a matrix operator, as explained in section 1.4.3:

$$\psi(p,q,z,t) = i\left[c_1\begin{pmatrix}\partial_t+m\\0\\-\partial_z\\\frac{-(\partial_u+i\partial_v)}{u-iv}\end{pmatrix}\varphi_1(p,q) + c_2\begin{pmatrix}0\\\partial_t+m\\\frac{-(\partial_u-i\partial_v)}{u+iv}\\\partial_z\end{pmatrix}\varphi_2(p,q)\right]\times e^{-i\omega t+ik_z z}. \quad (6.23)$$

Comparing this with the definition of $U^{\pm}$ (6.22) shows that the terms depending on u and v, are proportional to the ladder operators:

$$\frac{-(\partial_u+i\partial_v)}{u-iv} = -(\partial_u+i\partial_v)\frac{u+iv}{h^2} = -(\partial_u+i\partial_v)\frac{e^{i\beta}}{h} = -\sqrt{2}U^+,$$
$$\frac{-(\partial_u-i\partial_v)}{u+iv} = -(\partial_u-i\partial_v)\frac{u-iv}{h^2} = -(\partial_u-i\partial_v)\frac{e^{-i\beta}}{h} = -\sqrt{2}U^-.$$

Inserting these into (6.23) yields exactly the general spinor field expression (1.40). This shows that this general expression indeed holds in any coordinate system.

Spin-orbit coupling effects The vector and spinor field components in equations (1.38) and (1.40) are related to each other through the $U^{\pm}$ operators. If the $\hat{\mathbf{z}}$-component of a vector field is given by the scalar field solution φ, the transverse $\hat{\mathbf{e}}_{\pm}$ components are proportional to $U^{\mp}\varphi$. Each field component carries a different amount of SAM in this basis while the OAM value is shifted by the ladder operators $U^{\pm}$, conserving the total AM. Similarly for the spinor field; by raising or lowering the OAM value of one of the components the total AM of every component is the same. Thus, to find the corresponding expressions for parabolic vector and spinor harmonics the action of the $U^{\pm}$ operators on a scalar parabolic harmonic needs to be understood.

An important difference between the ladder operators in parabolic coordinates (6.22) and in cylindrical coordinates (1.16) is that the operators in parabolic coordinates are proportional to $e^{\pm i\beta} = e^{\pm i\phi/2}$. They do not raise or lower the OAM with one unit, but only with a half unit. With this definition, the action of the ladder operators can be divided into two parts. Firstly, the effect of taking derivatives of (6.16) with respect to u and v. These solutions can be expressed in

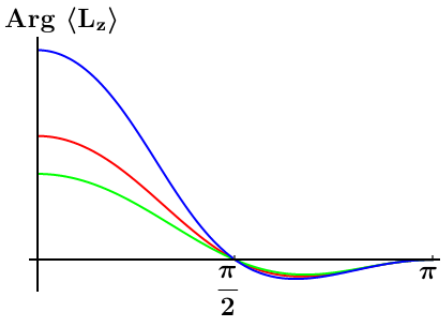

Figure 6.8: The shift in argument of the expectation value of the OAM induced by the ladder operators $U^{\pm}$. Shown are the arguments of the expectation value of L_z, (6.20) with $a = 2$, red line, and the arguments of the spectra when shifted by $+\phi/2$ (green) and $-\phi/2$ (blue).

Kummer functions (equations 12.14.15 and 12.14.16 in [182]) as:

$$U_{e,k,a}(u,v) \propto \exp\left(-i\frac{k_\perp}{2}(u^2+v^2)\right) \times \\ {}_1F_1\left(\frac{1}{4}-\frac{i}{2}a,\frac{1}{2};i\frac{k_\perp}{2}u^2\right)\ {}_1F_1\left(\frac{1}{4}+\frac{i}{2}a,\frac{1}{2};i\frac{k_\perp}{2}v^2\right),$$

$$U_{o,k,a}(u,v) \propto 2k_\perp uv \exp\left(-i\frac{k_\perp}{2}(u^2+v^2)\right) \times \\ {}_1F_1\left(\frac{3}{4}-\frac{i}{2}a,\frac{3}{2};i\frac{k_\perp}{2}u^2\right)\ {}_1F_1\left(\frac{3}{4}+\frac{i}{2}a,\frac{3}{2};i\frac{k_\perp}{2}v^2\right).$$

Derivatives of these functions can be expressed in other Kummer functions, for example (see equation 13.3.15 in [182])

$$\frac{\partial U_{e,k,a(u,v)}}{\partial u} = -i\frac{u}{2}U_{e,k,a(u,v)} + (1-2ia)u\exp\left(-i\frac{k_\perp}{2}(u^2+v^2)\right) \times \\ {}_1F_1\left(\frac{5}{4}-\frac{i}{2}a,\frac{3}{2};i\frac{k_\perp}{2}u^2\right)\ {}_1F_1\left(\frac{1}{4}+\frac{i}{2}a,\frac{1}{2};i\frac{k_\perp}{2}v^2\right) \quad (6.24)$$

However, how this result is related to the original function is not easily resolved. Hence it is not possible to interpret the action of the raising or lowering operators on the spatial dependence of the parabolic harmonics in a conclusive way.

Another way to investigate the effect of the $U^{\pm}$ operators is by studying their effect on the angular spectrum $A(\phi)$. This get multiplied by $e^{\pm i\phi/2}$, which does not change the amplitude. However, the complex argument of the expectation value of L_z, (6.20), gets shifted in value but is again equal to 0 for $\phi = \pi/2$. This is shown in figure 6.8.

A spectrum that is multiplied by $e^{in\phi/2}$ with $n \in \mathbb{Z}$ can be expressed in terms of the original spectrum, as expanding the spectrum in powers of ϕ around $\phi = \pi/2$ gives the following relationship:

$$A(\phi; a)e^{in\phi/2} \simeq e^{in\pi/2} A\left(\phi, a + \frac{n}{2}\right). \tag{6.25}$$

This equality is valid up to $\mathcal{O}\left(\phi^2\right)$, and shows that raising the OAM with a half-integer amount effectively changes the value of the parabolic momentum with a half quantum as well. This is not surprising, as it was concluded earlier that at $\phi = \pi/2$ the beam resembles an OAM eigenstate. Moreover, accelerating beams propagating in the $\hat{\mathbf{y}}$ direction are eigenstates of the p_y operator before they start to bend; the action of p_y on the beam returns the original field expression. The action of the parabolic momentum operator (6.11) is, as a result, equivalent to that of the OAM operator.

The effect of raising or lowering the OAM by one unit There is another approach to study the effect of raising and lowering the OAM on the parabolic harmonics. Since parabolic harmonics describe a complete and orthogonal set of functions, any modified parabolic harmonic can be expressed in the original set of functions. Similar to (6.19), the inner product of two parabolic harmonics with parabolic momentum a and a', of which one has its OAM value modified by ± 1, is given by

$$\begin{aligned}
\langle A(\phi; a)|A(\phi; a')e^{\pm i\phi}\rangle &= \int_0^{\pi} \frac{1}{2\pi \sin(\theta)} \exp\left\{ i(a' - a) \ln\left[\tan\left(\frac{\phi}{2}\right)\right]\right\} e^{\pm i\phi} d\phi \\
&= \int \frac{1}{2\pi} \exp\left(iwt\right) \exp\left[\pm 2i \arctan\left(e^t\right)\right] dt, \\
&= S_{\pm 1}(w),
\end{aligned}$$

where the same transformation as in (6.19) is implemented. The parameter $w = a' - a$ is a measure for the shift in parabolic momentum. This integral is the Fourier transform of the function $\exp\left[\pm 2i \arctan\left(e^t\right)\right]$ with respect to w. Instead of sines and cosines, this is a decomposition into parabolic harmonics. The Fourier transform $S_{\pm 1}(w)$ describes the weighting of the original parabolic harmonics in the decomposition of a modified parabolic harmonic, according to the shift in parabolic momentum. The real part of $S_{\pm 1}(w, t)$ is approximately zero, while the imaginary part is shown in figure 6.9.

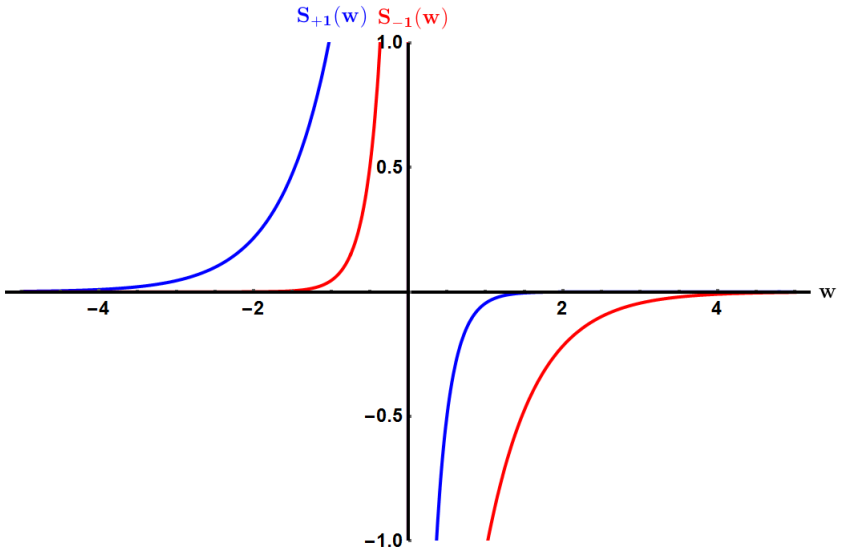

Figure 6.9: The imaginary part of the weight function $S_{\pm 1}(w)$. Blue: $+1$, red: -1. This figure shows clearly that $S_{\pm 1}$ has a singularity in the vicinity of $w = \mp 1$. The functions $S_{\pm 1}(w)$ are each others mirror image.

This weight function can be used to find an approximate expression for the modified spectrum $A(\phi; a')e^{\pm i\phi}$:

$$A(\phi; a')e^{\pm i\phi} = \int S_{\pm 1}(w) A(\phi; a' - w)\, dw. \tag{6.26}$$

The w-dependence of $S_{\pm 1}(w)$ leads to the prediction that $A(\phi; a \mp 1)e^{\pm i\phi} \simeq A(\phi; a)$, with possibly some smaller contributions from other parabolic harmonics. This is in agreement with the approximation (6.25) found earlier. However, the function $S_{\pm 1}(w)$ is not defined for half-integer units of ϕ.

The integral (6.26) can be approximated by a discrete sum over w, concentrated around the value $w = \pm 1$. For a parabolic harmonic with parabolic momentum a' and its spectrum multiplied by $e^{+i\phi}$, the term $S_{+1}(-1)A(\phi; a' + 1)$ describes the azimuthal dependence almost correctly, hence $a = a' + 1$. Similarly for an opposite shift in OAM, as shown in figure 6.10. This figure clearly shows that discrepancies increase for angles further away from $\phi = \pi/2$, in agreement with the approximation (6.25). By summing over more values of w better approximations of the modified spectrum can be found. This will be left for future considerations.

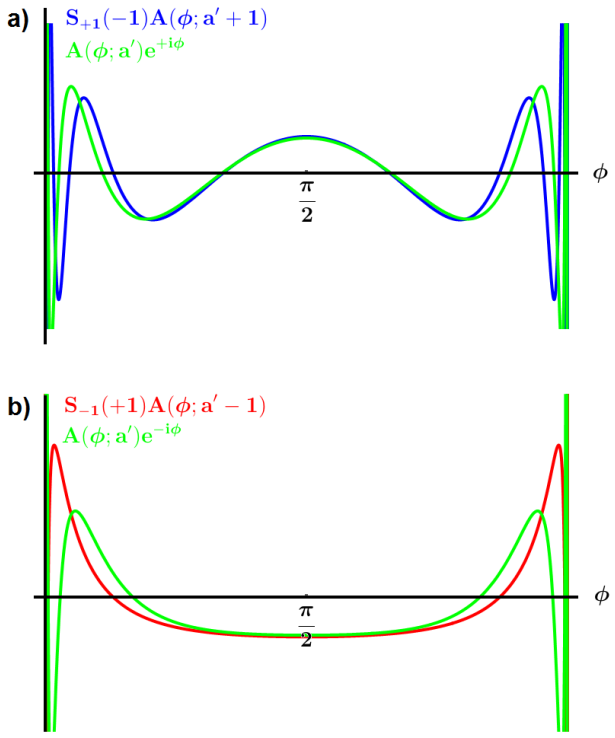

Figure 6.10: Comparison between the imaginary parts of the parabolic harmonic spectrum modified with $e^{\pm i\phi}$ and the first term in its decomposition. a) Comparison between the spectrum of a parabolic harmonic with $a = 2$, modified by $e^{+i\phi}$, i.e. $A(\phi;2)e^{+i\phi}$, and the first term in the decomposition $S_{+1}(-1)A(\phi;3)$. b)The same comparison, but now with $A(\phi;2)e^{-i\phi}$ and $S_{-1}(+1)A(\phi;1)$. These graphs show clearly that discrepancies increase further away from $\phi = \pi/2$.

It can be concluded that a general parabolic vector field, of which the transverse components are related to the longitudinal component through the $U^{\pm}$ operators, have a parabolic momentum of approximately $a \pm \frac{1}{2}$. Simultaneously, their OAM value is shifted to $\ell \pm \frac{1}{2}$ as well. This is surprising, as all spin-weighted vector fields encountered before had components of which their OAM was shifted with ± 1, keeping the total AM constant. However, the scalar field is not an eigenstate of the total AM to start with, hence there is no condition on the total AM of the vector field. Further, this approximation only holds in the vicinity of $\phi = \pi/2$. To study the actual effect of the ladder operators on the parabolic harmonics the whole transverse plane needs to be considered. The observation that the shift in OAM is equal to the shift in parabolic momentum around $\phi = \pi/2$ is confirmed from calculating the Fourier decomposition of the spectrum.

To summarize, there is an approximate spin-orbit coupling effect, equal to a coupling between the parabolic momentum and the SAM of the field components. This is only for a small region around $\phi = \pi/2$. For now, I cannot draw any conclusions about a coupling effect, neither between the spin and orbital AM nor between the SAM and parabolic momentum, over the total transverse plane.

6.4 Discussion

Field solutions in parabolic coordinates are characterized by their parabolic momentum, the anticommutator of the orbital angular momentum and the momentum operator in the $\hat{\mathbf{y}}$-direction. In contrast to Bessel beams, the angular spectrum of parabolic harmonics varies in amplitude with ϕ. It resembles the angular spectrum of an OAM eigenstate at the coordinate $\phi = \pi/2$ but is not an eigenstate of the OAM everywhere in the transverse plane.

Vector field expressions can be found from the scalar field by acting with ladder operators $U^{\pm}$ on them. However, these operators raise or lower the OAM value with half a unit in parabolic coordinates, in contrast to one unit of OAM in cylindrical coordinates. As a result, the vector field components, shifted in SAM value with ± 1, do not conserve the total AM. The parabolic momentum resembles the OAM at $\phi = \pi/2$, and is hence also shifted by $\pm\frac{1}{2}$ under the action of $U^{\pm}$. This implies that there is an effective spin-orbit coupling, equal to a coupling between the SAM and the parabolic momentum. However, these observations are only true in the vicinity of $\phi = \pi/2$. At the present moment, I am not able to draw conclusions about the effect over the whole transverse plane.

7 Conclusion

This thesis set out to investigate the coupling between orbital and spin angular momentum, occurring both in optical and electron fields. These fields are different in several characteristics; the optical field is massless, real and has spin 1, while the electron field is massive, complex and has spin $\frac{1}{2}$. Although different, these fields also share many similarities. These fields were studied using classical field theory, ignoring the differences between bosonic and fermionic characteristics. However, the value of the SAM was taken into account, allowing for a study into the spin-orbit coupling for different values of SAM.

Both fields can be described in either a spin or helicity representation. They are eigenstates of the total angular momentum $\mathbf{S} + \mathbf{L}$ or the sum of the helicity and orbital angular momentum $\mathcal{H} + \mathbf{L}$. Differences between these helicity and spin states are in general small and disappear in the paraxial limit.

When comparing the conserved quantities of the scalar field with those of the spinor and vector fields, there are two additional contributions that can be identified. The first one is the orbital contribution, arising from the multi-component wavefunctions describing spinor and vector fields. The second contribution comes from the spin current. If this current is not taken into account the energy-momentum tensor is found to be asymmetric, which does not comply with the principle of inertial movement.

The momentum density of the fields in the longitudinal direction is, in general, proportional to the field density and the longitudinal momentum vector. The azimuthal momentum density depends on the ratio of the OAM and radial distance and vanishes in the paraxial limit, while the momentum density in the radial direction is zero. Corrections to the spinor longitudinal current are many orders of magnitude smaller than the scalar part of the current, making them unlikely to be observed in experiments.

The orbital and spin contributions of the spinor fields are proportional to $\sin(\theta)$ for the spin-polarized states and $\sin(\theta/2)$ for the helicity states. In contrast, the radius of the quantum core approximates to the same dependence on θ for both the spin-polarized and helical fields, with the radius for the spin-polarized electrons a factor of $\sqrt{2}$ larger than the radius of the helical electrons. However, it will be impossible to measure this effect as the radius is of the order 10^{-13} m for electrons. The quantum core associated with the

helicity density is $\sim 10^{-6}$ m for photons. The problem arises here that this radius is not a measure of the regime where vector characteristics become apparent, as there is no scalar equivalent to the helicity density of a vector field.

Taking superpositions of the spin-polarized beams gives linearly (transversely) polarized beams. This is clearly reflected in the conserved quantities of the fields. Superpositions of the helicity states give the TE and TM modes for the optical field, although the OAM values need to be shifted. Constructing similar electron beams yields states similar to Majorana states; real solutions of the spinor field.

An important difference between electrons and photons is that the photon field is real while the electron field is complex. However, complex fields can be described in terms of real fields and vice versa. This distinction is equivalent to the choice of either considering standing or travelling waves, or describing fields in terms of circularly or linearly polarized waves.

From symmetry considerations it can be concluded that optical Majorana fields are real and linearly polarized. It depends on the frame of reference whether these are considered to be travelling or standing waves. Important characteristics of fermionic Majorana excitations, the halving of the number of degrees of freedom and being surface states, are mirrored in optical states such as surface plasmon polaritons at the interface between a metal and vacuum. There are also Majorana-like modes possible in the bulk of photonic crystals, but there is no fermionic analogue of these modes.

Orbital angular momentum arises naturally in a cylindrically symmetric system but is not a conserved quantity in parabolic coordinates; the basis solutions are eigenstates of the parabolic momentum instead. It is only in the vicinity of $\phi = \pi/2$ that these states resemble eigenstates of the OAM. In this region the OAM and parabolic momentum are similar to each other, and hence ladder operators of the OAM can be used to raise or lower both the OAM and parabolic momentum. Hence there is an effective coupling between both the SAM and OAM, and the SAM and the parabolic momentum. However, the ladder operators raise or lower the OAM with a half unit, in contrast with one unit of OAM in cylindrical coordinates. These observations are only valid in the region around $\phi = \pi/2$, and effects over the total transverse plane have not been considered yet.

Laser modes

Lasers produce electromagnetic fields that do not extend infinitely in the transverse plane. These fields diffract (spread upon propagation) as a result. Starting out from the focal plane with a diameter w_0, the distance over which the beam diameter increases by a factor $\sqrt{2}$ is called the Rayleigh length z_R:

$$z_R = \frac{\pi w_0^2}{\lambda}.$$

The total energy flux is characterized by two quantities; the divergence (the spread of the wave amplitude) and the transversal extension (the spread of the intensity)[194]. These are given by

$$\text{Divergence} \propto \int d^2\mathbf{k}_\perp \; k_\perp^2 |A|^2; \qquad \text{Extension} \propto \int d^2\mathbf{k}_\perp \; \nabla_\perp^2 A,$$

where A describes the field amplitude as a function of the transverse wavenumbers. The mode that minimizes both these quantities simultaneously is the Gaussian laser mode, of which the electric field amplitude is given by [194]

$$E^G(\mathbf{r}) \propto \frac{w_0}{w(z)} \exp\left(-\frac{r^2}{w^2(z)}\right) \exp\left(-\frac{ikzr^2}{2(z^2+z_R^2)}\right) e^{-ikz} e^{i\varphi(z)}. \tag{A.1}$$

Here r is the radius in the transverse plane only $r = \sqrt{x^2+y^2}$. The diameter of the beam is given by $w(z) = w_0\sqrt{1+z^2/z_R^2}$ and $\varphi(z) = \arctan z/z_R$ is the Gouy phase. This phase arises when a converging light ray moves through its focal point as the difference between its path length and that of a plane wave.

The fundamental Gaussian mode (A.1) is completely rotationally symmetric about the propagation axis, and the field intensity decreases monotonically away from the centre. More complicated structured laser modes include Hermite-Gaussian (HG) modes, that are not cylindrically symmetric but respect the Cartesian symmetry, and Laguerre-Gaussian (LG) modes that also have a cylindrical

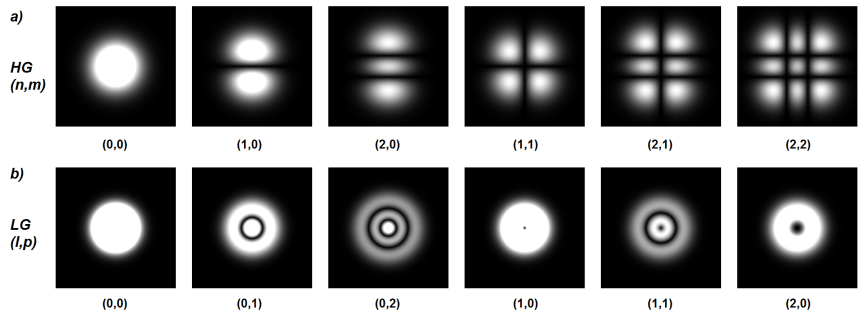

Figure A.1: The first HG and LG modes. a) HG modes are characterized by the order numbers n, m, which determine the number of nodes in the $\hat{\mathbf{y}}$ and $\hat{\mathbf{x}}$ direction respectively. b) LG modes are characterized by the azimuthal order number ℓ and the radial order number p, determining how many nodes there are in the radial direction. The value of ℓ is not observable from the light intensity.

symmetry along the propagation axis, but with a different radial intensity distribution.

The field amplitude of HG-modes is given by [195]:

$$E^{HG}_{m,n}(\mathbf{r}) \propto \frac{w_0}{w(z)} H_m\left(\frac{\sqrt{2}x}{w(z)}\right) H_n\left(\frac{\sqrt{2}y}{w(z)}\right) \exp\left(-\frac{r^2}{w^2(z)}\right) \times \exp\left(-\frac{ikzr^2}{2(z^2+z_R^2)}\right) e^{-ikz} e^{i\varphi_{mn}}. \quad \text{(A.2)}$$

The functions H_p are Hermite's polynomials, $H_p(x) = (-1)^p \exp(x^2) \frac{d^p}{dx^p} \exp(-x^2)$. These laser modes are characterized by two integers, one for each Cartesian coordinate. As a result the Gouy phase is modified to $\varphi_{mn} = (1 + m + n)\varphi(z)$.

Laguerre-Gaussian modes are cylindrically symmetric, with the field amplitude given by [195]

$$E^{LG}_{\ell,r}(\mathbf{r}) \propto \frac{1}{w(\zeta)} \left(\frac{r\sqrt{2}}{w(\zeta)}\right)^{|\ell|} L_p^{|\ell|}\left(\frac{2r^2}{w^2(z)}\right) \exp\left(-\frac{r^2}{w^2(z)}\right) \times \exp\left(-\frac{ikzr^2}{2(z^2+z_R^2)}\right) e^{-i\ell\phi - ikz} e^{i\varphi_{\ell r}}. \quad \text{(A.3)}$$

Here $L_p^{|\ell|}$ are generalized Laguerre's polynomials $L_p^{\ell}(r) = \frac{e^r r^{-\ell}}{p!} \frac{d^p}{dr^p}(e^{-r} r^{\ell+p})$ and $\varphi_{\ell p} = (|\ell| + 2p + 1)\varphi(z)$. The number ℓ determines how many times the phase changes from 0 to 2π when circling around the beam axis and is a measure of the orbital angular momentum, while p is the radial index.

As explained in section 1.2.2, Bessel beams need to be regularized by a Gaussian envelope, and are in the focal plane described by (1.11). Paraxially propagating this beam gives for a general coordinate z [196]:

$$\mathbf{E}^{BG}(\mathbf{r}) \propto \frac{w_0}{w(z)} e^{ikz} e^{-i\ell\phi} e^{-ik_r^2 z/2k} e^{-i\varphi(z)} J_\ell\left(\frac{w_0}{w(z)} k_r r e^{-i\varphi(z)}\right) \exp\left[\left(-\frac{1}{w^2(z)} + \frac{ikz}{2(z^2+z_R^2)}\right)\left(r^2 + \frac{k_r^2 r^2}{k^2}\right)\right]. \quad \text{(A.4)}$$

Bessel-Gauss beams are similar to LG beams [23, 33], as they are both rotationally symmetric and related to each other in the high order limit $p \ll \ell$.

Photonic eigenmodes in stratified media

B

Photonic modes in periodic media always appear in counterpropagating pairs [176]. This is a result of the periodicity of the lattice that implements restrictions on the electromagnetic fields. If the material has a periodicity in the $\hat{\mathbf{z}}$ direction, the electric and magnetic field solutions are given by

$$\mathbf{E}(t,\mathbf{r}) = e^{i(k_x x + k_y y)} e^{-i\omega t}\, \mathbf{E}(z), \qquad \mathbf{B}(t,\mathbf{r}) = e^{i(k_x x + k_y y)} e^{-i\omega t}\, \mathbf{B}(z),$$

i.e. the fields oscillate in the transverse directions and only vary in the longitudinal direction. Maxwell's equations can be written in terms of these fields as one differential equation

$$\partial_z \psi(z) = ikM(z)\psi(z); \qquad \psi = \begin{pmatrix} E_x \\ E_y \\ B_x \\ B_y \end{pmatrix}, \tag{B.1}$$

where $M(z)$ is not a Hermitian matrix, but J-Hermitian[1], $M^\dagger = JMJ^{-1}$ [176]. Since the waves are propagating in the $\hat{\mathbf{z}}$ direction and depend harmonically on time, the derivatives with respect to time and the z-coordinate are proportional to each other. This is similar to the derivative with respect to z in the paraxial wave equation (1.12). The relationship (B.1) can hence be regarded as a Hamiltonian operator $\partial_t \psi$ for the field.

[1] This is comparable to the $\mathcal{PT}$-symmetric Hamiltonians H that are not Hermitian, but related to a Hermitian operator h by $h = e^{-Q/2} H e^{Q/2}$ [157]. The matrix J is given by:

$$J = \begin{pmatrix} 0 & 0 & 0 & 1 \\ 0 & 0 & -1 & 0 \\ 0 & -1 & 0 & 0 \\ 1 & 0 & 0 & 0 \end{pmatrix}.$$

Since the lattice is periodic, the photonic modes are invariant under a translation in z by the periodic length L, and the matrix $M(z)$ is also periodic:

$$\psi_k(z+L) = e^{ikL}\psi_k(z), \qquad M(z+L) = M(z).$$

As a consequence, a transfer matrix $T(z, z_0)$ can be defined which transforms a mode at coordinate z_0 to a mode at coordinate z. This matrix satisfies the same differential equation (B.1) with the modes ψ_k:

$$\psi_k(z) = T(z, z_0)\psi_k(z_0).$$

This leads to the following relationship for the translation of the modes:

$$\psi_k(z+L) = T(z+L, z)\psi_k(z) = e^{ikL}\psi_k(z),$$

where $e^{ik_jL} = \zeta_j$ are the eigenvalues of the matrix T. These k_j can in general be four different wave numbers $\{k_1, k_2, k_3, k_4\}$. However, due to the J-Hermiticity of $M(z)$, the matrix T is J-unitary, $T^\dagger = JT^{-1}J$ [2] [197]. As a consequence the eigenvalues of T are restricted:

$$\{k_1, k_2, k_3, k_4\} = \{k_1^*, k_2^*, k_3^*, k_4^*\}.$$

This does not necessarily mean that the eigenvalues are real, ($k_1^* = k_1$), as they can also be complex, as long as they fulfil the condition $k_1 = k_2^*$ and $k_2 = k_1^*$, with a similar relation for k_3 and k_4. It can be concluded that the eigenvalues of this matrix are either real or appear in complex conjugate pairs. Since real wavenumbers correspond to propagating Bloch modes and complex wavenumbers to evanescent modes, there will always be an even number of either of these; the possibilities include four propagating, four evanescent, or two propagating and two evanescent modes.

[2] This can be derived from (B.1):

$$\partial_z T(z) = ikM(z)T(z) \rightarrow \partial_z T^\dagger(z) = -ikT^\dagger(z)M^\dagger(z). \tag{B.2}$$

Since $T(z)T^{-1}(z)$ is the identity matrix, the derivative of this product is $\partial_z(T(z)T^{-1}(z)) = 0$ and thus $T(z)\partial_z T^{-1}(z) = -(\partial_z T(z))T^{-1}(z)$. This gives

$$\partial_z T^{-1}(z) = -T^{-1}(\partial_z T)T^{-1} = -ikT^{-1}M(z).$$

Multiplying from the right and left by J and using that $J = J^{-1}$ gives

$$\partial_z(JT^{-1}(z)J) = -ik(JT^{-1}J)(JM(z)J) = -ik(JT^{-1}J)M^\dagger(z).$$

Comparing this with (B.2) shows that $T^\dagger = JT^{-1}J$.

If the transfer matrix is similar to its inverse, $T = U^{-1}T^{-1}U$, it is also similar to its Hermitian conjugate; $T = V^{-1}T^{\dagger}V$ with $V = JU$. This leads to the following constraint for the wavenumbers:

$$\{k_j\} = \{-k_j\}.$$

This relation is called *axial spectral symmetry*, as the dispersion relation is symmetric in $\mathbf{k}$. It applies both for the propagating and evanescent modes, and thus these modes will always appear in counterpropagating pairs.

The axial spectral symmetry agrees with the observation that Majorana fermions do not have a vector current but an axial vector current. If the axial symmetry of the optical crystal is conserved the only possible waves are standing waves.

C

Parabolic coordinate transformations

Parabolic coordinates are defined in terms of Cartesian and polar coordinates by the transformations

$$x \pm iy = re^{\pm i\phi} = \frac{1}{2}(u \pm iv)^2.$$

And the inverse transformations are given by

$$u = \frac{1}{\sqrt{2}}\left(\sqrt{x+iy} + \sqrt{x-iy}\right) = \sqrt{\frac{r}{2}}\left(e^{i\phi/2} + e^{-i\phi/2}\right), \tag{C.1a}$$

$$v = \frac{-i}{\sqrt{2}}\left(\sqrt{x+iy} - \sqrt{x-iy}\right) = -i\sqrt{\frac{r}{2}}\left(e^{i\phi/2} - e^{-i\phi/2}\right). \tag{C.1b}$$

The scale factors are given by

$$h_u = h_v = h = \sqrt{u^2+v^2} = \sqrt{2r}. \tag{C.2}$$

Now introducing an azimuthal angle [55]

$$\beta = \arcsin\left(\frac{v}{h}\right) = \frac{\phi}{2}, \tag{C.3}$$

gives the following identities:

$$e^{\pm i\beta} = \frac{u \pm iv}{h}, \tag{C.4a}$$

$$u = \sqrt{\frac{r}{2}}\left(e^{i\beta} + e^{-i\beta}\right) = h\cos(\beta), \tag{C.4b}$$

$$v = -i\sqrt{\frac{r}{2}}\left(e^{i\beta} - e^{-i\beta}\right) = h\sin(\beta). \tag{C.4c}$$

This is similar to transformations between cylindrical polar coordinates (r, ϕ) and Cartesian coordinates, under the substitutions $\phi \mapsto \frac{\phi}{2} = \beta,\ r \mapsto \sqrt{2r} = h$.

The divergence, curl and Laplacian operators in parabolic coordinates are transformed to

$$\nabla \cdot \mathbf{F} = \frac{1}{h^2}\left(\partial_u(hF_u) + \partial_v(hF_v)\right) + \partial_z F_z, \tag{C.5a}$$

$$\nabla \times \mathbf{F} = \left(\frac{1}{h}\partial_v F_z - \partial_z F_v\right)\hat{\mathbf{u}} + \left(\partial_z F_u - \frac{1}{h}\partial_u F_z\right)\hat{\mathbf{v}} + \frac{1}{h^2}\left(\partial_u(hF_v) - \partial_v(hF_u)\right)\hat{\mathbf{z}}, \tag{C.5b}$$

$$\nabla^2\varphi = \frac{1}{h^2}\left(\partial_u^2\varphi + \partial_v^2\varphi\right) + \partial_z^2\varphi. \tag{C.5c}$$

In parabolic coordinates, the expressions of the Lagrangian, Hamiltonian and OAM operator are given by:

$$\mathcal{L} = \frac{1}{2}m(u^2+v^2)(\dot{u}^2+\dot{v}^2), \tag{C.6a}$$

$$H = \frac{1}{u^2+v^2}\left(\frac{1}{2m}(p_u^2+p_v^2) - 2k\right), \tag{C.6b}$$

$$L_z = \frac{1}{2}(up_v - vp_u). \tag{C.6c}$$

Bibliography

[1] E. Kreyszig. *Advanced Engineering Mathematics*. John Wiley & Sons, Hoboken, New Jersey, 9th edition, (2006). ISBN: 9780471728979.

[2] M.R. Dennis *et al.* volume **53** of *Progress in Optics*, chapter Singular Optics; Optical Vortices and Polarization Singularities, pages 293–363. Elsevier, Amsterdam, (2009).

[3] A.D. Poularikas. *The Transforms and Applications Handbook*. CRC Press LLC, Boca Raton, Florida, 2nd edition, (2000). ISBN: 0849385954.

[4] D. McGloin and K. Dholakia. Bessel beams: diffraction in a new light. *Cont. Phys.*, **46**:15–28, (2005).

[5] J. Durnin. Exact solutions for nondiffracting beams. I. The scalar theory. *J. Opt. Soc. Am. A.*, **4**:651–654, (1987).

[6] J.A. Stratton. *Electromagnetic Theory*. McGraw-Hill Book Company Inc., New York, (1941).

[7] P.A.M. Dirac. Quantised singularities in the electromagnetic field. *Proc. R. Soc. A*, **133**:60–72, (1931).

[8] J.F. Nye and M.V. Berry. Dislocations in wave trains. *Proc. R. Soc. A.*, **336**:165–190, (1974).

[9] H. Wolter. Concerning the path of light upon total reflection. *J. Opt. A: Pure Appl. Opt.*, **11**:090401, (2009).

[10] V. Bazhenov, M.V. Vasnetsov, and M.S. Soskin. Laser beams with screw dislocations in their wavefronts. *JETP Lett.*, **52**:429–431, (1990).

[11] L. Allen, M.W. Bijersbergen, R.J.C. Spreeuw, and J.P. Woerdman. Orbital angular momentum of light and the transformation of Laguerre-Gaussian laser modes. *Phys. Rev. A*, **45**:8185–8189, (1992).

[12] M.W. Beijersbergen, R.P.C. Coerwinkel, M. Kristensen, and J.P. Woerdman. Helical-wavefront laser beams produced with a spiral phase plate. *Opt. Comm.*, **112**:321–327, (1994).

[13] N.R. Heckenberg, R. McDuff, C.P. Smith, and A. White. Generation of optical phase singularities by computer-generated holograms. *Opt. Lett.*, **17**:221–223, (1992).

[14] J. Harris *et al.* Structured quantum waves. *Nat. Phys.*, **11**:629–634, (2015).

[15] J. Masajada and B. Dubik. Optical vortex generation by three plane wave interference. *Opt. Comm.*, **198**:21–27, (2001).

[16] W. Braunbek. Zur Darstellung von Wellenfeldern. *Z. Naturforsch*, **6**:12–15, (1951).

[17] G.A. Turnbull *et al.* The generation of free-space Laguerre-Gaussian modes at millimetre-wave frequencies by use of a spiral phaseplate. *Opt. Comm.*, **127**:183–188, (1996).

[18] M. D. Williams *et al.* Optical vortex generation from molecular chromophore arrays. *Phys. Rev. Lett.*, **111**, (2013).

[19] S. Zheng and J. Wang. Measuring Orbital Angular Momentum (OAM) states of vortex beams with annular gratings. *Scientific Reports*, **7**(40781), (2017).

[20] H. Zhou *et al.* Measuring the orbital angular momentum state of light by coordinate transformation. *IEEE Phot. Tech. Lett.*, **29**:86–89, (2017).

[21] S. Franke-Arnold, L. Allen, and M. Padgett. Advances in optical angular momentum. *Laser & Photon. Rev.*, **2**:299–313, (2008).

[22] F. Gori, G. Guattari, and C. Padovani. Bessel-Gauss beams. *Opt. Comm.*, **64**:491–495, (1987).

[23] M.A. Porras, R. Borghi, and M. Santarsiero. Relationship between elegant Laguerre-Gauss and Bessel-Gauss beams. *J. Opt. Soc. Am. A*, **18**:177–184, (2001).

[24] J.E. Greivenkamp. *Field Guide to Geometrical Optics*, volume **FG01**. SPIE, Bellingham, Washington, (2004). ISBN: 9780819452948.

[25] J. Durnin, J.J. Micheli, and J.H. Eberly Jr. Diffraction-free beams. *Phys. Rev. Lett.*, **58**:1499–1501, (1987).

[26] J. Turunen, A. Vasara, and A.T. Friberg. Holographic generation of diffraction-free beams. *Appl. Opt.*, **27**:3959–3962, (1988).

[27] R.M. Herman and T.A. Wiggins. Production and uses of diffractionless beams. *J. Opt. Soc. Am. A*, **8**:932–942, (1991).

[28] J. Arlt and K. Dholakia. Generation of high-order Bessel beams by use of an axicon. *Opt. Comm.*, **177**:297–301, (2000).

[29] A. Vasara, J. Turunen, and A.T. Friberg. Realization of general nondiffracting beams with computer-generated holograms. *J. Opt. Soc. Am. A*, **6**:1748–1754, (1989).

[30] H.S. Lee, B.W. Stewart, K. Choi, and H. Fenichel. Holographic nondiverging hollow beam. *Phys. Rev. A*, **49**:4922–4927, (1994).

[31] C. Paterson and R. Smith. Higher-order Bessel waves produced by axicon-type computer-generated holograms. *Opt. Comm.*, **124**:121–130, (1996).

[32] A. April. Bessel-Gauss beams as rigorous solutions of the Helmholtz equation. *J. Opt. Soc. Am. A*, **28**:2100–2107, (2011).

[33] M.A. Bandres. Accelerating parabolic beams. *Opt. Lett.*, **33**:1678–1680, (2008).

[34] K.Y. Bliokh, Y.P. Bliokh, S. Savel'ev, and F. Nori. Semiclassical dynamics of electron wave packet states with phase vortices. *Phys. Rev. Lett.*, **99**:190404, (2007).

[35] V. Grillo *et al.* Generation of nondiffracting electron Bessel beams. *Phys. Rev. X.*, **4**:011013, (2014).

[36] P. Schattschneider and J. Verbeeck. Theory of free electron vortices. *Ultramicroscopy*, **111**:1461–1468, (2011).

[37] J. Verbeeck, H. Tian, and P. Schattschneider. Production and application of electron vortex beams. *Nature*, **467**:301–304, (2010).

[38] M. Uchida and A. Tonomura. Generation of electron beams carrying orbital angular momentum. *Nature*, **464**:737–739, (2010).

[39] Mc.Morran *et al*. Electron vortex beams with high quanta of orbital angular momentum. *Science*, **331**:192–195, (2011).

[40] S.M. Lloyd, M. Babiker, G. Thirunavukkarasu, and J. Yuan. Electron vortices: Beams with orbital angular momentum. *Rev. Mod. Phys.*, **89**:035004, (2017).

[41] P. Schattschneider, M. Stöger-Pollach, and J. Verbeeck. Novel vortex generator and mode converter for electron beams. *Phys. Rev. Lett.*, **109**(084801), (2012).

[42] L. Clark *et al.* Exploiting lens aberrations to create electron-vortex beams. *Phys. Rev. Lett.*, **111**(064801), (2013).

[43] K. Saitoh *et al.* Generation of electron Bessel beams with nondiffractive spreading by a nanofabricated annular slit. *J. Phys. Soc. Japan*, **85**, (2016). 043501.

[44] A. Béché, R. Van Boxem, G. Van Tendeloo, and J. Verbeeck. Magnetic monopole field exposed by electrons. *Nat. Phys.*, **10**:26–29, (2014).

[45] S.M. Lloyd, M. Babiker, and J. Yuan. Mechanical properties of electron vortices. *Phys. Rev. A*, **88**:031802(R), (2013).

[46] S.M. Lloyd, M. Babiker, J. Yuan, and C. Kerr-Edwards. Electromagnetic vortex fields, spin, and spin-orbit interactions in electron vortices. *Phys.*

Rev. Lett., **109**:254801, (2012).

[47] H. Laroque *et al.* Nondestructive measurement of orbital angular momentum for an electron beam. *Phys. Rev. Lett.*, **117**(154801), (2016).

[48] A.S. Konkov, A.P. Potylitsyn, and M.S. Polonskaya. Transition radiation of electrons with a nonzero orbital angular momentum. *JETP Letters*, **100**:421–425, (2014).

[49] L.H. Ryder. *Quantum Field Theory*. Cambridge University Press, Cambridge, 2nd edition, (1996). ISBN: 0521472423.

[50] M.D. Schwartz. *Quantum Field Theory and the Standard Model*. Cambridge University Press, Cambridge, (2014). ISBN: 9781107034730.

[51] D.M. Brink and G.R. Satchler. *Angular Momentum*. Clarendon Press, Oxford, 2nd edition, (1968).

[52] D.J. Griffiths. *Introduction to Quantum Mechanics*. Prentice-Hall, Upper Saddle River, New Jersey, 2nd edition, (2005). ISBN: 0131911759.

[53] W. Gerlach and O. Stern. Der experimentelle Nachweis der Richtungsquantelung im Magnetfeld. *Zeitschrift für Physik*, **9**:349–352, (1922).

[54] G. Gabrielse *et al.* New determination of the fine structure constant from the electron g value and QED. *Phys. Rev. Lett.*, **97**:030802, (2006).

[55] K. Volke-Sepulveda and E. Ley-Koo. General construction and connections of vector propagation invariant optical fields: TE and TM modes and polarization states. *J. Opt. A: Pure Appl. Opt.*, **8**:867–877, (2006).

[56] D. Stoler. Operator methods in physical optics. *J. Opt. Soc. Am.*, **71**:334–341, (1981.

[57] W. Greiner and J. Reinhardt. *Field Quantization*. Springer, Heidelberg, (1996). ISBN: 3540594796.

[58] S. Weinberg. *The Quantum Theory of Fields*. Cambridge University Press, Cambridge, (1995). ISBN: 0521550017.

[59] B. Thaller. *The Dirac equation*. Springer-Verlag, Heidelberg, (1992).

[60] D. Tong. Quantum field theory. Course Notes, Cambridge University, (2006-2007).

[61] D. Griffiths. *Introduction to Elementary Particles*. Wiley-VCH Verlag GmbH & Co, Weinheim, 2nd edition, (2004).

[62] O. Heaviside. *Electromagnetic Theory*, volume **2**. Cosimo, Inc, New York, (1971).

[63] J.T.M. Walraven. Atomic physics. Lecture Notes, University of Amsterdam, (2010).

[64] I. Bialynicki-Birula and Z. Bialynicka-Birula. Beams of electromagnetic radiation carrying angular momentum: The Riemann-Silberstein vector and the classical-quantum correpondence. *Opt. Comm.*, **264**:342–451, (2006).

[65] G.F. Torres del Castillo. Spinors in three dimensions. *Rev. Mex. de Fís.*, **38**:863–874, (1992).

[66] I. Bialynicki-Birula and Z. Bialynicka-Birula. Relativistic electron wave packets carrying angular momentum. *Phys. Rev. Lett.*, **118**:114801, (2017).

[67] G.F. Torres del Castillo. Solution of nonscalar equations in cylindrical coordinates. *Rev. Mex. de Fís.*, **38**:19–39, (1992).

[68] G.F. Torres del Castillo. Solution of nonscalar equations in cylindrical coordinates. II. *Rev. Mex. de Fís.*, **40**:833–845, (1994).

[69] M. Krenn and A. Zeilinger. On small beams with large topological charge: II. Photons, electrons and gravitational waves. *New J. Phys.*, **20**, (2018).

[70] S.J. van Enk and G. Nienhuis. Commutation rules and eigenvalues of spin and orbital angular momentum of radiation fields. *Europhys. Lett.*, **25**:497–501, (1994).

[71] K.Y. Bliokh, M.A. Alonso, E.A. Ostrovskaya, and A. Aiello. Angular momenta and spin-orbit interaction of nonparaxial light in free space. *Phys. Rev. A.*, **82**:063825, (2010).

[72] K.Y. Bliokh, M.R. Dennis, and F. Nori. Relativistic electron vortex beams: angular momentum and spin-orbit interaction. *Phys. Rev. Lett.*, **107**:174802(5), (2011).

[73] D.V. Karlovets. Electron with orbital angular momentum in a strong laser wave. *Phys. Rev. A.*, **86**:062102, (2012).

[74] I. Kaminer *et al.* Quantum Cherenkov radiation: Spectral cutoffs and the role of spin and orbital angular momentum. *Phys. Rev. X*, **6**:011006, (2016).

[75] J.D. Jackson. *Classical Electrodynamics*. Wiley, Hoboken, New Jersey, 3rd edition, (1999). ISBN: 047130932.

[76] J.H. Poynting. The wave motion of a revolving shaft, etc. *Proc. R. Soc. London A*, **82**:560–567, (1909).

[77] R.A. Beth. Mechanical detection and measurement of the angular momentum of light. *Phys. Rev.*, **50**:115–125, (1936).

[78] E.P. Wigner. On unitary representations of the inhomogeneous Lorentz group. *Ann. Math.*, **40**:149–204, (1939).

[79] K.Y. Bliokh *et al.* Spin-to-orbital angular momentum conversion in focusing, scattering, and imaging systems. *Opt. Expr.*, **19**:26432–26149, (2011).

[80] S. Chandra. The Chandrasekhar-Kendall functions. *Astrophysics and Space Science*, **136**:409–412, (1987).

[81] S. Chandrasekhar. On force-free magnetic fields. *PNAS*, **42**:1, (1956).

[82] A.M. Steane. An introduction to spinors. Lecture Notes Symmetry and Relativity, (2011). arXiv:1312.3824.

[83] S. Esposito, E. Recami, and A. van der Merwe, editors. *Ettore Majorana: unpublished Research Notes on Theoretical Physics*. Springer, Heidelberg, (2008). ISBN: 1402091133.

[84] R. Mignani *et al.* About a Dirac-like equation for photon according to Ettore Majorana. *Lett. al Nuovo Cimento*, **11**:568–572, (1974).

[85] P.B. Pal. Dirac, Majorana and Weyl fermions. *Am. J. Phys.*, **79**:485–498, (2011).

[86] A. Aste. A direct road to Majorana fields. *Symmetry*, **2**:1776–1809, (2010).

[87] H. F. Jones. *Groups, Representations and Physics*. Taylor & Francis Group, New York, 2nd edition, (1998).

[88] M.E. Peskin and D.V. Schroeder. *An Introduction to Quantum Field Theory*. Westview Press, Boulder, Colorado, (1995). ISBN: 100201503972.

[89] C.W.J. Beenakker. Search for Majorana fermions in superconductors. *Annu. Rev. Con. Mat. Phys.*, **4**(113-116), (2013).

[90] M. Leijnse and K. Flensberg. Introduction to topological superconductivity and Majorana fermions. *Semicond. Sci. Technol.*, **27**:124003, (2012).

[91] F. Wilczek. Majorana returns. *Nat. Phys.*, **5**:614–618, (2009).

[92] J. Alicea. New directions in the pursuit of Majorana fermions in solid state systems. *Rep. Prog. Phys.*, **75**(076501), (2012).

[93] L. Fu and C.L. Kane. Superconducting proximity effect and Majorana fermions at the surface of a topological insulator. *Phys. Rev. Lett.*, **100**(096407), (2008).

[94] A.Y. Kitaev. Unpaired Majorana fermions in quantum wires. *Phys.-Usp*, **44**:131, (2001).

[95] N. Read and D. Green. Paired states of fermions in two dimensions with breaking of parity and time-reversal symmetries and the fractional quantum Hall effect. *Phys. Rev. B*, **61**:10267–10297, (2000).

[96] V. Mourik *et al.* Signatures of Majorana fermions in hybrid superconductor-semiconductor nanowire devices. *Science*, **336**:1003–1007, (2012).

[97] M.T. Deng *et al.* Anomalous zero-bias conductance peak in a Nb-InSb nanowire-Nb hybrid device. *Nano Lett.*, **12**:6414–6419, (2012).

[98] L.P. Rokhinson. The fractional a.c. Josephson effect in a semiconductor-superconductor nanowire as a signature of Majorana particles. *Nat. Phys.*, **8**:795–799, (2012).

[99] S. Nadj-Perge *et al.* Observation of Majorana fermions in ferromagnetic atomic chains on a superconductor. *Science*, **346**:602–607, (2014).

[100] W. Greiner. *Relativistic Quantum Mechanics*. Springer, Heidelberg, 3rd edition, (2000). ISBN: 3540674578.

[101] E. Wigner. Über die Operation der Zeitumkehr in der Quantenmechanik. *Nachr. Ges. Wiss. Göttingen, Math.-Phys. Klasse*, **1932**:546–559, (1932).

[102] S.Q. Shen, W.-Y. Shan, and H.-Z. Lu. Topological insulator and the Dirac equation. *Spin*, **1**:33–44, (2011).

[103] P. M. Morse and H. Feshbach. *Methods of Theoretical Physics, Part I*. Mc Graw-Hill, New York, (1953).

[104] U.D. Jentschura and B.J. Wundt. Neutrino helicity reversal and fundamental symmetries. *J. Phys. G: Nucl. Part. Phys.*, **41**(075201), (2017).

[105] S. Weinberg and E. Witten. Limits on massless particles. *Phys. Lett.*, **96B**:59–60, (1980).

[106] J.D. Griffiths. *Introduction to Electrodynamics*. Prentice Hall, Upper Saddle River, New Jersey, 3rd edition, (2008). ISBN: 0139199608.

[107] E. Leader and C. Lorcé. The angular momentum controversy: What's it all about and does it matter? *Phys. Rep.*, **541**:163–248, (2014).

[108] R. Medina and J. Stephany. Belinfante-Rosenfeld tensor and the inertia principle. (2014). arXiv:1404.3334v1.

[109] L. Rosenfeld. "Sur le tenseur D'Impulsion-Energie". *Mémoires Acad. Roy. de Belgique*, **18**:1–30, (1940).

[110] F.J. Belinfante. On the current and the density of the electric charge, the energy, the linear momentum and the angular momentum of arbitrary fields. *Physica*, **7**:449–474, (1940).

[111] W. Gordon. "Der Strom der Diracschen Elektronentheorie". *Zeitschrift fur Physik*, **50**:630–632, September (1928).

[112] F.J. Belinfante. On the spin angular momentum of mesons. *Physica*, **6**:887–898, (1939).

[113] A. Bandyopadhyay. *Improvement of stress-energy tensor using space-time symmetries*. PhD thesis, University of Illinois, (2001).

[114] G. Sterman. *An Introduction to Quantum Field Theory*. Cambridge University Press, Cambridge, (1993). ISBN: 1316583287.

[115] M. V. Berry. Optical currents. *J. Opt. A*, **11**(094001), (2009).

[116] R.P. Cameron, S.M. Barnett, and A.M. Yao. Optical helicity, optical spin and related quantities in electromagnetic theory. *New J. Phys.*, **14**(053050), (2012).

[117] D.L. Andrews. Symmetries, conserved properties, tensor representations, and irreducible forms in molecular quantum electrodynamics. *Symmetry*, **10**(298), (2018).

[118] D.L. Andrews and M.M. Coles. Measures of chirality and angular momentum in the electromagnetic field. *Opt. Lett.*, **37**:3009–3011, (2012).

[119] M.G. Calkin. An invariance property of the free electromagnetic field. *Am. J. Phys.*, **33**:958–960, (1965).

[120] I. Fernandez-Corbaton *et al.* Electromagnetic duality symmetry and helicity conservation for the macroscopic Maxwell's equations. *Phys. Rev. Lett.*, **111**(060401), (2013).

[121] R.P. Cameron. On the "second potential" in electrodynamics. *J. Opt.*, **16**(015708), (2014).

[122] K.Y. Bliokh, A.Y. Bekshaev, and F. Nori. Dual electromagnetism: helicity, spin, momentum and angular momentum. *New J. Phys.*, **15**(033026), (2013).

[123] A. Aiello and M.V. Berry. Note on the helicity decomposition of spin and orbital optical currents. *J. Opt.*, **17**(062001), (2015).

[124] S.M. Barnett. Rotation of electromagnetic fields and the nature of optical angular momentum. *J. Mod. Opt.*, **57**:1339–1343, (2010).

[125] T.G. Philbin. Lipkin's conservation law, Noether's theorem, and the relation to optical helicity. *Phys. Rev. A*, **87**:043843, (2013).

[126] E.A. Jeffery. Component minimization of the Bargmann-Wigner wavefunction. *Aust. J. Phys.*, **31**:137–149, (1978).

[127] R.P. Feynman, R.B. Leighton, and M. Sands. *The Feynman Lectures in Physics Volume 3, Quantum Mechanics*. Addison-Wesley, Boston, Massachusetts, (1964, revised 2005).

[128] S.R. Mishra. A vector wave analysis of a Bessel beam. *Opt. Comm.*, **85**:159–161, (1991).

[129] R.H. Jordan and D.G. Hall. Free-space azimuthal paraxial wave equation: the azimuthal Bessel-Gauss solution. *Opt. Lett.*, **19**:427–429, (1994).

[130] Z. Bouchal and M. Olivík. Non-diffractive vector Bessel beams. *J. Mod. Opt.*, **42**:1555–1566, (1995).

[131] D.G. Hall. Vector-beam solutions of Maxwell's wave equation. *Opt. Lett.*, **21**:9–11, (1996).

[132] P.L. Greene and D.G. Hall. Properties and diffraction of vector Bessel-Gauss beams. *J. Opt. Soc. Am. A*, **15**:3020–3027, (1998).

[133] V. Garcés-Chávez *et al.* Observation of the transfer of the local angular momentum density of a multiringed light beam to an optically trapped particle. *Phys. Rev. Lett.*, **91**:093602, (2003).

[134] G. Milione *et al.* Measuring the self-healing of the spatially inhomogeneous states of polarization of vector Bessel beams. *J. Opt.*, **17**:035617, (2015).

[135] A. Dudley *et al.* Generating and measuring non-diffracting vector Bessel beams. *Proc. SPIE*, **8999**, (2014).

[136] L. Marrucci. The q-plate and its future. *J. Nanophotonics*, **7**:078598, (2013).

[137] N. Tischler *et al.* Experimental control of optical helicity in nanophotonics. *Light: Science & Applications*, **3**:e183, (2014).

[138] C. Pfeiffer and A. Grbic. Controlling vector Bessel beams with metasurfaces. *Phys. Rev. Appl.*, **2**:044012, (2014).

[139] S. Fu, S. Zhang, and C. Gao. Bessel beams with spatial oscillating polarization. *Scientific Reports*, **6**:30765, (2016).

[140] M. He, Z. Chen, S. Sun, and J. Pu. Propagation properties and self-reconstruction of azimuthally polarized non-diffracting beams. *Opt. Comm.*, **294**:36–42, (2013).

[141] G. Wu, F. Yang, and Y. Cai. Generation and self-healing of a radially polarized Bessel-Gauss beam. *Phys. Rev. A*, **89**:043807, (2014).

[142] K.Y. Bliokh *et al.* Spin-orbit interactions of light. *Nat. Phot.*, **9**:796–808, (2015).

[143] R.Y. Chiao and W.S. Wu. Manifestations of Berry topological phase for the photon. *Phys. Rev. Lett.*, **57**:933–936, (1986).

[144] A. Tomita and R.Y. Chiao. Observation of Berry topological phase by use of an optical fiber. *Phys. Rev. Lett.*, **57**:937–940, (1986).

[145] R. Bhandari. Polarization of light and topological phases. *Phys. Rep.*, **281**:1–54, (1997).

[146] R.V. Boxem, J. Verbeeck, and B. Partoens. Spin effects in electron vortex states. *Europhys. Lett.*, **102**:40010, (2013).

[147] L. Marks. Viewpoint: what are the resolution limits in an electron micro-

scope? *Physics*, **6**:82, (2013).

[148] K.Y. Bliokh *et al.* Theory and applications of free-electron vortex states. *Phys. Rep.*, **690**:1–70, (2017).

[149] K.Y. Bliokh, M.R. Dennis, and F. Nori. Position, spin and orbital angular momentum of a relativistic electron. *Phys. Rev. A*, **96**:023622, (2017).

[150] S.M. Barnett. Relativistic electron vortices. *Phys. Rev. Lett.*, **118**:114802, (2017).

[151] K. Volke-Sepulveda *et al.* Orbital angular momentum of a high-order Bessel light beam. *J. Opt. B: Quantum Semiclass. Opt.*, **4**:S82–89, (2002).

[152] A. Flores-Pérez, J. Hernandez-Hernandez, R. Jauregui, and K. Volke-Sepulveda. Experimental generation and analysis of first-order TE and TM Bessel modes in free space. *Opt. Lett.*, **31**:1732–1734, (2006).

[153] A. Niv, G. Biener, V. Kleiner, and E. Hasman. Propagation-invariant vectorial bessel beams obtained by use of quantized Pancharatnam-Berry phase optical elements. *Opt. Lett.*, **29**:238–240, (2004).

[154] K.Y. Bliokh, A.Y. Bekshaev, and F. Nori. Extraordinary momentum and spin in evanescent waves. *Nat. Comm.*, **5**:3300, (2014).

[155] C.M. Bender. Introduction to $\mathcal{PT}$-symmetric quantum theory. *Contemp. Phys.*, **46**:277–292, (2005).

[156] C.M. Bender and P.D. Mannheim. $\mathcal{PT}$-symmetry in relativistic quantum mechanics. *Phys. Rev. D*, **84**:105038, (2011).

[157] C.M. Bender, H.F. Jones, and R.J. Rivers. Dual $\mathcal{PT}$-symmetric quantum field theories. *Phys. Lett. B*, **625**:333–340, (2005).

[158] J.R. Oppenheimer. Note on light quanta and the electromagnetic field. *Phys. Rev.*, **38**:725–746, (1931).

[159] O. Laporte and G.E. Uhlenbeck. Application of spinor analysis to the Maxwell and Dirac equation. *Phys. Rev.*, **37**:1380–1397, (1931).

[160] M.V. Berry. *Anomalies, Phases, Defects*, chapter Quantum adiabatic Anholonomy, pages 125–181. Bibliopolis, Naples, (1990).

[161] S.M. Barnett. Optical Dirac equation. *New J. Phys.*, **16**:093008, (2014).

[162] L. Siberstein. Electromagnetic basic equations in bivectoral treatment. *Ann. Phys.*, **22**:579–86, (1907).

[163] L. Silberstein. Addendum to the treatise "Basic electromagnetic equations in bivectorial form". *Ann. Phys.*, **24**:783–4, (1907).

[164] I. Bialynicki-Birula. Photon wave function. *Progress in Optics*, **36**:245–294, (1996).

[165] P.J. Mohr. Solutions of the Maxwell equations and photon wave functions. *Ann. Phys.*, **325**:607–63, (2010).

[166] C.-E. Bardyn and A. İmamoğlu. Majorana-like modes of light in a one-dimensional array of nonlinear cavities. *Phys. Rev. Lett.*, **109**:253606, (2012).

[167] J.-S. Xu *et al.* Simulating the exchange of Majorana zero modes with a photonic system. *Nat. Comm.*, **7**:13194, (2016).

[168] B.M. Rodrígues-Lara and H.M. Moya-Cessa. Optical simulation of Majorana physics. *Phys. Rev. A*, **89**(015803), (2014).

[169] W. Tan, L. Chen, X. Ji, and H.-Q. Lin. Photonic simulation of topological superconductor edge state and zero-energy mode at a vortex. *Scientific Reports*, **4**:7381, (2014).

[170] K.Y. Bliokh, D. Smirnova, and F. Nori. Quantum spin Hall effect of light. *Science*, **348**:1448–1451, (2015).

[171] W.L. Barnes, A. Dereux, and T.W. Ebbesen. Surface plasmon subwavelength optics. *Nature*, **424**:824–830, (2003).

[172] A.V. Zayats and I.I. Smolyaninov. Near-field photonics: surface plasmon polaritons and localized surface plasmons. *J. Opt. A: Pure Appl. Opt.*, **5**:S16–S50, (2003).

[173] G. Isfort, K. Schierbaum, and D. Zerulla. Polarization dependence of surface plasmon polariton emission. *Phys. Rev. B*, **7**:033404, (2006).

[174] T. Baba and D. Mori. Slow light engineering in photonic crystals. *J. Phys. D: Appl. Phys.*, **40**:2659–2665, (2007).

[175] B. Lang, D.M. Breggs, and R. Oulton. Time-reversal constraint limits unidirectional photon emission in slow-light photonic crystals. *Phil. Trans. R. Soc. A*, **374**:20150263, (2016).

[176] A. Figotin and I. Vitebskiy. Slow light in photonic crystals. *Waves in random and complex media*, **16**:293–382, (2006).

[177] M. Burresi *et al.* Observation of polarization singularities at the nanoscale. *Phys. Rev. Lett.*, **102**:033902, (2009).

[178] M.R. Dennis and J.D. Ring. Propagation-invariant beams with quantum pendulum spectra: from Bessel beams to Gaussian beam-beams. *Opt. Lett.*, **38**:3325–3328, (2013).

[179] M.A. Bandres, J.C. Gutiérrez-Vega, and S. Chávez-Cerda. Parabolic non-diffracting optical wave fields. *Opt. Lett.*, **29**:44–46, (2004).

[180] N. Wheeler. Reduced Kepler problem in elliptical coordinates. Lecture

Notes Reed College, (1991).

[181] M.A. Bandres and B.M. Rodríguez-Lara. Nondiffracting accelerating waves: Weber waves and parabolic momentum. *New J. Phys.*, **15**:013054, (2013).

[182] Nist Digital Library of Mathematical Functions. https://dlmf.nist.gov.

[183] E.M. Ovsiyuk, A.N. Red'ko, V. Balan, and V.M. Red'kov. The Dirac equation in parabolic cylindric coordinates and possible effects of the spinor structures in quantum physics. *Applied Sciences*, **18**:84–107, (2016).

[184] C.T. Sosa-Sánchez *et al.* Parabolic non-diffracting beams: geometrical approach. *J. Opt.*, **19**:085604, (2017).

[185] C. López-Mariscal, M.A. Bandres, and J.C. Gutiérrez-Vega. Observation of parabolic nondiffracting optical fields. *Opt. Expr.*, **13**:2364–2369, (2005).

[186] B.M. Rodríguez-Lara. Normalization of optical Weber waves and Weber-Gauss beams. *J. Opt. Soc. Am. A*, **27**:327–332, (2010).

[187] P. Zhang *et al.* Nonparaxial Mathieu and Weber accelerating beams. *Phys. Rev. Lett.*, **109**:193901, (2012).

[188] Y. Wen *et al.* Tailoring accelerating beams in phase space. *Phys. Rev. A*, **95**:023825, (2017).

[189] Y. Wen, Y. Zhang, H. Chen, and S. Yu. Winding light beams along elliptical helical trajectories. *Phys. Rev. A*, **94**:013829, (2016).

[190] I. Kaminer, R. Bekenstein, J. Nemirovsky, and M. Segev. Nondiffracting accelerating wave packets of Maxwell's equations. *Phys. Rev. Lett.*, **108**:163901, (2012).

[191] A. Ortiz-Ambriz, J.C. Gutiérrez-Vega, and D. Petrov. Manipulation of dielectric particles with nondiffracting parabolic beams. *J. Opt. Soc. Am. A*, **31**:2759–2762, (2014).

[192] Y. Kang *et al.* Nonparaxial accelerating electron beams. *IEEE J. Quant. Electronics*, **53**:9200206, (2017).

[193] I. Rondón-Ojeda and F. Soto-Eguibar. Properties of the Poynting vector for invariant beams: Negative propagation in Weber beams. *Wave Motion*, **78**:176–184, (2018).

[194] F. Pampaloni and J. Enderlein. Gaussian, Hermite-Gaussian, and Laguerre-Gaussian beams: A primer. (2004). arXiv:physics/0410021v1.

[195] O. Svelto and D.C. Hanna. *Principles of Lasers*. Springer Science and Business Media, Heidelberg, 3rd edition, (1989). ISBN: 9781441913012.

[196] C. Palma, R. Borghi, and G. Cincotti. Beams originated by J_0-correlated Schell-model planar sources. *Opt. Comm.*, **125**:113–121, (1996).

[197] A. Figotin and I. Vitebskiy. Oblique frozen modes in periodic layered media. *Phys. Rev. E*, **68**:036609, (2003).